



APPROVED FOR PUBLIC RELEASE, DISTRIBUTION UNLIMITED

ALEX(01)-TR-77-11

2

12

**DETERMINATION OF SEISMIC SOURCE PARAMETERS
FROM LONG-PERIOD SURFACE WAVE DATA**

**TECHNICAL REPORT NO. 11
VELA NETWORK EVALUATION AND AUTOMATIC PROCESSING RESEARCH**

Prepared by
David Sun

TEXAS INSTRUMENTS INCORPORATED
Equipment Group
Post Office Box 6015
Dallas, Texas 75222

DDC
RECEIVED
FEB 9 1978
F

Prepared for
**AIR FORCE TECHNICAL APPLICATIONS CENTER
Alexandria, Virginia 22314**

Sponsored by
**ADVANCED RESEARCH PROJECTS AGENCY
Nuclear Monitoring Research Office
ARPA Program Code No. 7F10
ARPA Order No. 2551**

31 August 1977

Acknowledgment: This research was supported by the Advanced Research Projects Agency, Nuclear Monitoring Research Office, under Project VELA-UNIFORM, and accomplished under the technical direction of the Air Force Technical Applications Center under Contract Number F08606-77-C-0004.

Equipment Group

AD A 049759

AD No. *1*
JDC FILE COPY



APPROVED FOR PUBLIC RELEASE, DISTRIBUTION UNLIMITED

ALEX(01)-TR-77-11

**DETERMINATION OF SEISMIC SOURCE PARAMETERS
FROM LONG-PERIOD SURFACE WAVE DATA**

**TECHNICAL REPORT NO. 11
VELA NETWORK EVALUATION AND AUTOMATIC PROCESSING RESEARCH**

Prepared by
David Sun

TEXAS INSTRUMENTS INCORPORATED
Equipment Group
Post Office Box 6015
Dallas, Texas 75222



Prepared for
AIR FORCE TECHNICAL APPLICATIONS CENTER
Alexandria, Virginia 22314

Sponsored by
ADVANCED RESEARCH PROJECTS AGENCY
Nuclear Monitoring Research Office
ARPA Program Code No. 7F10
ARPA Order No. 2551

31 August 1977

Acknowledgment: This research was supported by the Advanced Research Projects Agency, Nuclear Monitoring Research Office, under Project VELA-UNIFORM, and accomplished under the technical direction of the Air Force Technical Applications Center under Contract Number F08606-77-C-0004.

UNCLASSIFIED

SECURITY CLASSIFICATION OF THIS PAGE (When Data Entered)

REPORT DOCUMENTATION PAGE		READ INSTRUCTIONS BEFORE COMPLETING FORM
1. REPORT NUMBER	2. GOVT ACCESSION NO.	3. RECIPIENT'S CATALOG NUMBER
4. TITLE (and Subtitle) 6 DETERMINATION OF SEISMIC SOURCE PARAMETERS FROM LONG-PERIOD SURFACE WAVE DATA.		5. TYPE OF REPORT & PERIOD COVERED 9 Technical rept.
7. AUTHOR(s) 10 David/Sun		8. PERFORMING ORG. REPORT NUMBER 14 TI-ALEX(81)-TR-77-11
9. PERFORMING ORGANIZATION NAME AND ADDRESS Texas Instruments Incorporated Equipment Group Dallas, Texas 75222		10. PROGRAM ELEMENT, PROJECT, TASK AREA & WORK UNIT NUMBERS 15 F08606-77-C-0004 V ARPA Order-2551 VELA T/7705/B/ETR
11. CONTROLLING OFFICE NAME AND ADDRESS Advanced Research Projects Agency Nuclear Monitoring Research Office Arlington, Virginia 22209		12. REPORT DATE 11 31 Aug 77
14. MONITORING AGENCY NAME & ADDRESS (if different from Controlling Office) Air Force Technical Applications Center VELA Seismological Center Alexandria, Virginia 22314		13. NUMBER OF PAGES 34 12 351 p
16. DISTRIBUTION STATEMENT (of this Report) APPROVED FOR PUBLIC RELEASE, DISTRIBUTION UNLIMITED		15. SECURITY CLASS. (of this report) UNCLASSIFIED
17. DISTRIBUTION STATEMENT (of the abstract entered in Block 20, if different from Report)		
18. SUPPLEMENTARY NOTES ARPA Order No. 2551		
19. KEY WORDS (Continue on reverse side if necessary and identify by block number) Seismology Long-period seismic surface waves Amplitude spectral fitting Presumed underground nuclear explosions Seismic source parameter estimations Rayleigh and Love wave amplitude spectra and ratios		
20. ABSTRACT (Continue on reverse side if necessary and identify by block number) ✓ Far-field Rayleigh and Love waves observed on a long-period seismic network were studied to characterize presumed underground nuclear explosions. These occurred at the United States Nevada Test Site (NTS), the Russian eastern Kazakh (EKZ) region, and at the site of presumed peaceful nuclear explosions (PNE) in the north Caspian Sea region. The observation stations available for this study included Alaskan Long Period Array (ALPA), Large Aperture Seismic Array (LASA), Norwegian Seismic Array (NCRSAR),		

DD FORM 1 JAN 73 1473

EDITION OF 1 NOV 65 IS OBSOLETE

UNCLASSIFIED 405076
SECURITY CLASSIFICATION OF THIS PAGE (When Data Entered)

UNCLASSIFIED

SECURITY CLASSIFICATION OF THIS PAGE(When Data Entered)

20. continued

the Very Long Period Experiment (VLPE) stations, the Seismic Research Observatories (SRO), and the Special Data Collection System (SDCS) stations. The purpose of this study was to determine the seismic source parameters from long-period surface wave data and to investigate the influence of geological and near-source propagation effects on the frequency content of the surface wave signals. ↑

The surface wave group velocities were measured for travel paths from NTS, EKZ, and PNE to all available observation stations. Results were examined using all selected NTS, EKZ, and PNE events. The collective behavior of the surface wave group velocities for each travel path were then obtained.

Amplitude spectra of the NTS, EKZ, and PNE events under study were examined in the period range between 10 and 50 seconds. The amplitude spectral ratios of the Love wave to Rayleigh wave (LQ/LR) were calculated for each event at all available observation stations. These ratios were then compared among the NTS, EKZ, and PNE events for any indications of geological and/or source-oriented dependence, such as the correlation between the LQ/LR ratio and the event m_b , and any apparent differences in the LQ/LR ratios among the NTS, EKZ, and PNE events, or between the source types, i. e., explosion versus earthquake. Also, the relative excitations of the Love waves for a suite of NTS events were examined.

The average surface wave attenuation coefficients along the travel paths between the NTS and the observation stations and those along the travel paths between the EKZ and the observation stations were estimated by the isotropic-source method. All available events were used. The travel paths between the NTS and the observation stations were divided into two groups: purely oceanic path and mostly continental path. In addition, whenever applicable, the two-station method was employed to calculate the surface wave attenuation coefficients for the travel path between two observation stations. These results were compared with the existing results on the surface wave attenuation.

Finally, the seismic source parameters were estimated for all selected NTS, EKZ, and PNE events based on the observed long-period surface wave spectra. The estimated seismic source parameters included (1) relative strength of the explosive source and double-couple source which modeled the possible tectonic strain release associated with the explosion, (2) focal depth, and (3) the source mechanism of the possible tectonic strain release, i. e., the dip, slip, and strike angle. Layered half-space earth models were obtained for the NTS, the EKZ, and the north Caspian Sea region. This, together with the theoretical source model consisting of point explosive source and point double-couple source, was used to generate theoretical surface wave spectra. The results from the source parameter estimations were then used in a comparative study of NTS, EKZ, and PNE events for possible application to discrimination of earthquakes from explosions.

UNCLASSIFIED

SECURITY CLASSIFICATION OF THIS PAGE(When Data Entered)

ABSTRACT

ACCESSION for	
NTS	Write Section <input checked="" type="checkbox"/>
ROC	Bull Section <input type="checkbox"/>
MANUSCRIPT	<input type="checkbox"/>
BY	
DISTRIBUTION/AVAILABILITY CODES	
JUL 1974 SPECIAL	
A	

Far-field Rayleigh and Love waves observed on a long-period seismic network were studied to characterize presumed underground nuclear explosions. These occurred at the United States Nevada Test Site (NTS), the Russian eastern Kazakh (EKZ) region, and at the site of presumed peaceful nuclear explosions (PNE) in the north Caspian Sea region. The observation stations available for this study included Alaskan Long Period Array (ALPA), Large Aperture Seismic Array (LASA), Norwegian Seismic Array (NORSAR), the Very Long Period Experiment (VLPE) stations, the Seismic Research Observatories (SRO), and the Special Data Collection System (SDCS) stations. The purpose of this study was to determine the seismic source parameters from long-period surface wave data and to investigate the influence of geological and near-source propagation effects on the frequency content of the surface wave signals.

The surface wave group velocities were measured for travel paths from NTS, EKZ, and PNE to all available observation stations. Results were examined using all selected NTS, EKZ, and PNE events. The collective behavior of the surface wave group velocities for each travel path were then obtained.

Amplitude spectra of the NTS, EKZ, and PNE events under study were examined in the period range between 10 and 50 seconds. The amplitude spectral ratios of the Love wave to Rayleigh wave (LQ/LR) were calculated for each event at all available observation stations. These ratios were then compared among the NTS, EKZ, and PNE events for any indications of geological and/or source-oriented dependence, such as the correlation between the LQ/LR ratio and the event m_b , and any apparent differences in the

LQ/LR ratios among the NTS, EKZ, and PNE events, or between the source types, i. e., explosion versus earthquake. Also, the relative excitations of the Love waves for a suite of NTS events were examined.

The average surface wave attenuation coefficients along the travel paths between the NTS and the observation stations and those along the travel paths between the EKZ and the observation stations were estimated by the isotropic-source method. All available events were used. The travel paths between the NTS and the observation stations were divided into two groups: purely oceanic path and mostly continental path. In addition, whenever applicable, the two-station method was employed to calculate the surface wave attenuation coefficients for the travel path between two observation stations. These results were compared with the existing results on the surface wave attenuation.

Finally, the seismic source parameters were estimated for all selected NTS, EKZ, and PNE events based on the observed long-period surface wave spectra. The estimated seismic source parameters included (1) relative strength of the explosive source and double-couple source which modeled the possible tectonic strain release associated with the explosion, (2) focal depth, and (3) the source mechanism of the possible tectonic strain release, i. e., the dip, slip, and strike angle. Layered half-space earth models were obtained for the NTS, the EKZ, and the north Caspian Sea region. This, together with the theoretical source model consisting of point explosive source and point double-couple source, was used to generate theoretical surface wave spectra. The results from the source parameter estimations were then used in a comparative study of NTS, EKZ, and PNE events for possible application to discrimination of earthquakes from explosions.

ACKNOWLEDGMENTS

The author wishes to thank Mrs. Cherylann B. Saunders for preparing the tables, captioning the figures, and typing the manuscript.

Neither the Advanced Research Projects Agency nor the Air Force Technical Applications Center will be responsible for information contained herein which has been supplied by other organizations or contractors, and this document is subject to later revision as may be necessary. The views and conclusions presented are those of the authors and should not be interpreted as necessarily representing the official policies, either expressed or implied, of the Advanced Research Projects Agency, the Air Force Technical Applications Center, or the US Government

TABLE OF CONTENTS

SECTION	TITLE	PAGE
	ABSTRACT	iii
	ACKNOWLEDGMENTS	v
I.	INTRODUCTION	I-1
II.	DATA BASE	II-1
	A. SELECTION OF THE EVENTS	II-1
	B. DATA AVAILABILITY AND QUALITY	II-1
	C. DATA HANDLING	II-8
III.	EXAMINATION OF THE OBSERVED SURFACE WAVES	III-1
	A. TRAVEL PATH GROUP VELOCITIES	III-1
	B. OBSERVED SURFACE WAVE AMPLITUDE SPECTRA	III-31
IV.	TRAVEL PATH ATTENUATION	IV-1
	A. METHODS	IV-2
	B. RESULTS	IV-6
V.	SOURCE PARAMETER ESTIMATES OF THE SELECTED NTS, EKZ, AND PNE EVENTS	V-1
	A. A PROCEDURE OF SOURCE PARAMETER ESTIMATION USING FAR-FIELD SURFACE WAVE DATA	V-3
	B. EARTH MODELS	V-10
	C. SOURCE PARAMETER ESTIMATIONS	V-14
VI.	CONCLUSIONS	VI-1
VII.	REFERENCES	VII-1

LIST OF FIGURES

FIGURE	TITLE	PAGE
III-1	LOCATIONS OF THE OBSERVATION STATIONS AND TRAVEL PATHS ENCOUNTERED TO THE NTS	III-3
III-2	LOCATIONS OF THE OBSERVATION STATIONS AND TRAVEL PATHS ENCOUNTERED TO THE EKZ	III-4
III-3	OBSERVED RAYLEIGH WAVE GROUP VELOCITIES ALONG THE TRAVEL PATHS FROM THE NTS TO OBSERVATION STATIONS	III-5
III-4	OBSERVED LOVE WAVE GROUP VELOCITIES ALONG THE TRAVEL PATHS FROM THE NTS TO OBSERVATION STATIONS	III-12
III-5	OBSERVED RAYLEIGH WAVE GROUP VELOCITIES ALONG THE TRAVEL PATHS FROM THE EKZ TO OBSERVATION STATIONS	III-19
III-6	OBSERVED LOVE WAVE GROUP VELOCITIES ALONG THE TRAVEL PATHS FROM THE EKZ TO OBSERVATION STATIONS	III-24
III-7	OBSERVED RAYLEIGH WAVE GROUP VELOCITIES ALONG THE TRAVEL PATHS FROM THE PNE TO OBSERVATION STATIONS	III-26
III-8	OBSERVED LOVE WAVE GROUP VELOCITIES ALONG THE TRAVEL PATHS FROM THE PNE TO OBSERVATION STATIONS	III-28
III-9	OBSERVED SURFACE WAVE SPECTRA: NTS/926/74	III-32
III-10	OBSERVED SURFACE WAVE SPECTRA: NTS/430/75	III-34
III-11	OBSERVED SURFACE WAVE SPECTRA: NTS/514/75	III-36
III-12	OBSERVED SURFACE WAVE SPECTRA: NT1/603/75	III-41
III-13	OBSERVED SURFACE WAVE SPECTRA: NT2/603/75	III-45

LIST OF FIGURES
(continued)

FIGURE	TITLE	PAGE
III-14	OBSERVED SURFACE WAVE SPECTRA: NTS/619/75	III-47
III-15	OBSERVED SURFACE WAVE SPECTRA: NTS/626/75	III-53
III-16	OBSERVED SURFACE WAVE SPECTRA: NTS/1028/5	III-57
III-17	OBSERVED SURFACE WAVE SPECTRA: NTS/103/76	III-63
III-18	OBSERVED SURFACE WAVE SPECTRA: NT1/204/76	III-65
III-19	OBSERVED SURFACE WAVE SPECTRA: NT2/204/76	III-67
III-20	OBSERVED SURFACE WAVE SPECTRA: NTS/212/76	III-69
III-21	OBSERVED SURFACE WAVE SPECTRA: NTS/309/76	III-73
III-22	OBSERVED SURFACE WAVE SPECTRA: NTS/314/76	III-78
III-23	OBSERVED SURFACE WAVE SPECTRA: NT1/317/76	III-84
III-24	OBSERVED SURFACE WAVE SPECTRA: NT2/317/76	III-89
III-25	OBSERVED SURFACE WAVE SPECTRA: EKZ/723/73	III-94
III-26	OBSERVED SURFACE WAVE SPECTRA: EKZ/1026/3	III-96
III-27	OBSERVED SURFACE WAVE SPECTRA: EKZ/1214/3	III-98
III-28	OBSERVED SURFACE WAVE SPECTRA: EKZ/220/75	III-100

LIST OF FIGURES
(continued)

FIGURE	TITLE	PAGE
III-29	OBSERVED SURFACE WAVE SPECTRA: EKZ/311/75	III-102
III-30	OBSERVED SURFACE WAVE SPECTRA: EKZ/427/75	III-104
III-31	OBSERVED SURFACE WAVE SPECTRA: EKZ/1029/5	III-107
III-32	OBSERVED SURFACE WAVE SPECTRA: EKZ/704/76	III-109
III-33	OBSERVED SURFACE WAVE SPECTRA: PNE/1222/1	III-113
III-34	OBSERVED SURFACE WAVE SPECTRA: PNE/820/72	III-115
III-35	OBSERVED SURFACE WAVE SPECTRA: PNE/729/76	III-117
IV-1	AVERAGE RAYLEIGH WAVE AMPLITUDE ATTENUATION FOR TRAVEL PATHS IN THE PACIFIC OCEAN	IV-9
IV-2	AVERAGE RAYLEIGH WAVE AMPLITUDE ATTENUATION FOR TRAVEL PATHS FROM THE NTS TO OBSERVATION STATIONS	IV-10
IV-3	RAYLEIGH WAVE AMPLITUDE ATTENUATION FOR TRAVEL PATHS IN THE ATLANTIC OCEAN	IV-14
IV-4	AVERAGE RAYLEIGH WAVE AMPLITUDE ATTENUATION FOR TRAVEL PATH FROM THE EKZ TO OBSERVATION STATIONS	IV-15
V-1	SCHEMATIC DIAGRAM SHOWING A PROCEDURE TO OBTAIN THE SEISMIC SOURCE PARAMETER ESTIMATION USING FAR-FIELD SURFACE WAVE DATA	V-4
V-2	GEOMETRY OF THE DOUBLE-COUPLE SOURCE WHICH MODELS THE EXPLOSION-ASSOCIATED TECTONIC STRAIN RELEASE	V-7

LIST OF FIGURES
(continued)

FIGURE	TITLE	PAGE
V-3	LOCATIONS OF THE SELECTED EKZ AND PNE EVENTS, AND LOCAL GEOLOGY	V-13
V-4	CRUSTAL CROSS SECTION ALONG LINE XIV-XIV'	V-15
V-5	CRUSTAL CROSS SECTION ALONG LINE C-C'	V-16
V-6	RESULTS FROM AMPLITUDE SPECTRAL FITTING: NTS/926/74	V-25
V-7	RESULTS FROM AMPLITUDE SPECTRAL FITTING: NTS/430/75	V-27
V-8	RESULTS FROM AMPLITUDE SPECTRAL FITTING: NTS/514/75	V-29
V-9	RESULTS FROM AMPLITUDE SPECTRAL FITTING: NT1/603/75	V-32
V-10	RESULTS FROM AMPLITUDE SPECTRAL FITTING: NT2/603/75	V-34
V-11	RESULTS FROM AMPLITUDE SPECTRAL FITTING: NTS/619/75	V-36
V-12	RESULTS FROM AMPLITUDE SPECTRAL FITTING: NTS/626/75	V-39
V-13	RESULTS FROM AMPLITUDE SPECTRAL FITTING: NTS/1028/5	V-41
V-14	RESULTS FROM AMPLITUDE SPECTRAL FITTING: NTS/103/76	V-44
V-15	RESULTS FROM AMPLITUDE SPECTRAL FITTING: NTS/212/76	V-46
V-16	RESULTS FROM AMPLITUDE SPECTRAL FITTING: NTS/309/76	V-48
V-17	RESULTS FROM AMPLITUDE SPECTRAL FITTING: NTS/314/76	V-51
V-18	RESULTS FROM AMPLITUDE SPECTRAL FITTING: NT1/317/76	V-54

LIST OF FIGURES
(continued)

FIGURE	TITLE	PAGE
V-19	RESULTS FROM AMPLITUDE SPECTRAL FITTING: NT2/317/76	V-57
V-20	RESULTS FROM AMPLITUDE SPECTRAL FITTING: NT1/204/76	V-60
V-21	RESULTS FROM AMPLITUDE SPECTRAL FITTING: NT2/204/76	V-62
V-22	SURFACE WAVE RADIATION PATTERNS FOR EVENT NTS/1028/5	V-67
V-23	RESULTS FROM AMPLITUDE SPECTRAL FITTING: EKZ/723/73	V-88
V-24	RESULTS FROM AMPLITUDE SPECTRAL FITTING: EKZ/1026/3	V-90
V-25	RESULTS FROM AMPLITUDE SPECTRAL FITTING: EKZ/1214/3	V-92
V-26	RESULTS FROM AMPLITUDE SPECTRAL FITTING: EKZ/220/75	V-94
V-27	RESULTS FROM AMPLITUDE SPECTRAL FITTING: EKZ/311/75	V-96
V-28	RESULTS FROM AMPLITUDE SPECTRAL FITTING: EKZ/427/75	V-98
V-29	RESULTS FROM AMPLITUDE SPECTRAL FITTING: EKZ/1029/5	V-101
V-30	RESULTS FROM AMPLITUDE SPECTRAL FITTING: EKZ/704/76	V-103
V-31	SURFACE WAVE RADIATION PATTERNS FOR EVENT EKZ/704/76	V-106
V-32	RESULTS FROM AMPLITUDE SPECTRAL FITTING: PNE/1222/1	V-127
V-33	RESULTS FROM AMPLITUDE SPECTRAL FITTING: PNE/820/74	V-129

LIST OF FIGURES
(continued)

FIGURE	TITLE	PAGE
V-34	RESULTS FROM AMPLITUDE SPECTRAL FITTING: PNE/729/76	V-131
V-35	SURFACE WAVE RADIATION PATTERNS FOR EVENT PNE/729/76	V-133
V-36	TYPICAL RESIDUAL VARIATION WITH RESPECT TO THE TESTED F VALUES FOR THE SELECTED NTS, EKZ, AND PNE EVENTS	V-153
V-37	ESTIMATED F VALUES OF THE SELECTED NTS, EKZ, AND PNE EVENTS VERSUS THE EVENT m_b	V-154
V-38	MOMENT VERSUS m_b PLOT	V-155

LIST OF TABLES

TABLE	TITLE	PAGE
I-1	SOURCE PARAMETERS FOR THREE EARTH- QUAKES FROM DIFFERENT METHODS	I-3
II-1	LIST OF THE SELECTED EVENTS AND THEIR DATA AVAILABILITY	II-3
II-2	DESCRIPTION OF OBSERVATION STATIONS	II-7
II-3	STATION AZIMUTHAL ANGLES AND EPICENTER DISTANCES FROM THE SELECTED EVENTS	II-9
III-1	TYPICAL LQ/LR SPECTRAL RATIOS FOR THE SELECTED NTS EVENTS	III-123
III-2	TYPICAL LQ/LR SPECTRAL RATIOS FOR THE SELECTED EKZ EVENTS	III-126
III-3	TYPICAL LQ/LR SPECTRAL RATIOS FOR THE SELECTED PNE EVENTS	III-127
III-4	LOVE WAVE AMPLITUDE RATIOS OF THE SELECTED NTS EVENTS: REFERENCE EVENT NTS/619/75 $m_b = 6.1$	III-130
III-5	ESTIMATED SEISMIC MOMENTS OF THE TECTONIC STRAIN RELEASES ASSOCIATED WITH THE SELECTED NTS EVENTS	III-132
V-1	STRUCTURE PROFILE OF THE NTS EARTH MODEL (37°N, 116°W)	V-11
V-2	SURFACE WAVE DISPERSION FOR THE NTS EARTH MODEL (37°N, 116°W)	V-12
V-3	STRUCTURE PROFILE OF THE EKZ EARTH MODEL (BALKHASH-CHINGIZ FOLDBELT)	V-17
V-4	SURFACE WAVE DISPERSION FOR THE EKZ EARTH MODEL (BELKHASH-CHINGIZ FOLDBELT)	V-18
V-5	STRUCTURE PROFILE OF THE PNE EARTH MODEL (NORTH CASPIAN BASIN)	V-19
V-6	SURFACE WAVE DISPERSION FOR THE PNE EARTH MODEL (NORTH CASPIAN BASIN)	V-20

LIST OF TABLES
(continued)

TABLE	TITLE	PAGE
V-7	ESTIMATIONS OF SOURCE PARAMETERS OBTAINED BY AMPLITUDE SPECTRAL FITTING BASED ON THE MINIMUM-RESIDUAL CRITERION: SELECTED NTS EVENTS	V-21
V-8	ESTIMATIONS OF SOURCE PARAMETERS OBTAINED BY AMPLITUDE SPECTRAL FITTING BASED ON THE RESIDUAL DISTRIBUTIONS: SELECTED NTS EVENTS	V-65
V-9	ESTIMATIONS OF SOURCE PARAMETERS OBTAINED BY AMPLITUDE SPECTRAL FITTING BASED ON THE MINIMUM-RESIDUAL CRITERION: SELECTED EKZ EVENTS	V-86
V-10	ESTIMATIONS OF SOURCE PARAMETERS OBTAINED BY AMPLITUDE SPECTRAL FITTING BASED ON THE RESIDUAL DISTRIBUTIONS: SELECTED EKZ EVENTS	V-87
V-11	ESTIMATIONS OF SOURCE PARAMETERS OBTAINED BY AMPLITUDE SPECTRAL FITTING BASED ON THE MINIMUM-RESIDUAL CRITERION: SELECTED PNE EVENTS	V-125
V-12	ESTIMATIONS OF SOURCE PARAMETERS OBTAINED BY AMPLITUDE SPECTRAL FITTING BASED ON THE RESIDUAL DISTRIBUTIONS: SELECTED PNE EVENTS	V-126

SECTION I

INTRODUCTION

This report presents the results from a continuing effort at Texas Instruments Incorporated to obtain the seismic source parameter estimates and to investigate the travel path effects using long-period teleseismic surface wave data. Previous work (Tsai, 1972a, 1972b; Tsai and Shen, 1972; Turnbull, et al., 1973, 1974, 1975; Sun, 1976) has been mainly concerned with methodology (such as the development of multi-period multi-site amplitude spectral fitting process), study of the theoretical surface wave spectra and radiation patterns, and verification and application of the methods to synthetic events and earthquakes. All these studies have been aimed toward the better understanding and utilization of the long-period teleseismic surface waves for source characterization and possibly for source discrimination. Previously developed methods of narrowband filtering and amplitude spectral fitting have been proved to be efficient and quite satisfactory for the extraction of the demultipathed seismic surface wave spectra and the determination of seismic source parameters from the far-field seismic surface waves of earthquakes. In this report, we apply the same techniques, making necessary modifications, to underground nuclear explosions for similar purposes, namely the determination of the seismic source parameters from long-period seismic surface wave data and investigation of the influence of the geological and near-source propagation effects on the frequency content of these surface waves.

Since Tsai's method was established, many seismic events have been analyzed by several authors using this method. An error analysis was attempted during their application of this technique. However, their endeavor was defeated by many unsolvable difficulties. First, there was no standard solution which they could compare their result with, so no definite

error could be estimated. Secondly, errors for a system depend upon basic assumptions, the procedures used, the technique of computation, and analyst's judgments. There are some high degree of uncertainties such as the earth model assumptions, travel path attenuations, data processing etc. Most of these uncertainties are complexly interrelated. This causes the different type of errors to be interlocked in a way difficult to analyze. Therefore, it is not now known by us how to calculate individual error of each step of processing and to accurately estimate confidence limits of our resultant source mechanism solutions.

Even though the extent of the errors could not be determined, the authors still thought this method reliable after comparing their results with those obtained by other means.

Battis and Hill (1977) used this method to analyze the Pocatello Valley earthquake. The results were similar to the composite fault based on a microearthquake study of the source region by Smith and Shar (1974), and also agreed closely with that obtained by Arabasz, et al. (1975) and Rodgers (1977, from T. C. Bache's report). Battis and Hill (1977) also calculated the fault plane by this method for the main shock and the foreshock of Yellowstone earthquake. Their solutions are nearly identical to a composite fault plane constructed for the same earthquake and its aftershocks by the U. S. G. S. based on data from a local array (C. Weaver, 1976, personal communication). Turnbull, Sun, and Battis (1975) analyzed a Bear Valley event. The mechanism of that event was reasonably close to the solution estimated by other means. After using this method to analyze seven Eurasian events, Turnbull, Sun, and Black (1974) found that depth estimates can be obtained which closely agree with those determined from bodywave depth phases (see Table I-1).

Previous studies on the determination of source parameters of underground nuclear explosions using far-field surface waves have been reported by several authors for various purposes (Toksöz, et al., 1964, 1965;

TABLE I-1
SOURCE PARAMETERS FOR THREE EARTHQUAKES FROM DIFFERENT METHODS

Event I. D.	Source of Data	Strike ϕ_0	Dip δ_0	Slip λ_0	M_0 (dyne-cm)	Depth h km
Pocatello Earthquake	Arabasz, et al. (1975), Geology	N10E	--	-90	1×10^{25}	5.0
	Battis and Hill (1977), Surface Wave	N15E	60	-90	7.2×10^{24}	5.0
	Rodgers (1977), Bodywave	N13E	45	-90	-	-
Yellowstone Earthquake	Battis and Hill (1977), Surface Wave	N130W	40	-90	7.7×10^{24}	4.0
	Weaver (1976), Bodywave	N135W	40	-83	-	-
Bear Valley Earthquake	Turnbull, et al. (1975), Surface Wave Far-Field	N55W	90	0	0.74×10^{22}	11.5
	Turnbull, et al. (1974), Near-Field	N40W	75	-	1.2×10^{23}	10.5

Lambert, et al., 1972; Mitchell, 1975). However, there are several common features in all of these studies: (1) they analyzed a small number of events from the United States Nevada Test Site, typically two or three explosions, (2) they used radiation pattern fitting requiring many well distributed observation stations, (3) they assumed that explosions took place at the surface and that the source mechanism of the explosion-associated tectonic strain release was identical to that of the local earthquakes in the region, and (4) hence, to obtain the best fit between the observed and theoretical radiation patterns, they only estimated two parameters - the strike angle, adjusting it around the vicinity of the strike direction of local earthquakes; and the relative strength of the explosion and explosion-associated tectonic strain release i. e., the so-called F value. In this report, we analyze a total of twenty-seven underground nuclear explosions from three different regions, the United States Nevada Test Site (NTS), the Russian eastern Kazakh (EKZ), and the north Caspian Sea area. Also, we estimate all six source parameters of a given underground explosion, namely the F value, focal depth, dip angle, slip angle, strike angle, and seismic moment of the explosion-associated tectonic strain release.

The following sections present the results of research on long-period teleseismic surface waves of twenty-seven NTS, EKZ, and PNE events. In Section II, we discuss the data base used in this study, such as data availability, data quality, and the data reduction procedure. The results from the examination of the observed surface waves are presented in Section III, where the surface wave group velocities for various travel paths, the observed amplitude spectra, and spectral ratios are given and discussed. Section IV briefly describes the methods which are used for the estimation of the surface wave travel path attenuations and shows the attenuation coefficients along various travel paths obtained from this study. The source parameter estimations of the selected explosions are detailed in Section V. Finally, in Section VI, a summary of the results given in the previous sections is presented.

SECTION II

DATA BASE

A. SELECTION OF THE EVENTS

In the selection of the events to be analyzed in this study, we tried to include as many recent NTS, EKZ, and PNE events as possible. The NTS and the EKZ events are underground nuclear explosions from the United States Nevada Test Site and from the Russian eastern Kazakh, respectively, while the PNE events are peaceful nuclear explosions in the Russian Eurasian continent some distance away from the normal Russian test sites. A list of the events was obtained for the NTS and EKZ events by means of a chronological search (starting from 1976 and progressing backward into 1975, 1974, and so on) through the NORSAR (Norwegian Seismic Array) bulletin, and the PDE (Preliminary Determination of Epicenters) bulletin. For the PNE events, the list was obtained mainly from the list of the Eurasian PNE events given by Nordyke (1974). The preliminary list of events consisted of twenty-four NTS events (ten in 1976, eleven in 1975, and three in 1974), twenty-five EKZ events (five in 1976, seven in 1975, seven in 1974, and six in 1973) and ten PNE events (one in 1976, four in 1973, three in 1972, and two in 1971). Based on this preliminary list, the availability of the long-period teleseismic surface wave data with good quality was examined and the final list of the selected NTS, EKZ, and PNE events, as given in Table II-1, was obtained.

B. DATA AVAILABILITY AND QUALITY

In the work statement of this task, we were requested to use the surface wave data from the observation stations which included the Very Long Period Experiment (VLPE) Stations, the Seismic Research Observatories

(SRO), Special Data Collection System (SDCS) stations, Large Aperture Seismic Array (LASA), Norwegian Seismic Array (NORSAR), Iranian Long Period Array (ILPA), and Korean Seismic Research Station (KSRS). The intention of including as many existing long-period recording stations as possible is understandable - it provides better azimuthal coverage and better data availability. Unfortunately, the ILPA data were not available, since ILPA started operation on 1 May 1976 and almost all of the events in our preliminary list occurred before that time; while the KSRS data were not available because no software was available for editing the KSRS long-period field tapes. To make up for the loss of data from the ILPA and the KSRS, we included the Alaskan Long Period Array (ALPA).

After checking the availability of the surface wave recordings and examining the results of the processed surface wave signals from all available recordings, the final list of the selected NTS, EKZ, and PNE events was obtained as shown in Table II-1. Table II-1 gives the event name, date, origin time, location, and PDE m_b , together with the availability of good quality surface wave recordings indicated by the letter 'B', 'R', or 'L' under the 'Station I. D.' heading. Stations are identified by the station number (1, 2, ...) or letter (A, L, and N). 'B' means that both Rayleigh and Love wave recordings are useable, 'R' means that only the Rayleigh wave recording is useable, and 'L' means that only the Love wave recording is useable. The descriptions of the available observation stations are given in Table II-2, including station name, location, and identification number or letter. It can be seen that the final list of the selected events consists of twenty-seven events (sixteen NTS events, eight EKZ events, and three PNE events) instead of fifty-nine events in the preliminary list. The loss of the events from the preliminary list was mainly caused by (1) bad field tapes which could not be edited for the desired events, (2) bad edited traces which contained no apparent desired surface wave signals due to the noise or contained uncorrectable spikes in the signal gate, and (3) mixed events. In addition, we

TABLE II-1
LIST OF THE SELECTED EVENTS AND THEIR DATA AVAILABILITY
(PAGE 1 OF 4)

(a) NTS Events

Event I. D. Date	Location		Origin Time	m _b	Station I. D.																						
	Lat. °N	Lon. °W			VLPE										SRO			Array			SDCS						
					1	2	4	5	6	7	8	9	10	11	1	6	7	12	A	L	N	1	2	3	4	5	
NTS/926/74 09/26/74	37.1	116.1	15.05.00	5.6																							
NTS/430/75 04/30/75	37.2	116.3	15.00.01	5.2					B					R					B	B	B						
NTS/514/75 05/14/75	38.2	115.6	14.00.00	6.0					B			B	R						B	R	R	B				B	
NT1/603/75 06/03/75	37.0	116.0	14.20.00	5.9					B	B									B	B	R	B				B	
NT2/603/75 06/03/75	37.0	116.0	14.40.00	5.7					B	B									B	B	B						
NTS/619/75 06/19/75	37.0	116.0	13.00.00	6.1					B	B	B								B	B	B	R				B	
NTS/626/75 06/26/75	37.0	116.0	12.30.00	6.2					B					R					B	R		B	B			B	
NTS/1028/5 10/28/75	38.0	116.0	14.30.06	6.4					R	B	B	B	R	R					B		R	B	B			B	

B: Both Rayleigh and Love Wave R: Only Rayleigh Wave L: Only Love Wave

TABLE II-1
LIST OF THE SELECTED EVENTS AND THEIR DATA AVAILABILITY
(PAGE 2 OF 4)

(a) NTS Events

Event I. D. Date	Location		Origin Time	m _b	Station I. D.																																																																																																																																																																																																																																																																																																																																																																																																																																																																																																																																																																																																																																																																																																																																																																																																																																																																																																																																																																																																																																																																																																																																																																																																																																																																																																																																																																																																																																																																																																																																																																																																																																												
	Lat. ON	Lon. OW			VLPE												SRO			Array			SDCS																																																																																																																																																																																																																																																																																																																																																																																																																																																																																																																																																																																																																																																																																																																																																																																																																																																																																																																																																																																																																																																																																																																																																																																																																																																																																																																																																																																																																																																																																																																																																																																																																										
					1	2	4	5	6	7	8	9	10	11	1	6	7	12	A	L	N	1	2	3	4	5																																																																																																																																																																																																																																																																																																																																																																																																																																																																																																																																																																																																																																																																																																																																																																																																																																																																																																																																																																																																																																																																																																																																																																																																																																																																																																																																																																																																																																																																																																																																																																																																																							
NTS/103/76 01/03/76	38.0	116.0	19.15.05	6.2	B					R									B																																																																																																																																																																																																																																																																																																																																																																																																																																																																																																																																																																																																																																																																																																																																																																																																																																																																																																																																																																																																																																																																																																																																																																																																																																																																																																																																																																																																																																																																																																																																																																																																																														

B: Both Rayleigh and Love Wave R: Only Rayleigh Wave L: Only Love Wave

TABLE II-1
LIST OF THE SELECTED EVENTS AND THEIR DATA AVAILABILITY
(PAGE 3 OF 4)

(b) EKZ Events

Event I. D. Date	Location		Origin Time	m _b	Station I. D.																						
	Lat. °N	Lon. °E			VLPE										SRO			Array	SDCS								
					1	2	4	5	6	7	8	9	10	11	1	6	7		12	A	L	N	1	2	3	4	5
EKZ/723/73 07/23/73	50.0	78.9	01.22.58	6.3																							
EKZ/1026/3 10/26/73	49.8	78.2	04.26.58	5.3																							
EKZ/1214/3 12/14/73	50.0	79.0	07.46.57	6.0																							
EKZ/220/75 02/20/75	49.8	78.1	05.32.58	5.7																							
EKZ/311/75 03/11/75	49.8	78.3	05.42.58	5.4																							
EKZ/427/75 04/27/75	50.0	79.0	05.36.57	5.6										R	R	R											
EKZ/1029/5 10/29/75	50.0	79.0	04.47.00	5.8																							
EKZ/704/76 07/04/76	49.0	80.0	02.56.50	5.8																							

B: Both Rayleigh and Love Wave R: Only Rayleigh Wave L: Only Love Wave

TABLE II-1
LIST OF THE SELECTED EVENTS AND THEIR DATA AVAILABILITY
(PAGE 4 OF 4)

(c) PNE Events

Event I. D. Date	Location		Origin Time	m _b	Station I. D.																						
	Lat. °N	Lon. °E			VLPE										SRO			Array			SDCS						
					1	2	4	5	6	7	8	9	10	11	1	6	7	12	A	L	N	1	2	3	4	5	
PNE/1222/1 12/22/71	47.9	48.2	06.59.56	6.0																							
PNE/820/72 08/20/72	49.5	48.2	02.59.58	5.7																							
PNE/729/76 07/29/76	48.0	47.0	05.00.00	5.9*															R		B	R					

B: Both Rayleigh and Love Wave R: Only Rayleigh Wave L: Only Love Wave

* NEIS (National Earthquake Information Service) m_b

TABLE II-2
DESCRIPTION OF OBSERVATION STATIONS

	Station I. D.		Station Location		
	#	Name	City and Country	Lat. °N	Lon. °E
VLPE Stations	1	CTA	Charters Towers, Australia	-20.1	146.3
	2	CHG	Chiang Mai, Thailand	18.8	99.0
	4	TLO	Toledo, Spain	39.0	-4.0
	5	EIL	Eilat, Israel	29.6	35.0
	6	KON	Kongsberg, Norway	59.7	9.6
	7	OGD	Ogdensburg, New Jersey	41.1	-74.6
	8	KIP	Kipapa, Hawaii	21.4	-158.0
	9	ALQ	Albuquerque, New Mexico	34.9	-106.5
	10	ZLP	La Paz, Bolivia	-16.5	-68.1
	11	MAT	Matsushiro, Japan	36.5	138.2
SRO	1	ANMO	Albuquerque, New Mexico	34.9	-106.5
	6	GUMO	Guam, Marianas Island	13.6	144.9
	7	MAIO	Mashhad, Iran	36.3	59.5
	12	TATO	Taipei, Taiwan	25.0	121.5
Array	A	ALPA	Alaska	65.2	-147.7
	L	LASA	Montana	46.7	-106.2
	N	NORSAR	Norway	60.8	10.9
SDCS Stations	1	FN-WV	Franklin, N. Virginia	38.6	-79.5
	2	HN-ME	Houlton, Maine	46.2	-68.0
	3	RK-ON	Red Lake, Ontario	50.8	-93.7
	4	WH2YK	White Horse, Yukon	60.7	-135.0
	5	CPSO	McMinnville, Tennessee	35.6	85.6

discarded those events which had less than three good edited surface wave traces at two observation stations. This last condition for rejecting an event was based on the previous result that the source parameters of a given seismic event could be satisfactorily estimated with good quality surface wave recordings at two observation stations in two consecutive quadrants (Turnbull, et al., 1973). From the data availability indicated in Table II-1, it is clear that the NTS events have fairly good station coverage while for the EKZ and the PNE events we mostly have to rely on the array stations.

The selected NTS events took place at five different locations; the EKZ events at three different locations. Table II-3 presents the station azimuthal angles with respect to those event locations and the epicenter distances from those event locations to each observation station. In general, the station coverage for the selected events is thought to be satisfactory in terms of station azimuthal distribution and epicenter distances for the purposes of this study.

C. DATA HANDLING

The observed surface wave data needed in the analysis of this study are the amplitude spectra from ten to fifty seconds for the following three purposes:

- Examination of the surface wave spectral contents and spectral ratios,
- Estimation of the surface wave travel path attenuation, and
- Estimation of the seismic source parameters.

In order to obtain the desired surface wave amplitude spectra, the field tapes containing the surface wave recordings for the selected NTS, EKZ, and PNE events at all available observation stations were processed as follows:

TABLE II-3
STATION AZIMUTHAL ANGLES AND EPICENTER DISTANCES FROM THE SELECTED EVENTS
(PAGE 1 OF 6)

(a) NTS Events

Station I.D.		NTS-1 *		NTS-2		NTS-3		NTS-4		NTS-5	
#	Name	AZ	Δ	AZ	Δ	AZ	Δ	AZ	Δ	AZ	Δ
1	CTA	-101.4	108.1	-100.8	108.8	-101.7	107.9	-101.8	107.7	-101.1	108.4
2	CHG	-36.5	114.5	-35.6	115.0	-36.8	115.3	-37.0	115.0	-36.1	114.5
4	TLO	46.2	80.4	46.8	79.9	46.1	81.1	46.0	81.2	46.5	80.1
5	EIL	26.2	107.4	27.1	107.0	26.4	108.3	26.1	108.2	26.5	107.0
6	KON	25.5	72.7	25.9	72.4	25.4	73.6	25.3	73.5	25.7	72.4
7	OGD	71.2	31.8	71.4	31.1	69.7	32.1	70.0	32.3	71.6	31.4
8	KIP	-102.4	39.7	-101.6	40.5	-101.2	39.5	-101.7	39.3	-102.3	40.0
9	ALQ	108.8	8.3	111.3	7.5	102.0	8.0	102.9	8.3	111.1	8.0

AZ = Station Azimuth at Source (+ for NE)

Δ = Distance between Station and Source in degrees

* = NTS Event Location

TABLE II-3
STATION AZIMUTHAL ANGLES AND EPICENTER DISTANCES FROM THE SELECTED EVENTS
(PAGE 2 OF 6)

(a) NTS Events (continued)

	Station I. D.	NTS-1 *		NTS-2		NTS-3		NTS-4		NTS-5	
		38.0W	116.0W	38.0N	115.0W	37.0N	116.0W	37.2N	116.3W	38.2N	115.6W
#	Name	AZ	Δ	AZ	Δ	AZ	Δ	AZ	Δ	AZ	Δ
10	ZLP	130.9	70.5	131.7	69.9	130.6	69.9	130.4	70.2	131.2	70.4
11	MAT	-52.0	78.9	-51.5	79.5	-51.9	79.5	-52.0	79.2	-51.8	79.0
1	ANMO	108.8	8.3	111.3	7.5	102.0	8.0	102.9	8.3	111.1	8.0
6	GUMO	-73.6	88.7	-73.0	89.5	-73.6	89.0	-73.8	88.7	-73.4	89.0
7	MAIO	3.8	105.8	4.6	105.7	3.8	106.8	3.5	106.6	4.1	105.5
12	TATO	-50.3	97.2	-49.7	97.8	-50.4	97.8	-50.6	97.5	-50.0	97.3
A	ALPA	-24.0	32.9	-24.5	33.2	-23.4	33.8	-23.4	33.6	-24.3	32.9
L	LASA	36.6	11.3	34.0	10.8	33.9	12.1	35.1	12.1	36.2	10.9

AZ = Station Azimuth at Source (+ for NE)

Δ = Distance between Station and Source in degrees

* = NTS Event Location

TABLE II-3
STATION AZIMUTHAL ANGLES AND EPICENTER DISTANCES FROM THE SELECTED EVENTS
(PAGE 3 OF 6)

(a) NTS Events (continued)

#	Station I. D. Name	NTS-1 38.0N 116.0W *		NTS-2 38.0N 115.0W		NTS-3 37.0N 116.0W		NTS-4 37.2N 116.3W		NTS-5 38.2N 115.6W	
		AZ	Δ	AZ	Δ	AZ	Δ	AZ	Δ	AZ	Δ
N	NORSAR	24.2	72.3	24.6	71.9	24.1	73.2	24.0	73.1	24.4	71.9
1	FN-WV	77.4	28.5	77.7	27.7	75.6	28.7	75.9	28.9	77.9	28.1
2	HN-ME	61.2	36.0	61.3	35.3	60.1	36.5	60.3	36.6	61.5	35.7
3	RK-ON	43.8	20.4	42.8	19.8	42.0	21.1	42.6	21.1	43.8	20.0
4	WH2YK	-21.6	25.6	-22.5	25.9	-20.9	26.6	-20.8	26.3	-22.2	25.6
5	CPSO	86.2	24.4	86.7	23.6	84.0	24.5	84.3	24.7	86.9	24.1

SDCS Stations

AZ = Station Azimuth at Source (+ for NE)
 Δ = Distance between Station and Source in degrees
 * = NTS Event Location

TABLE II-3
STATION AZIMUTHAL ANGLES AND EPICENTER DISTANCES FROM THE SELECTED EVENTS
(PAGE 4 OF 6)

(b) EKZ Events

Station I.D.		EKZ-1 49.0N 80.0E		EKZ-2 49.8N 78.2E		EKZ-3 50.0N 79.0E	
#	Name	AZ	Δ	AZ	Δ	AZ	Δ
1	CTA	120.5	90.5	119.1	92.0	119.7	91.6
2	CHG	146.3	33.8	144.2	35.2	145.6	35.0
4	TLO	-64.7	57.7	-66.2	56.3	-65.9	56.7
5	EIL	-102.7	39.2	-105.4	38.2	-104.9	38.8
6	KON	-47.4	40.4	-48.5	39.0	-48.5	39.3
7	OGD	-18.9	87.4	-20.2	86.2	-19.6	86.2
8	KIP	52.2	92.9	50.7	93.3	51.3	92.7
9	ALQ	5.3	96.0	3.8	95.3	4.5	95.1

AZ = Station Azimuth at Source (+ for NE)
 Δ = Distance between Station and Source in degrees
 * = EKZ Event Location

TABLE II-3
STATION AZIMUTHAL ANGLES AND EPICENTER DISTANCES FROM THE SELECTED EVENTS
(PAGE 5 OF 6)

(b) EKZ Events (continued)

	Station I. D.		EKZ-1 *		EKZ-2		EKZ-3	
	#	Name	49.0N	80.0E	49.8N	78.2E	50.0N	79.0E
VLPE	10	ZLP	AZ	Δ	AZ	Δ	AZ	Δ
			-49.5	138.5	-51.0	137.1	-49.9	137.3
SRO	11	MAT	84.0	43.4	83.6	44.5	84.3	44.0
	1	ANMO	5.3	96.0	3.8	95.3	4.5	95.1
Array	7	MAIO	-122.6	19.6	-127.8	19.1	-126.7	19.7
	A	ALPA	21.0	60.1	20.4	59.8	20.8	59.4
	L	LASA	4.3	84.3	3.0	83.6	3.6	83.4
	N	NORSAR	-45.9	39.5	-47.0	38.1	-47.0	38.3

AZ = Station Azimuth at Source (+ for NE)

Δ = Distance between Station and Source in degrees

* = EKZ Event Location

TABLE II-3
STATION AZIMUTHAL ANGLES AND EPICENTER DISTANCES FROM THE SELECTED EVENTS
(PAGE 6 OF 6)

(c) PNE Events

Station I. D.	PNE-1 *		PNE-2		PNE-3		
	47.9N	48.2E	49.5N	48.2E	48.0N	47.0E	
#	Name	AZ	Δ	AZ	Δ	AZ	Δ
A	ALPA	7.2	66.4	7.3	64.8	-	-
L	LASA	-17.4	83.0	-17.4	81.5	-18.2	82.7
N	NORSAR	-44.8	24.9	-47.3	23.8	-44.6	24.2
1	ANMO	-	-	-	-	-21.5	93.9
7	MAIO	-	-	-	-	137.1	14.9
12	TATO	-	-	-	-	83.2	61.6

AZ = Station Azimuth at Source (+ for NE)

Δ = Distance between Station and Source in degrees

* = PNE Event Location

- The desired surface wave recordings on the field tape are edited to yield the edited event signal which usually consists of $3 \cdot N$ signal traces, where N is the number of recording sites in a station, i. e., $N=1$ for a single-site station. In general, the $3 \cdot N$ signal traces in the edited event signal are the vertical and two horizontal (oriented in N-S and E-W direction) recordings. The vertical Rayleigh wave signal is obtained from the vertical recording while the radial Rayleigh wave and transverse Love wave signal are obtained by properly rotating the two horizontal recordings. For the array stations, in addition to the rotation of horizontal recordings, the edited event signal is beamformed.
- The edited event signal with proper rotation of its traces (and beamforming for array stations) is reformatted to form the event files on 7-track tape to drive the processing programs in the PDP-15/50 computer.
- For each event signal in the event files, each component trace (Rayleigh or Love wave) is analyzed for evidence of multipathing by applying a series of narrowband filters (as discussed by Turnbull, et al., 1974; Sun and Shaub, 1977). At each period, group velocities are determined for each multipath, and then compared to the standard group velocity curves for the type of travel path encountered (see example in Sun, 1976). Estimating the correct multipath from this comparison, the amplitude spectra are obtained. These raw observed amplitude spectra are then corrected for the station instrument response to yield the desired observed amplitude spectra for the estimation of the surface wave travel path attenuation. These raw observed amplitude spectra with appropriate instrument

response correction are further corrected for the geometrical spreading and the travel path attenuation to yield the corrected observed amplitude spectra for the examination of the surface wave spectra and the estimation of the seismic source parameters.

In the above described surface wave data reduction procedure, the first two steps and the spectral correction in the third step are carried out by batch processing on the IBM 360/44 computer. The third step involving the narrowband filtering is done via the Interactive Seismic Processing System (ISPS) developed by Texas Instruments using PDP-15/50 interactive graphics.

SECTION III

EXAMINATION OF THE OBSERVED SURFACE WAVES

Before applying the amplitude spectral fitting technique to selected NTS, EKZ, and PNE events, the observed surface waves from these events will be first examined in terms of (1) observed fundamental mode group velocities and spectra, (2) amplitude spectra and spectral ratios between periods of 10 to 50 seconds, and (3) average surface wave attenuation coefficients estimated from observed amplitude spectra along various travel paths. The reasons for this examination, aside from fulfilling the work statement of this task, are twofold: (1) the results might be used to guide future processing and analysis of the surface waves of other NTS, EKZ, and PNE events, and (2) the results might yield a better geophysical understanding of the excitation and propagation of seismic surface waves from the NTS, EKZ, and PNE events. The results of the group velocity and amplitude spectral analyses are presented and discussed in this section. The determination of the average surface wave travel path attenuation will be given in Section IV.

A. TRAVEL PATH GROUP VELOCITIES

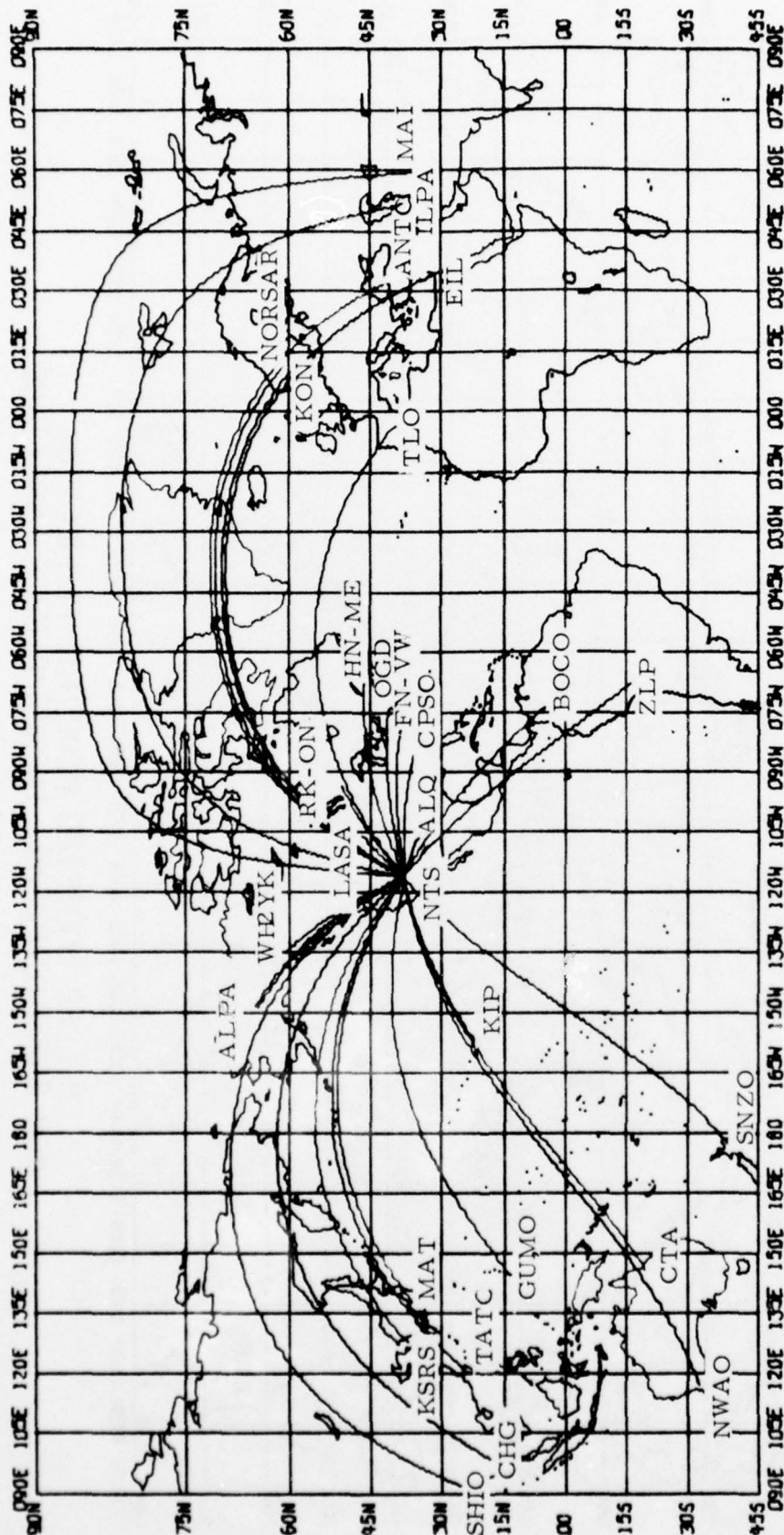
In narrowband filtering to demultipath surface wave spectra of selected NTS, EKZ, and PNE events, group velocities were determined for the fundamental mode great circle path arrival. This was done for all observation stations and was repeated for all selected NTS, EKZ, and PNE events. Therefore, for each event-station path (e. g., from the NTS to ALPA), N group velocity measurements were determined from N available events from the same vicinity. Theoretically, these N sets of group velocities for the same event-station path should be identical since the surface wave

group velocities for a given mode depend only on the medium through which the surface wave propagates, regardless of different seismic sources. However, in the real world, there may exist variations among these N sets of group velocities caused by some natural (known or unknown) or man-made factors. By examining these N sets of group velocities, some collective behavior of the group velocities along a given event-station path can be obtained and might be used for the calibration of this particular event-station path for future use.

Figures III-1 and III-2 show the geographical locations of the available observation stations in relation to the NTS and the EKZ events, together with the event-station travel paths. Except for the travel paths from NTS to the observation stations in the Pacific Ocean which are entirely oceanic, the travel paths are either entirely continental or mixed. Figures III-3 and III-4 present the Rayleigh and Love wave group velocities, respectively, for the travel paths from NTS to the observation stations, using all selected NTS events. Similar results are shown in Figures III-5, III-6, III-7, and III-8 for the travel paths from EKZ and PNE to the observation stations. In these figures, N is the number of events used in forming the average group velocities for the indicated travel path, the vertical bar at each given period indicates the range of the variation in the group velocities obtained from these N events, and the solid dot is the mid-point of this range. Two solid curves, which represent the theoretical group velocity curves for the typical continental and oceanic paths, are superimposed in these figures for reference purposes.

Referring to Figure III-3, which gives the Rayleigh wave group velocities for the travel paths from NTS to the observation stations, the following remarks about the behavior of these group velocities can be made:

- If we take the solid dots as the average group velocities for the indicated travel path and connect them with straight lines,

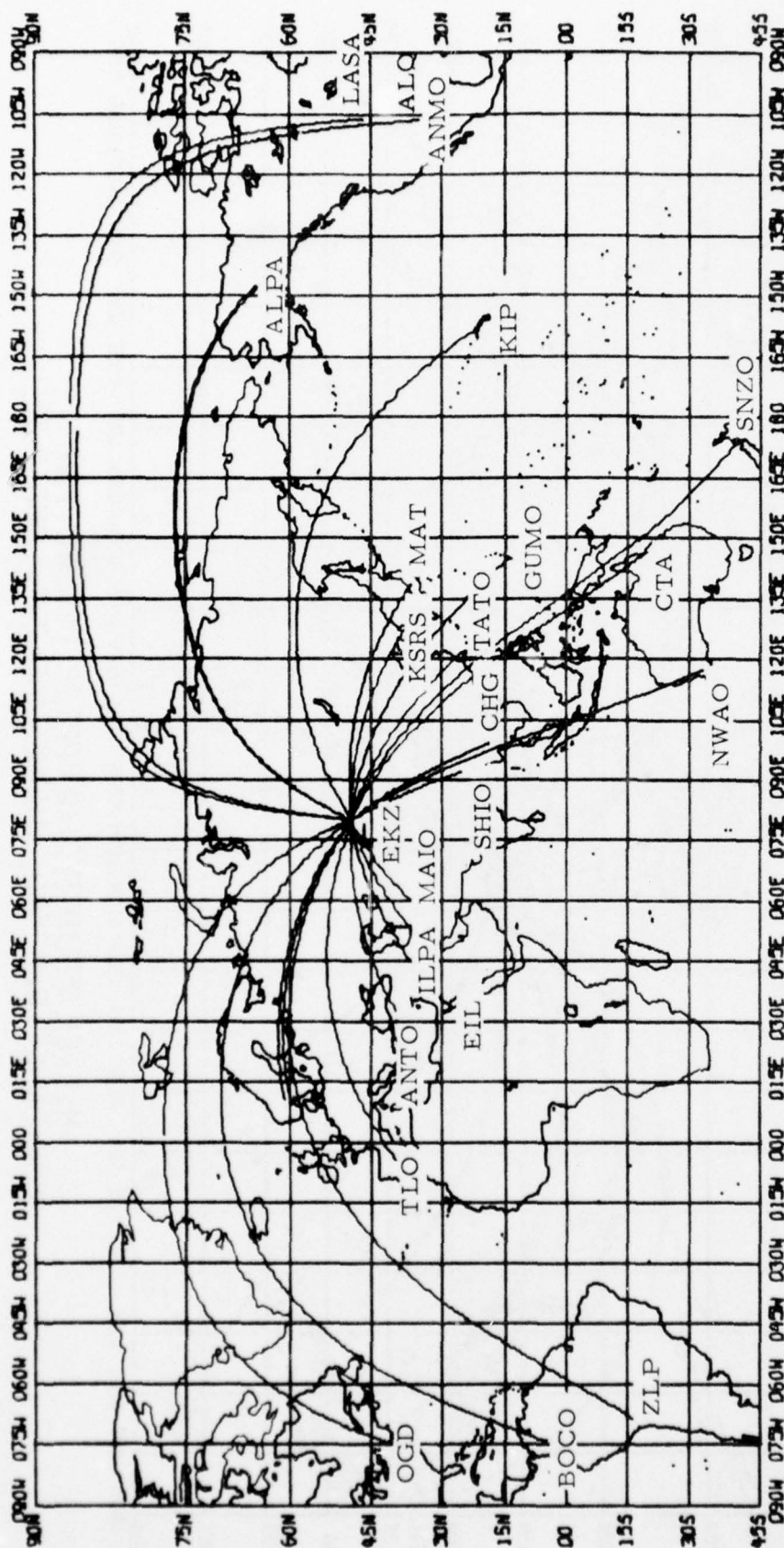


III-3

MILLER MODIFIED MERCATOR PROJECTION
MAP SCALE 0.02500 INCHES/DEGREE LONGITUDE

FIGURE III-1

LOCATIONS OF THE OBSERVATION STATIONS AND TRAVEL PATHS ENCOUNTERED TO THE NTS



III-4

MILLER MODIFIED MERCATOR PROJECTION
MAP SCALE 0.02500 INCHES/DEGREE LONGITUDE

FIGURE III-2

LOCATIONS OF THE OBSERVATION STATIONS AND TRAVEL PATHS ENCOUNTERED TO THE EKZ

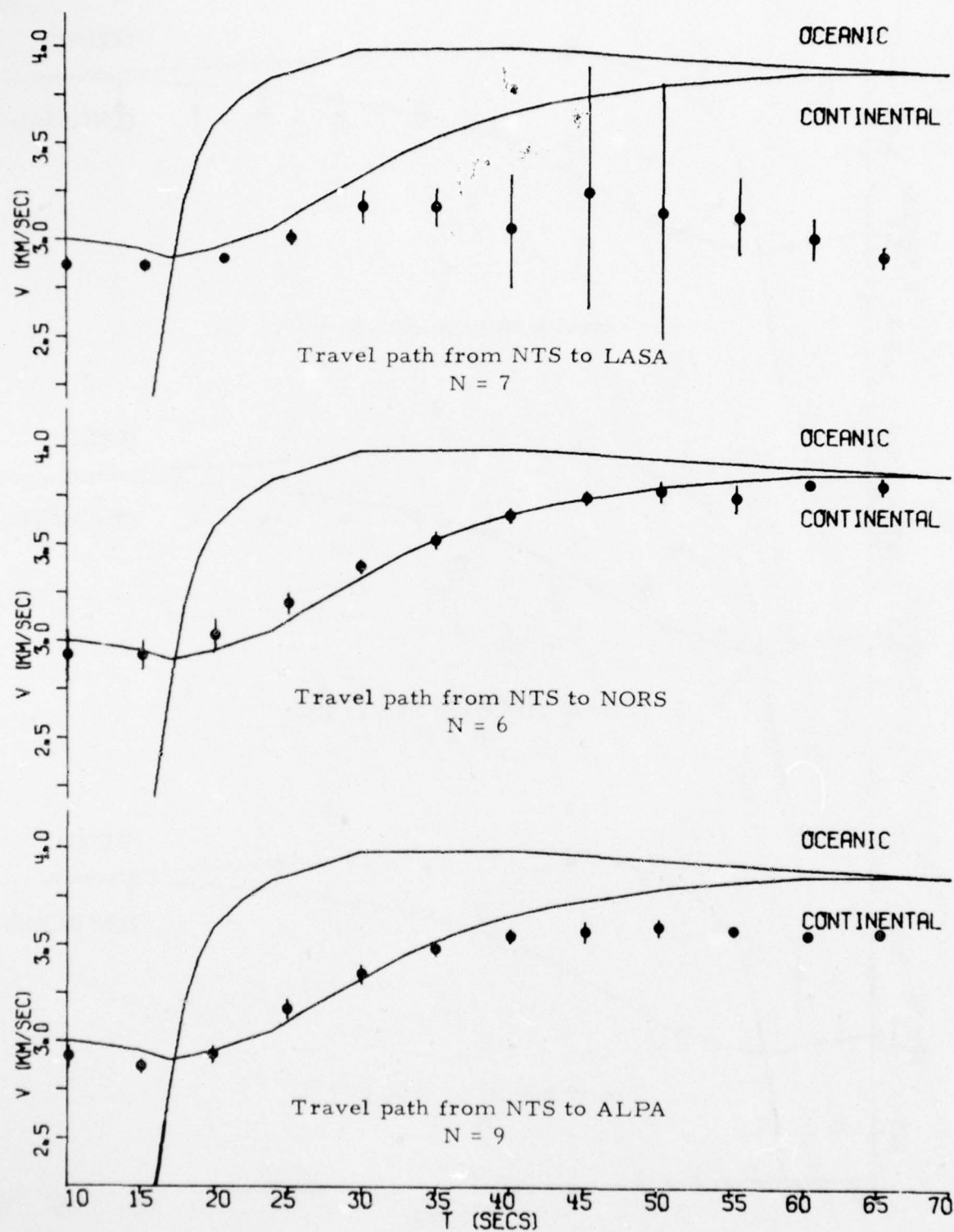


FIGURE III-3

OBSERVED RAYLEIGH WAVE GROUP VELOCITIES ALONG
THE TRAVEL PATHS FROM THE NTS TO OBSERVATION STATIONS
(PAGE 1 OF 7)

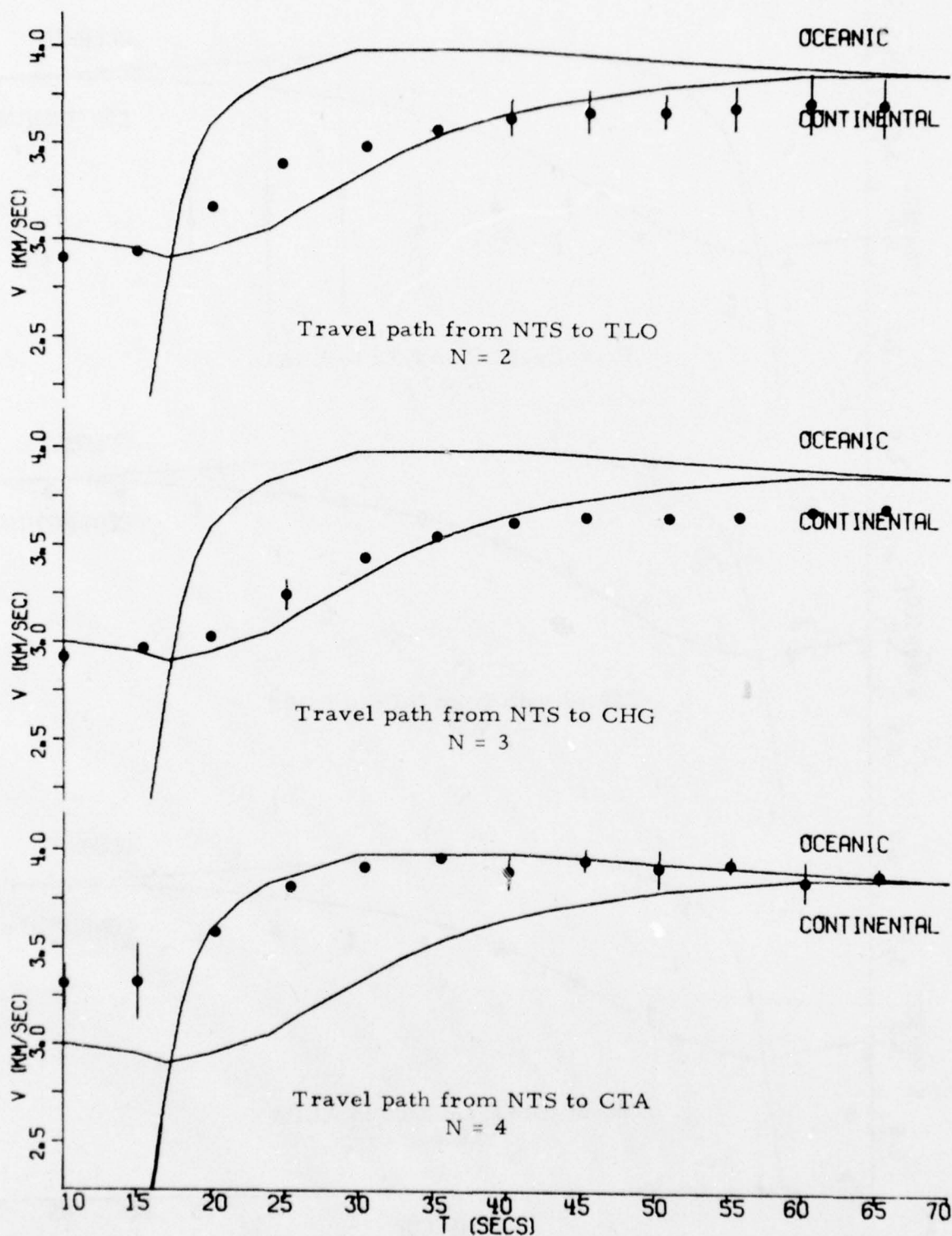


FIGURE III-3

OBSERVED RAYLEIGH WAVE GROUP VELOCITIES ALONG
THE TRAVEL PATHS FROM THE NTS TO OBSERVATION STATIONS
(PAGE 2 OF 7)

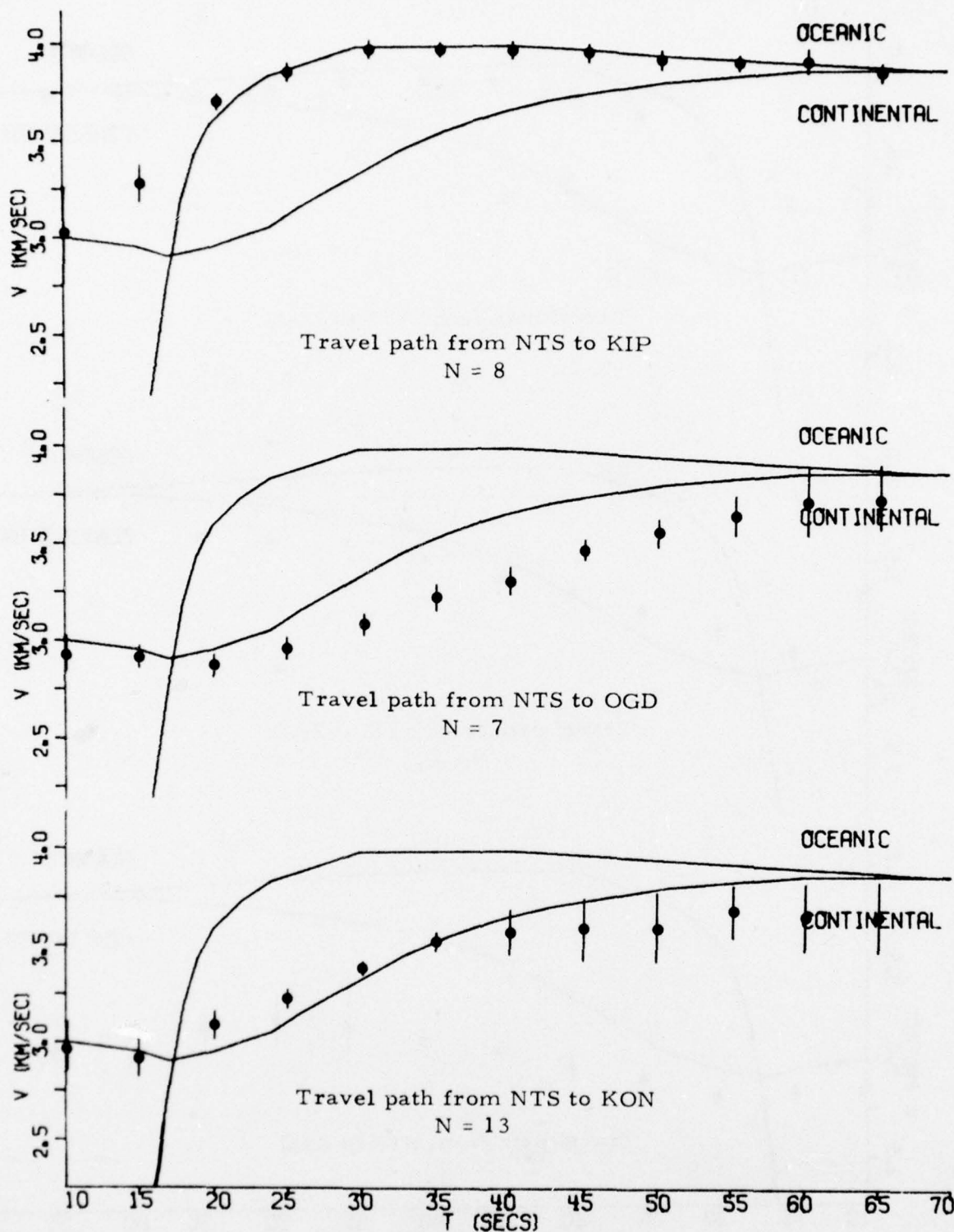


FIGURE III-3

OBSERVED RAYLEIGH WAVE GROUP VELOCITIES ALONG
THE TRAVEL PATHS FROM THE NTS TO OBSERVATION STATIONS
(PAGE 3 OF 7)

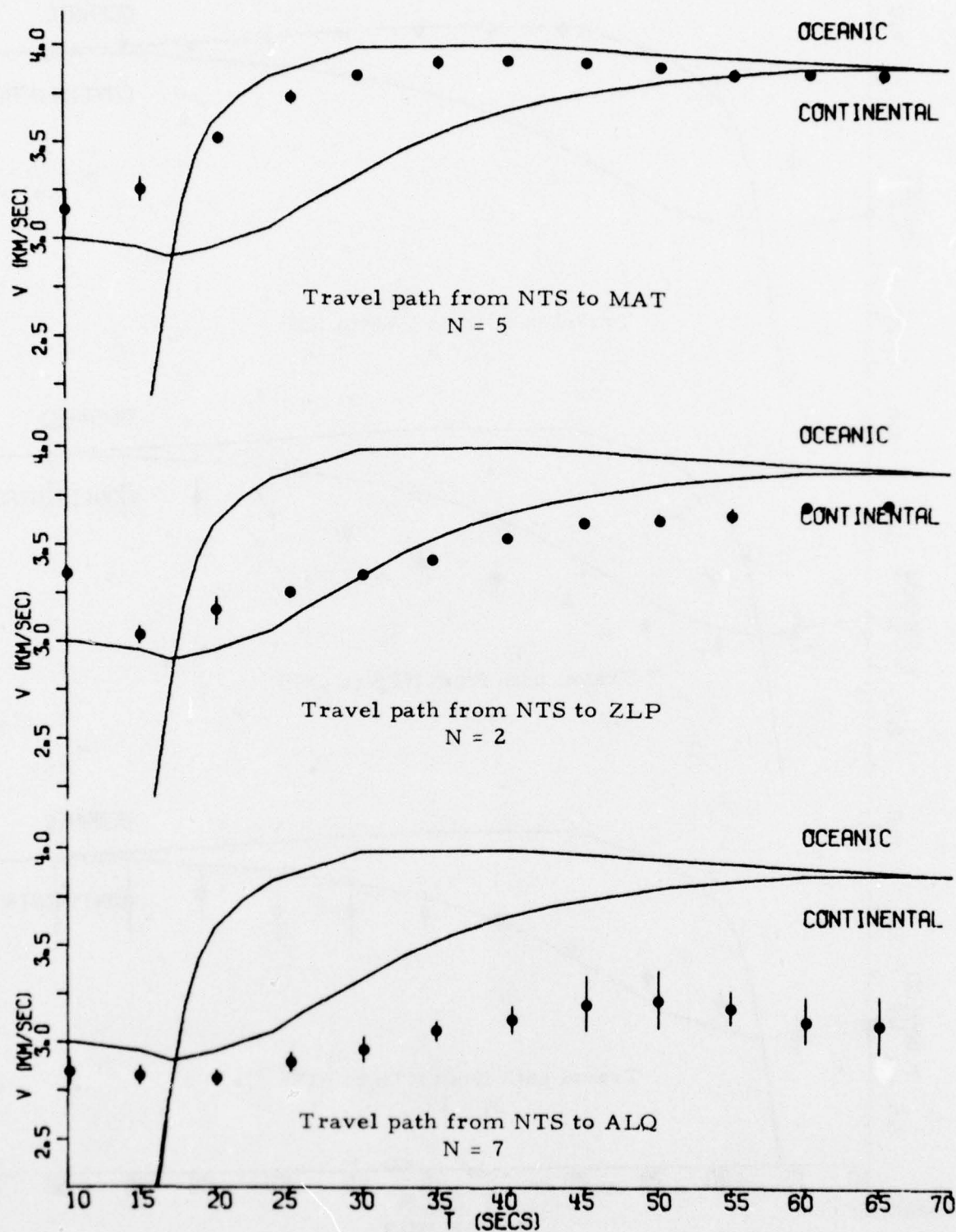


FIGURE III-3

OBSERVED RAYLEIGH WAVE GROUP VELOCITIES ALONG
THE TRAVEL PATHS FROM THE NTS TO OBSERVATION STATIONS
(PAGE 4 OF 7)

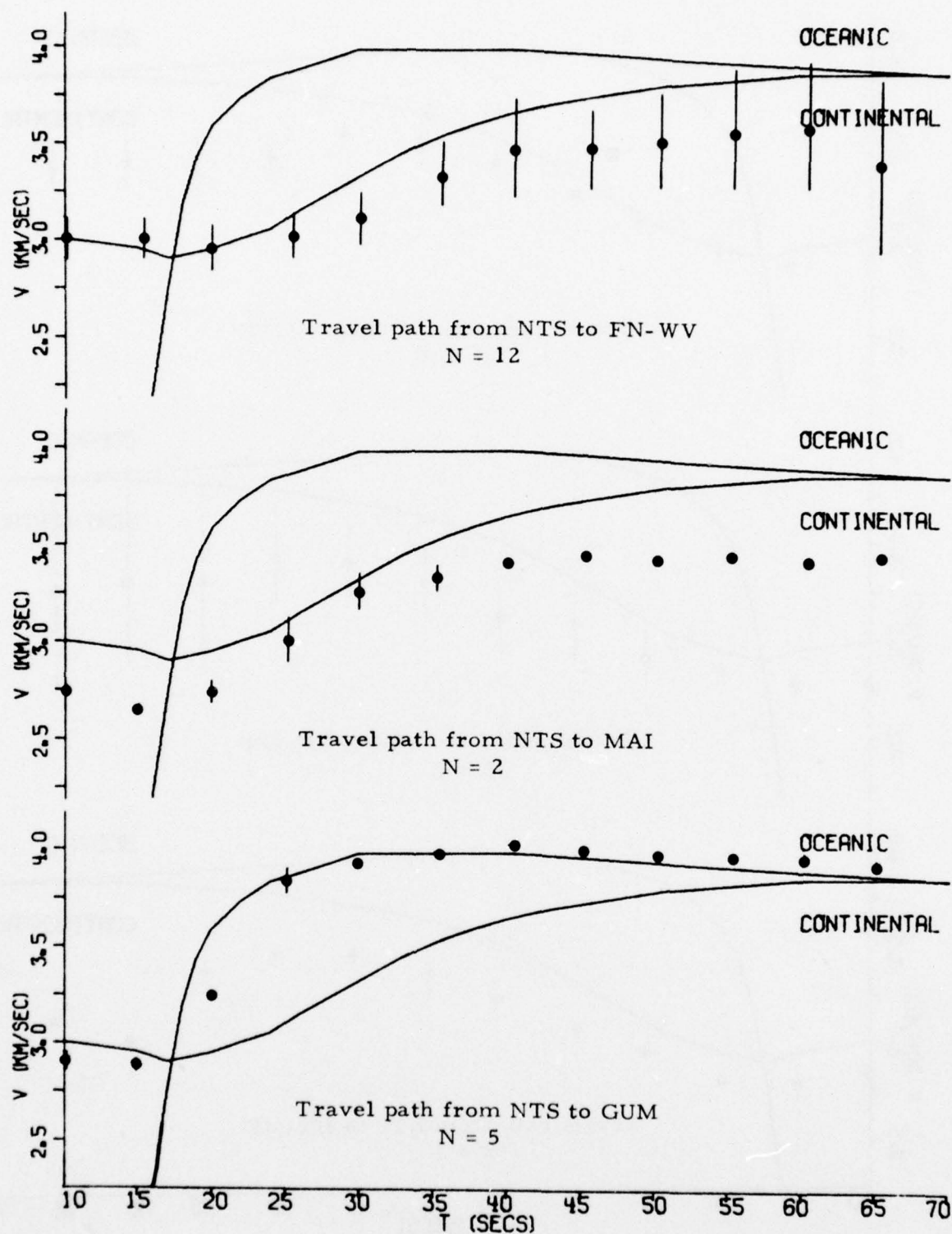


FIGURE III-3

OBSERVED RAYLEIGH WAVE GROUP VELOCITIES ALONG
THE TRAVEL PATHS FROM THE NTS TO OBSERVATION STATIONS
(PAGE 5 OF 7)

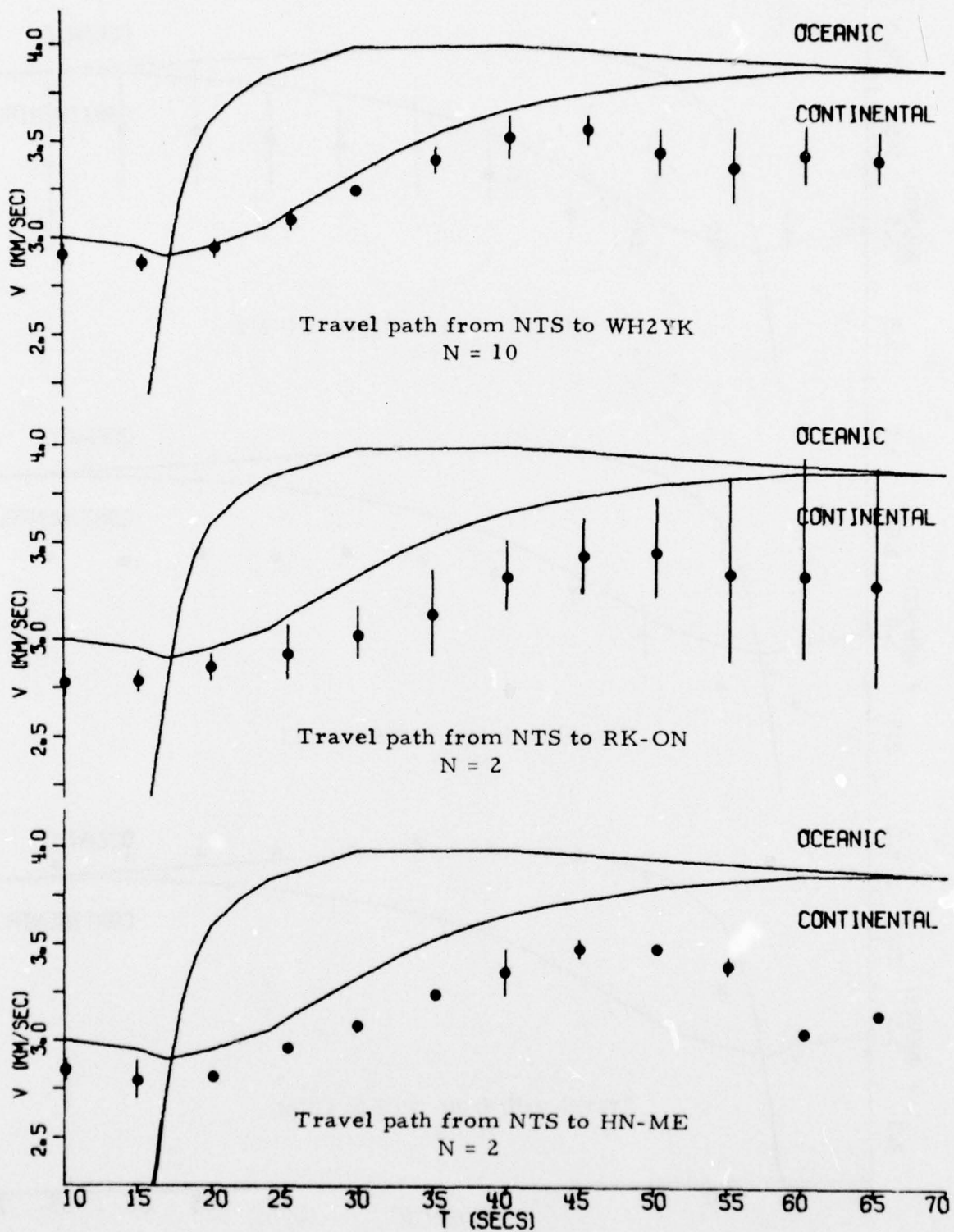


FIGURE III-3

OBSERVED RAYLEIGH WAVE GROUP VELOCITIES ALONG
THE TRAVEL PATHS FROM THE NTS TO OBSERVATION STATIONS
(PAGE 6 OF 7)

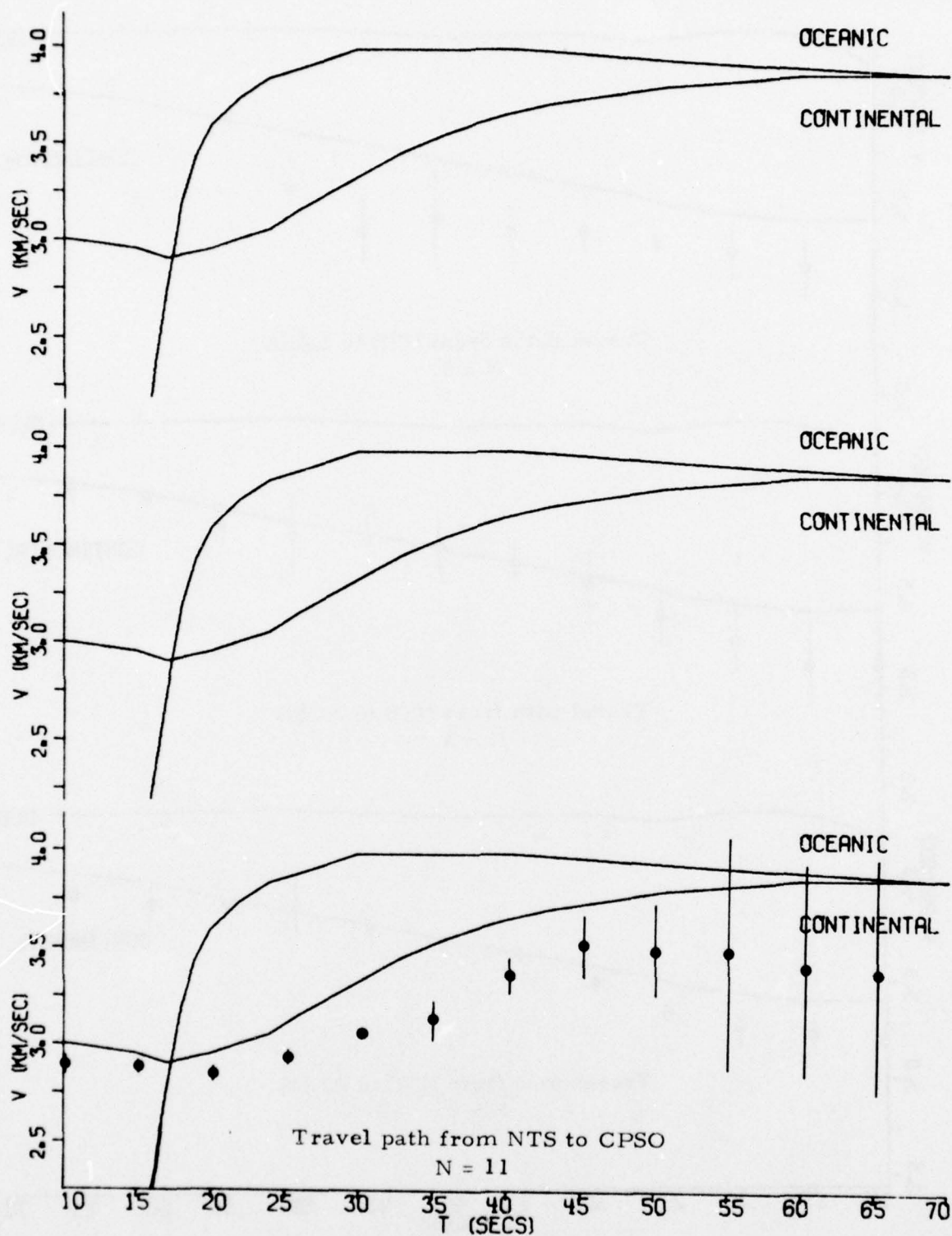


FIGURE III-3

OBSERVED RAYLEIGH WAVE GROUP VELOCITIES ALONG
THE TRAVEL PATHS FROM THE NTS TO OBSERVATION STATIONS
(PAGE 7 OF 7)

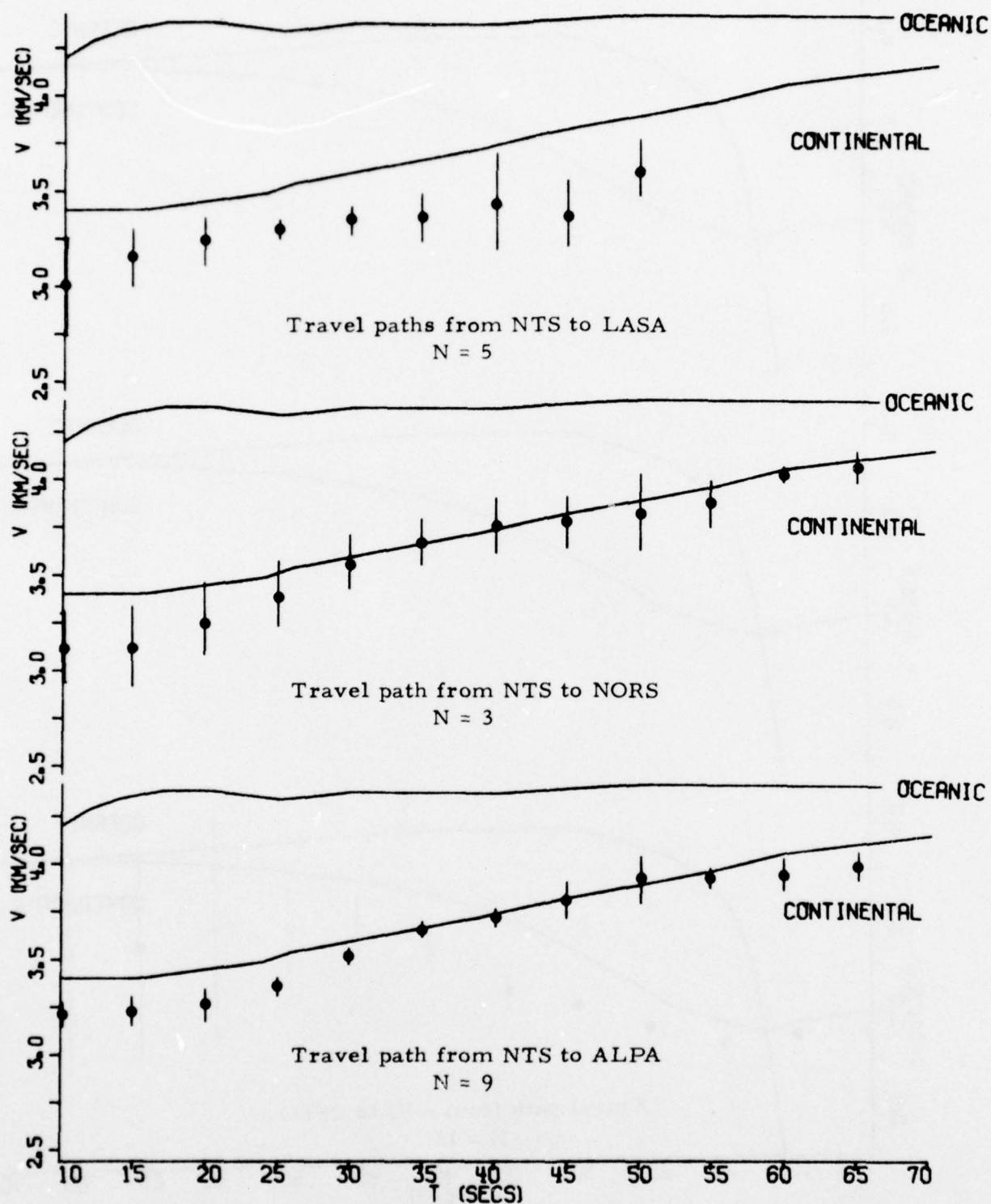


FIGURE III-4
OBSERVED LOVE WAVE GROUP VELOCITIES ALONG
THE TRAVEL PATHS FROM THE NTS TO OBSERVATION STATIONS
(PAGE 1 OF 7)

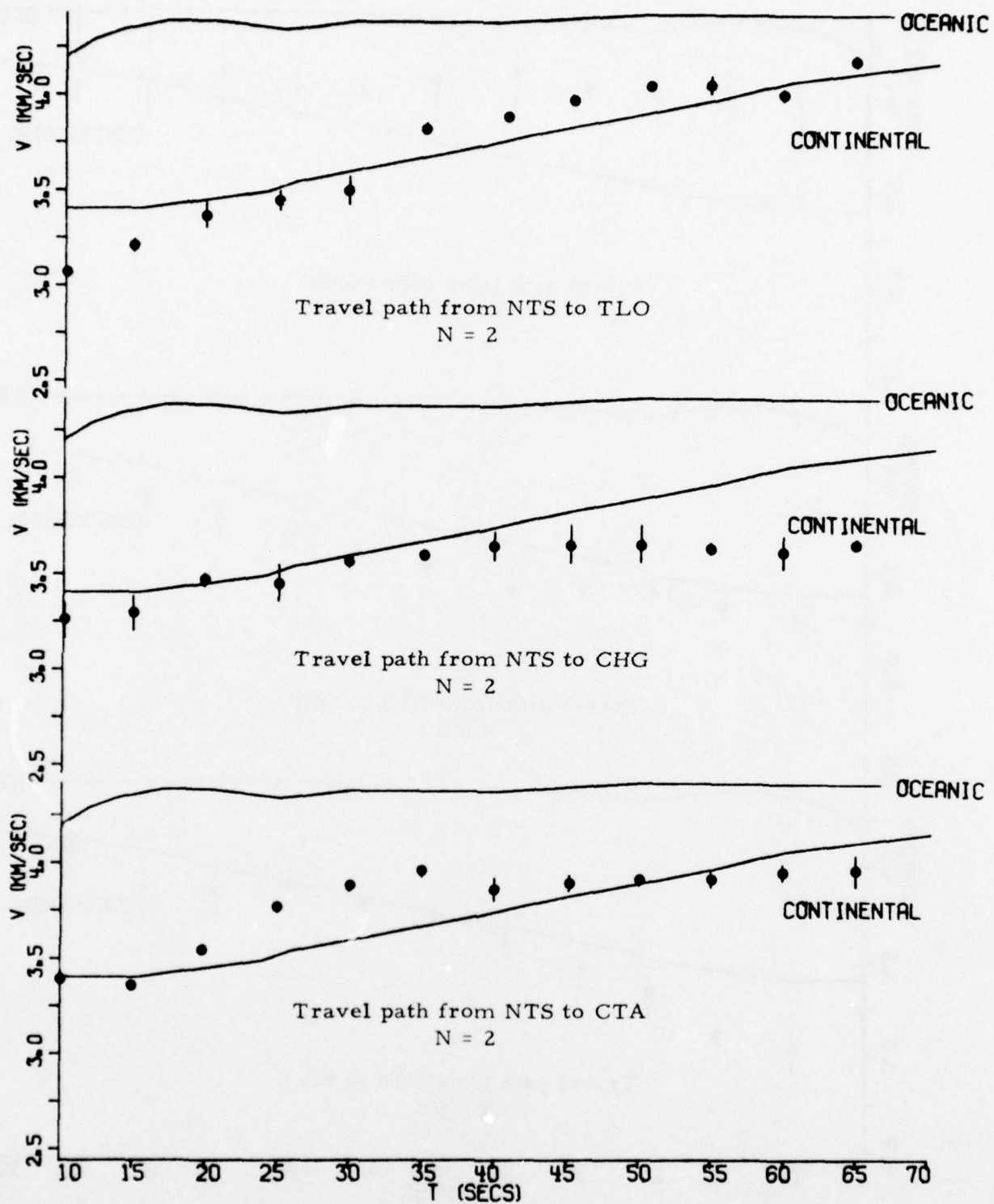


FIGURE III-4

OBSERVED LOVE WAVE GROUP VELOCITIES ALONG
THE TRAVEL PATHS FROM THE NTS TO OBSERVATION STATIONS
(PAGE 2 OF 7)

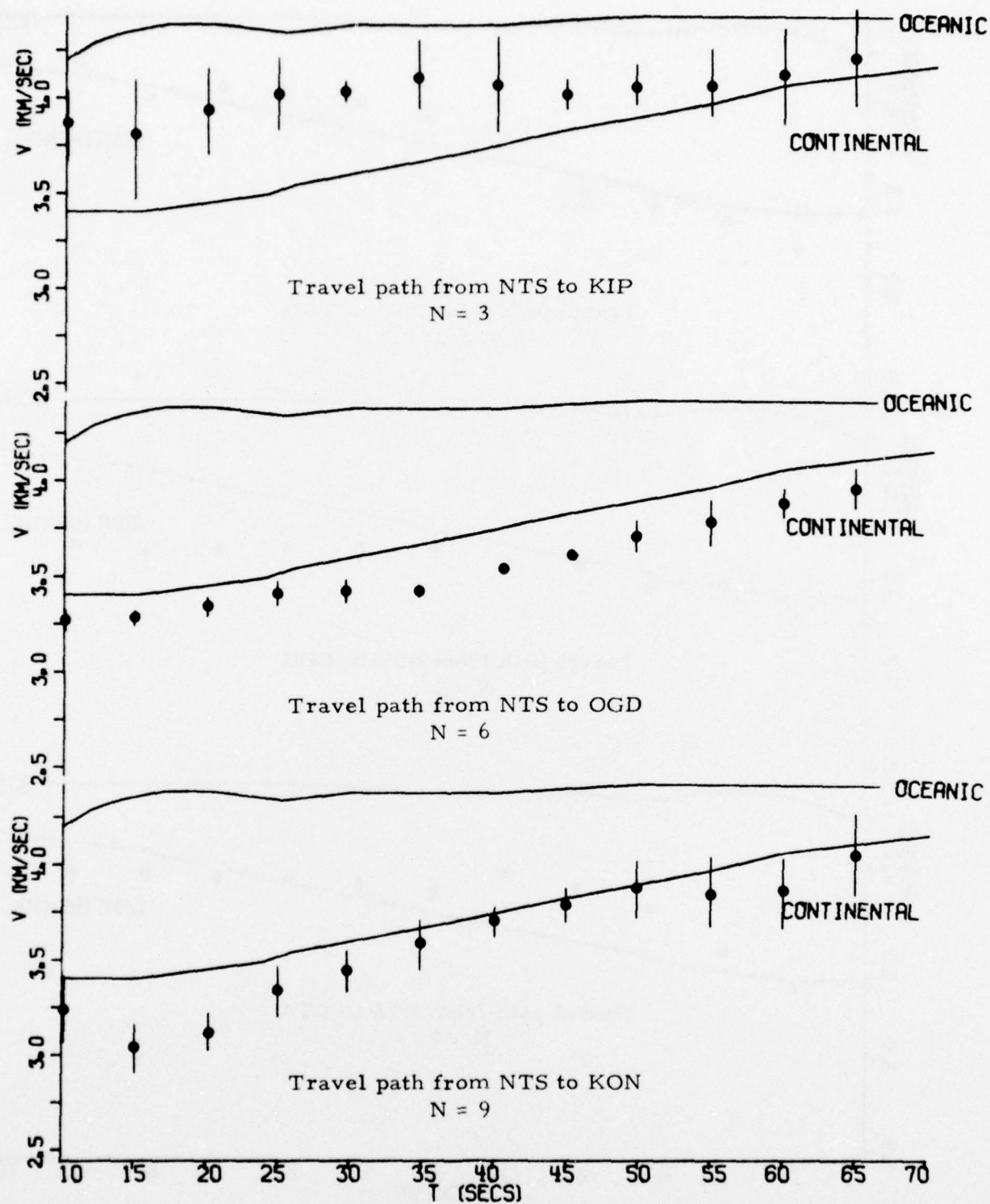


FIGURE III-4

OBSERVED LOVE WAVE GROUP VELOCITIES ALONG
THE TRAVEL PATHS FROM THE NTS TO OBSERVATION STATIONS
(PAGE 3 OF 7)

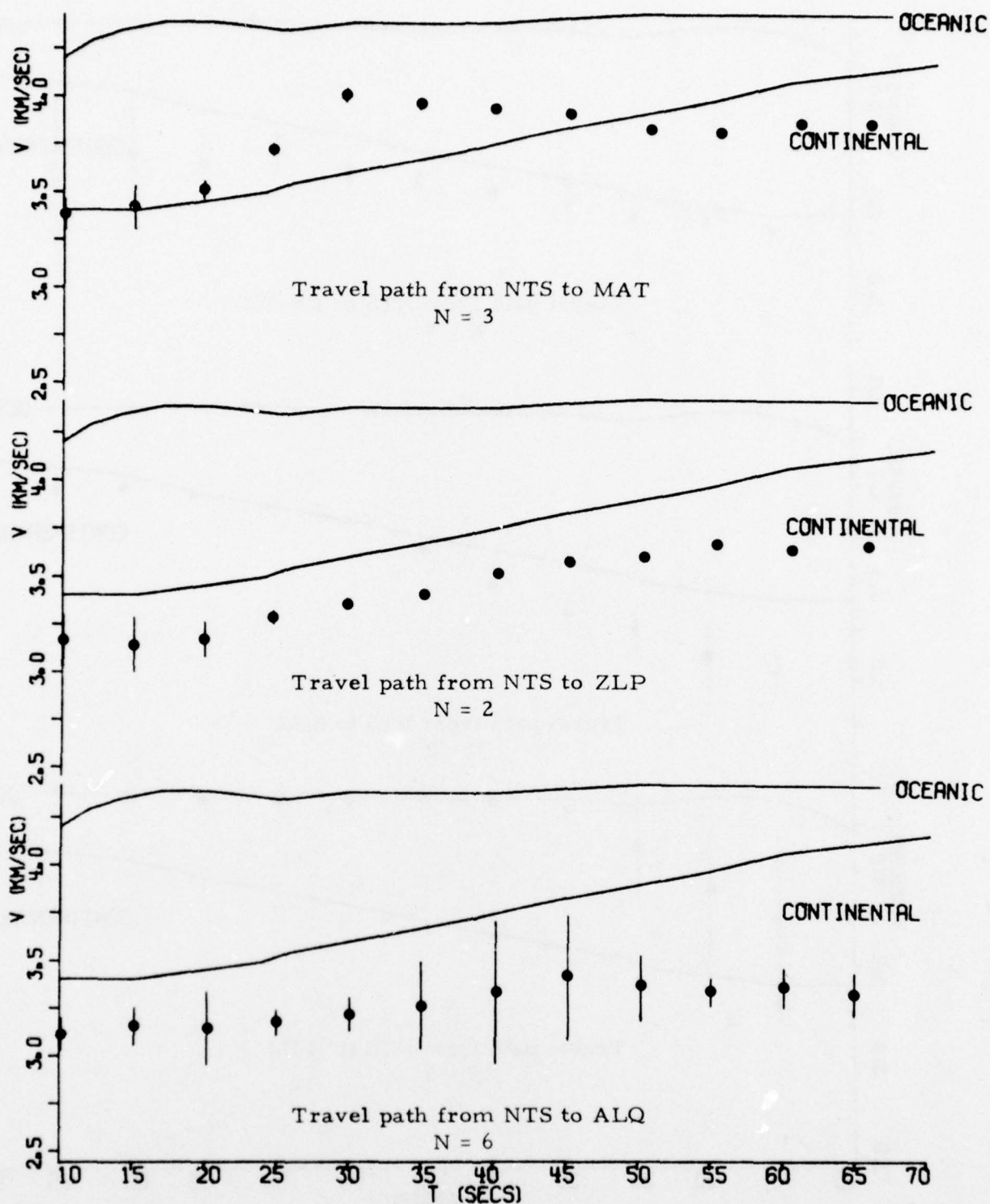


FIGURE III-4

OBSERVED LOVE WAVE GROUP VELOCITIES ALONG
THE TRAVEL PATHS FROM THE NTS TO OBSERVATION STATIONS
(PAGE 4 OF 7)

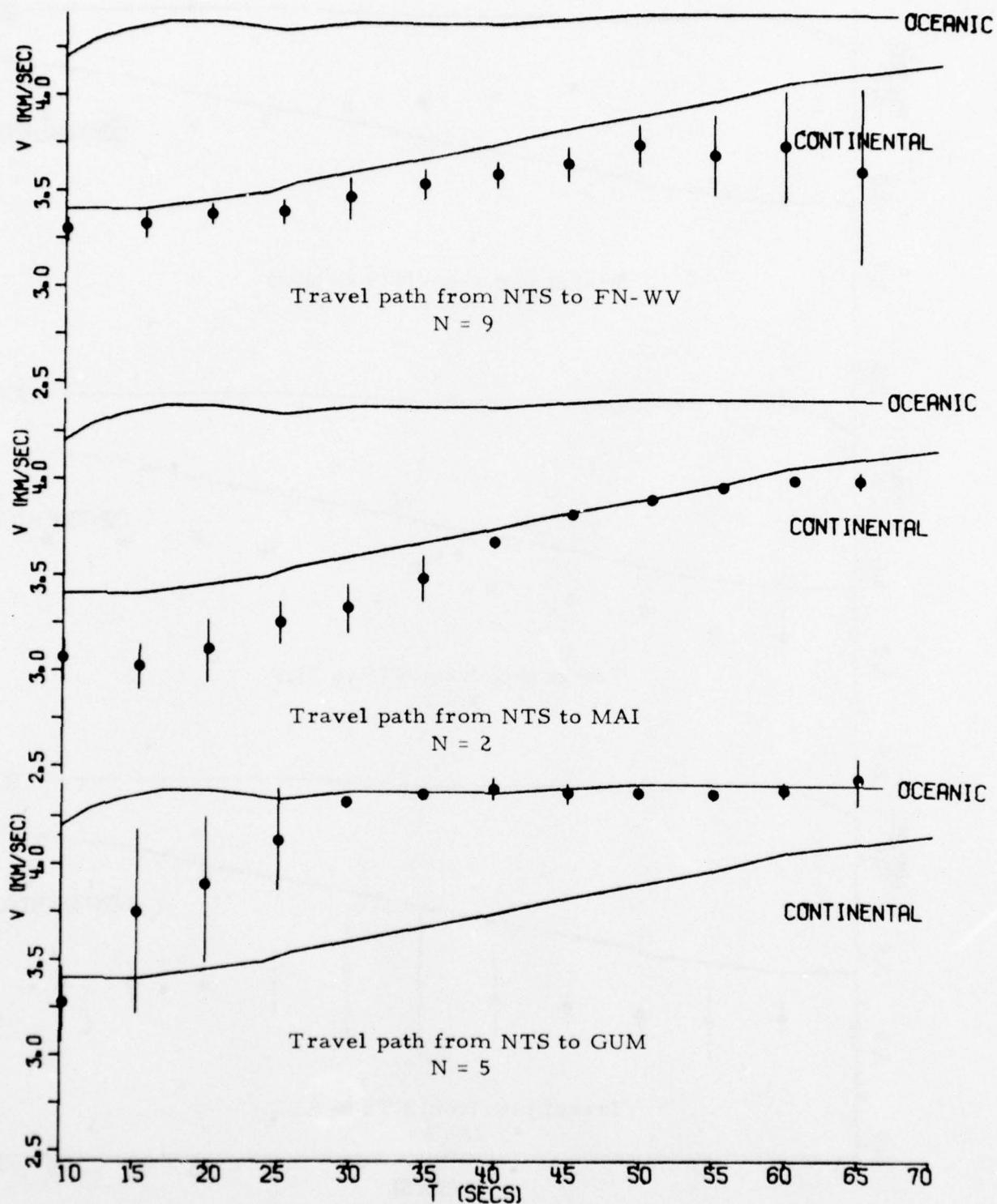


FIGURE III-4

OBSERVED LOVE WAVE GROUP VELOCITIES ALONG
THE TRAVEL PATHS FROM THE NTS TO OBSERVATION STATIONS
(PAGE 5 OF 7)

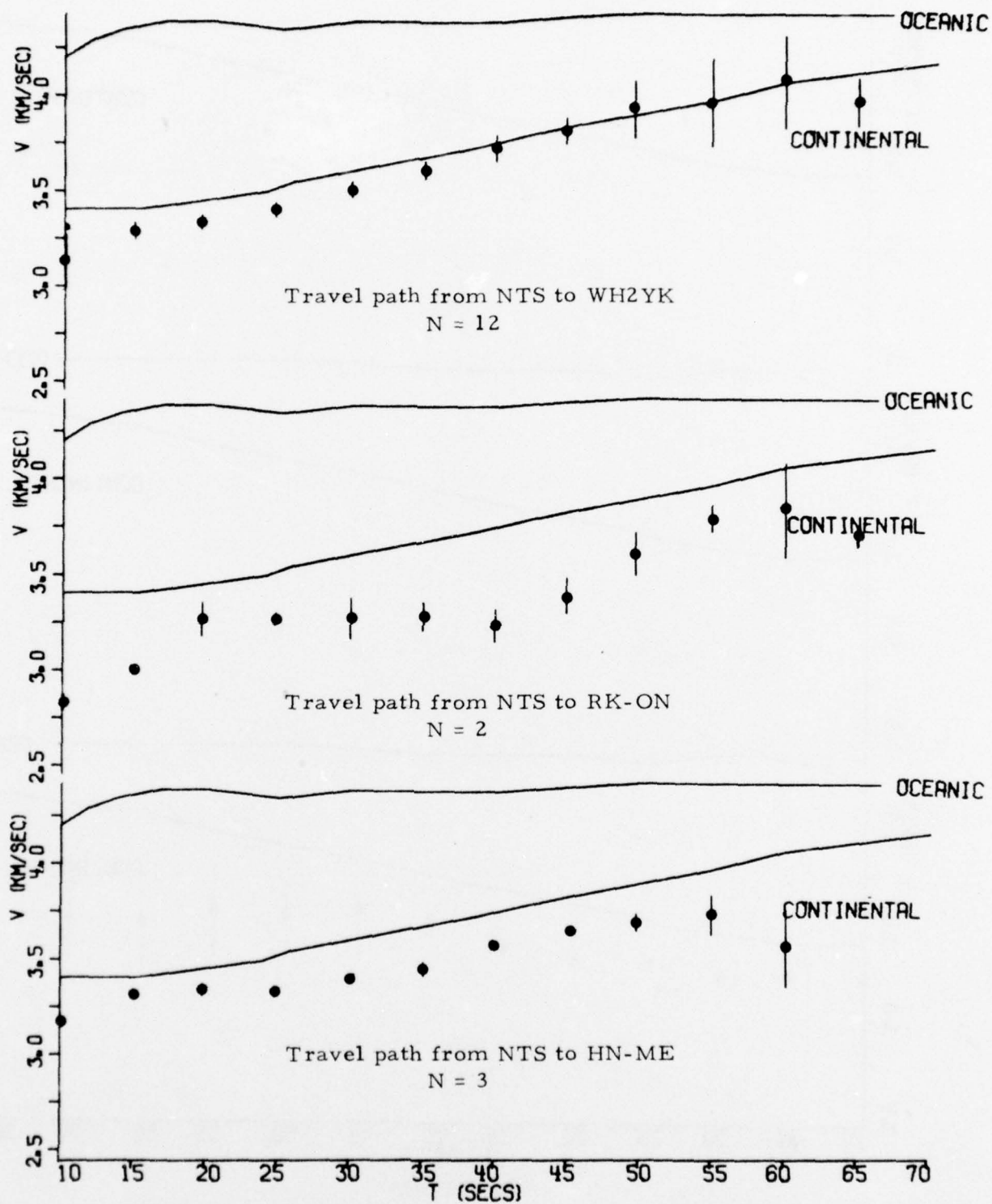


FIGURE III-4

OBSERVED LOVE WAVE GROUP VELOCITIES ALONG
THE TRAVEL PATHS FROM THE NTS TO OBSERVATION STATIONS
(PAGE 6 OF 7)

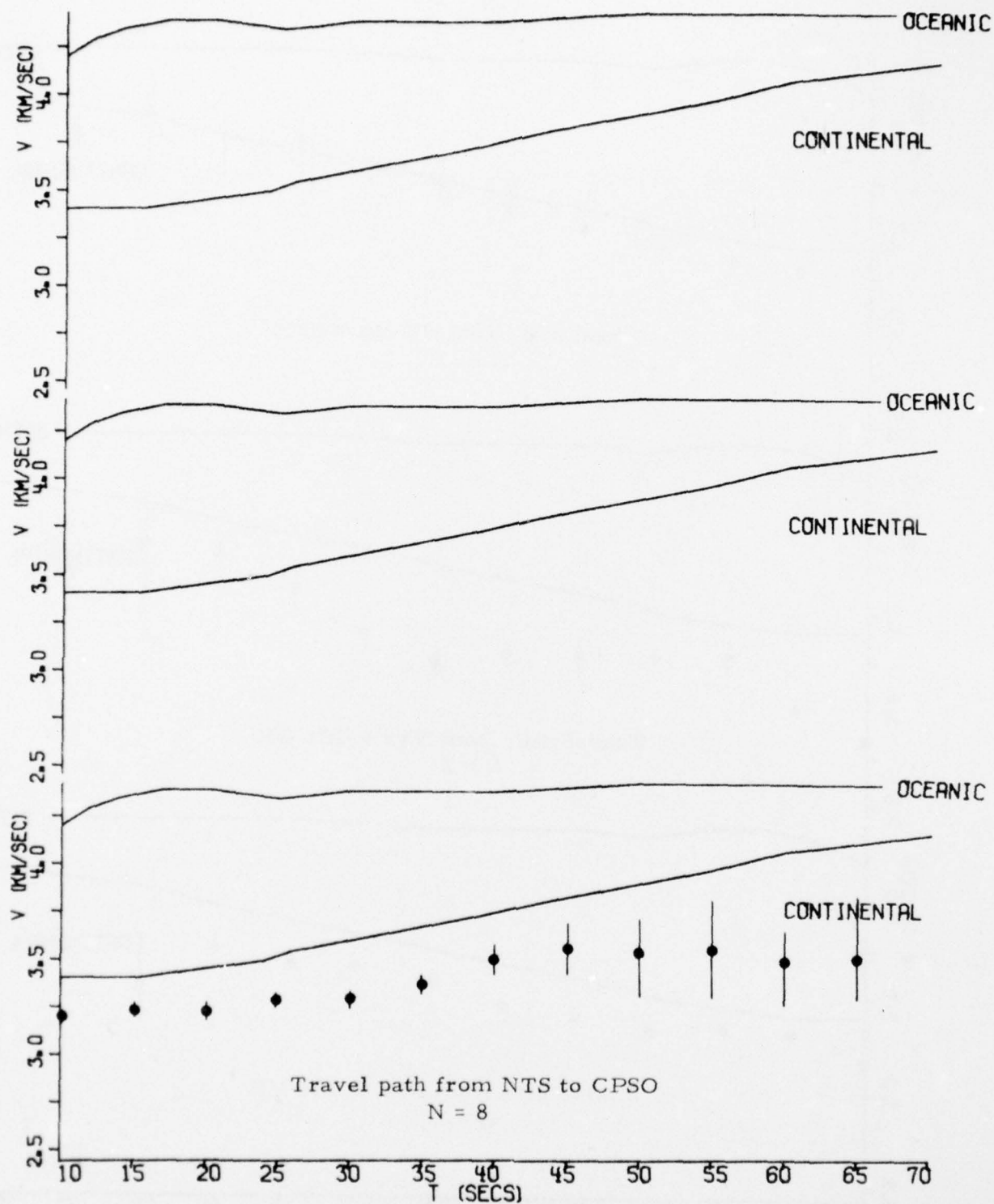


FIGURE III-4

OBSERVED LOVE WAVE GROUP VELOCITIES ALONG
THE TRAVEL PATHS FROM THE NTS TO OBSERVATION STATIONS
(PAGE 7 OF 7)

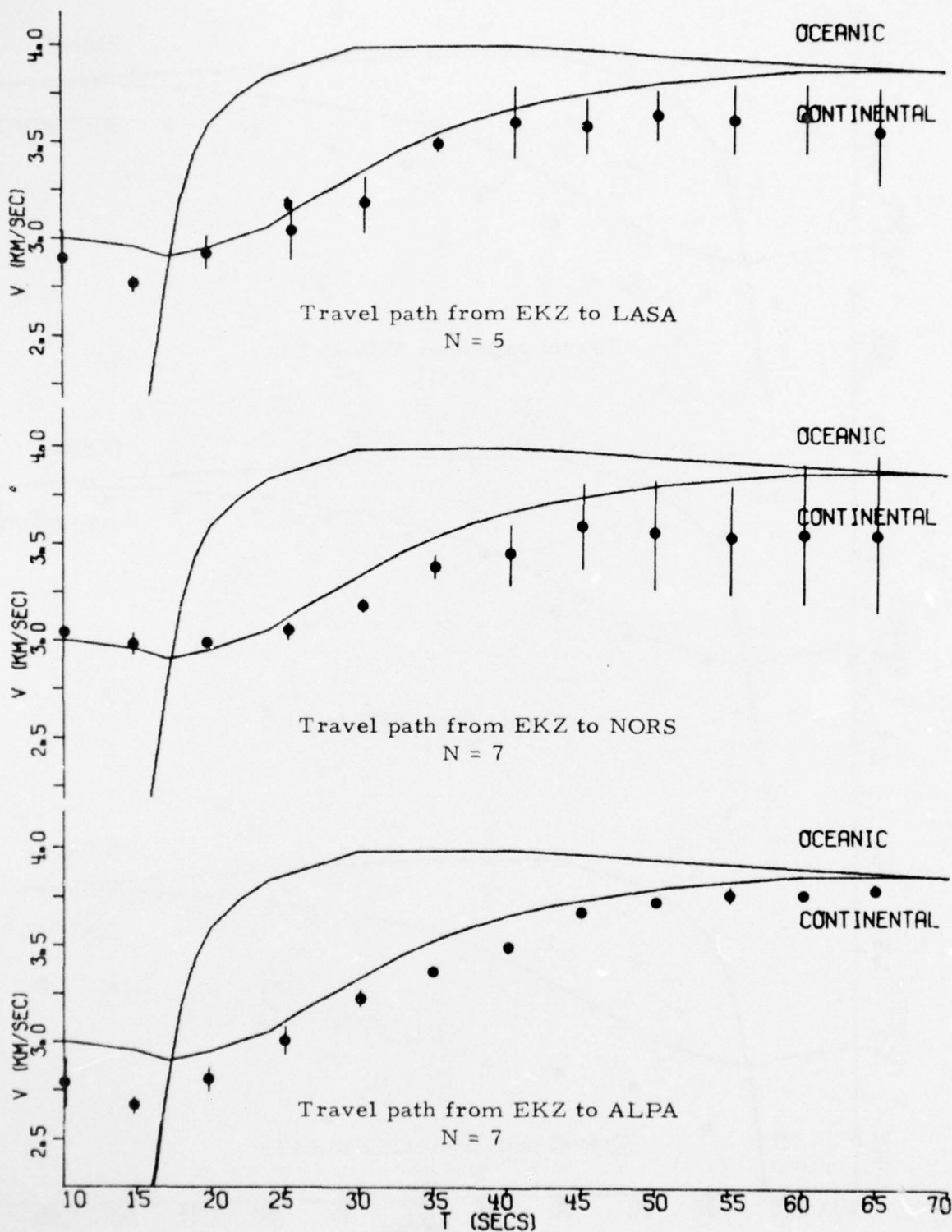


FIGURE III-5

OBSERVED RAYLEIGH WAVE GROUP VELOCITIES ALONG
THE TRAVEL PATHS FROM THE EKZ TO OBSERVATION STATIONS
(PAGE 1 OF 5)

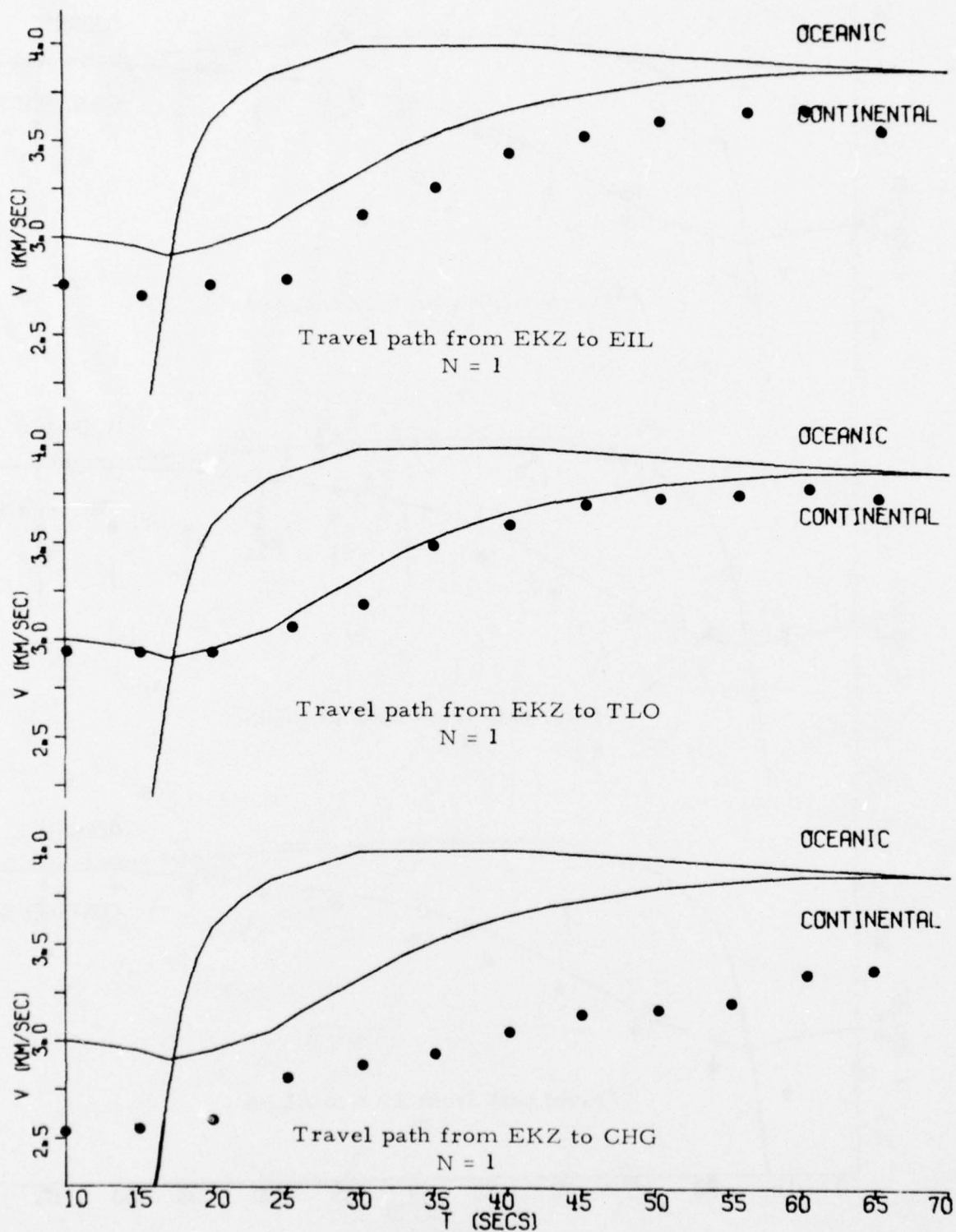


FIGURE III-5
OBSERVED RAYLEIGH WAVE GROUP VELOCITIES ALONG
THE TRAVEL PATHS FROM THE EKZ TO OBSERVATION STATIONS
(PAGE 2 OF 5)

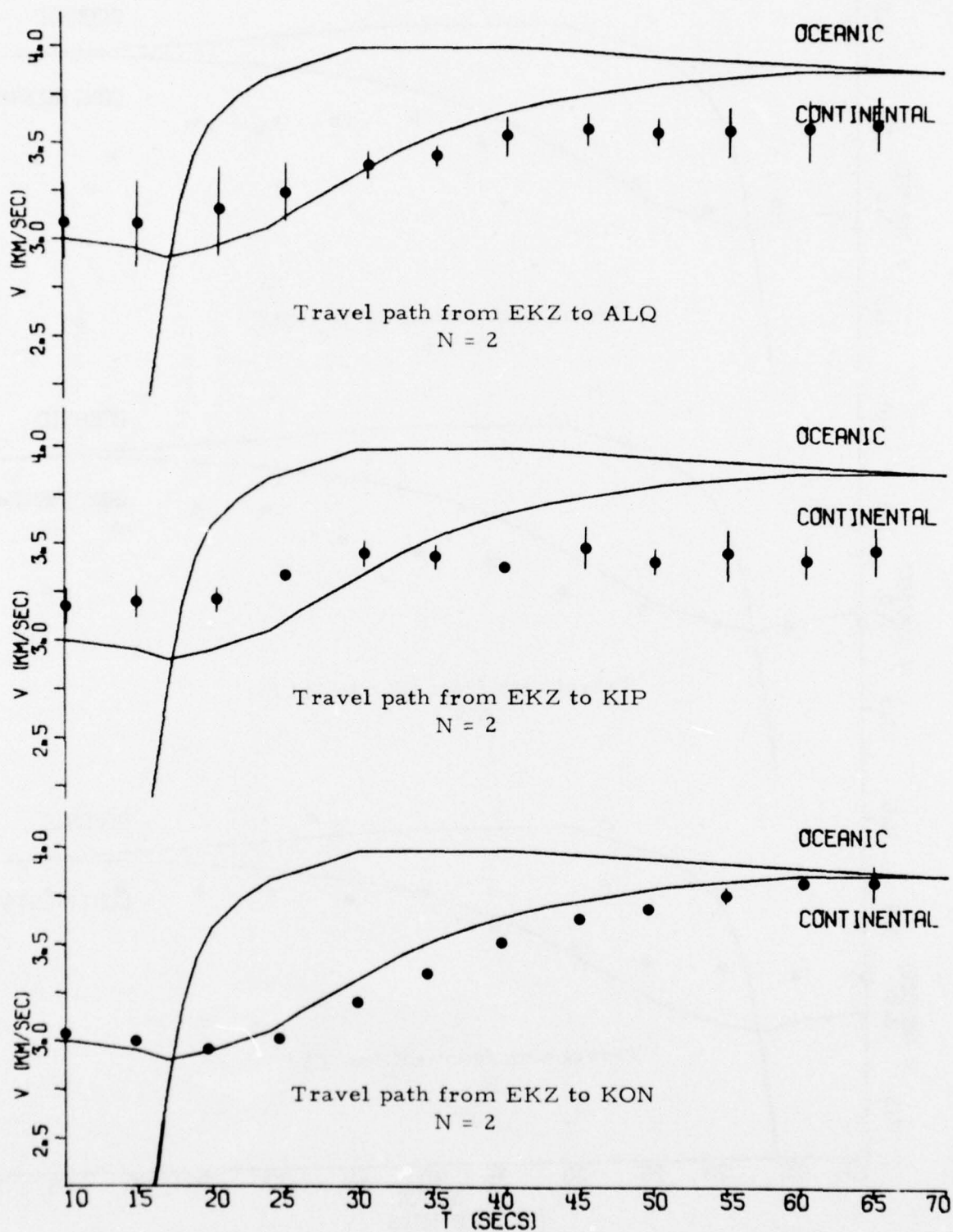


FIGURE III-5

OBSERVED RAYLEIGH WAVE GROUP VELOCITIES ALONG
THE TRAVEL PATHS FROM THE EKZ TO OBSERVATION STATIONS
(PAGE 3 OF 5)

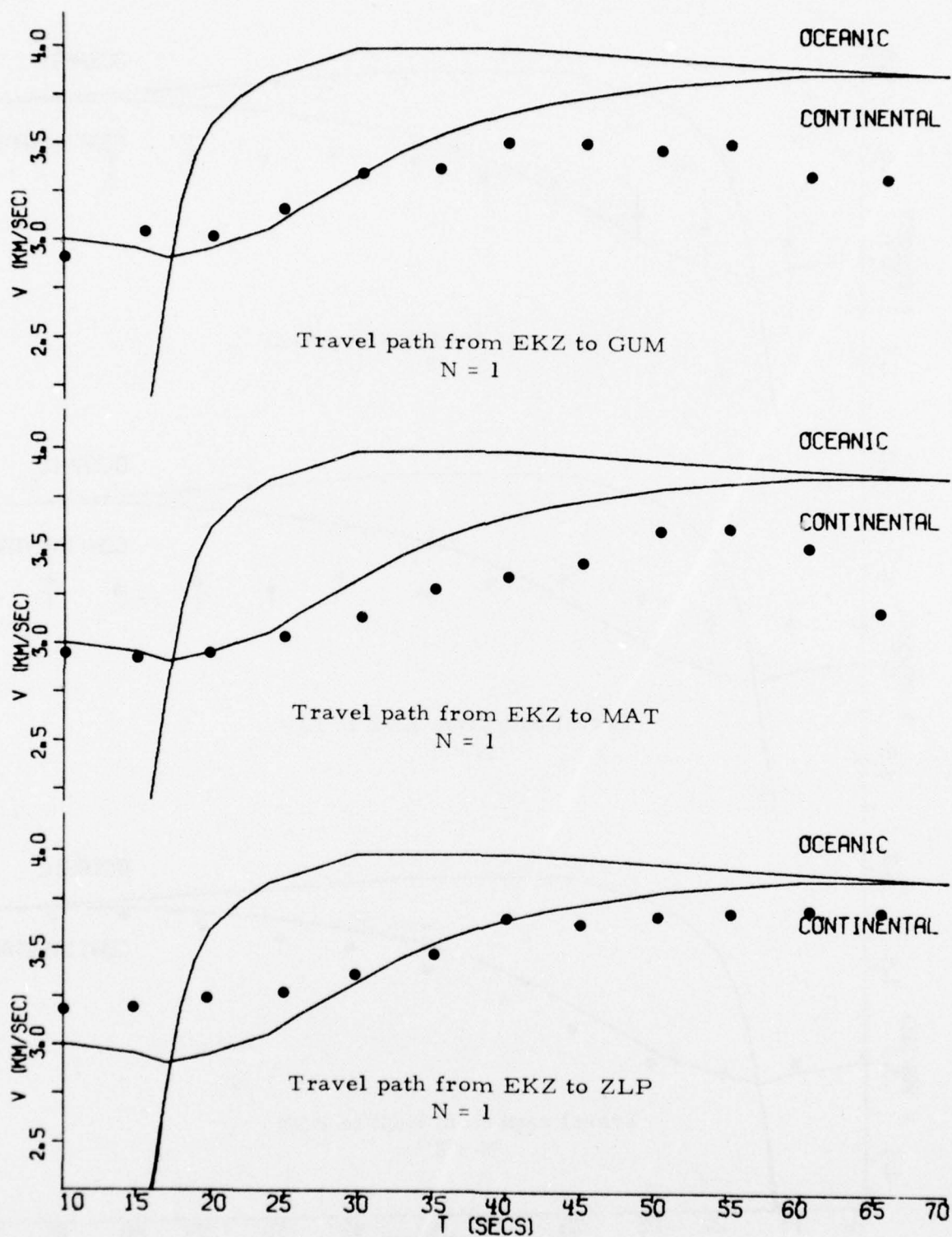


FIGURE III-5

OBSERVED RAYLEIGH WAVE GROUP VELOCITIES ALONG
THE TRAVEL PATHS FROM THE EKZ TO OBSERVATION STATIONS
(PAGE 4 OF 5)

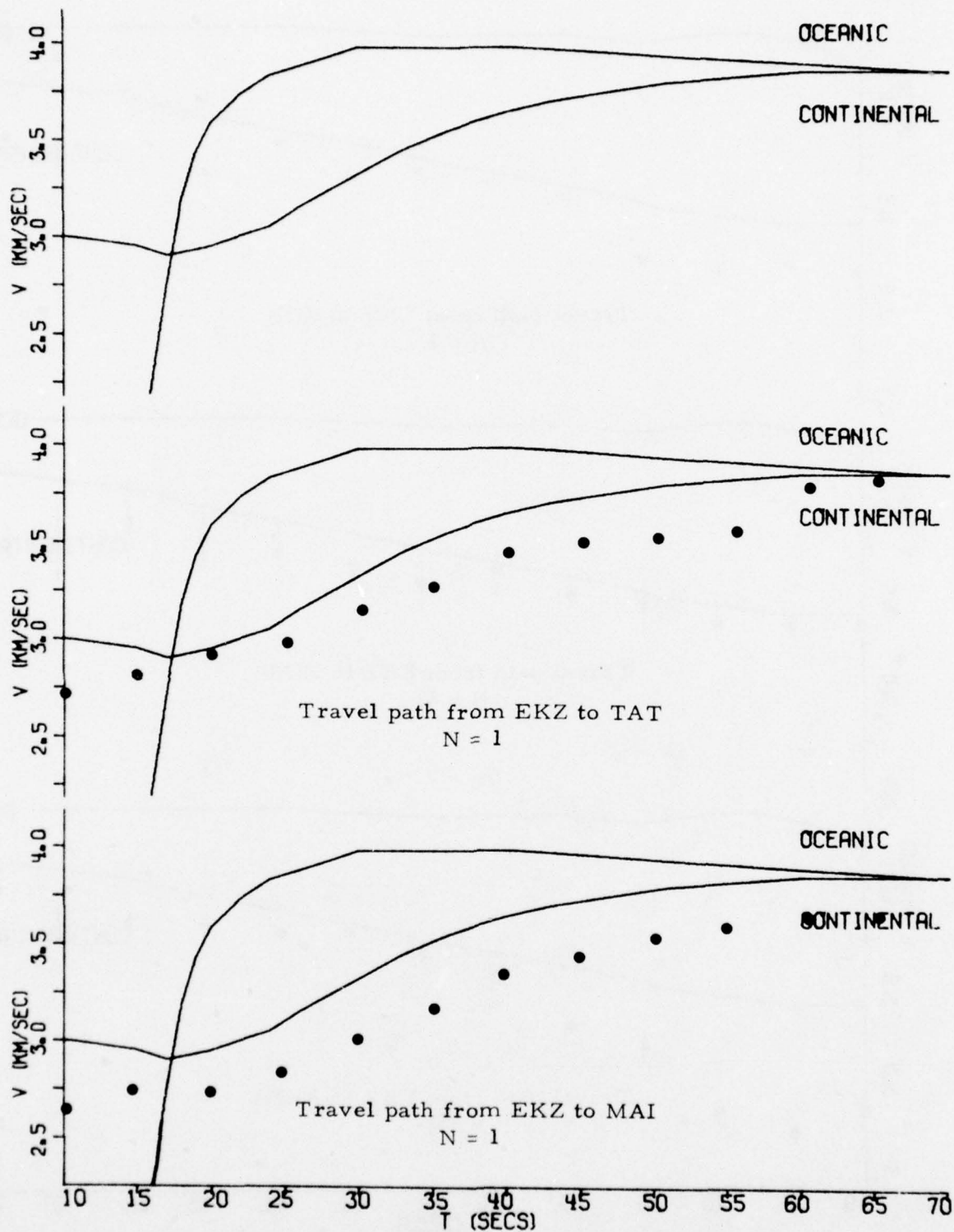


FIGURE III-5

OBSERVED RAYLEIGH WAVE GROUP VELOCITIES ALONG
THE TRAVEL PATHS FROM THE EKZ TO OBSERVATION STATIONS
(PAGE 5 OF 5)

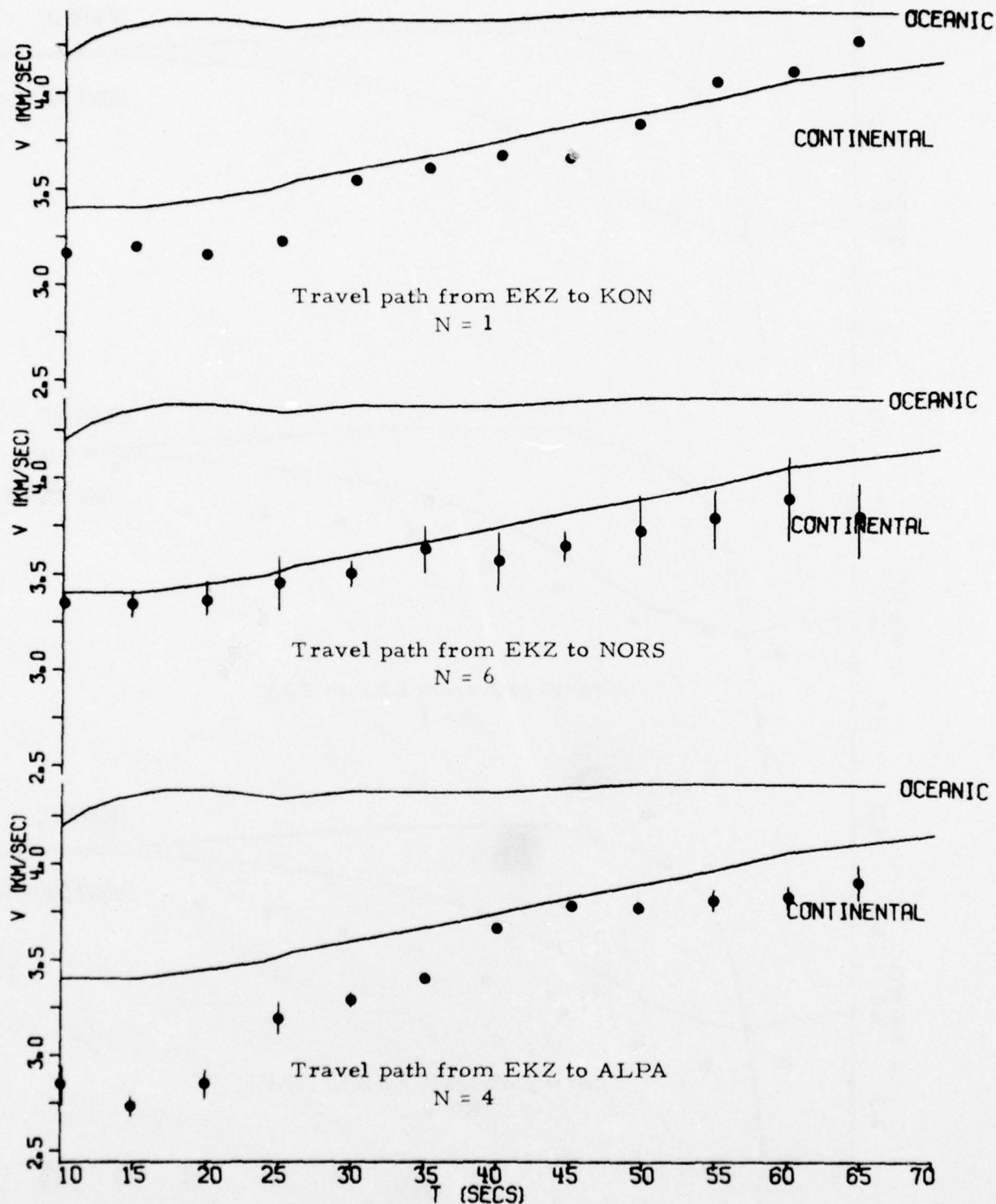


FIGURE III-6

OBSERVED LOVE WAVE GROUP VELOCITIES ALONG
THE TRAVEL PATHS FROM THE EKZ TO OBSERVATION STATIONS
(PAGE 1 OF 2)

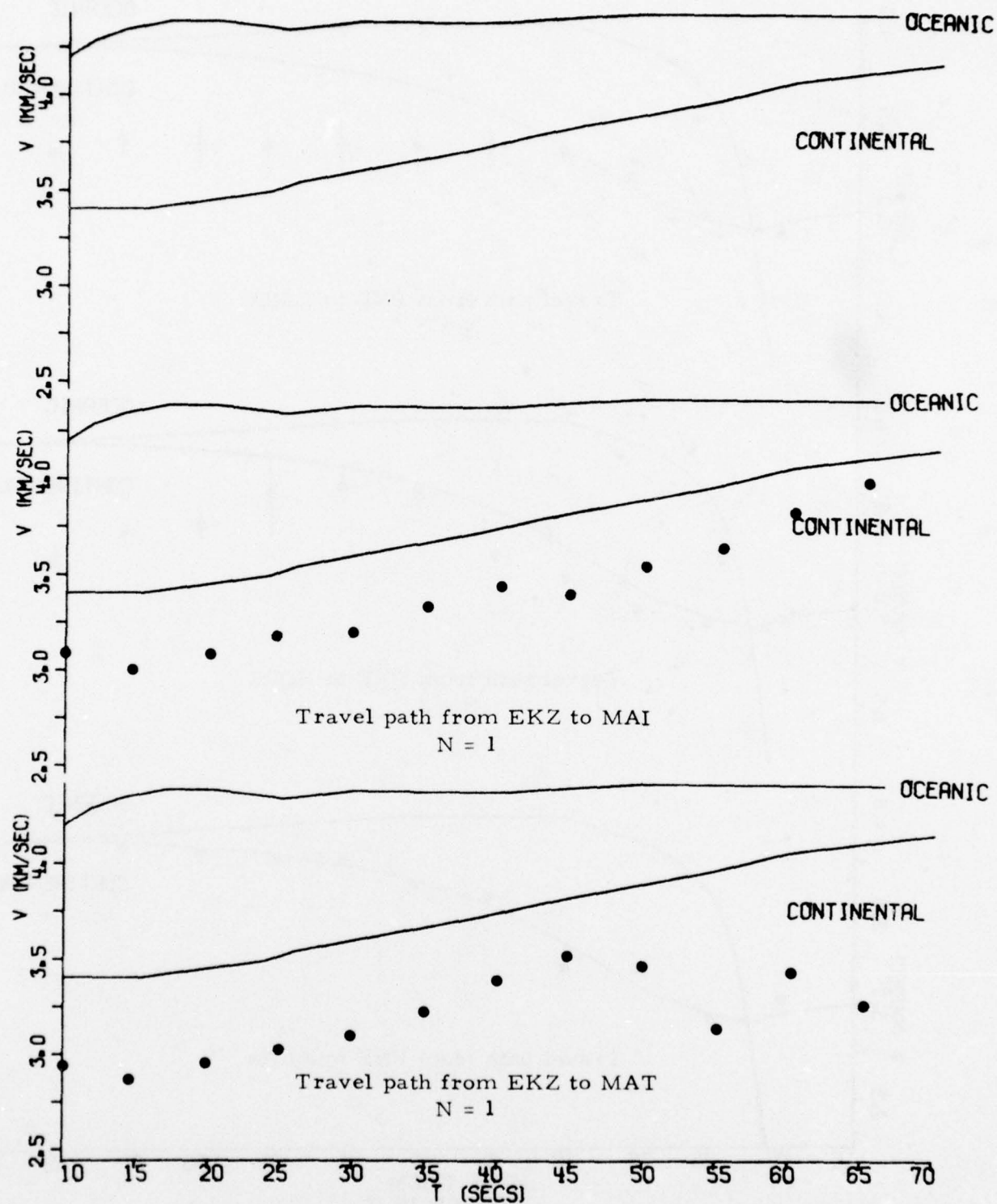
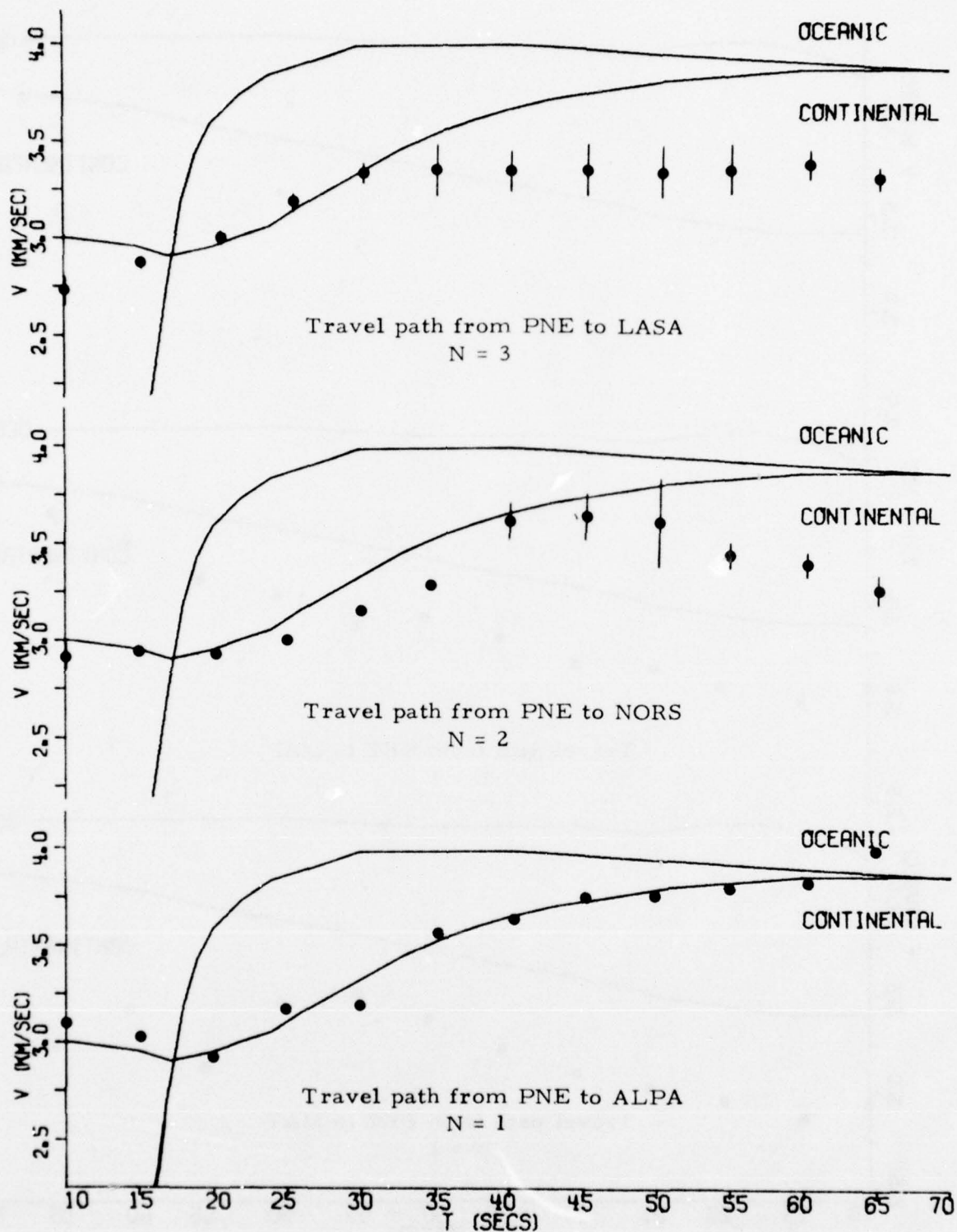


FIGURE III-6
OBSERVED LOVE WAVE GROUP VELOCITIES ALONG
THE TRAVEL PATHS FROM THE EKZ TO OBSERVATION STATIONS
(PAGE 2 OF 2)



OBSERVED RAYLEIGH WAVE GROUP VELOCITIES ALONG
 THE TRAVEL PATHS FROM THE PNE TO OBSERVATION STATIONS
 (PAGE 1 OF 2)

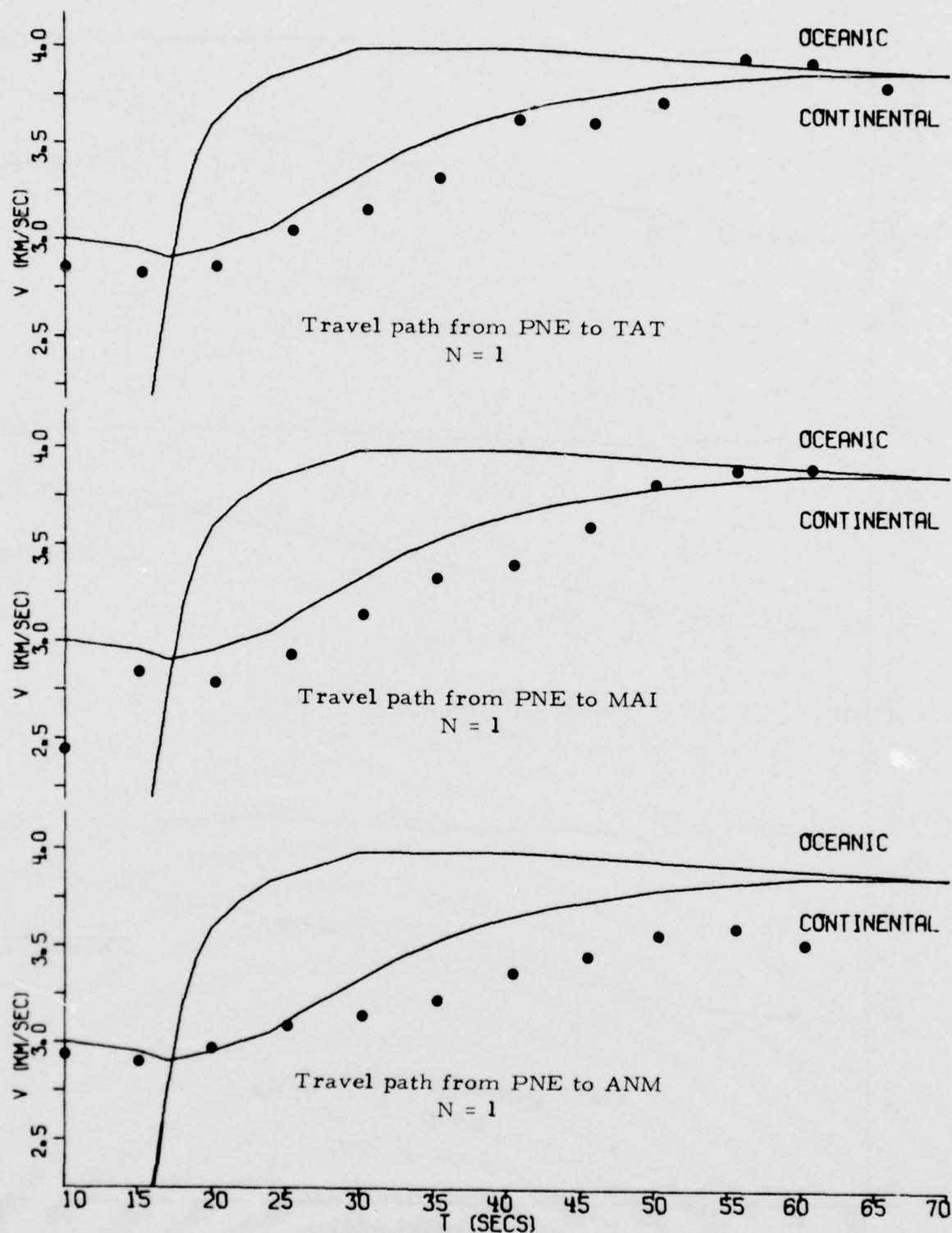


FIGURE III-7

OBSERVED RAYLEIGH WAVE GROUP VELOCITIES ALONG
THE TRAVEL PATHS FROM THE PNE TO OBSERVATION STATIONS
(PAGE 2 OF 2)

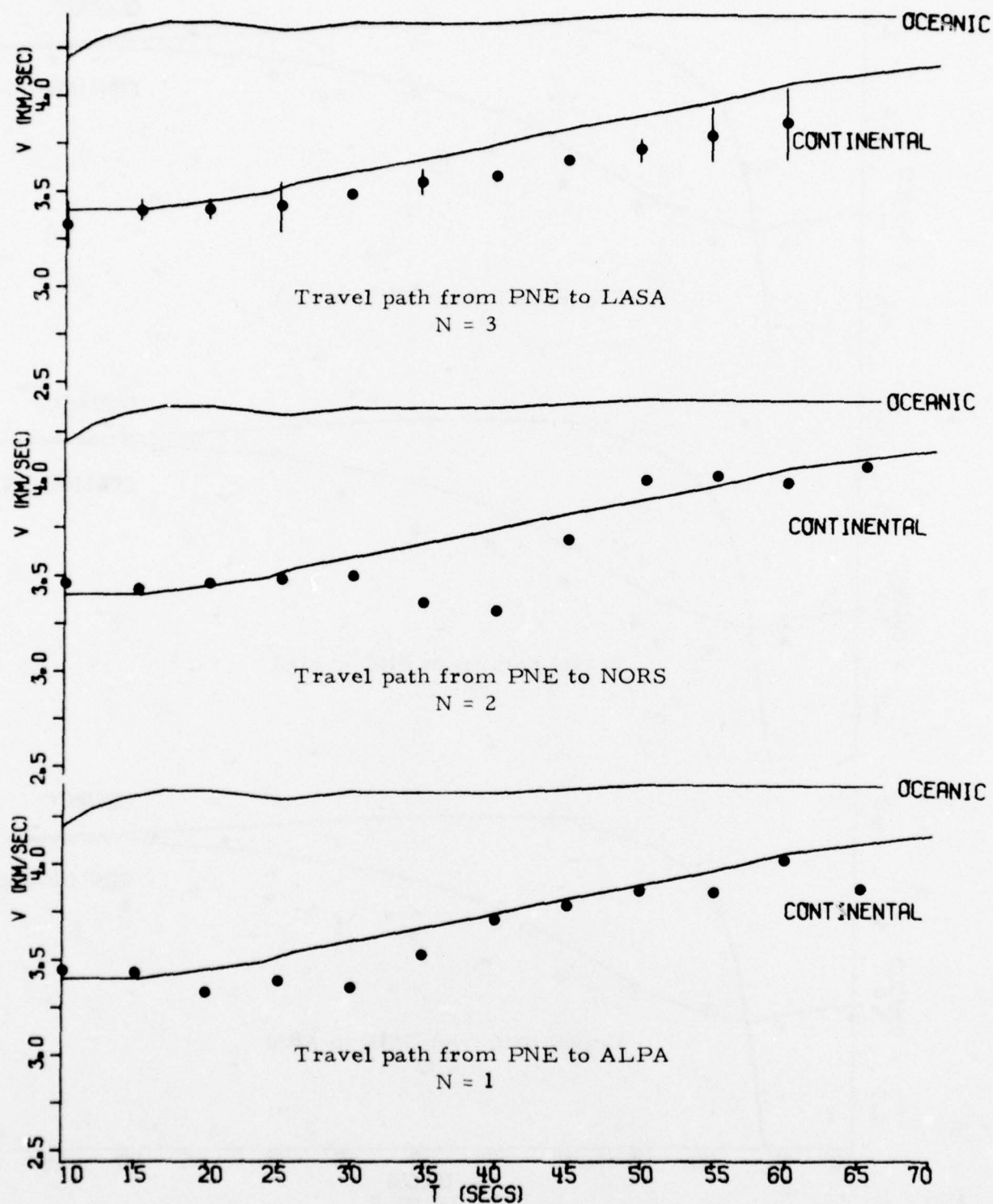


FIGURE III-8

OBSERVED LOVE WAVE GROUP VELOCITIES ALONG
THE TRAVEL PATHS FROM THE PNE TO OBSERVATION STATIONS

a fairly smooth group velocity curve can be formed, except for the travel path from NTS to LASA. Thus no sudden changes in the velocity profiles of the earth along these travel paths are encountered.

- The level of the average group velocity curves can be well explained as typical continental or oceanic paths, except for the travel paths to the observation stations which are to the east of the NTS on the northern American continent.
- For the travel paths to the observation stations at LASA, OGD, ALQ, FN-WV, HN-ME, RK-ON, and CPSO which are on the northern American continent and east of NTS, the levels of the average group velocity curves are lower than that for the typical continental path, especially at the longer periods and for the travel paths to LASA and ALQ which are very close to the NTS. For the travel paths to LASA and ALQ, the deviation of the group velocities from the rest of the travel paths might be partially due to the fact that the epicentral distance is short. For such a short epicentral distance, the surface waves might not be well dispersed and the calculated group velocities are very sensitive to the accuracy of the event locations and the origin times and to the analyst's arrival time picks. In addition, for these travel paths, the group velocities exhibit with varying degree reverse dispersion (i. e., group velocity decreasing with increasing period) at periods above 50 seconds.

Referring to Figure III-4, which gives the Love wave group velocities for the travel paths from NTS to the observation stations, the above remarks for the Rayleigh wave group velocities along the same travel paths are thought, in general, to be applicable here. However, it is noticed that the group velocities for the travel paths to CTA, KIP, MAT, and GUM,

which are entirely oceanic, are more irregular and deviate more from those for the typical oceanic path as compared to those for the Rayleigh waves along the same travel paths. Considering that the observed Rayleigh wave group velocities can be well explained with a typical ocean path Rayleigh wave group velocity curve, the large deviations of observed Love wave group velocities from those for the typical oceanic path seem surprising. Although the physical irregularities involved in these travel paths are not known, these observed irregularities in the obtained Love wave group velocities might be due to the inherent nature of the Love wave propagation which is more sensitive to travel path irregularities and is more susceptible to multipath effects than is the Rayleigh wave.

Figures III-5 and III-6 show measured Rayleigh and Love wave group velocities from EKA to the observation stations. As compared to travel paths from NTS to the observation stations, there are fewer events used to form the average group velocities for these travel paths. In fact, the Rayleigh wave group velocities for half of the event-station paths shown in Figure III-5 are obtained from just one EKZ event, and the Love wave group velocities as shown in Figure III-6 are obtained only for five event-station paths. That is due to the fact that there are fewer events and observation stations available for EKZ. Also, Love wave recordings for the EKZ events, in general, are scarce. Nevertheless, the Rayleigh wave group velocities shown in Figure III-5 are thought to be well behaved, even for those event-station paths where the group velocities are obtained from just one EKZ event. It is obvious, however, that the travel path from EKZ to CHG shows very low group velocities. These low group velocities are consistent with the previous observations at CHG for the central Eurasian earthquakes and the eastern Kazakh explosions (Turnbull, et al., 1973). The travel paths from central Eurasia to CHG encounter fairly complicated geological features in central Eurasia: the abnormally thick crust (about 60 km thickness) of the Tibet platform, and the

Himalayan fold system. Thus, these low group velocities are thought to be normal for the central Eurasia to CHG travel paths.

The average group velocities, as shown in Figures III-7 and III-8, for the travel paths from the north Caspian Sea region to the observation stations are determined from just three PNE events. Except for the travel paths to NORSAR and LASA, the group velocities for the other four travel paths as indicated in Figure III-7 represent the results from just one PNE event. However, judging from the fairly smooth variation of these group velocities, similar results probably can be expected for the same travel paths from examining more events in this region.

B. OBSERVED SURFACE WAVE AMPLITUDE SPECTRA

1. Spectral Contents and Spectral Ratios

The observed surface wave amplitude spectra at all available observation stations for all selected events listed in Table II-1 have been obtained in the manner discussed in Subsection II-C and are displayed in Figures III-9 through III-35. For each event, the observed spectra have been equalized at all observation stations in order to make direct comparison possible. The spectral equalization means that raw observed surface wave spectra have been corrected for the station's instrument response, geometric spreading, and travel path attenuation. Hence, the spectra shown in Figures III-9 through III-35 are the spectra as they would be observed at the source. For the travel path correction, Tryggvason's attenuation correction (1965) has been employed for all event-station paths, except for the travel paths from EKZ and PNE to CHG where the attenuation coefficients calculated specifically for these travel paths (Turnbull, et al., 1973) have been used. The reason for using Tryggvason's correction will be given later when we discuss the travel path attenuation in Section IV. In each figure, available observed Rayleigh and Love wave spectra are displayed in part (a), side-by-side for each

(a) Amplitude Spectra

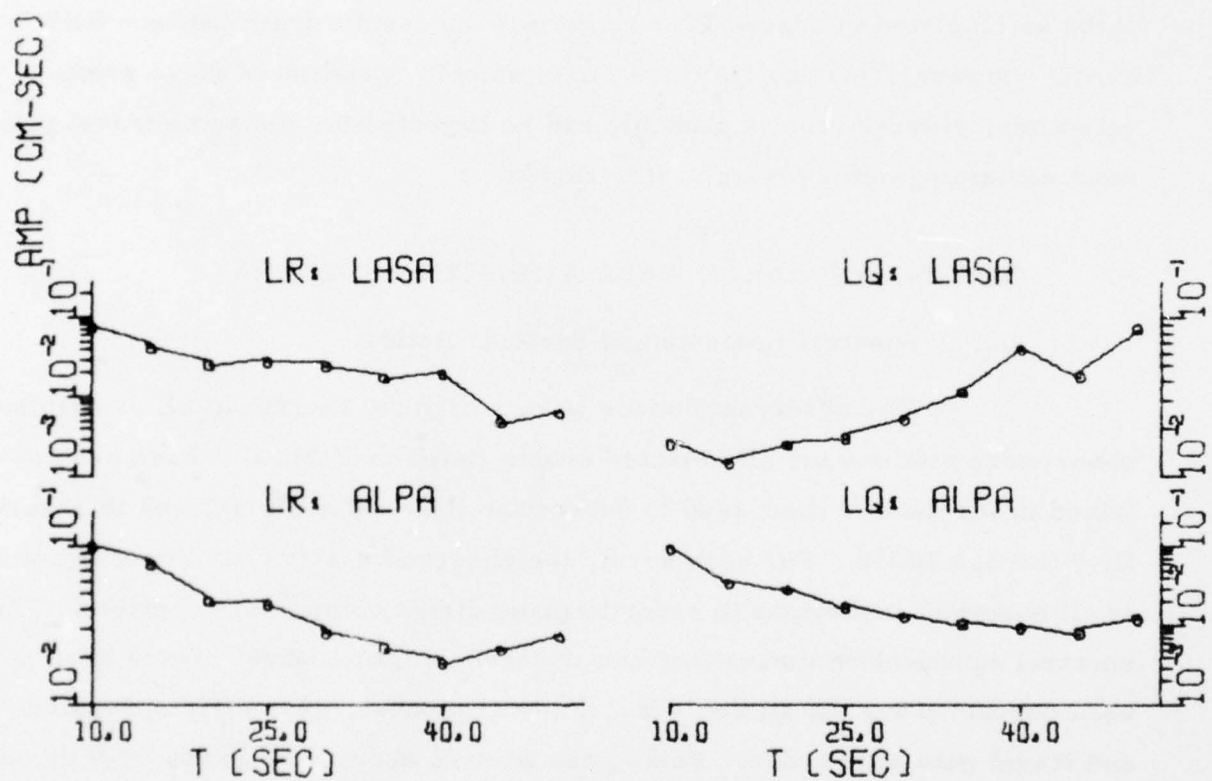


FIGURE III-9
OBSERVED SURFACE WAVE SPECTRA: NTS/926/74
(PAGE 1 OF 2)

(b) LQ/LR Amplitude Spectral Ratios

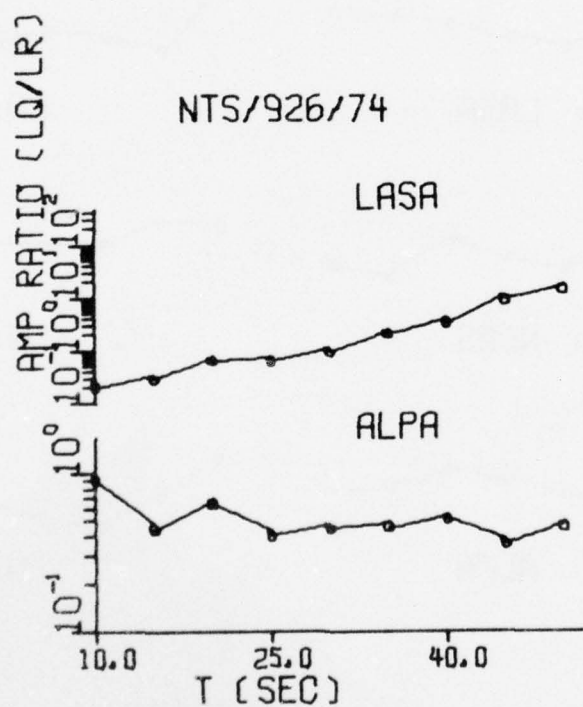


FIGURE III-9
OBSERVED SURFACE WAVE SPECTRA: NTS/926/74
(PAGE 2 OF 2)

(a) Amplitude Spectra

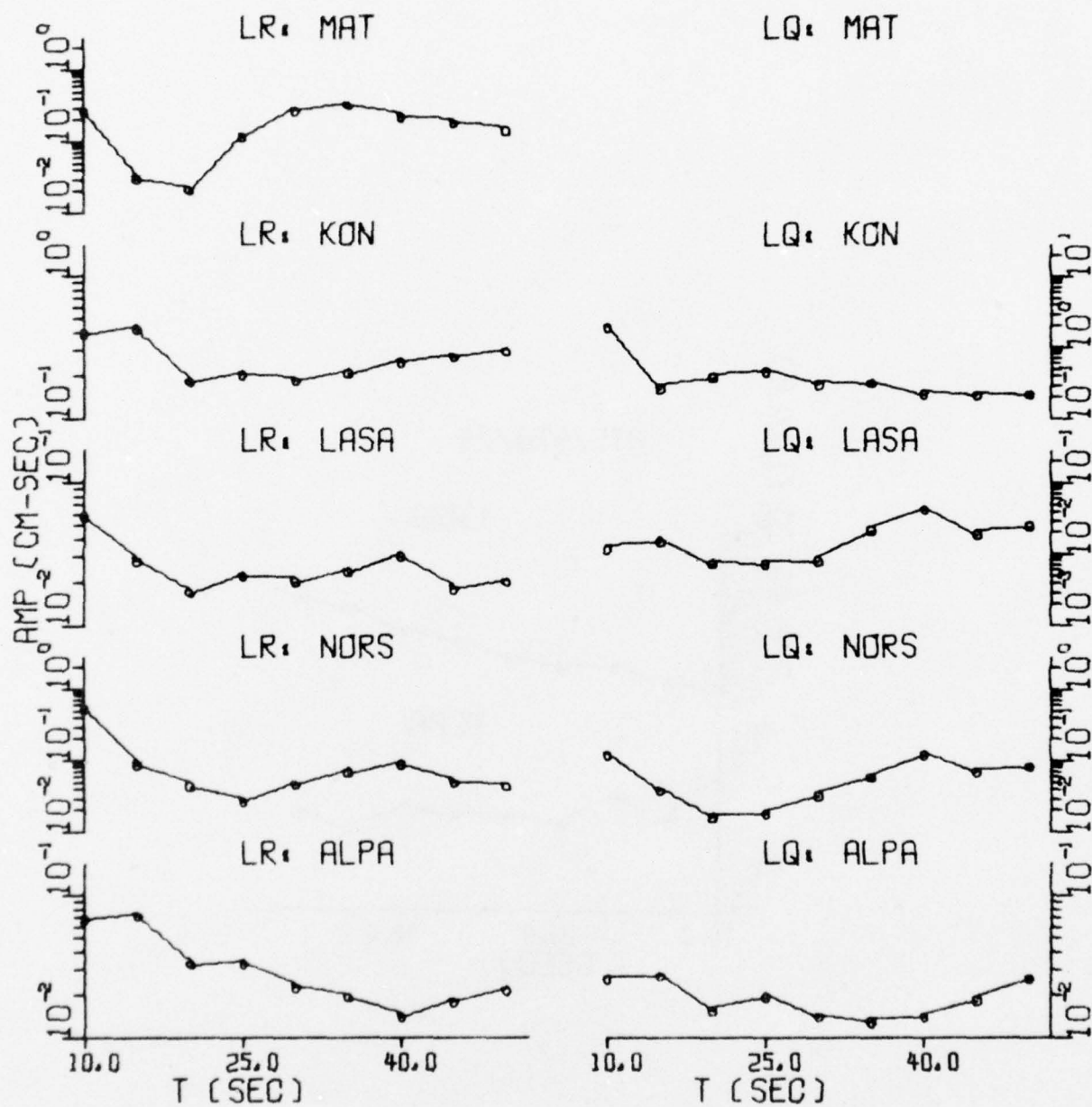


FIGURE III-10
OBSERVED SURFACE WAVE SPECTRA: NTS/430/75
(PAGE 1 OF 2)

(b) LQ/LR Amplitude Spectral Ratios

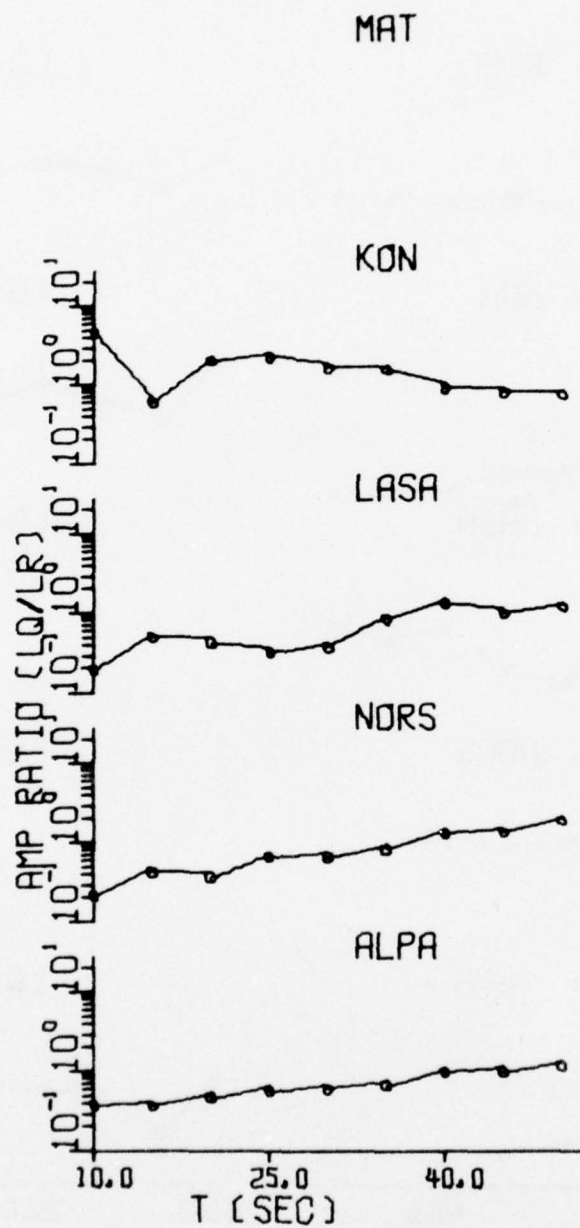


FIGURE III-10
OBSERVED SURFACE WAVE SPECTRA: NTS/430/75
(PAGE 2 OF 2)

(a) Amplitude Spectra

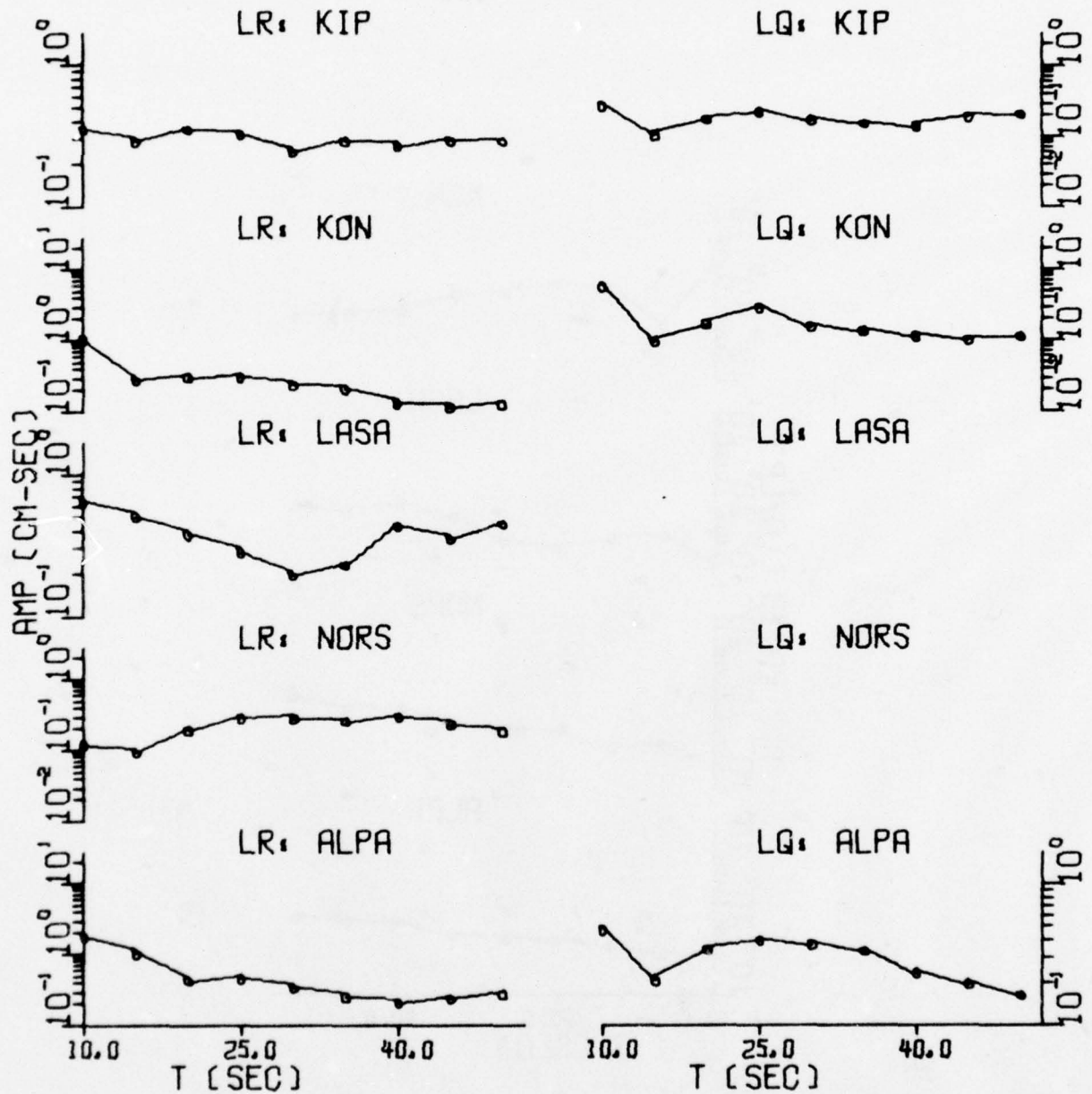


FIGURE III-11
OBSERVED SURFACE WAVE SPECTRA: NTS/514/75
(PAGE 1 OF 5)

(a) Amplitude Spectra

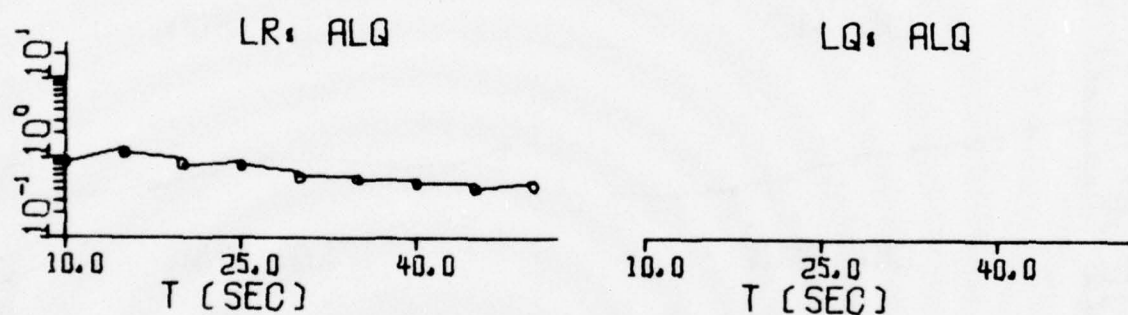


FIGURE III-11
OBSERVED SURFACE WAVE SPECTRA: NTS/514/75
(PAGE 2 OF 5)

(a) Amplitude Spectra

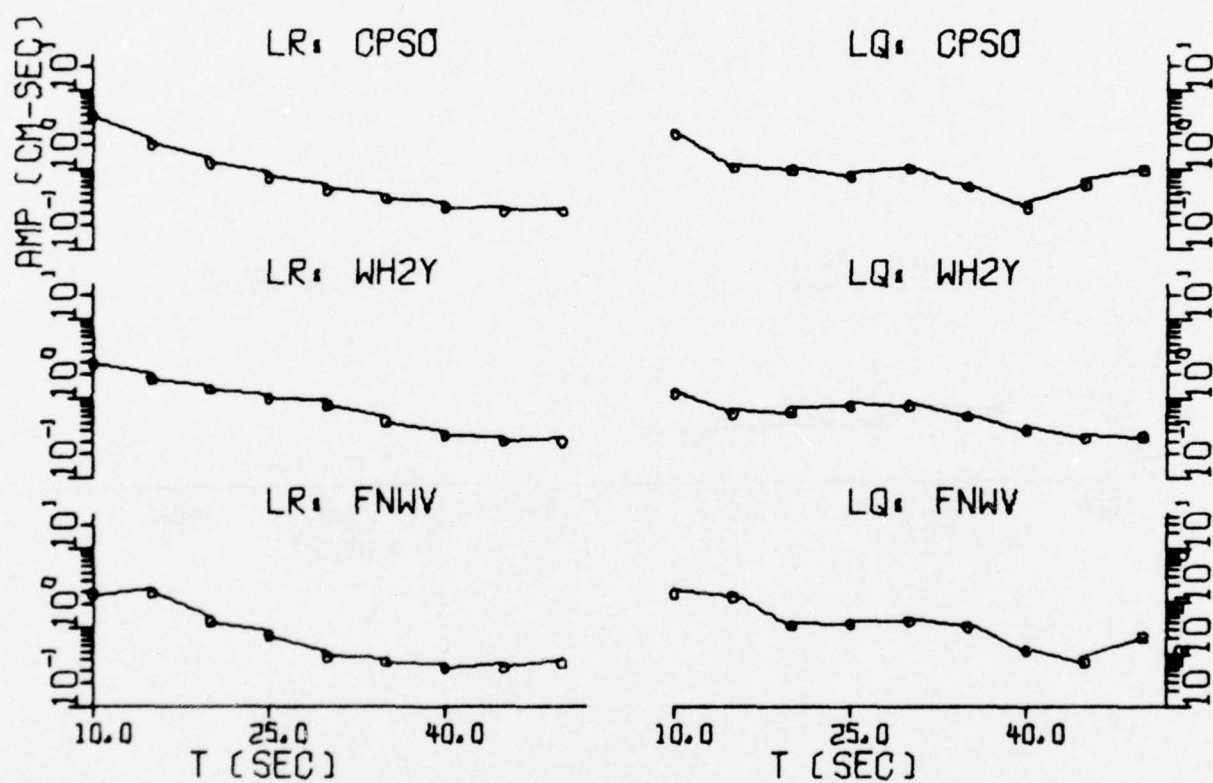


FIGURE III-11
OBSERVED SURFACE WAVE SPECTRA: NTS/514/75
(PAGE 3 OF 5)

(b) LQ/LR Amplitude Spectral Ratios

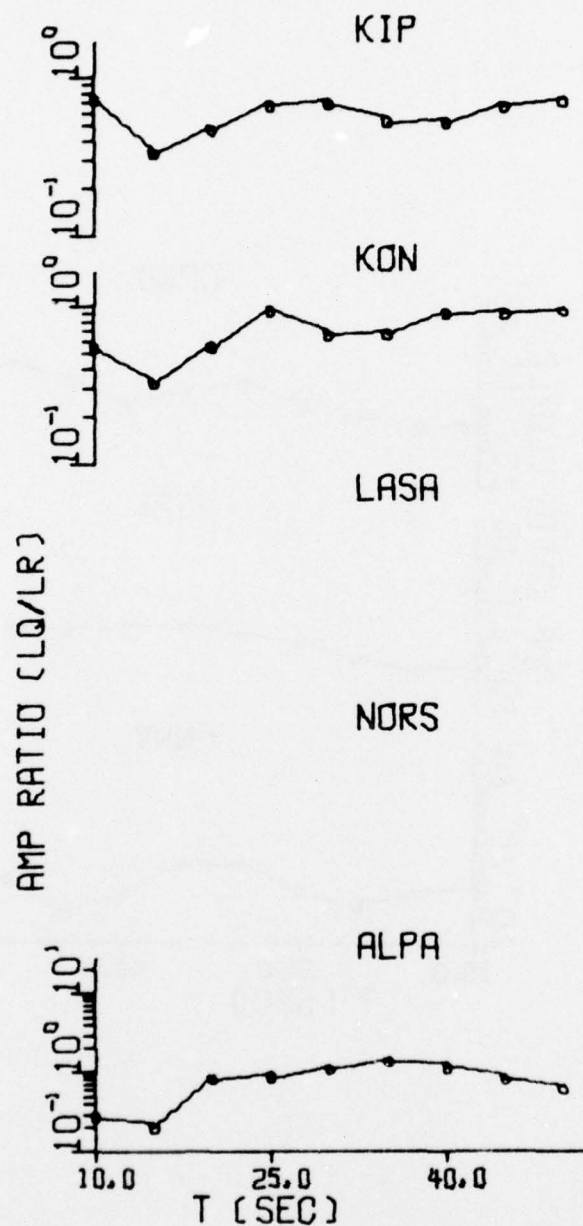


FIGURE III-11
OBSERVED SURFACE WAVE SPECTRA: NTS/514/75
(PAGE 4 OF 5)

(b) LQ/LR Amplitude Spectral Ratio

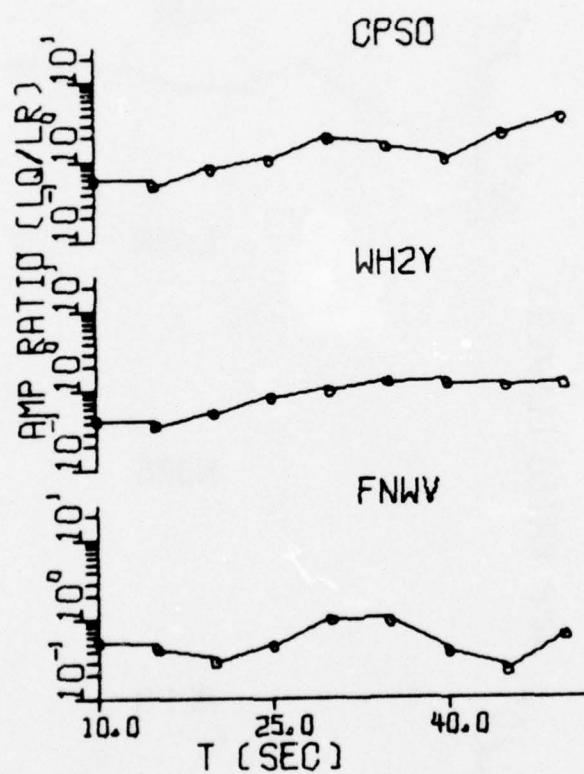


FIGURE III-11
OBSERVED SURFACE WAVE SPECTRA: NTS/514/75
(PAGE 5 OF 5)

(a) Amplitude Spectra

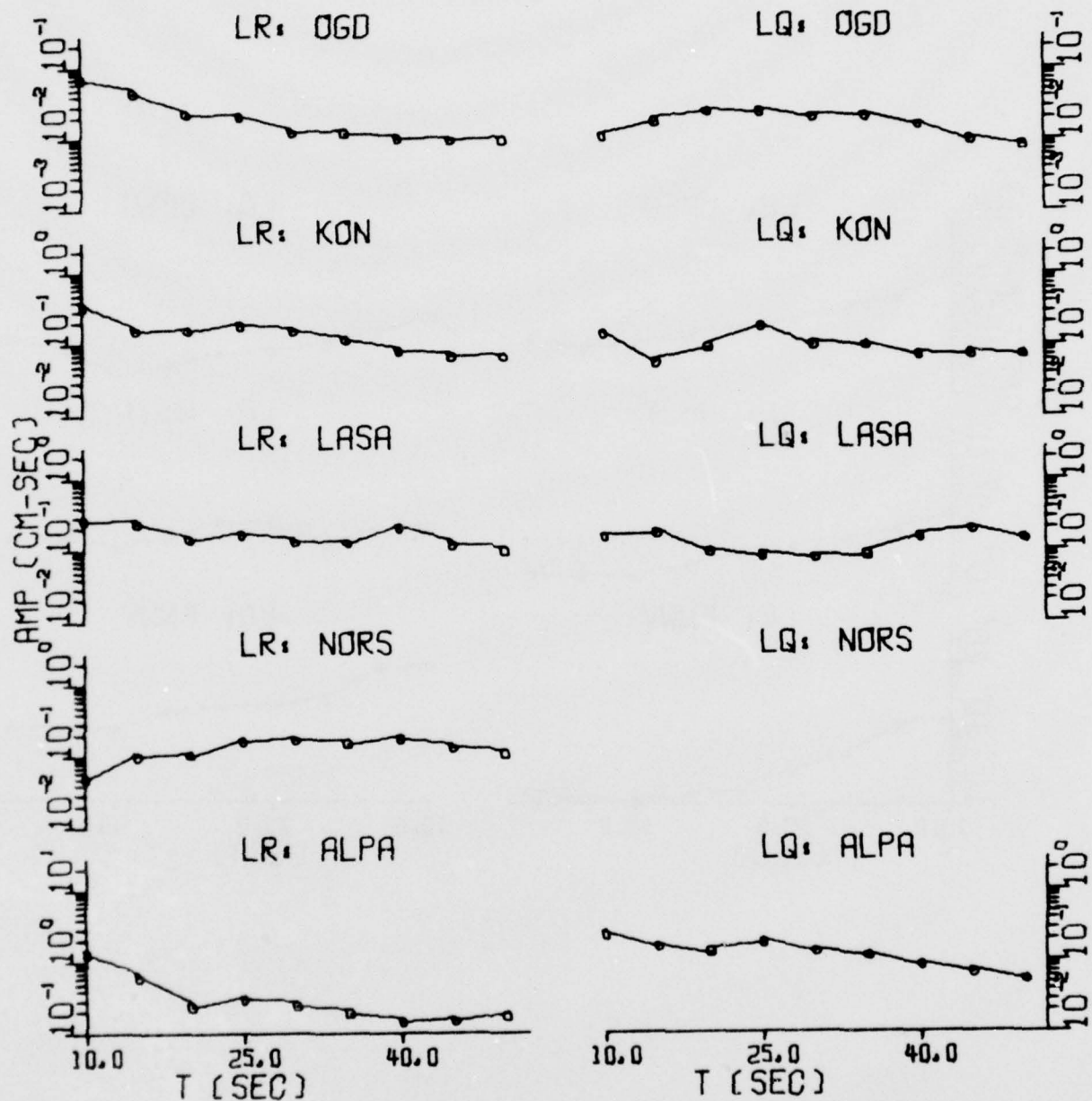


FIGURE III-12
OBSERVED SURFACE WAVE SPECTRA: NT1/603/75
(PAGE 1 OF 4)

(a) Amplitude Spectra

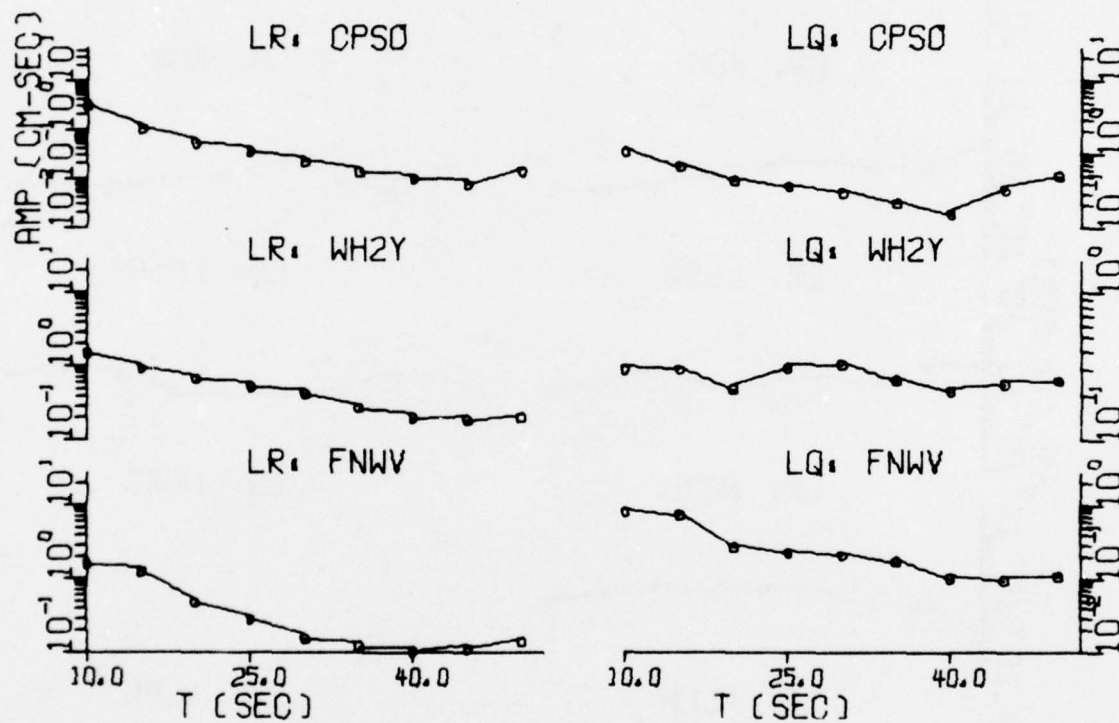


FIGURE III-12
OBSERVED SURFACE WAVE SPECTRA: NT1/603/75
(PAGE 2 OF 4)

(b) LQ/LR Amplitude Spectral Ratio

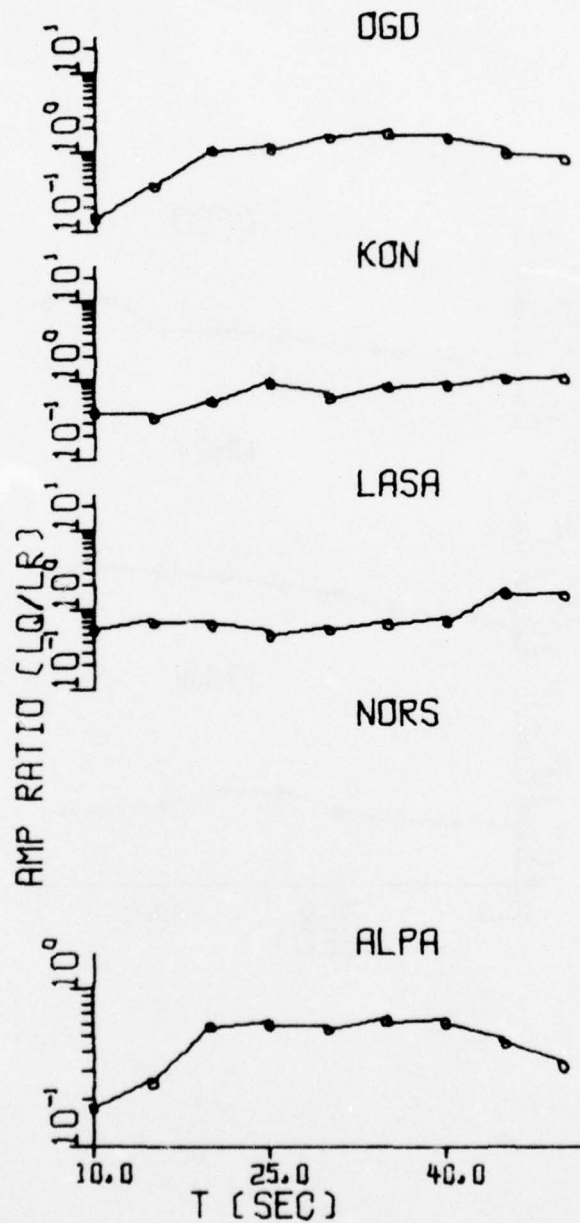


FIGURE III-12

OBSERVED SURFACE WAVE SPECTRA: NT1/603/75
(PAGE 3 OF 4)

(b) LQ/LR Amplitude Spectral Ratio

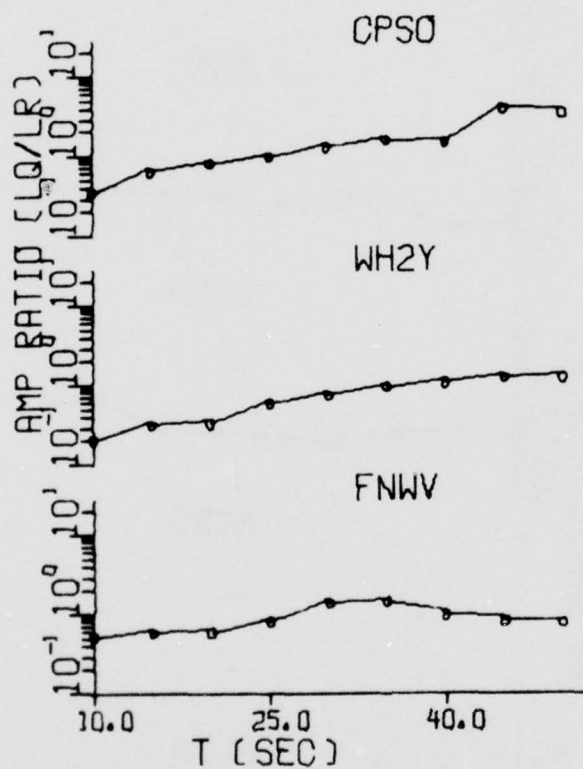


FIGURE III-12
OBSERVED SURFACE WAVE SPECTRA: NT1/603/75
(PAGE 4 OF 4)

(a) Amplitude Spectra

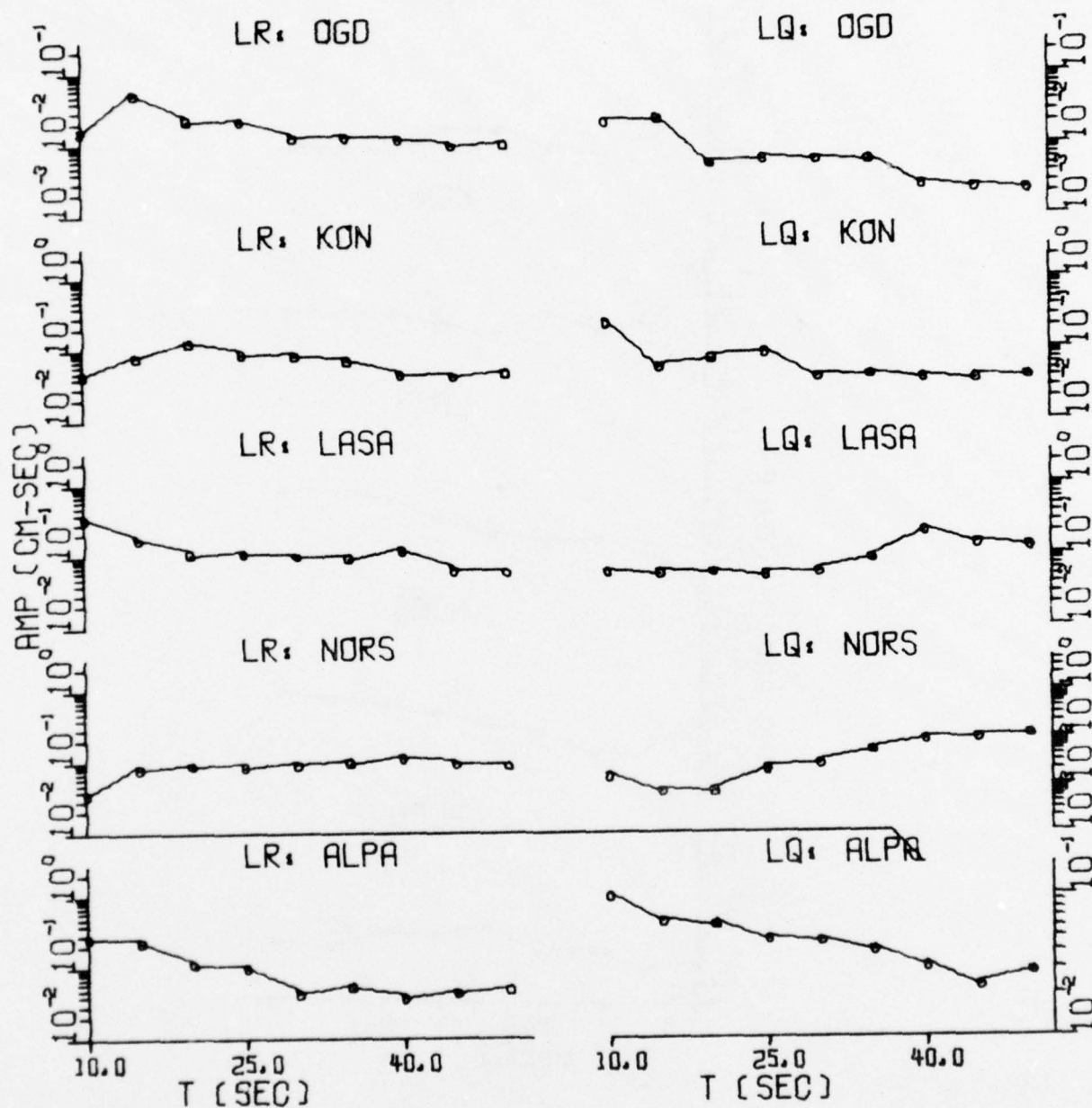


FIGURE III-13
OBSERVED SURFACE WAVE SPECTRA: NT2/603/75
(PAGE 1 OF 2)

(b) LQ/LR Amplitude Spectral Ratio

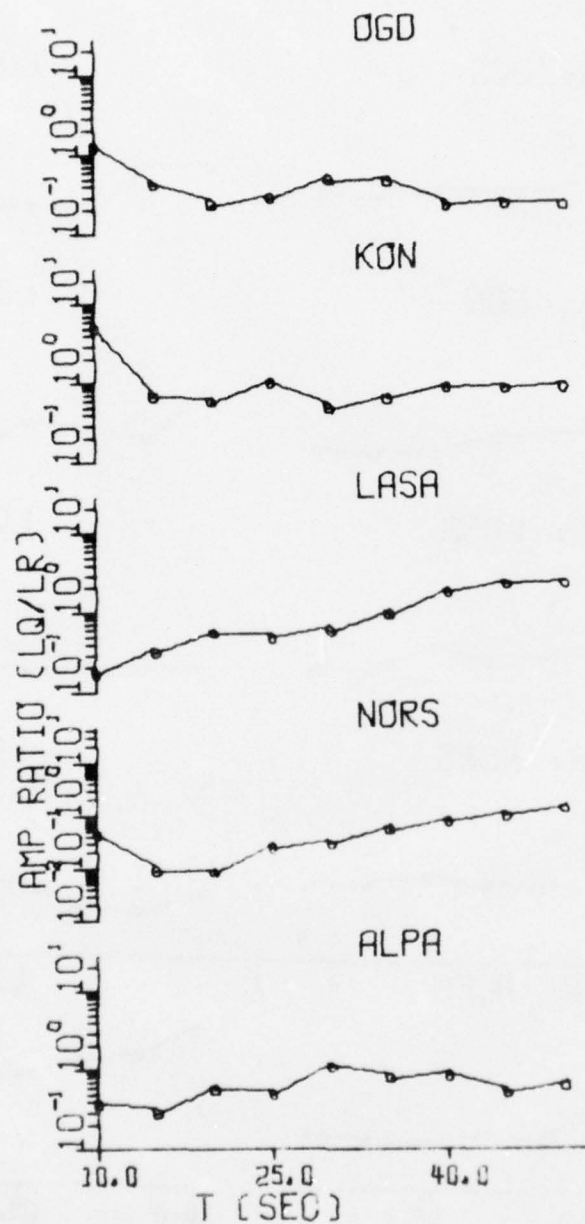


FIGURE III-13
OBSERVED SURFACE WAVE SPECTRA: NT2/603/75
(PAGE 2 OF 2)

(a) Amplitude Spectra

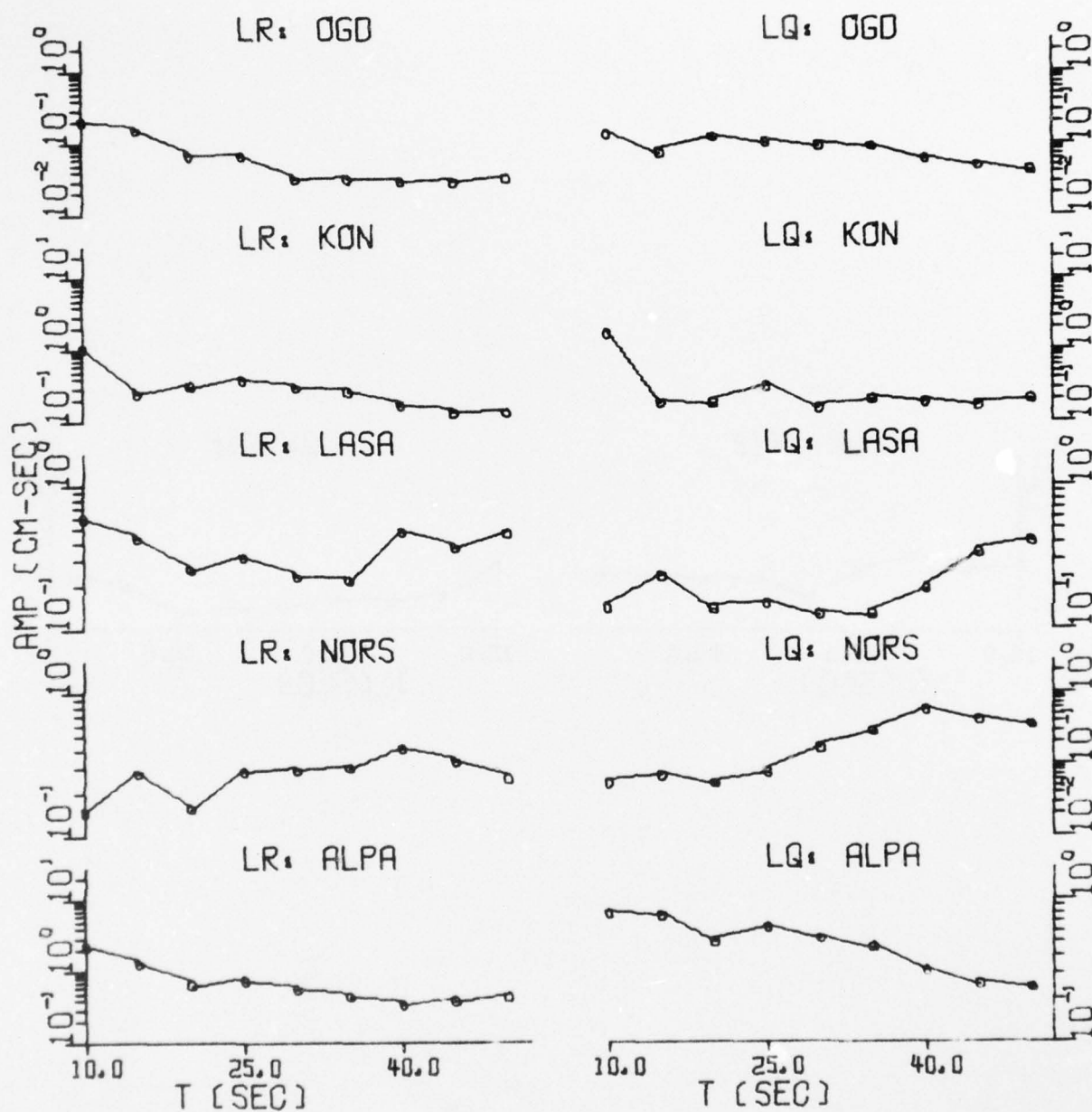


FIGURE III-14
OBSERVED SURFACE WAVE SPECTRA: NTS/619/75
(PAGE 1 OF 6)

(a) Amplitude Spectra

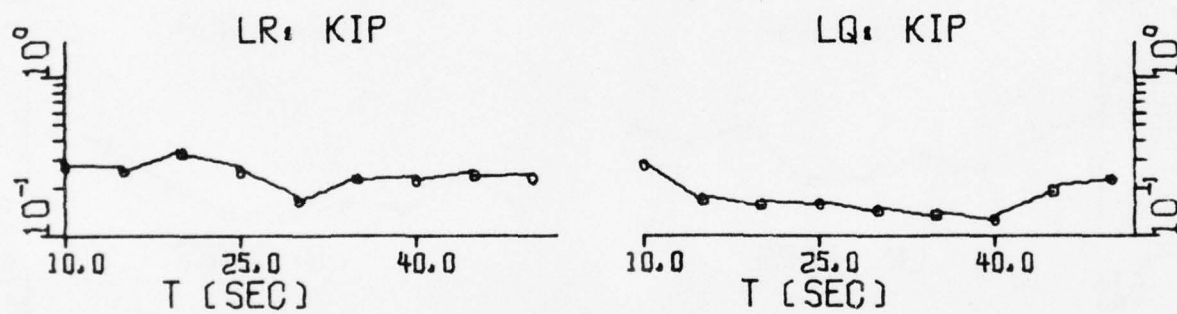


FIGURE III-14
OBSERVED SURFACE WAVE SPECTRA: NTS/619/75
(PAGE 2 OF 6)

(a) Amplitude Spectra

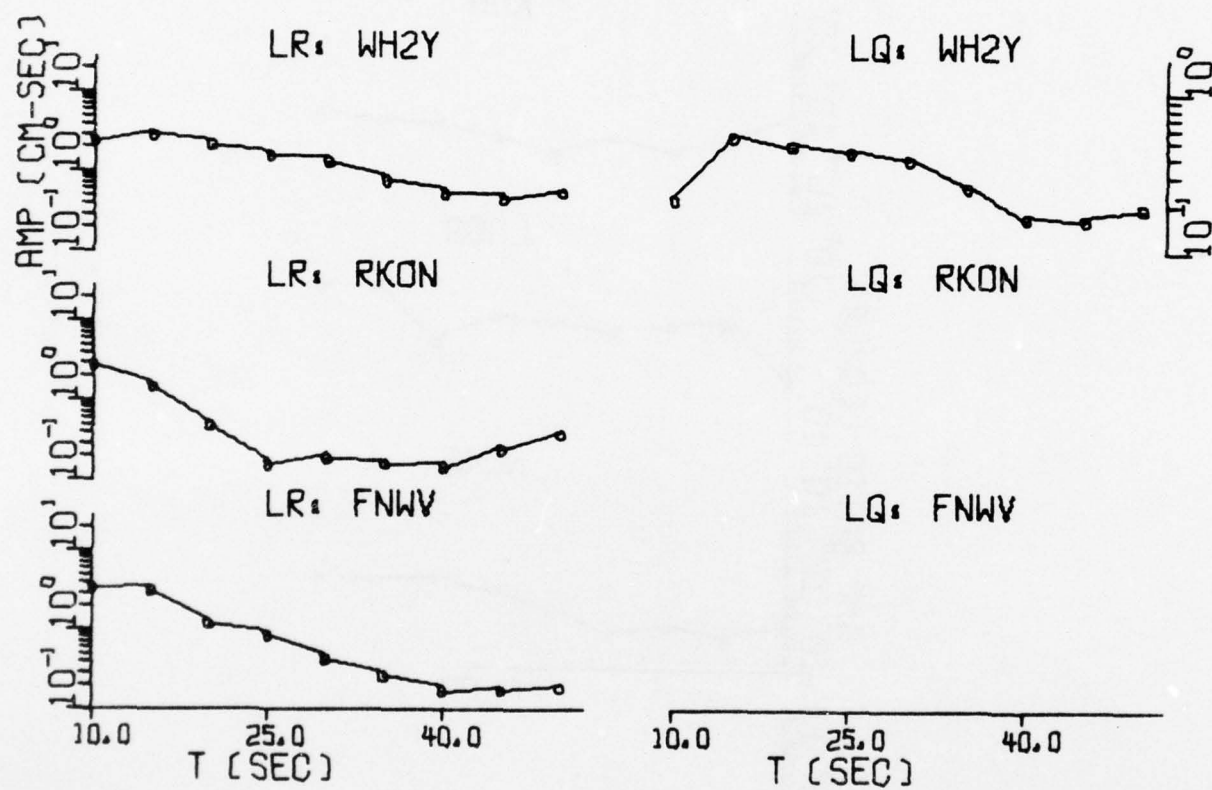


FIGURE III-14
OBSERVED SURFACE WAVE SPECTRA: NTS/619/75
(PAGE 3 OF 6)

(b) LQ/LR Amplitude Spectral Ratio

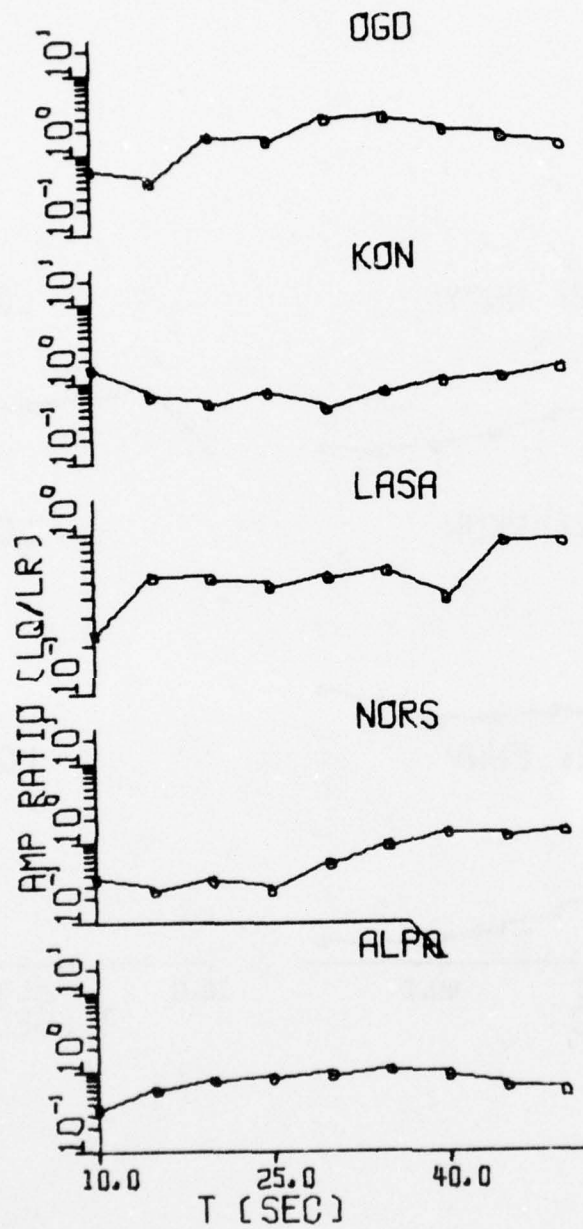


FIGURE III-14

OBSERVED SURFACE WAVE SPECTRA: NTS/619/75
(PAGE 4 OF 6)

(b) LQ/LR Amplitude Spectral Ratio

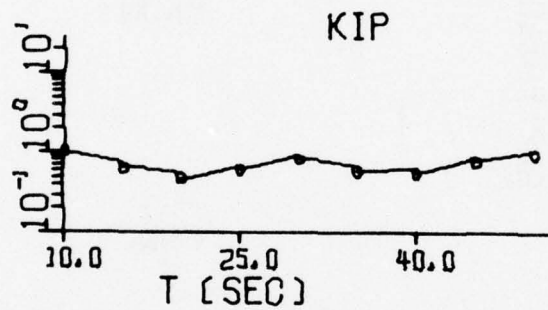


FIGURE III-14
OBSERVED SURFACE WAVE SPECTRA: NTS/619/75
(PAGE 5 OF 6)

(b) LQ/LR Amplitude Spectral Ratio

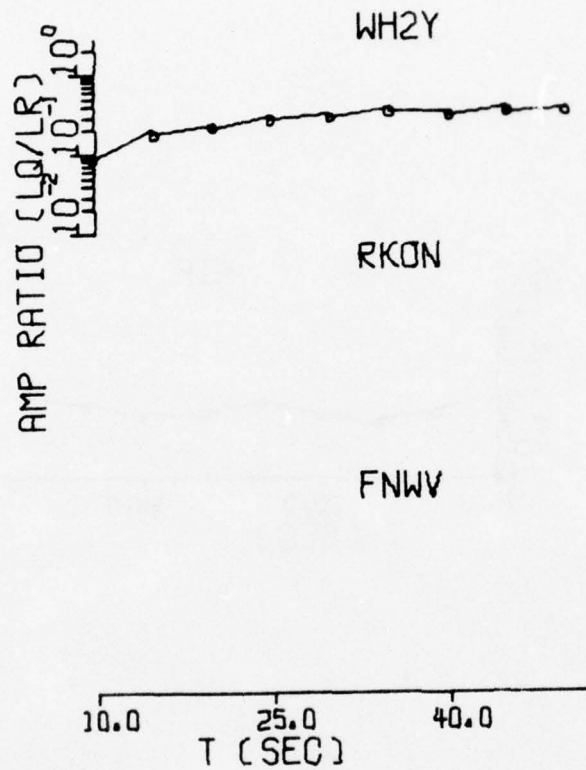


FIGURE III-14
OBSERVED SURFACE WAVE SPECTRA: NTS/619/75
(PAGE 6 OF 6)

(a) Amplitude Spectra

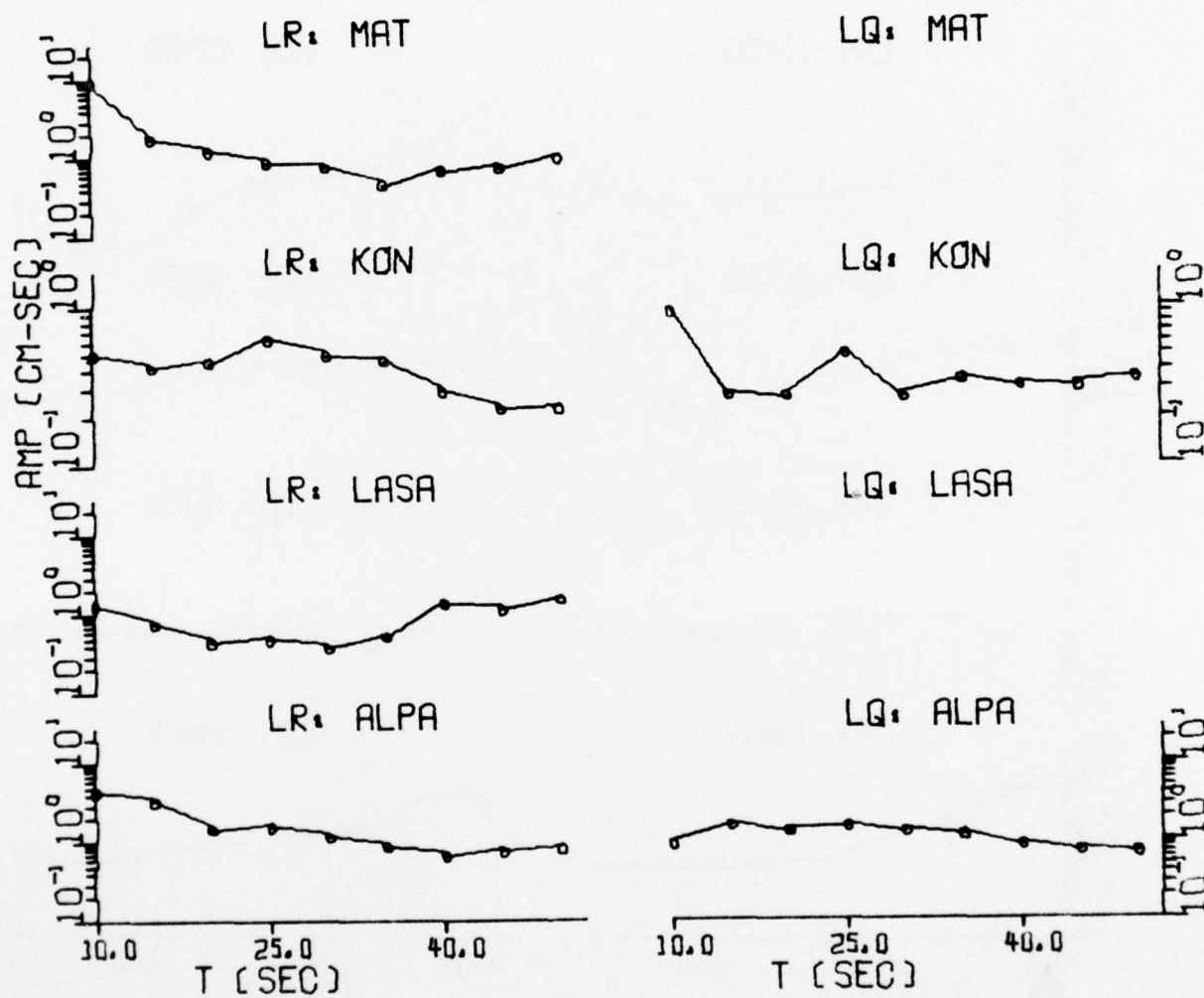


FIGURE III-15
OBSERVED SURFACE WAVE SPECTRA: NTS/626/75
(PAGE 1 OF 4)

(a) Amplitude Spectra

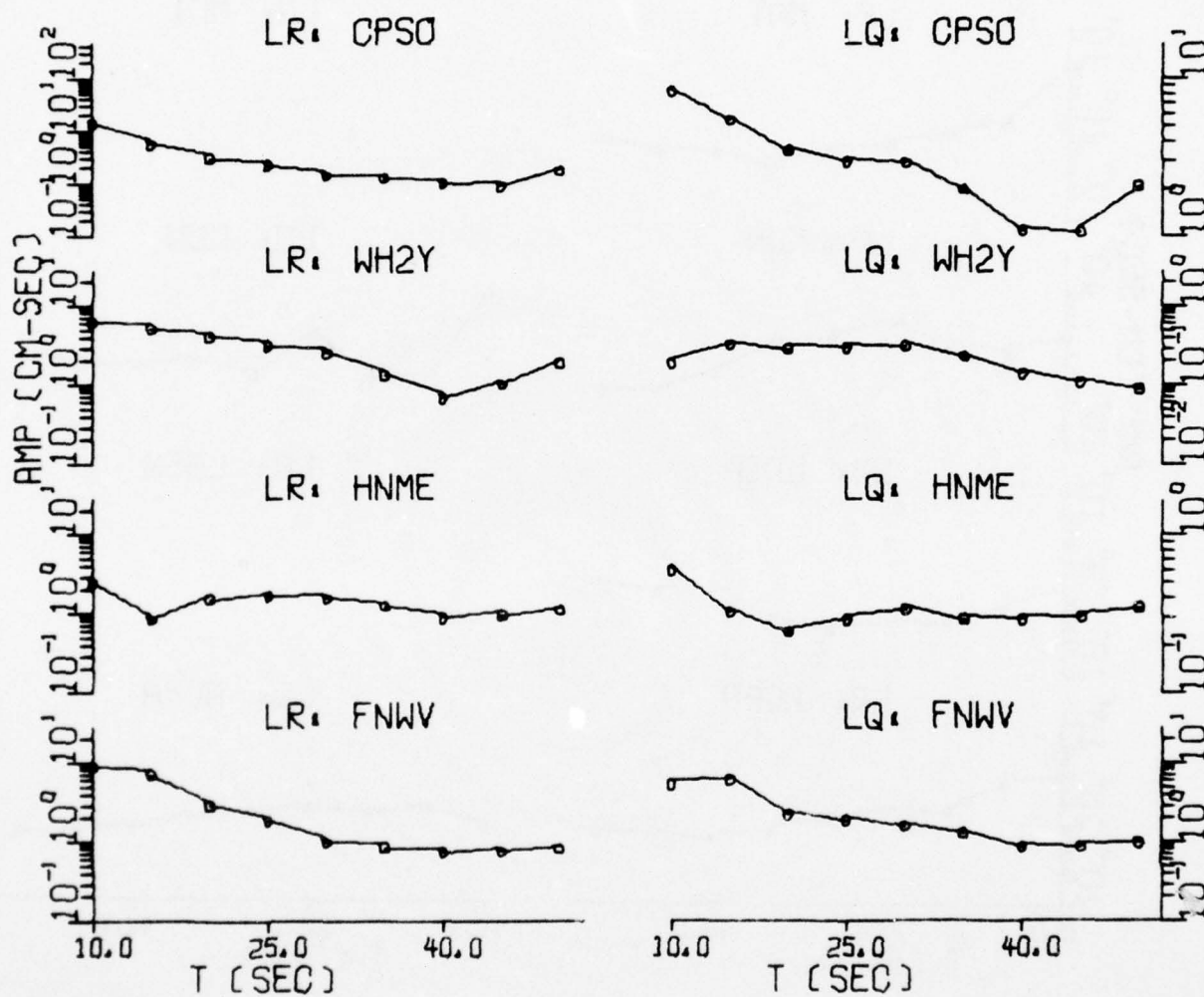


FIGURE III-15
OBSERVED SURFACE WAVE SPECTRA: NTS/626/75
(PAGE 2 OF 4)

(b) LQ/LR Amplitude Spectral Ratio

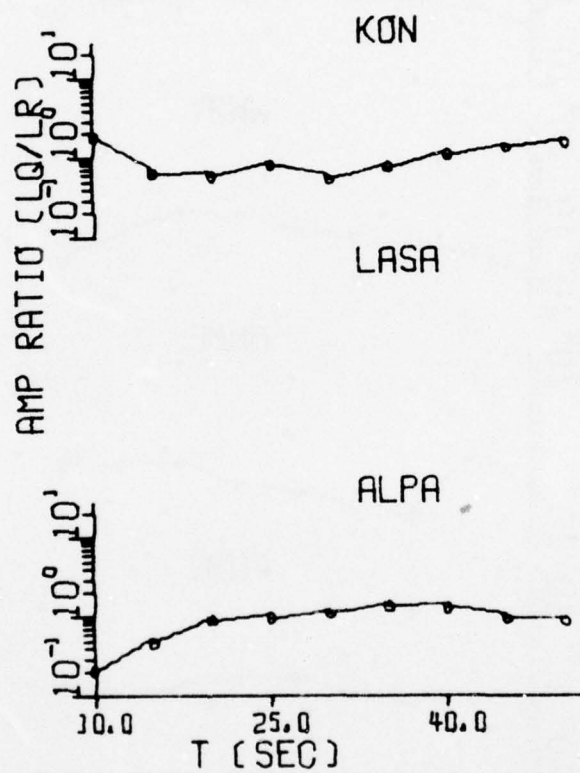


FIGURE III-15
OBSERVED SURFACE WAVE SPECTRA: NTS/626/75
(PAGE 3 OF 4)

(b) LQ/LR Amplitude Spectral Ratio

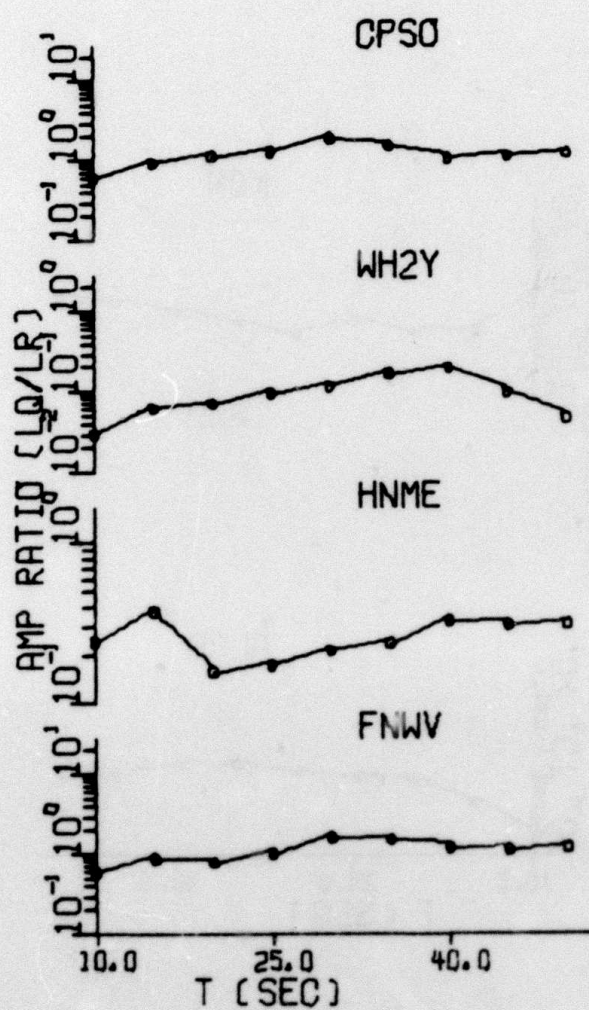


FIGURE III-15
OBSERVED SURFACE WAVE SPECTRA: NTS/626/75
(PAGE 4 OF 4)

(a) Amplitude Spectra

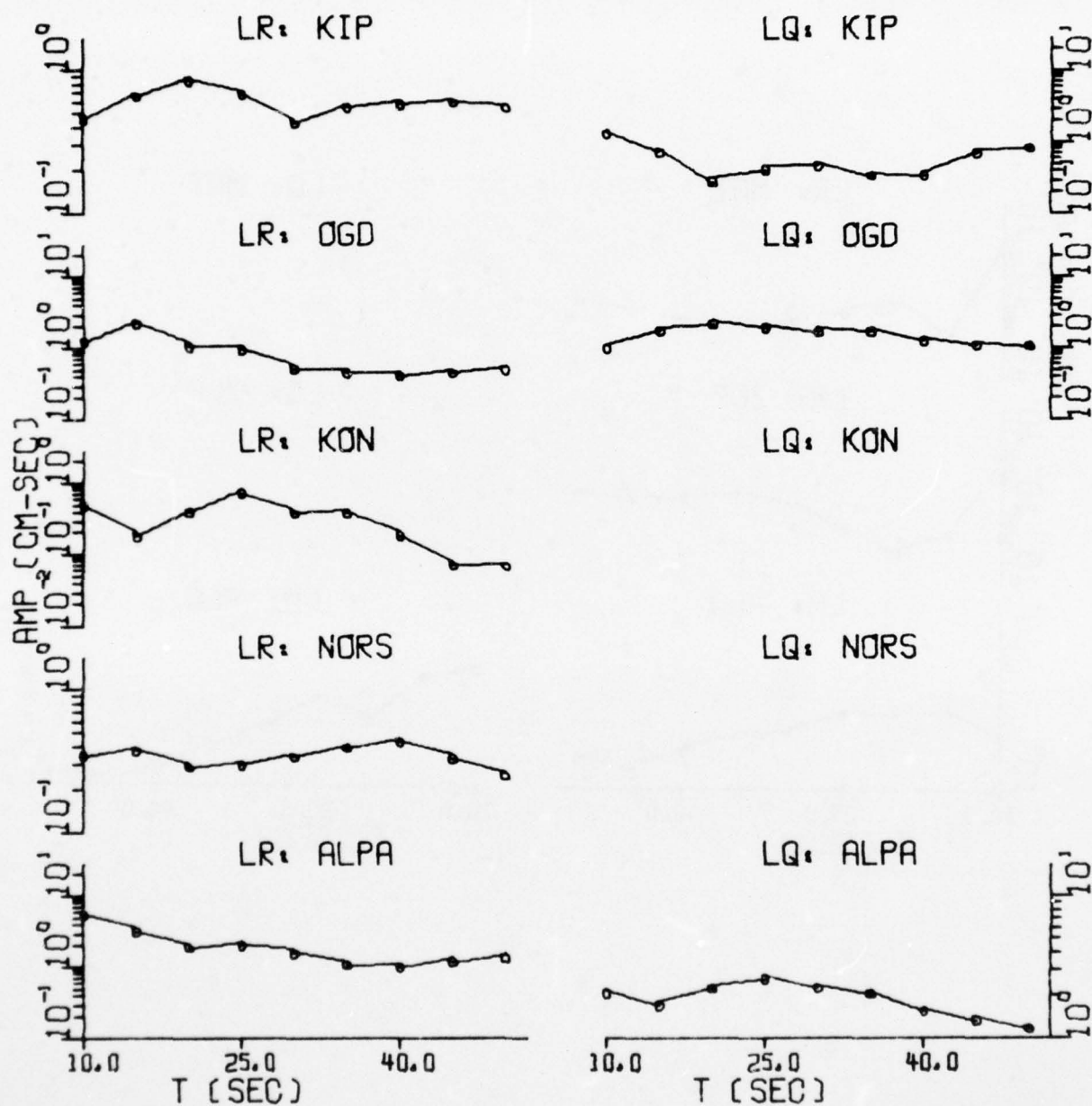


FIGURE III-16
OBSERVED SURFACE WAVE SPECTRA: NTS/1028/5
(PAGE 1 OF 6)

(a) Amplitude Spectra

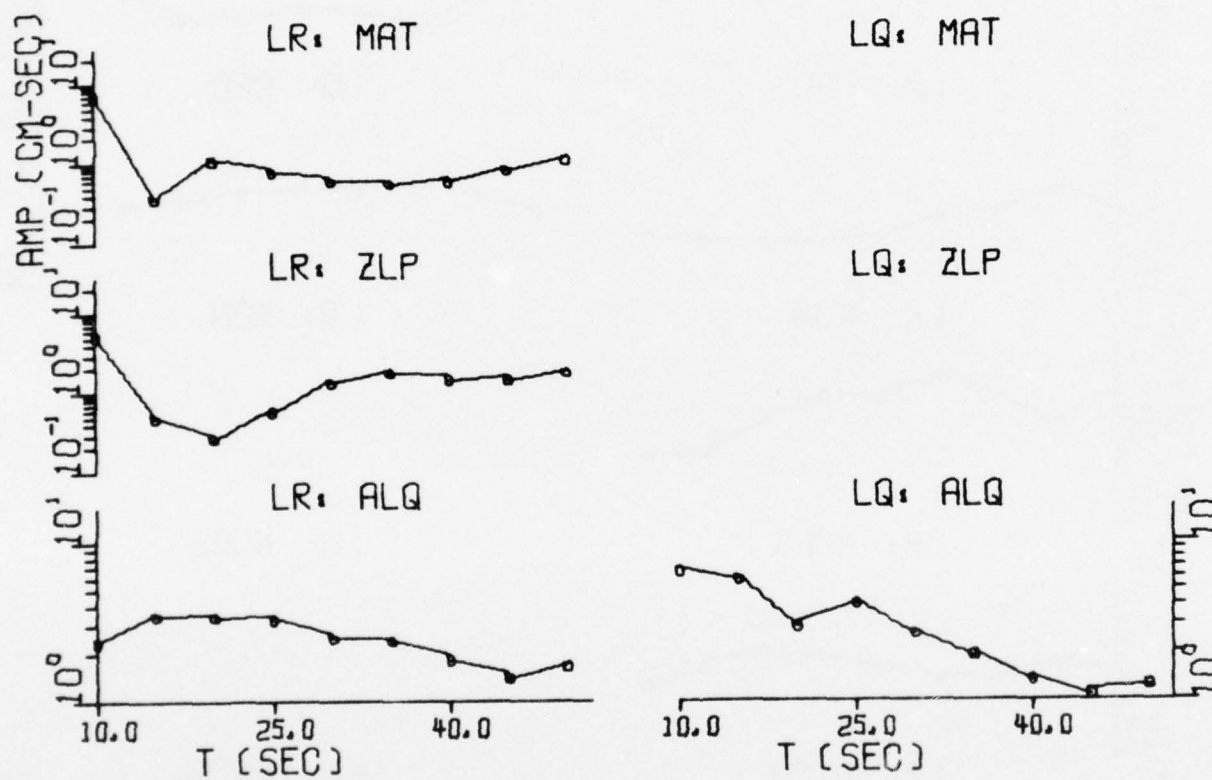


FIGURE III-16

OBSERVED SURFACE WAVE SPECTRA: NTS/1028/5
(PAGE 2 OF 6)

(a) Amplitude Spectra

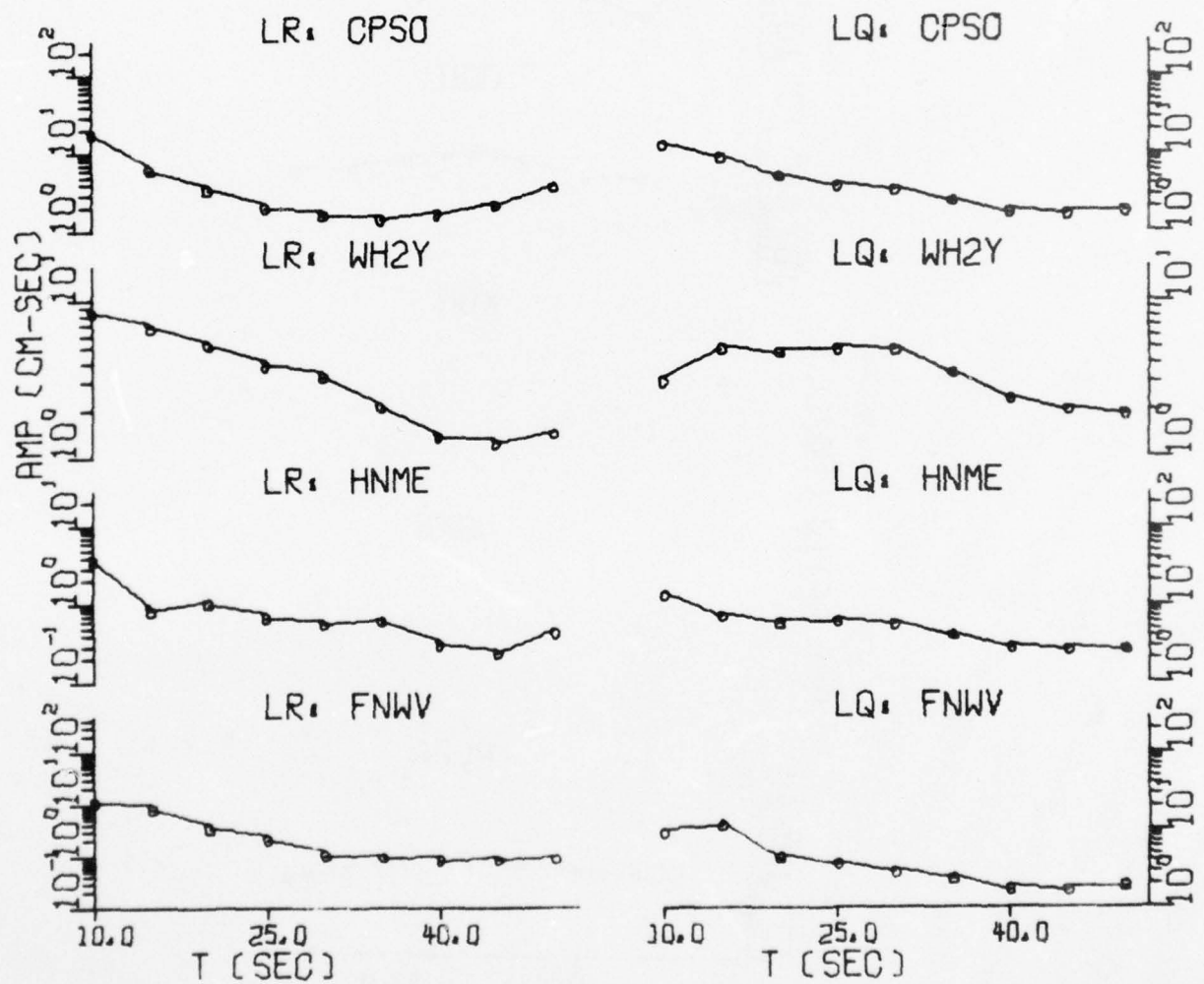


FIGURE III-16
OBSERVED SURFACE WAVE SPECTRA: NTS/1028/5
(PAGE 3 OF 6)

(b) LQ/LR Amplitude Spectral Ratio

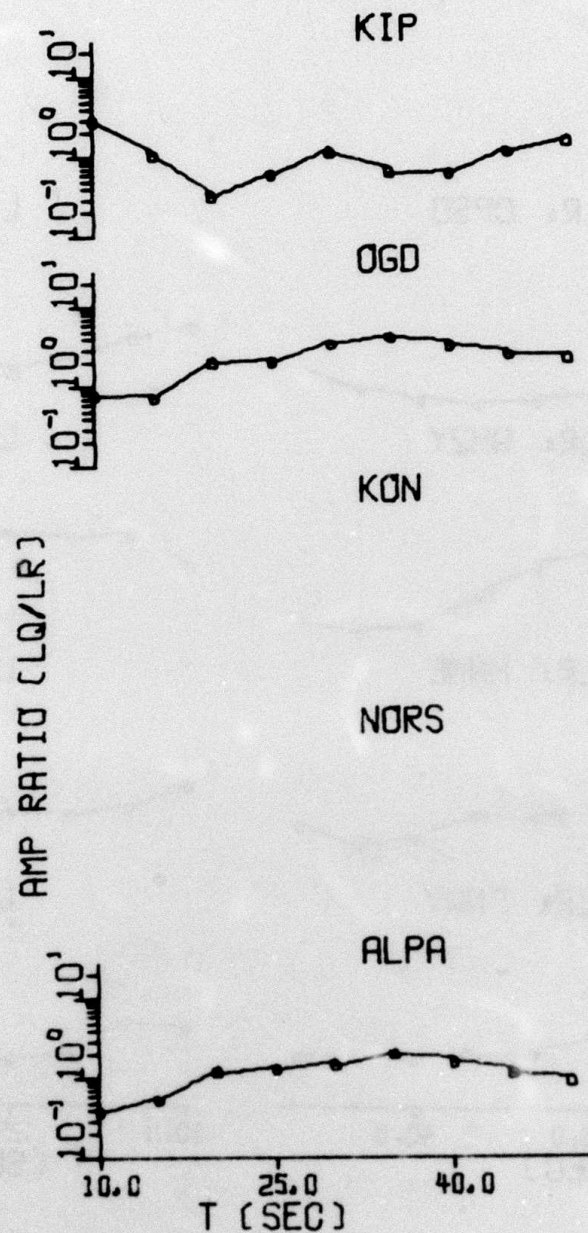


FIGURE III-16
OBSERVED SURFACE WAVE SPECTRA: NTS/1028/5
(PAGE 4 OF 6)

(b) LQ/LR Amplitude Spectral Ratio

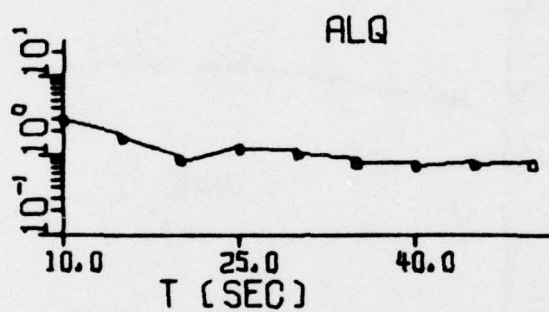


FIGURE III-16
OBSERVED SURFACE WAVE SPECTRA: NTS/1028/5
(PAGE 5 OF 6)

(b) LQ/LR Amplitude Spectral Ratio

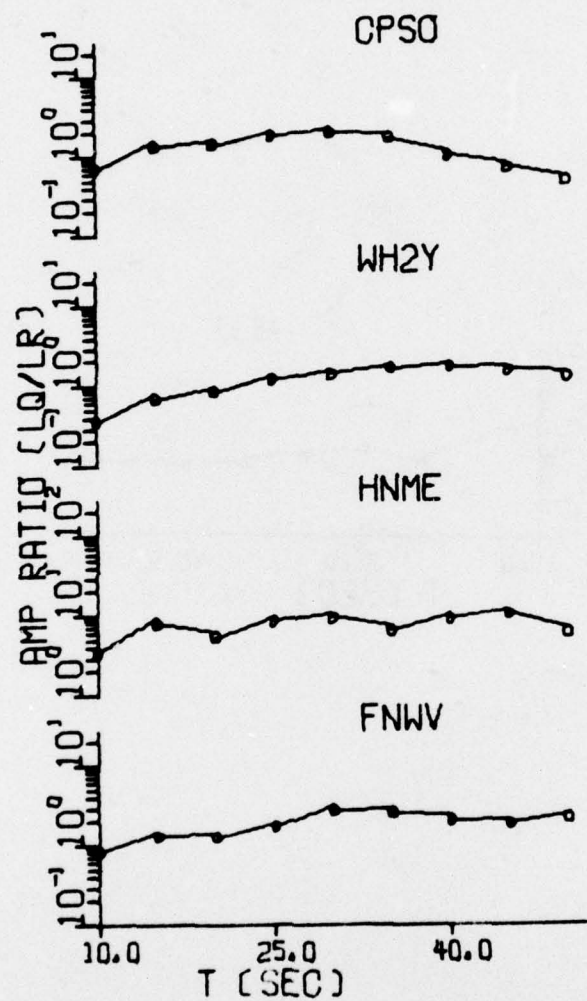


FIGURE III-16
OBSERVED SURFACE WAVE SPECTRA: NTS/1028/5
(PAGE 6 OF 6)

(a) Amplitude Spectra

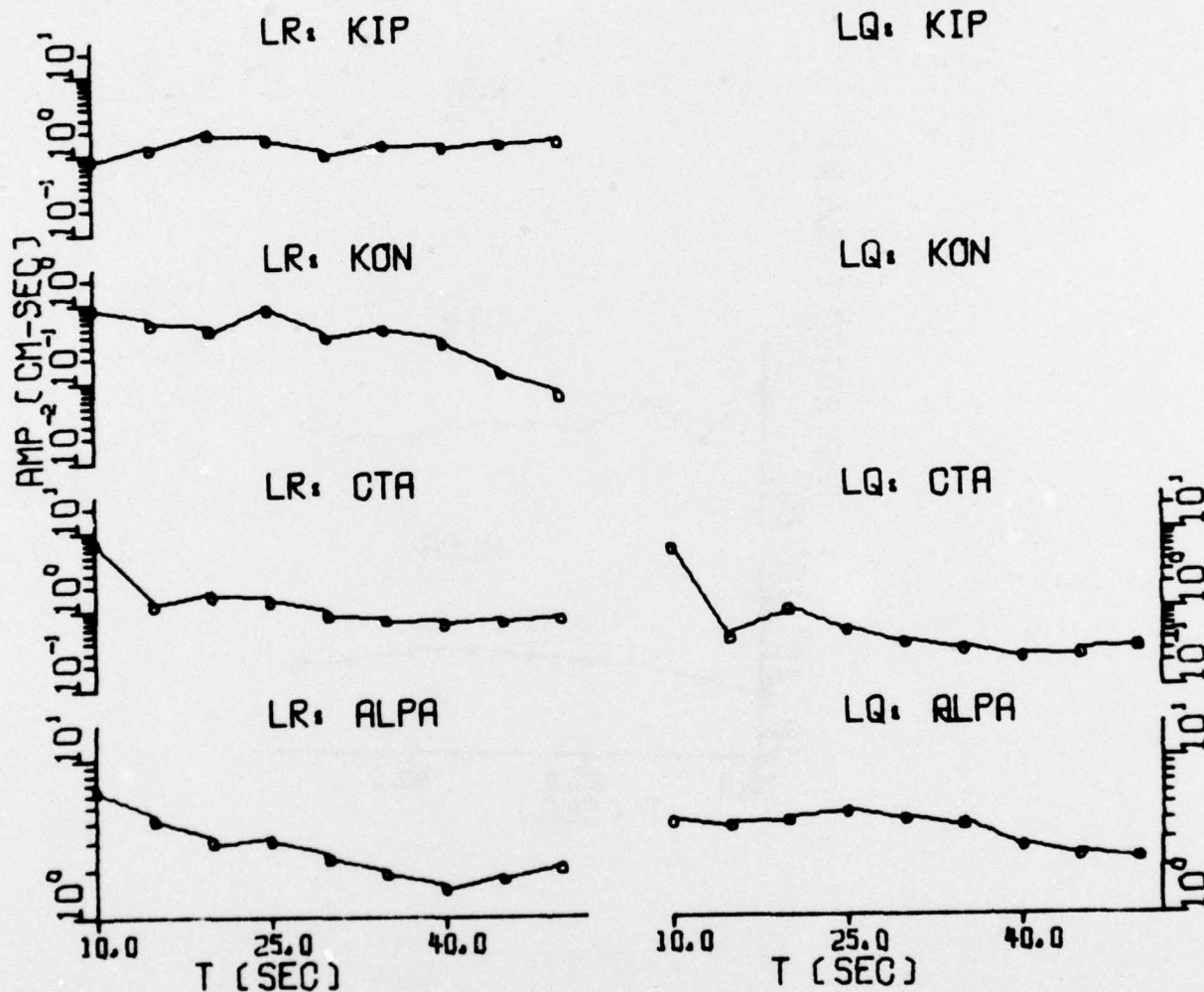


FIGURE III-17
OBSERVED SURFACE WAVE SPECTRA: NTS/103/76
(PAGE 1 OF 2)

(b) LQ/LR Amplitude Spectral Ratio

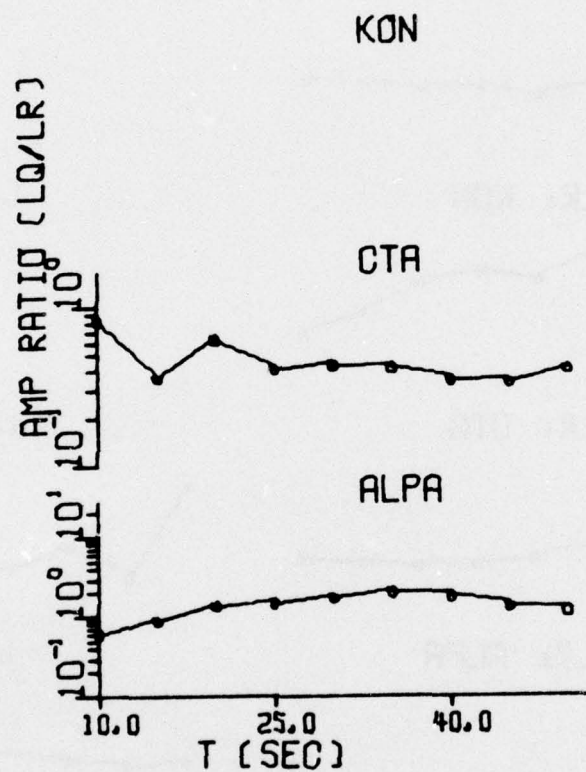


FIGURE III-17
OBSERVED SURFACE WAVE SPECTRA: NTS/103/76
(PAGE 2 OF 2)

(a) Amplitude Spectra

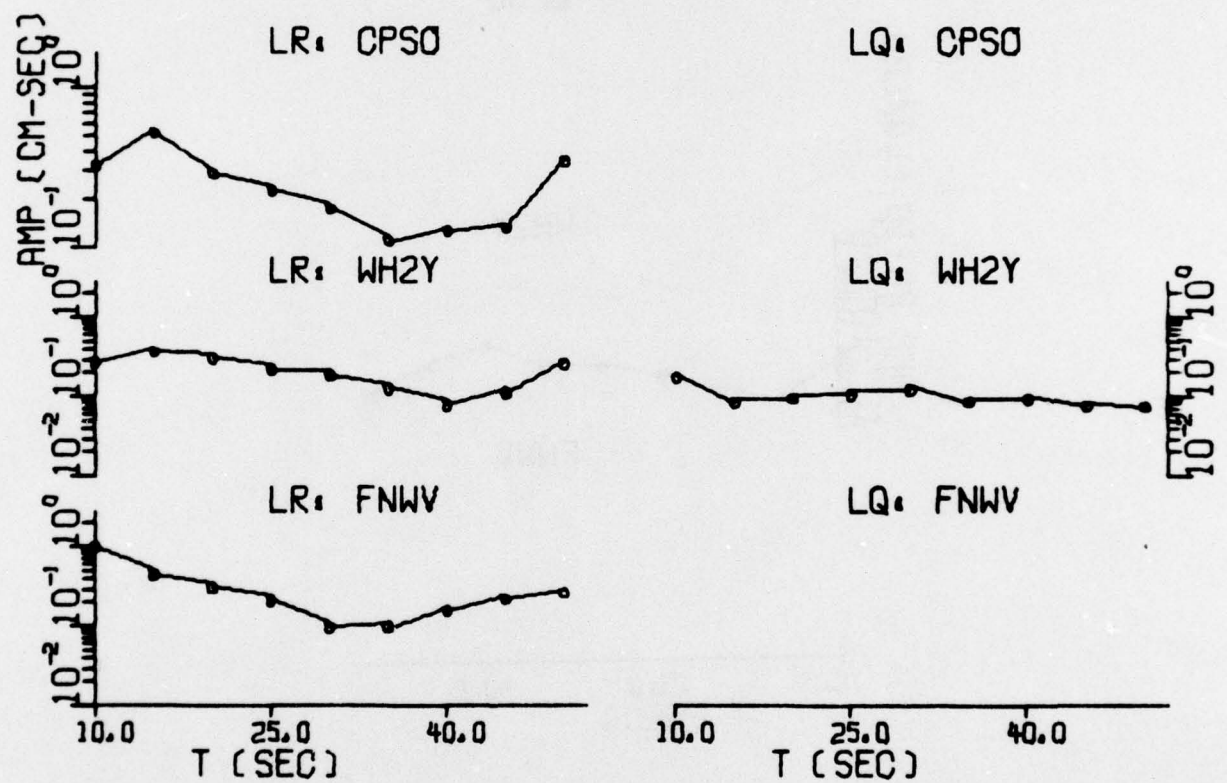


FIGURE III-18
OBSERVED SURFACE WAVE SPECTRA: NT1/204/76
(PAGE 1 OF 2)

(b) LQ/LR Amplitude Spectral Ratio

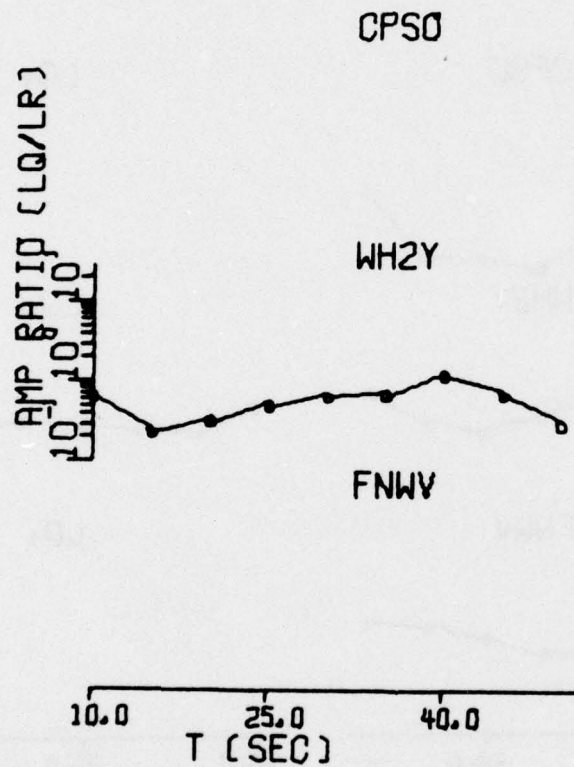


FIGURE III-18
OBSERVED SURFACE WAVE SPECTRA: NT1/204/76
(PAGE 2 OF 2)

(a) Amplitude Spectra

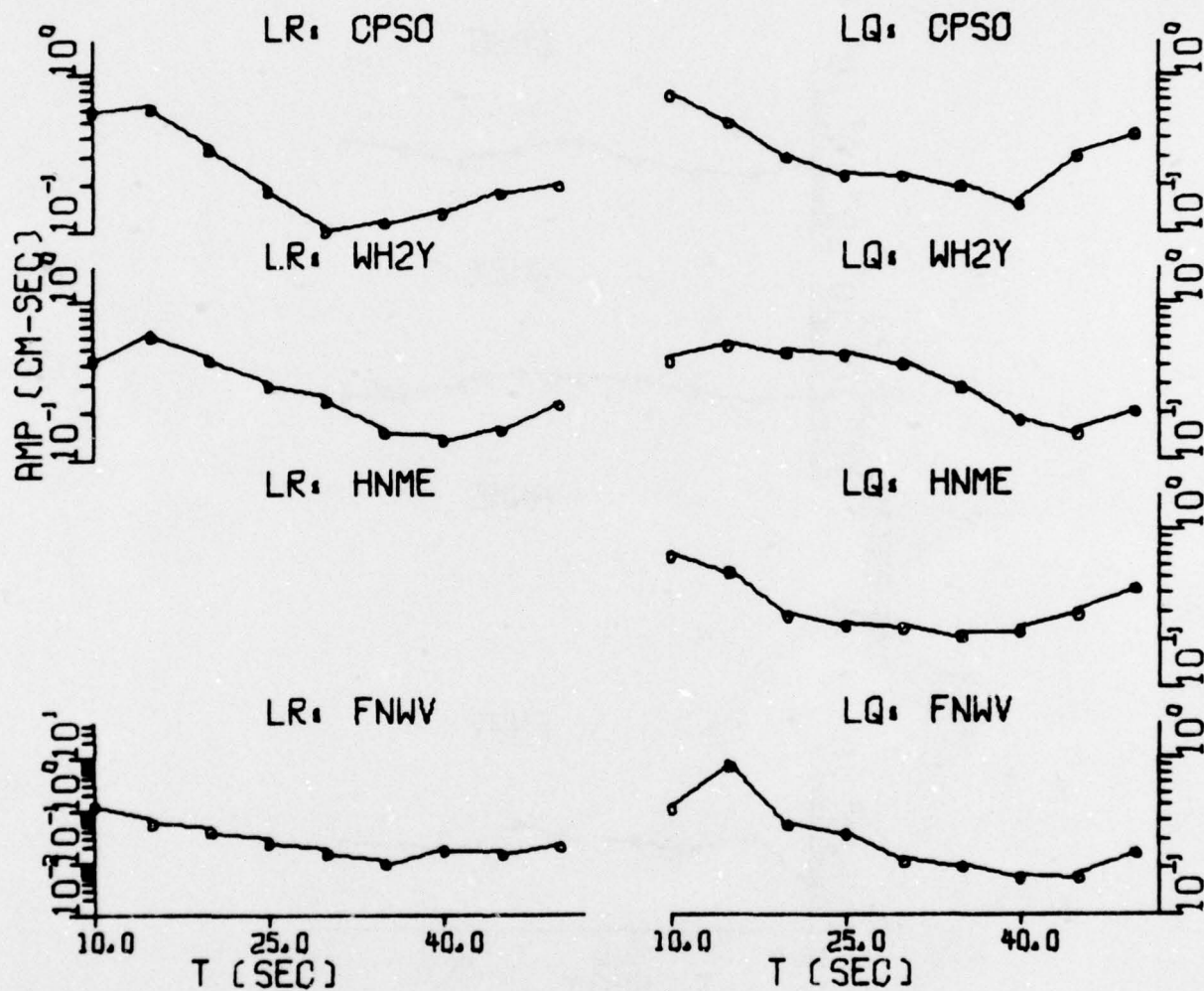


FIGURE III-19
OBSERVED SURFACE WAVE SPECTRA: NT2/204/76
(PAGE 1 OF 2)

(b) LQ/LR Amplitude Spectral Ratio

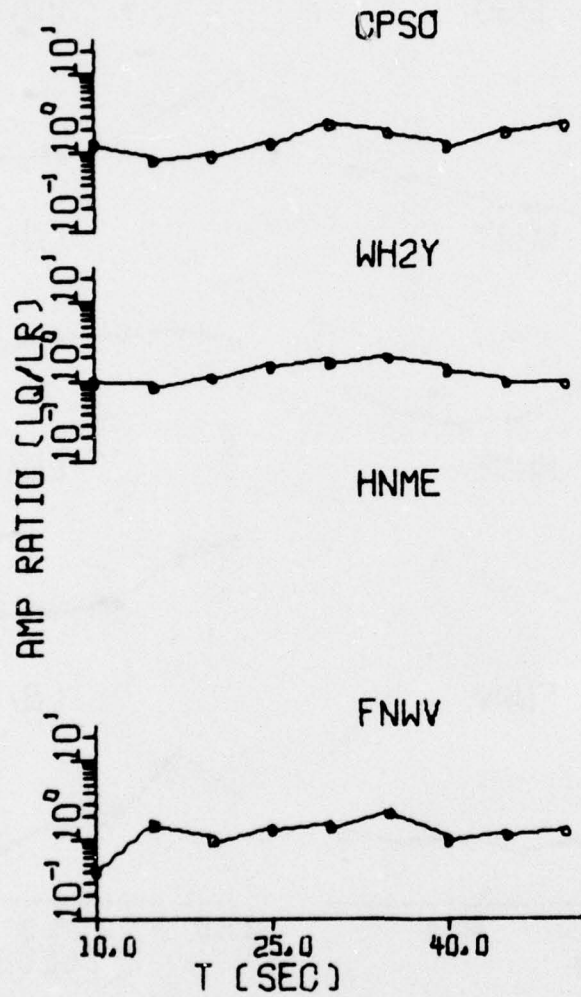


FIGURE III-19
OBSERVED SURFACE WAVE SPECTRA: NT2/204/76
(PAGE 2 OF 2)

(a) Amplitude Spectra

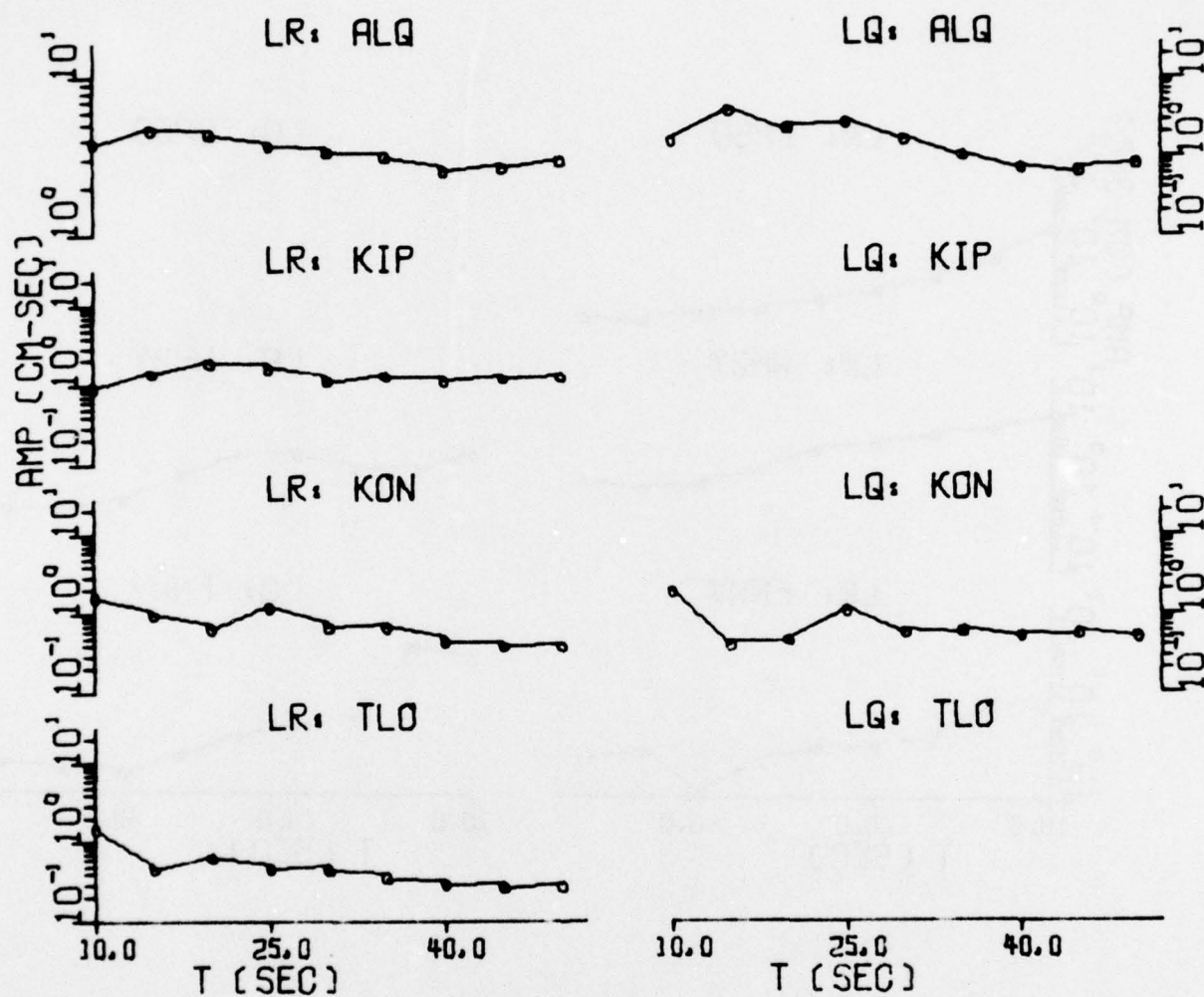


FIGURE III-20
OBSERVED SURFACE WAVE SPECTRA: NTS/212/76
(PAGE 1 OF 4)

(a) Amplitude Spectra

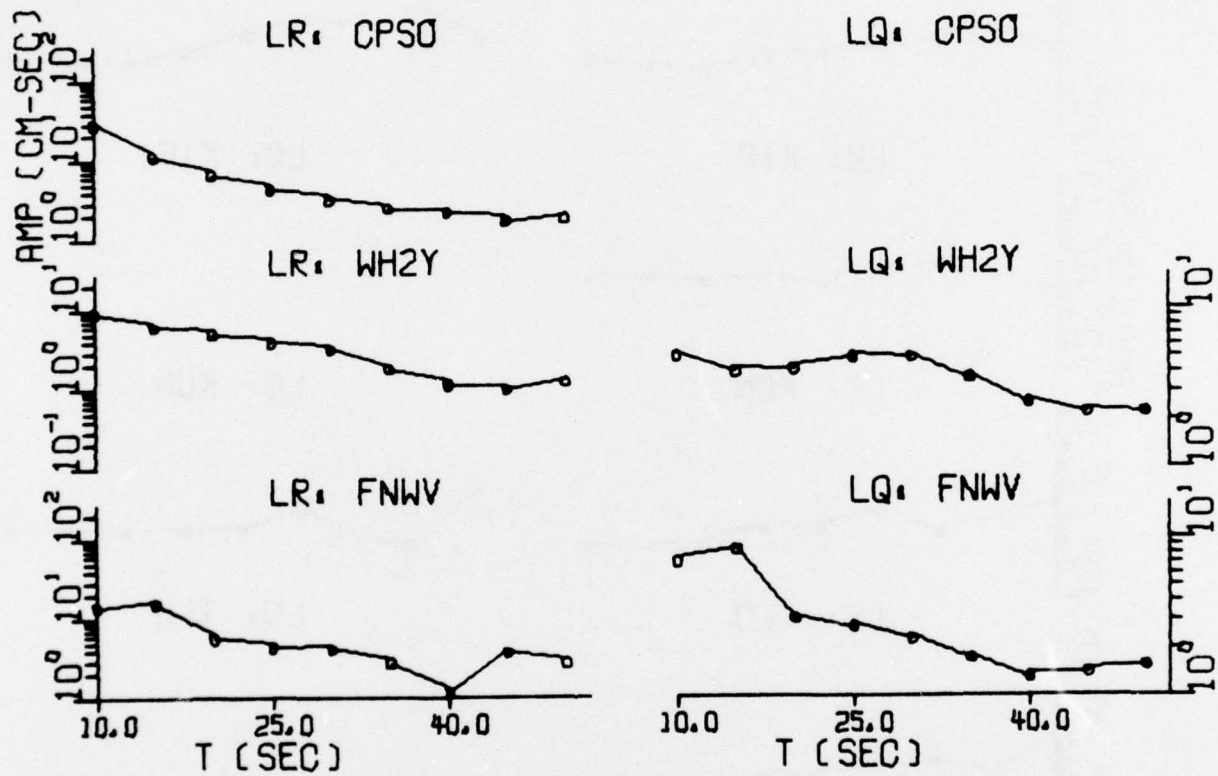


FIGURE III-20
OBSERVED SURFACE WAVE SPECTRA: NTS/212/76
(PAGE 2 OF 4)

(b) LQ/LR Amplitude Spectral Ratio

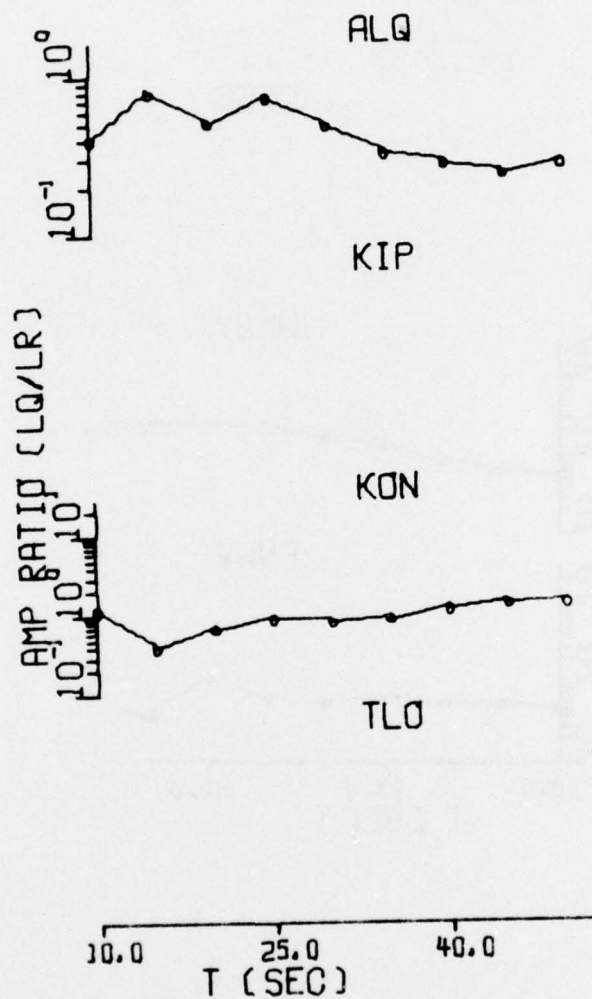


FIGURE III-20
OBSERVED SURFACE WAVE SPECTRA: NTS/212/76
(PAGE 3 OF 4)

(b) LQ/LR Amplitude Spectral Ratio

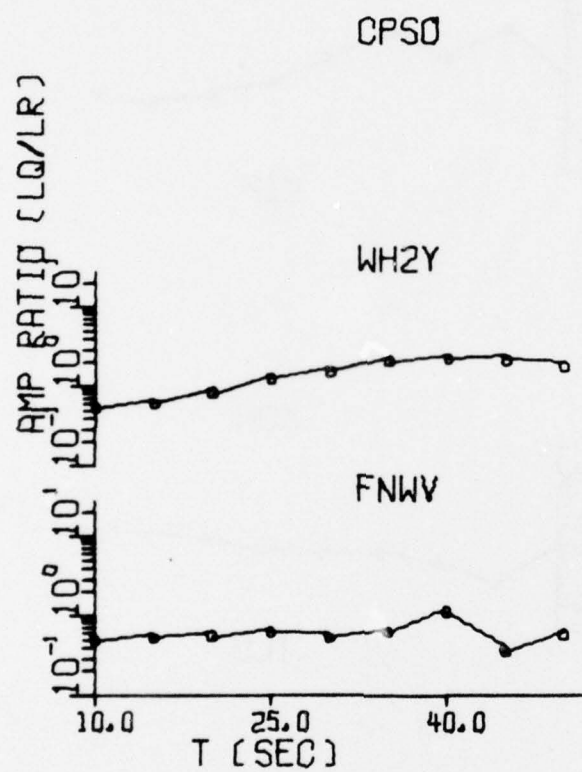


FIGURE III-20
OBSERVED SURFACE WAVE SPECTRA: NTS/212/76
(PAGE 4 OF 4)

(a) Amplitude Spectra

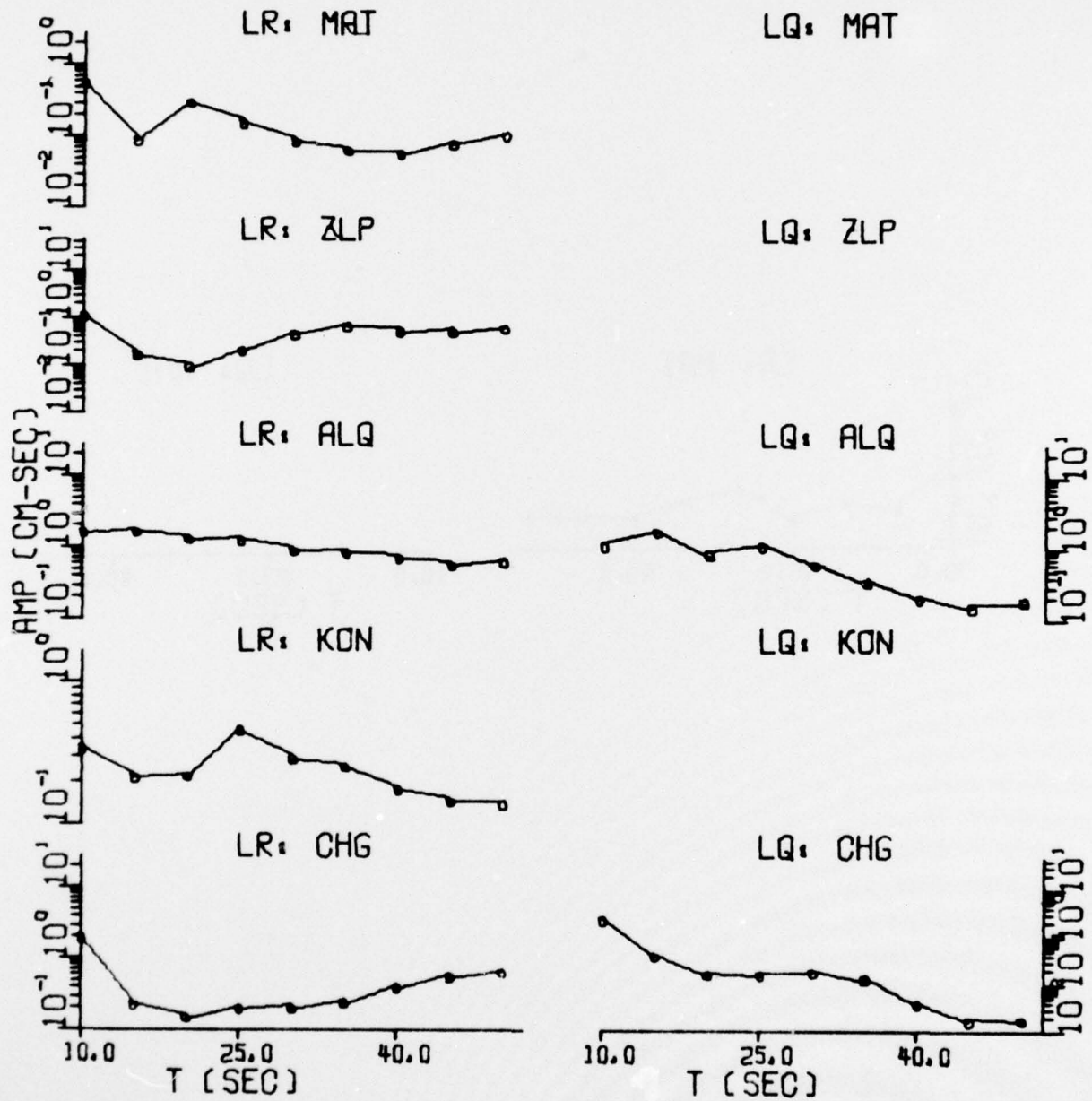


FIGURE III-21
OBSERVED SURFACE WAVE SPECTRA: NTS/309/76
(PAGE 1 OF 5)

(a) Amplitude Spectra

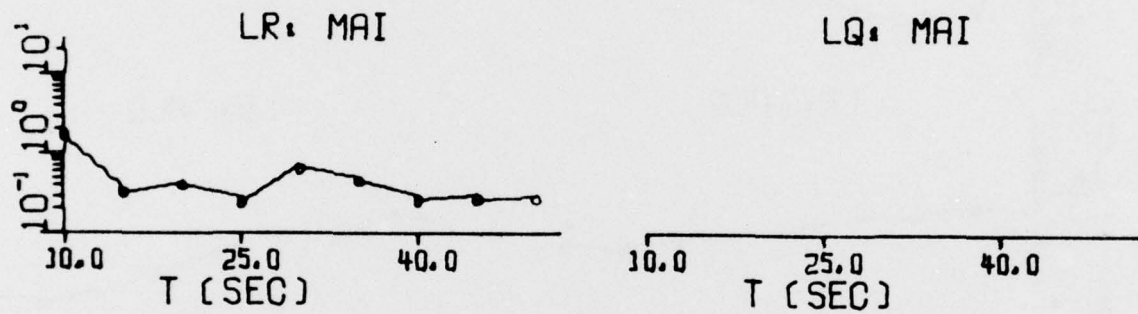


FIGURE III-21
OBSERVED SURFACE WAVE SPECTRA: NTS/309/76
(PAGE 2 OF 5)

(a) Amplitude Spectra

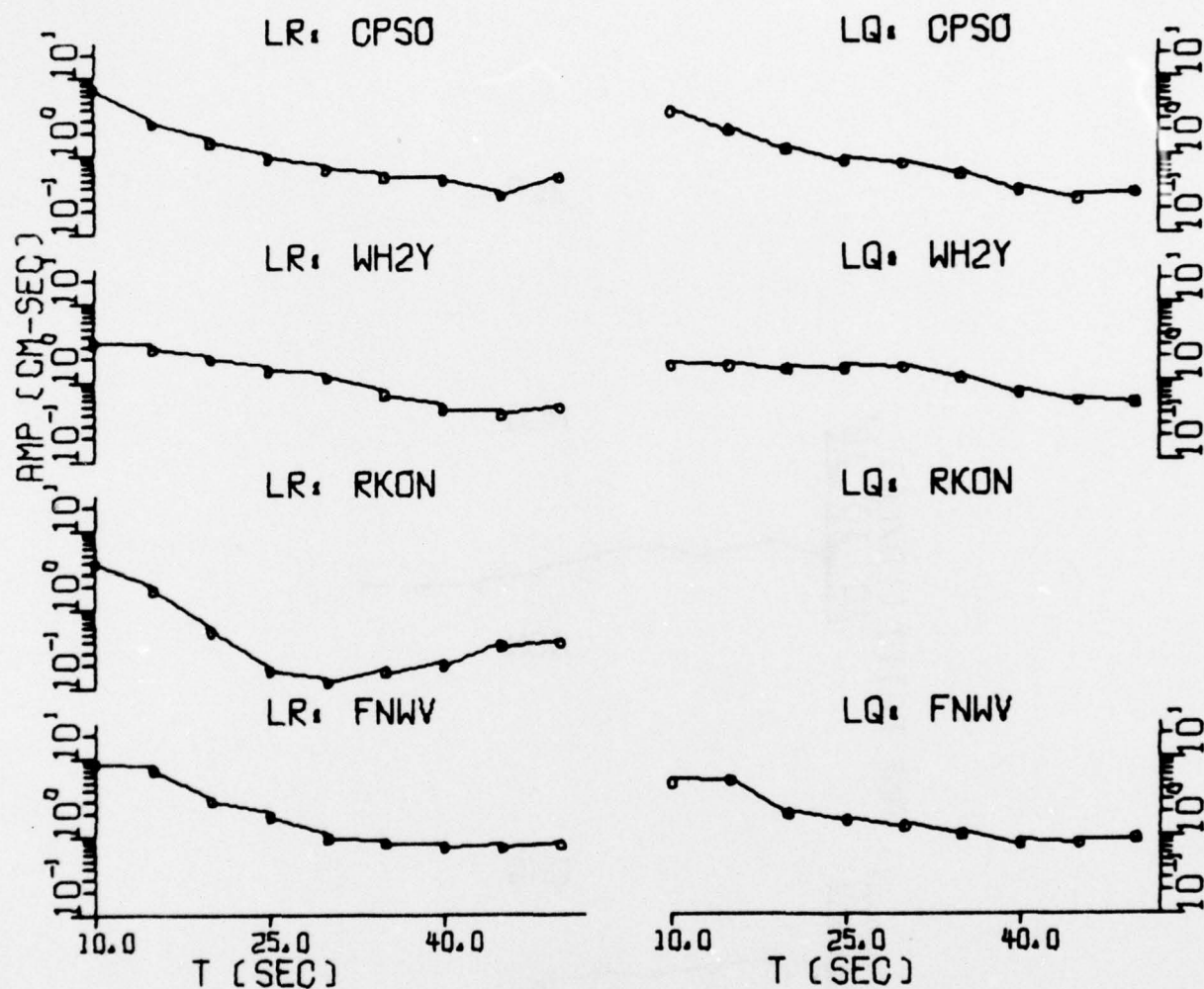


FIGURE III-21
OBSERVED SURFACE WAVE SPECTRA: NTS/309/76
(PAGE 3 OF 5)

(b) LQ/LR Amplitude Spectral Ratio

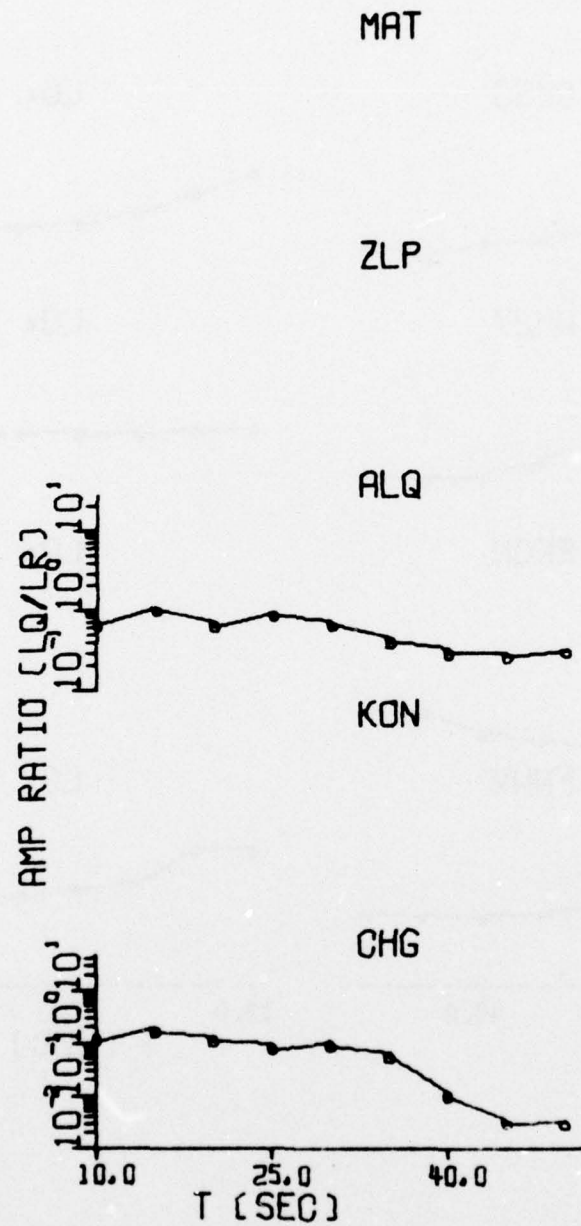


FIGURE III-21
OBSERVED SURFACE WAVE SPECTRA: NTS/309/76
(PAGE 4 OF 5)

(b) LQ/LR Amplitude Spectral Ratio

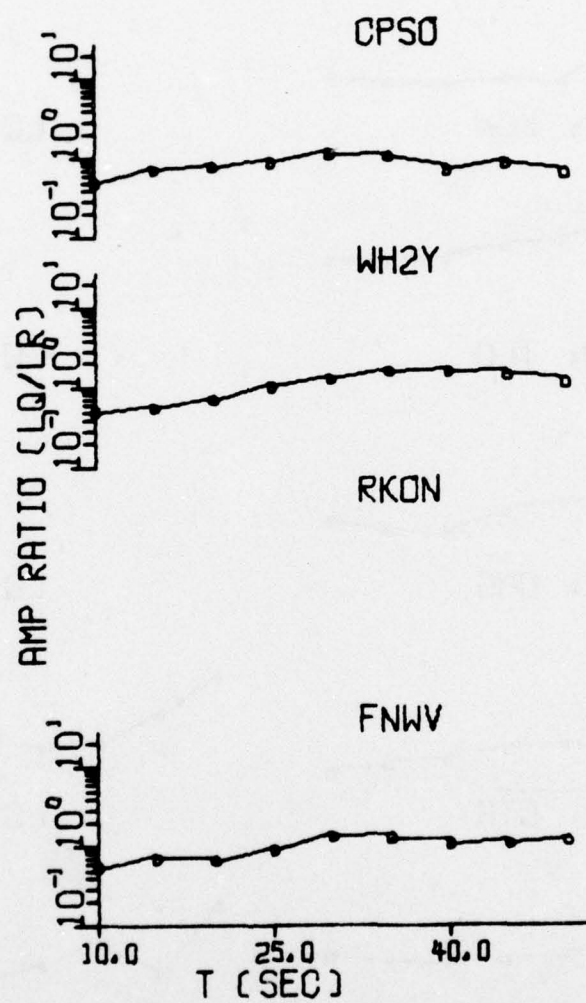


FIGURE III-21
OBSERVED SURFACE WAVE SPECTRA: NTS/309/76
(PAGE 5 OF 5)

(a) Amplitude Spectra

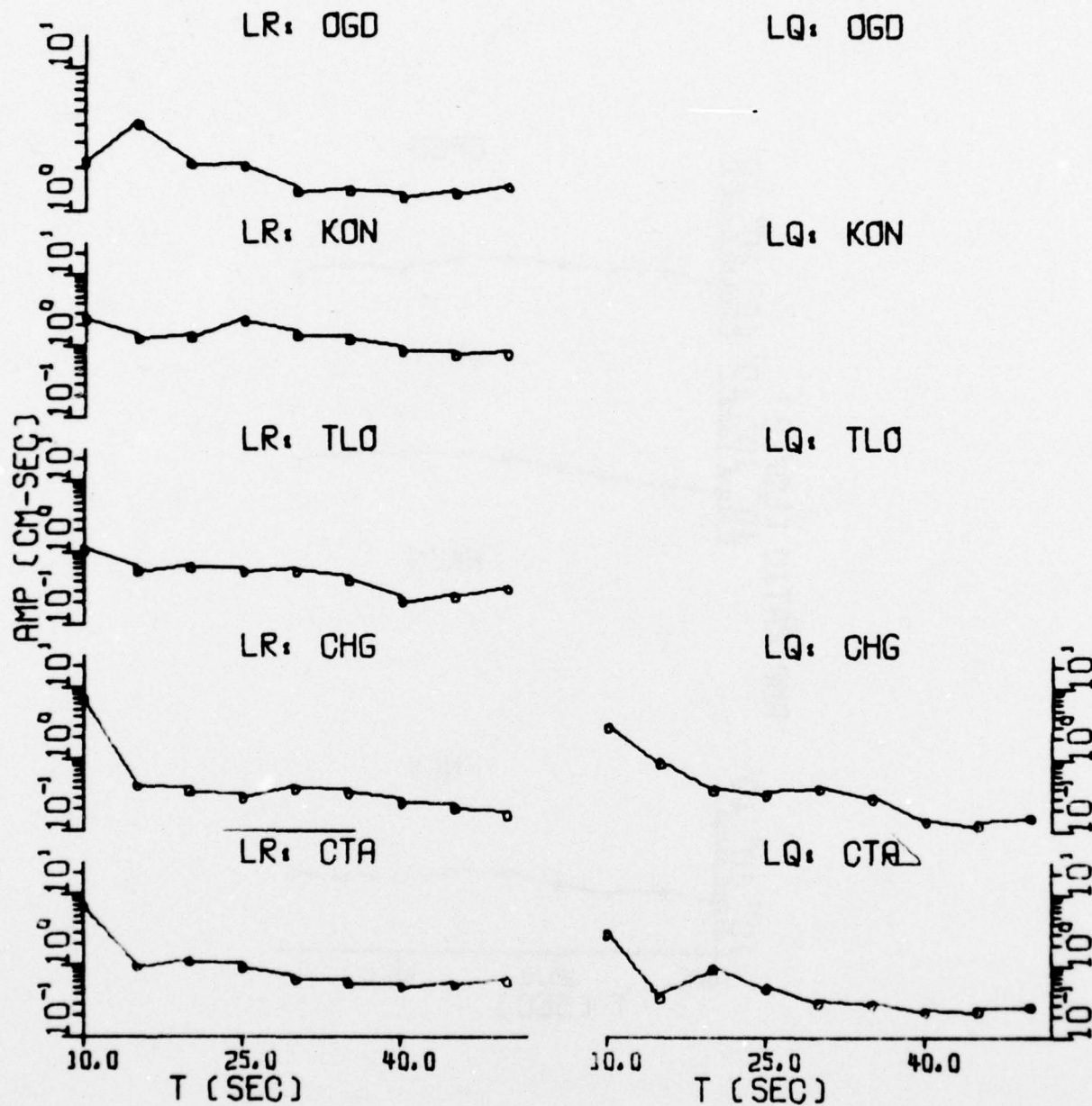


FIGURE III-22
OBSERVED SURFACE WAVE SPECTRA: NTS/314/76
(PAGE 1 OF 6)

(a) Amplitude Spectra

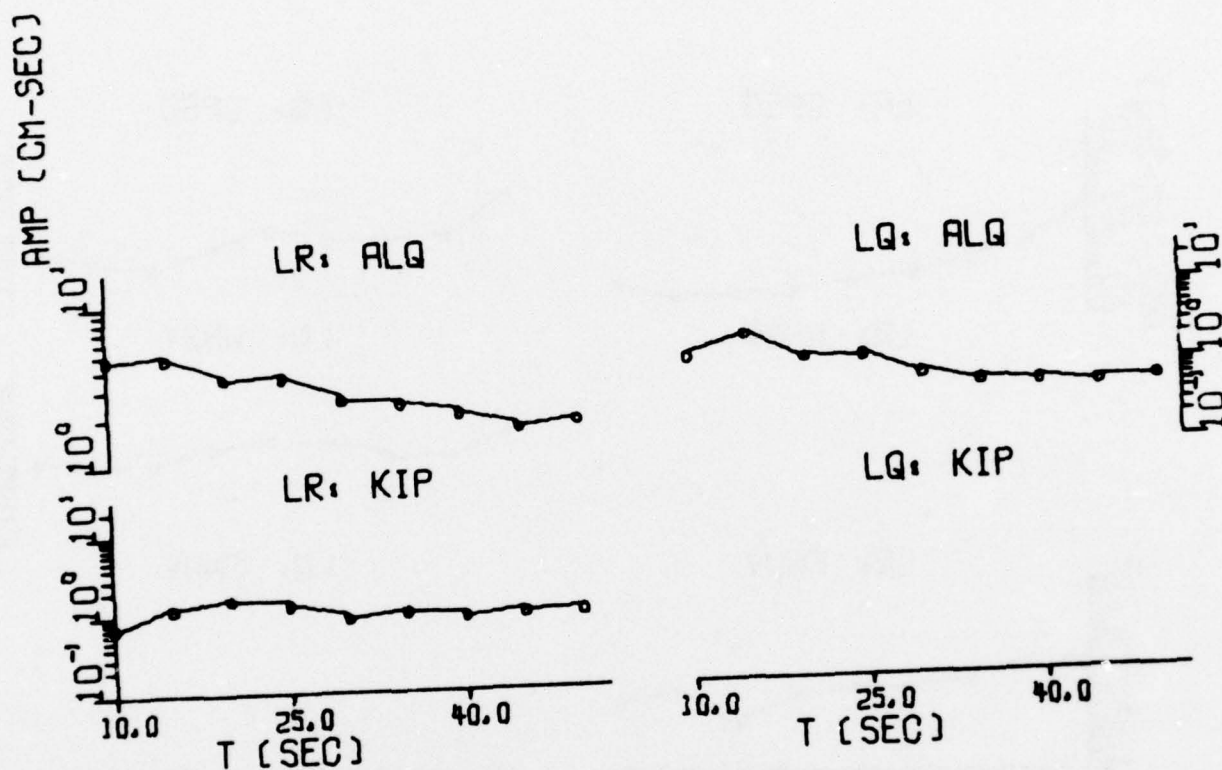


FIGURE III-22
OBSERVED SURFACE WAVE SPECTRA: NTS/314/76
(PAGE 2 OF 6)

(a) Amplitude Spectra

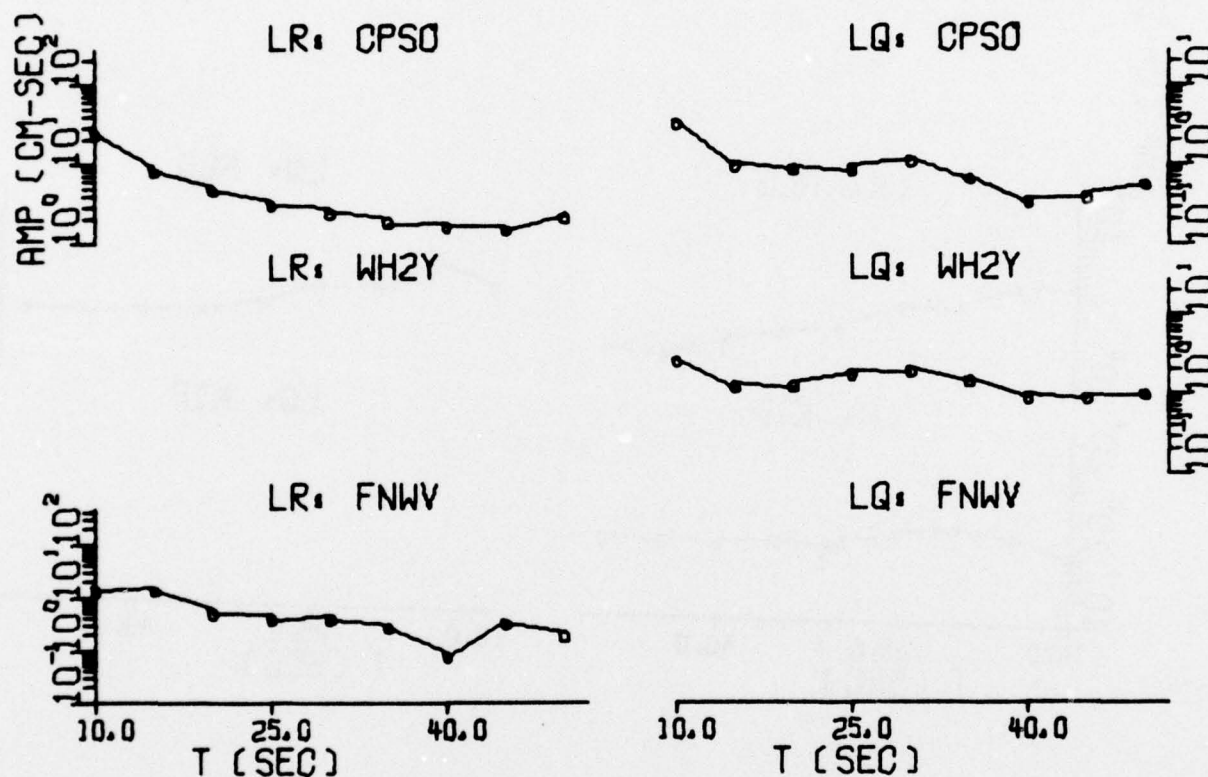


FIGURE III-22
OBSERVED SURFACE WAVE SPECTRA; NTS/314/76
(PAGE 3 OF 6)

(b) LQ/LR Amplitude Spectral Ratio

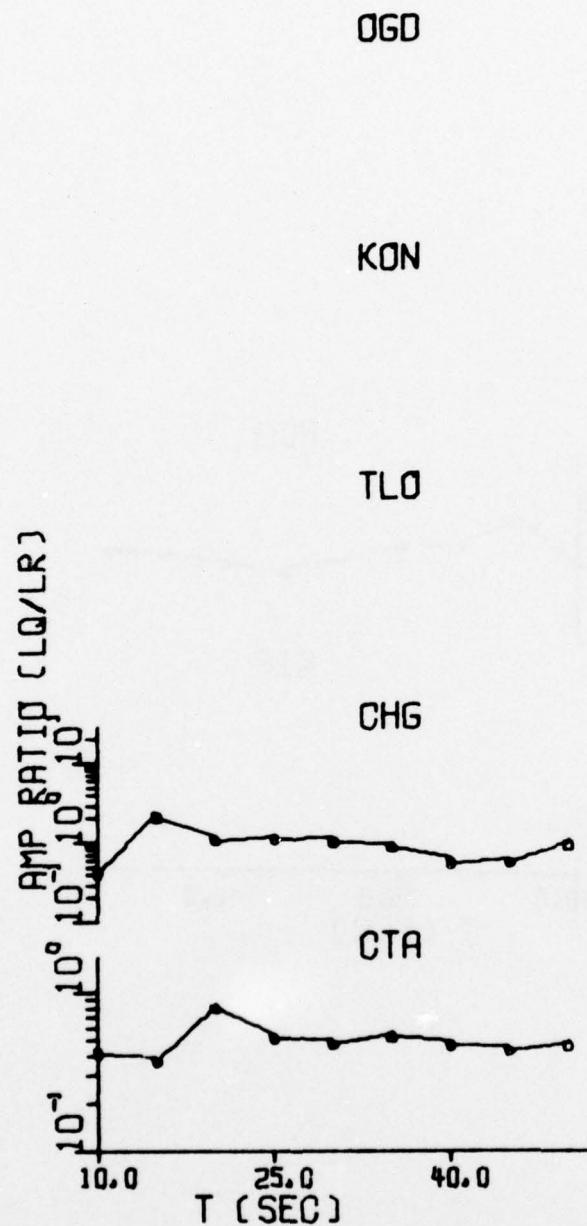


FIGURE III-22
OBSERVED SURFACE WAVE SPECTRA: NTS/314/76
(PAGE 4 OF 6)

(b) LQ/LR Amplitude Spectral Ratio

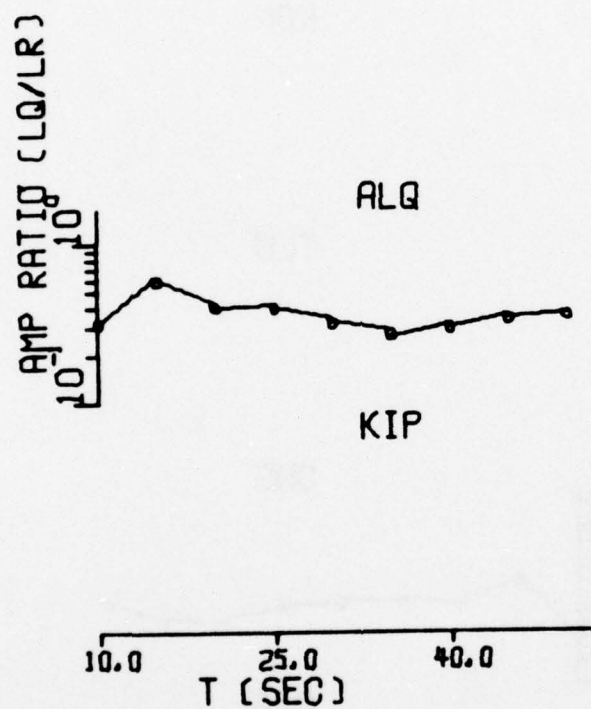


FIGURE III-22
OBSERVED SURFACE WAVE SPECTRA: NTS/314/76
(PAGE 5 OF 6)

(b) LQ/LR Amplitude Spectral Ratio

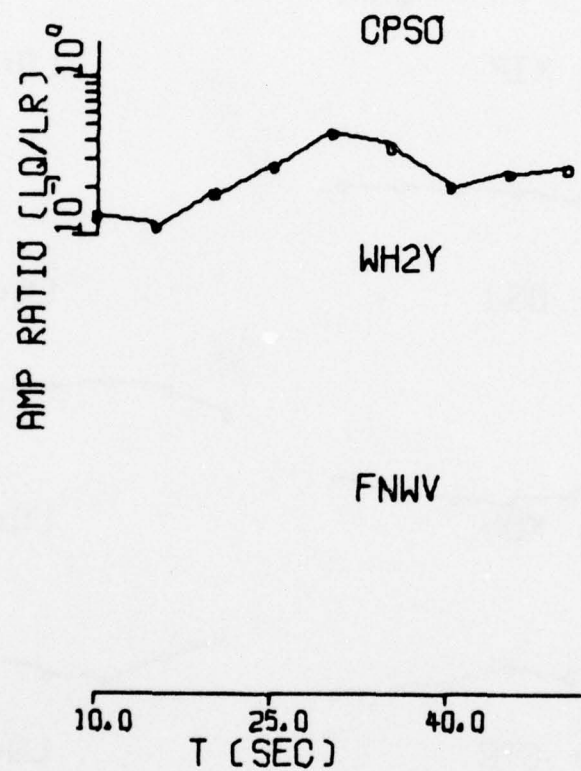


FIGURE III-22
OBSERVED SURFACE WAVE SPECTRA: NTS/314/76
(PAGE 6 OF 6)

(a) Amplitude Spectra

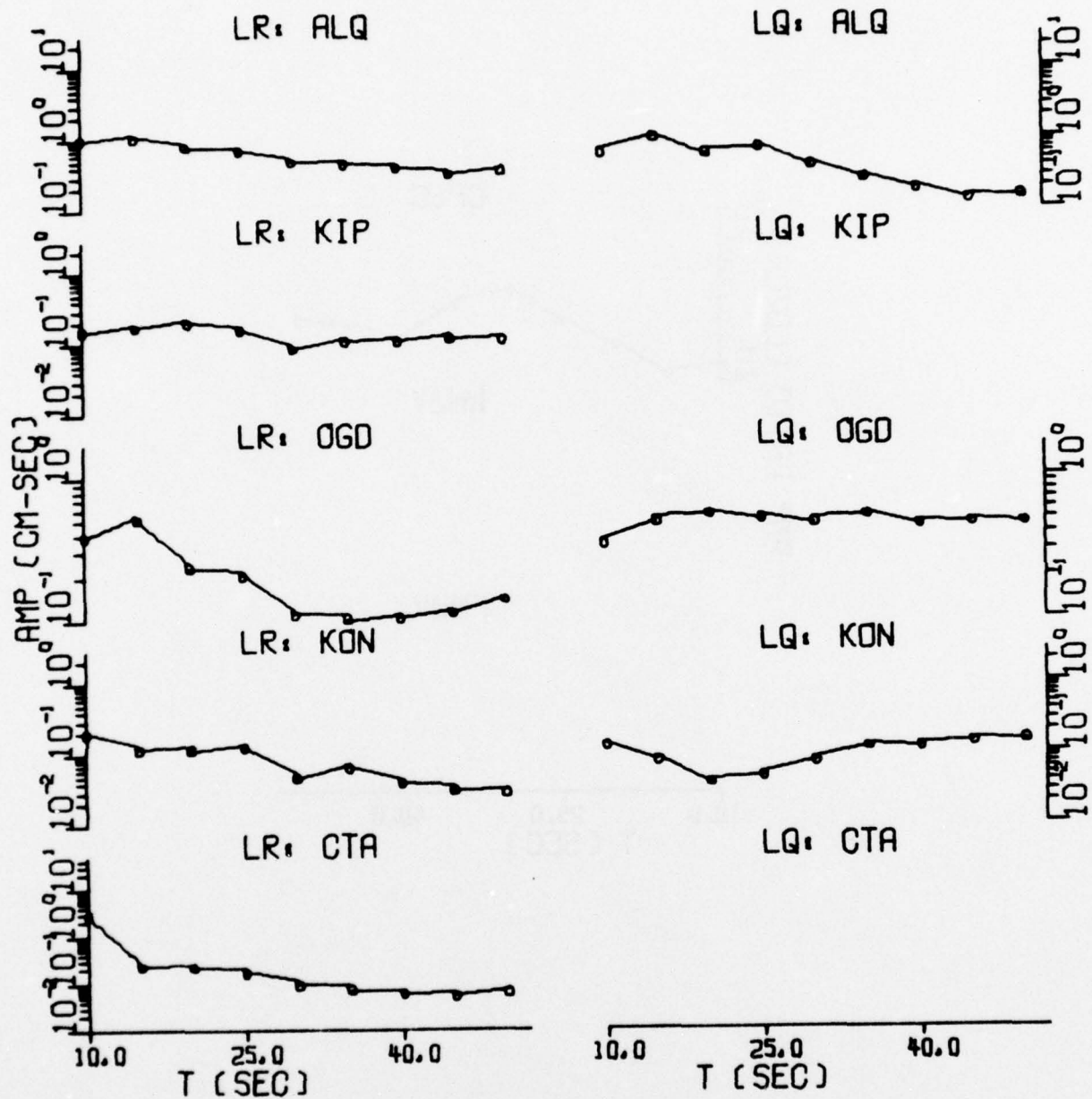


FIGURE III-23
OBSERVED SURFACE WAVE SPECTRA: NT1/317/76
(PAGE 1 OF 5)

(a) Amplitude Spectra

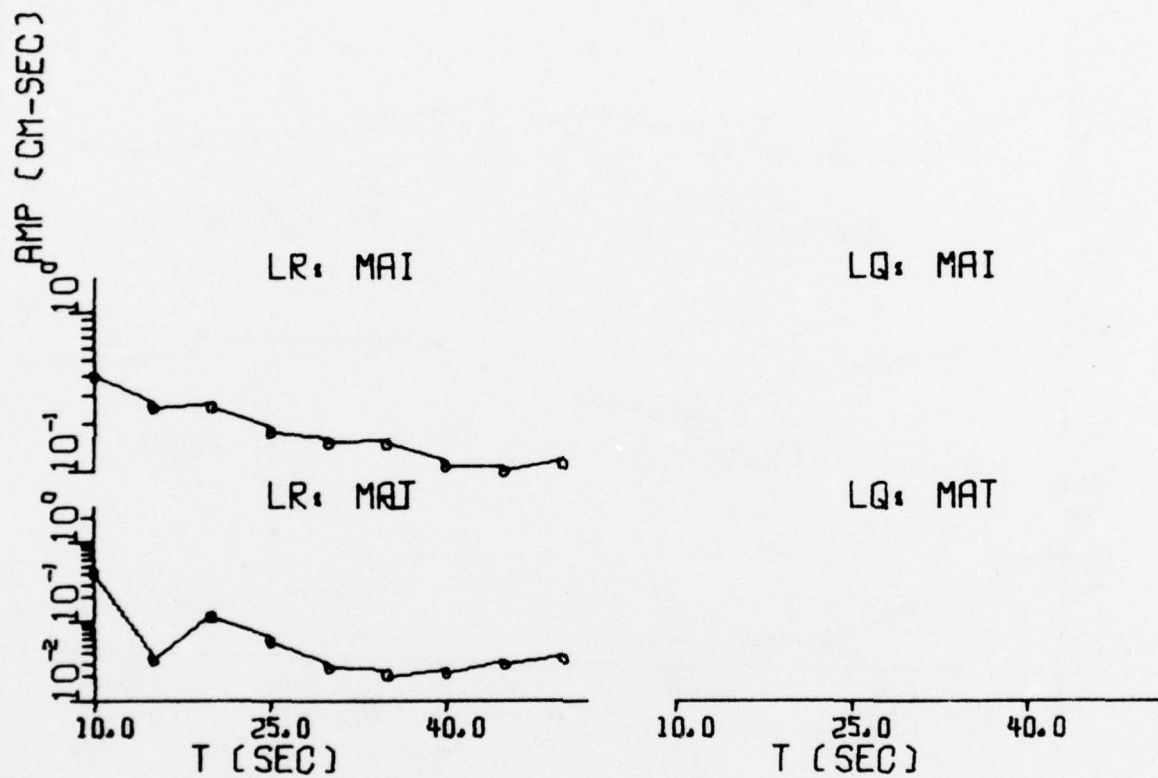


FIGURE III-23
OBSERVED SURFACE WAVE SPECTRA: NT1/317/76
(PAGE 2 OF 5)

(a) Amplitude Spectra

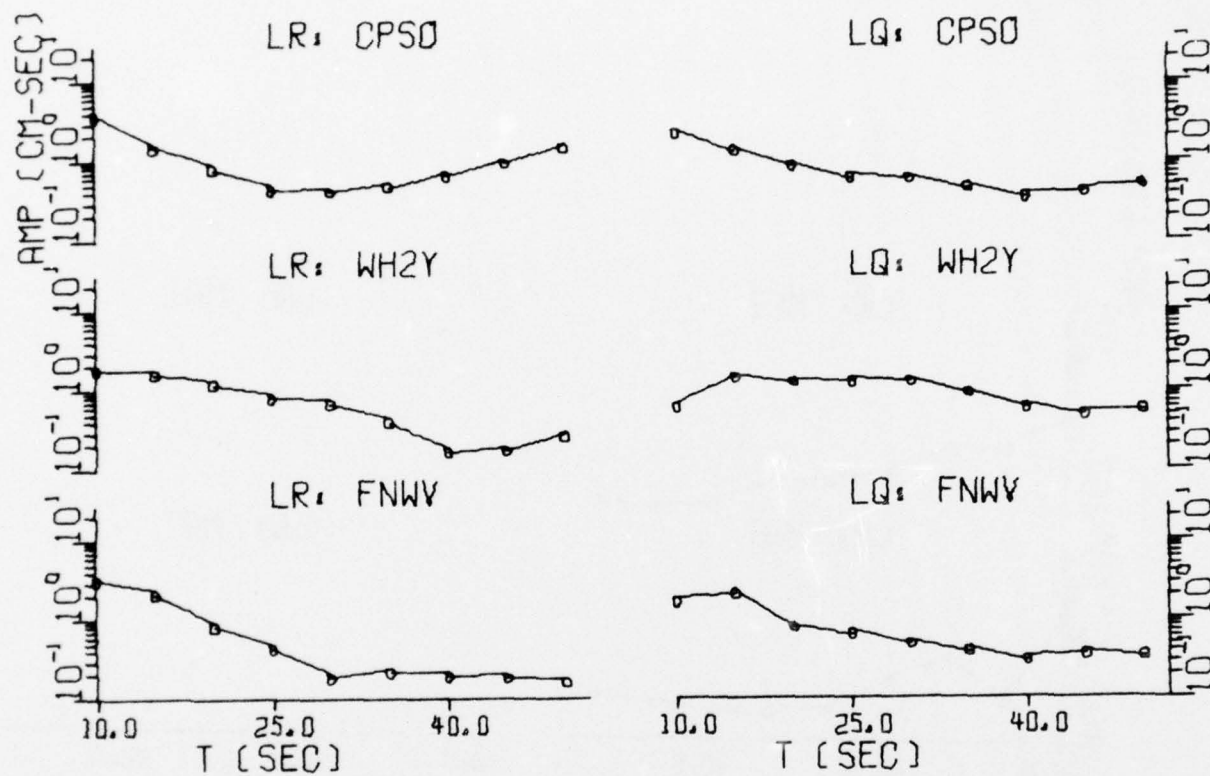


FIGURE III-23
OBSERVED SURFACE WAVE SPECTRA: NT1/317/76
(PAGE 3 OF 5)

(b) LQ/LR Amplitude Spectral Ratio

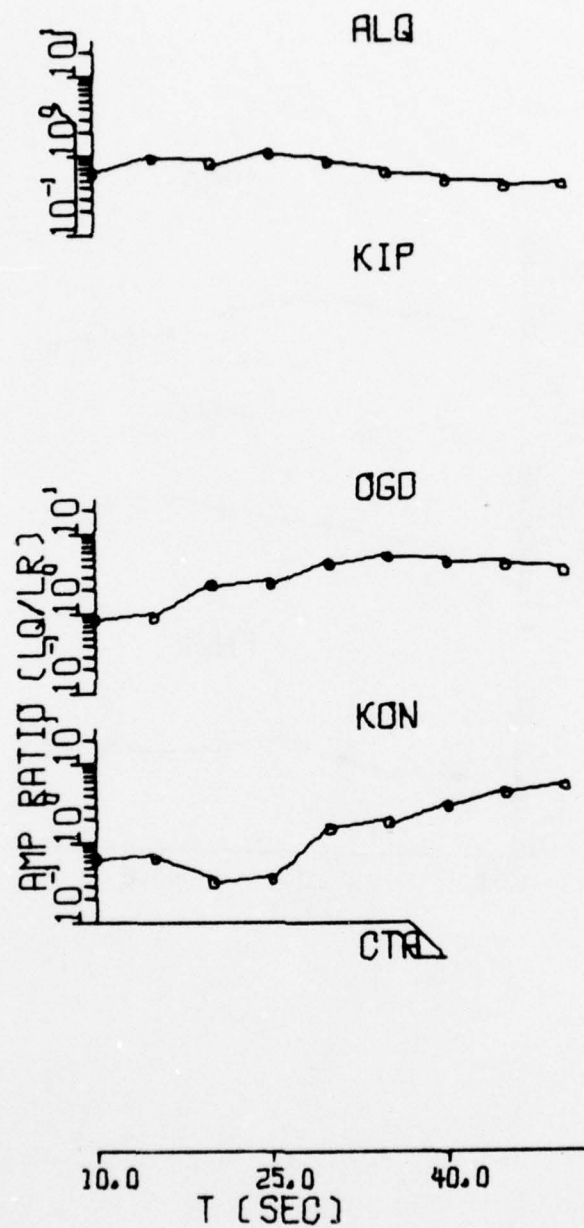


FIGURE III-23
OBSERVED SURFACE WAVE SPECTRA: NT1/317/76
(PAGE 4 OF 5)

(b) LQ/LR Amplitude Spectral Ratio

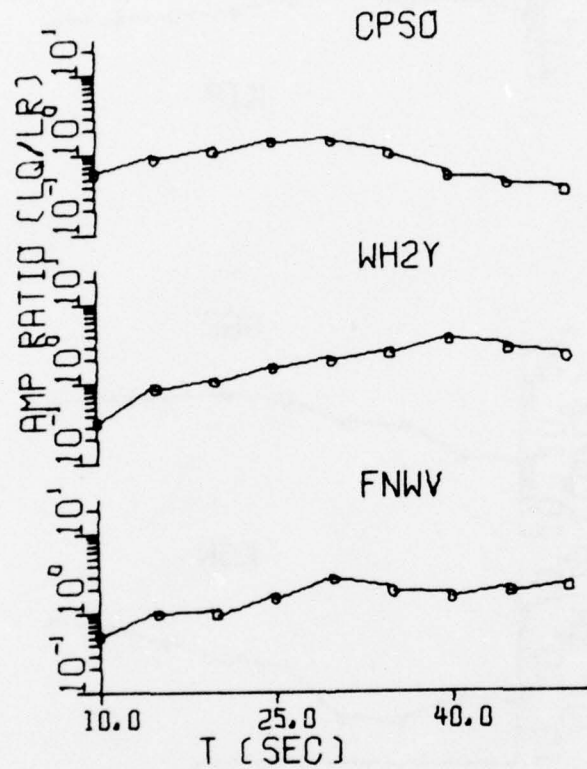


FIGURE III-23
OBSERVED SURFACE WAVE SPECTRA: NT1/317/76
(PAGE 5 OF 5)

(a) Amplitude Spectra

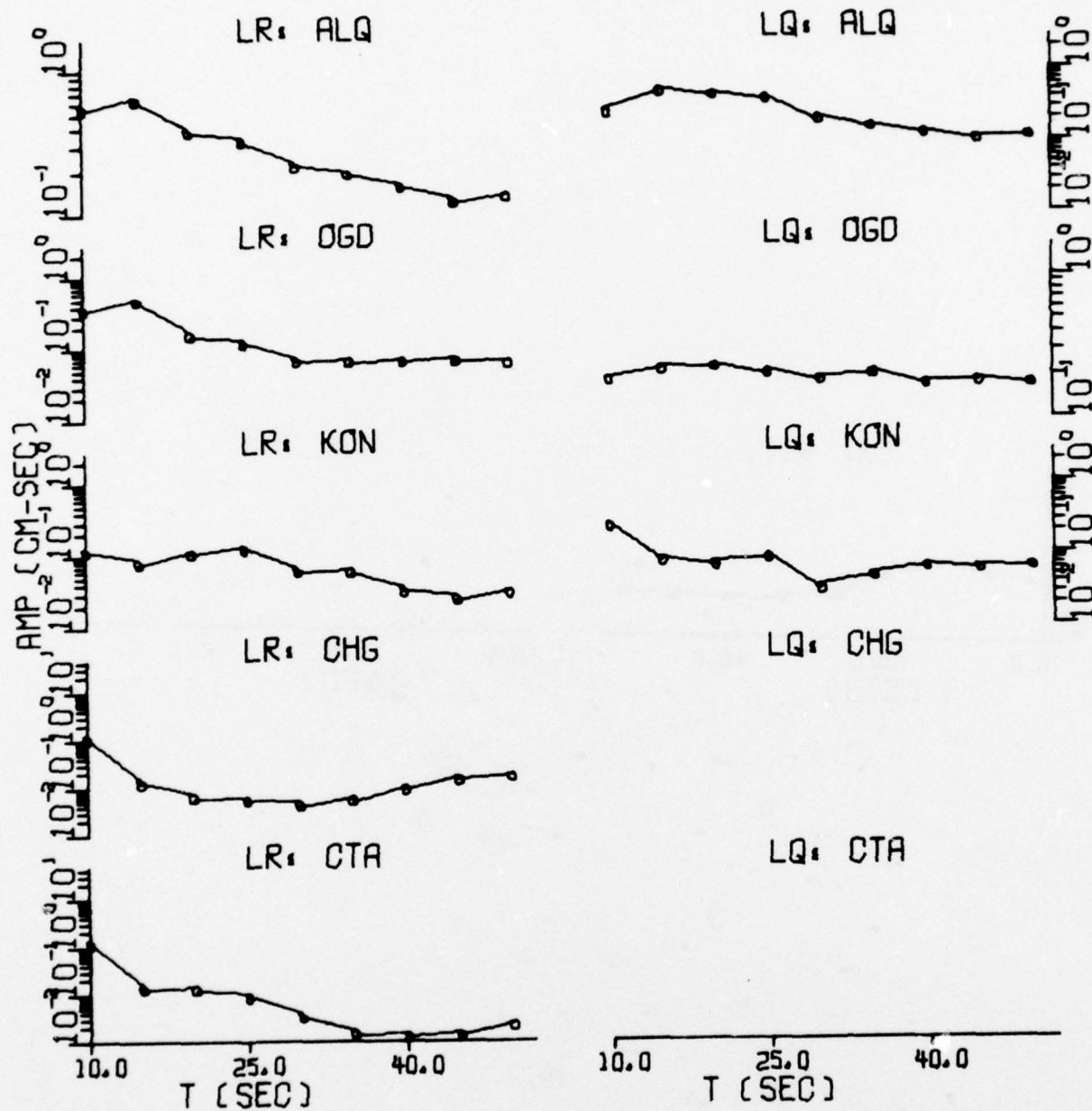


FIGURE III-24
OBSERVED SURFACE WAVE SPECTRA: NT2/317/76
(PAGE 1 OF 5)

(a) Amplitude Spectra

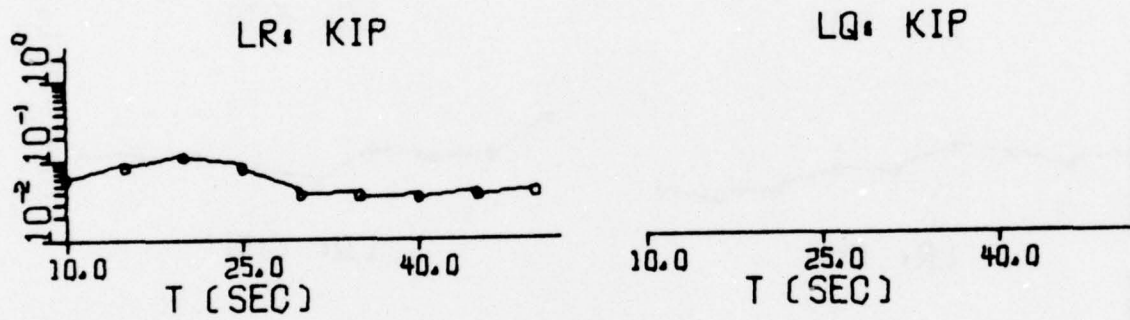


FIGURE III-24
OBSERVED SURFACE WAVE SPECTRA: NT2/317/76
(PAGE 2 OF 5)

(a) Amplitude Spectra

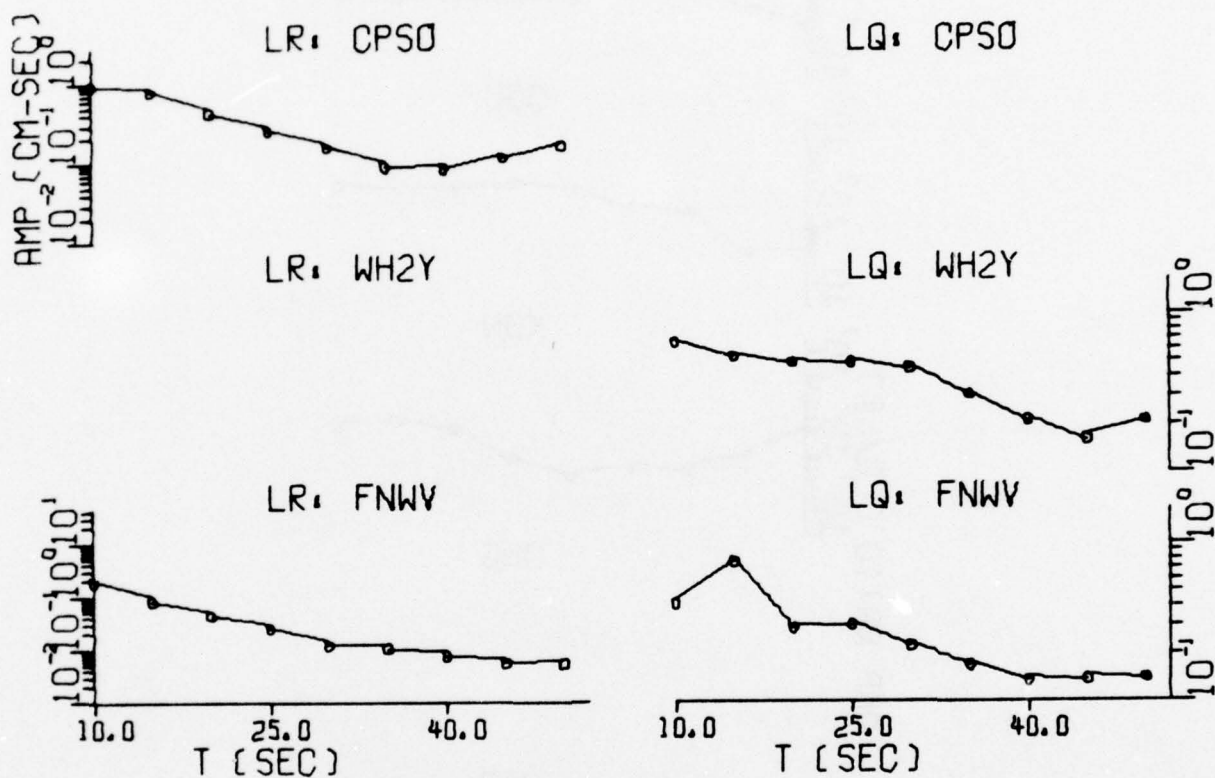


FIGURE III-24
OBSERVED SURFACE WAVE SPECTRA: NT2/317/76
(PAGE 3 OF 5)

(b) LQ/LR Amplitude Spectral Ratio

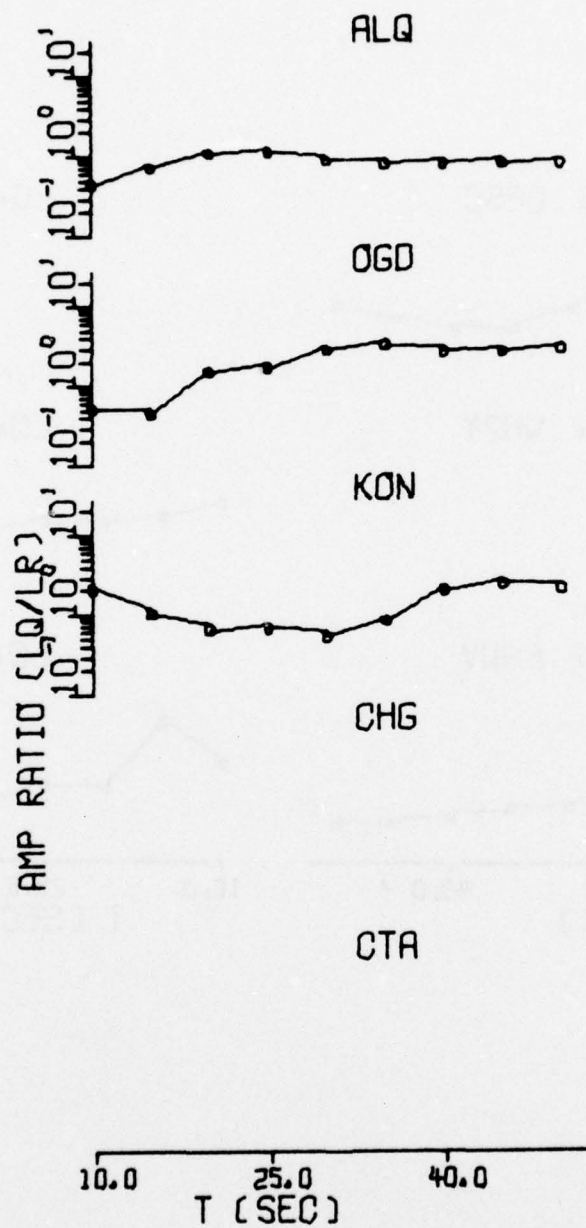


FIGURE III-24
OBSERVED SURFACE WAVE SPECTRA: NT2/317/76
(PAGE 4 OF 5)

(b) LQ/LR Amplitude Spectral Ratio

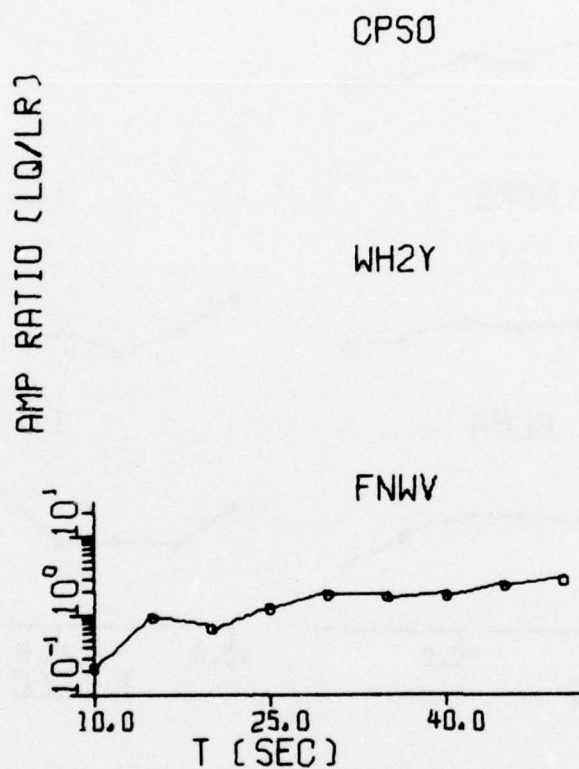


FIGURE III-24
OBSERVED SURFACE WAVE SPECTRA: NT2/317/76
(PAGE 5 OF 5)

(a) Amplitude Spectra

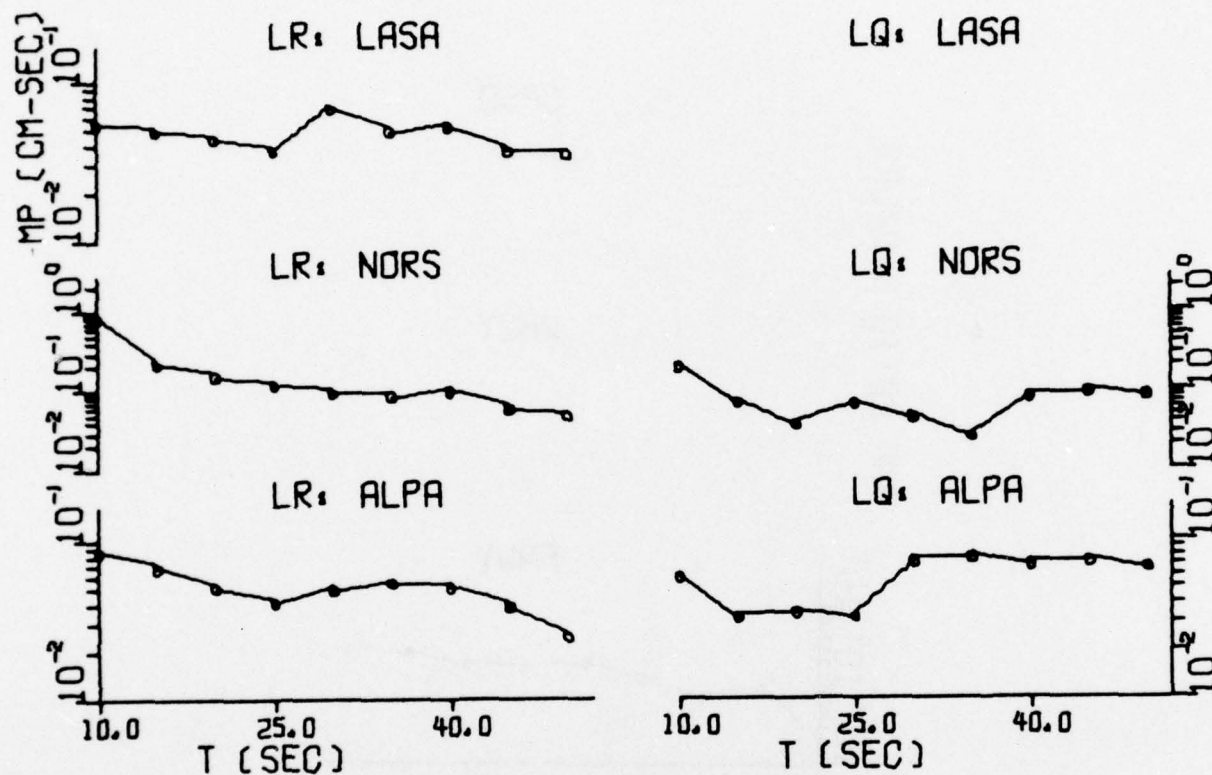


FIGURE III-25
OBSERVED SURFACE WAVE SPECTRA: EKZ/723/73
(PAGE 1 OF 2)

(b) LQ/LR Amplitude Spectral Ratio

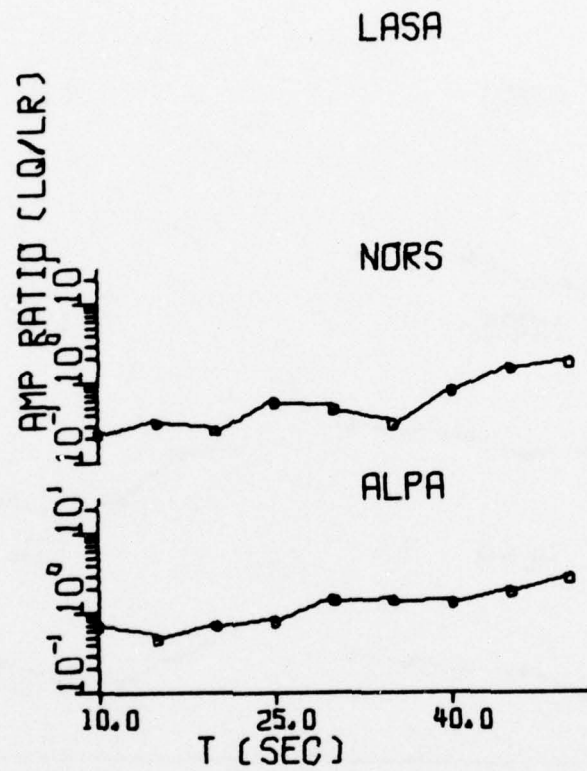


FIGURE III-25
OBSERVED SURFACE WAVE SPECTRA: EKZ/723/73
(PAGE 2 OF 2)

(a) Amplitude Spectra

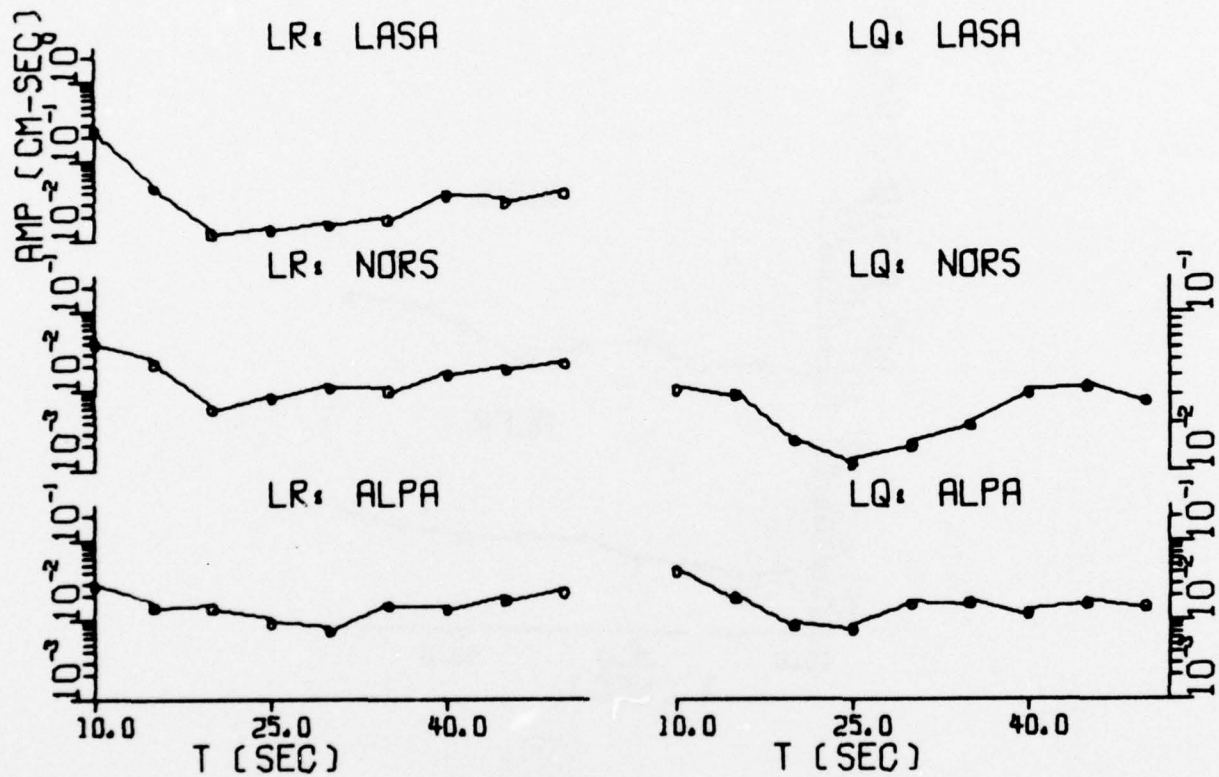


FIGURE III-26
OBSERVED SURFACE WAVE SPECTRA: EKZ/1026/3
(PAGE 1 OF 2)

(b) LQ/LR Amplitude Spectral Ratio

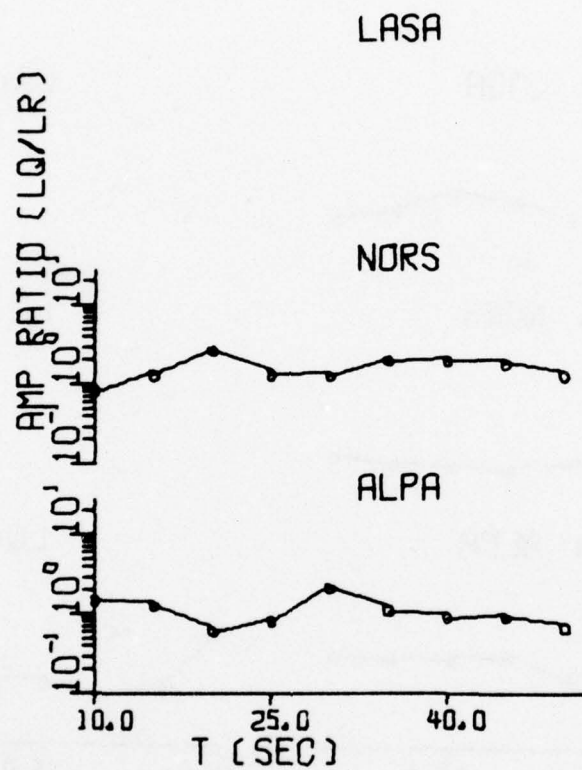


FIGURE III-26
OBSERVED SURFACE WAVE SPECTRA: EKZ/1026/3
(PAGE 2 OF 2)

(a) Amplitude Spectra

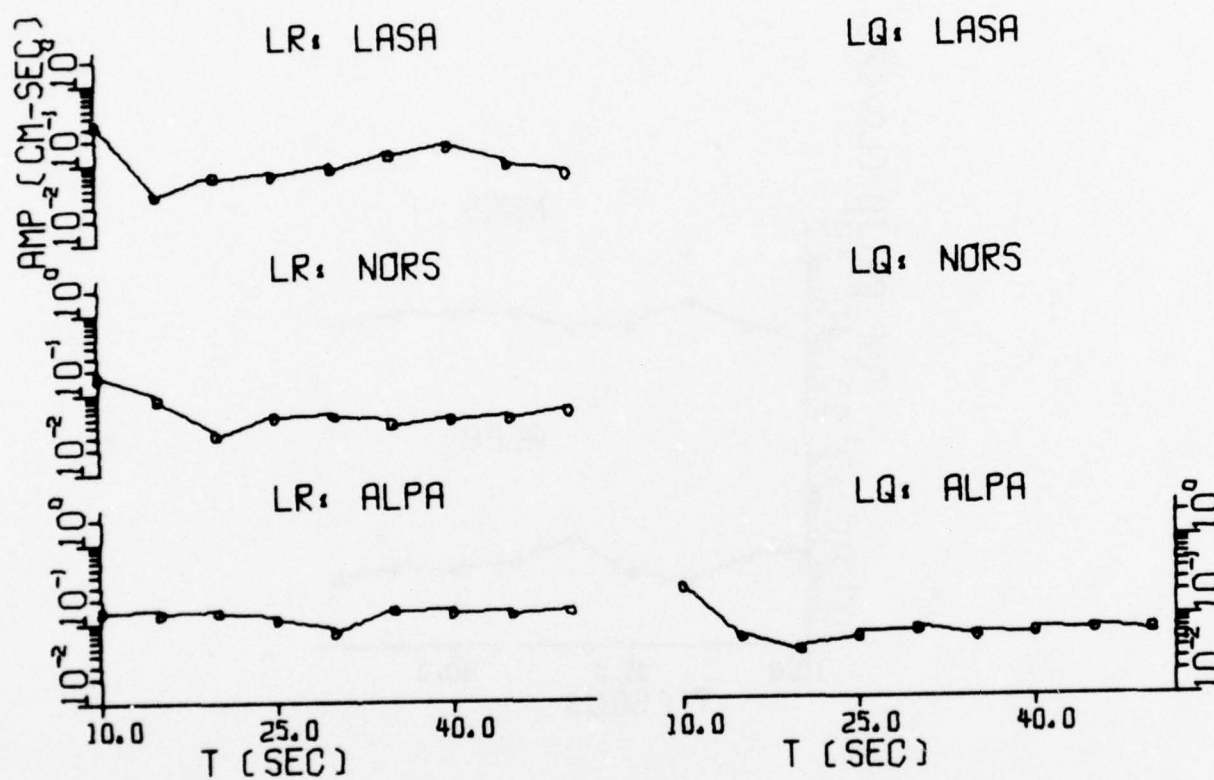


FIGURE III-27
OBSERVED SURFACE WAVE SPECTRA: EKZ/1214/3
(PAGE 1 OF 2)

(b) LQ/LR Amplitude Spectral Ratio

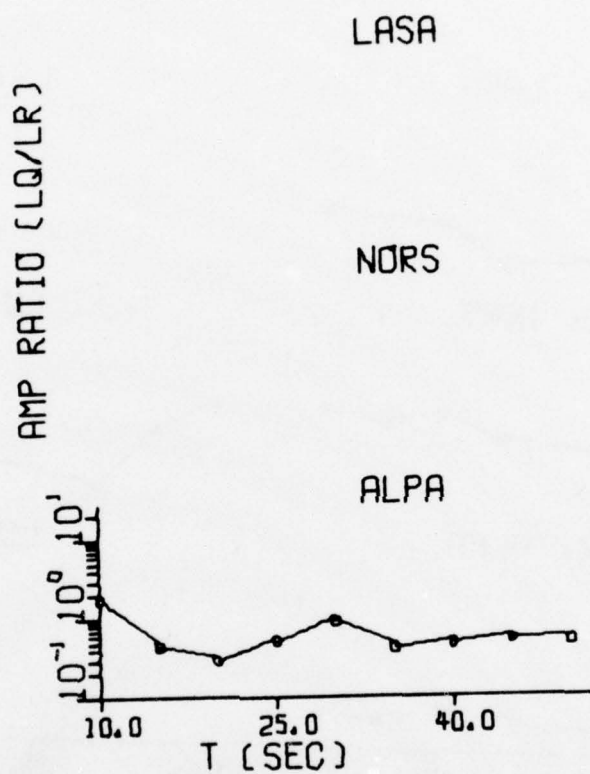


FIGURE III-27
OBSERVED SURFACE WAVE SPECTRA: EKZ/1214/3
(PAGE 2 OF 2)

(a) Amplitude Spectra

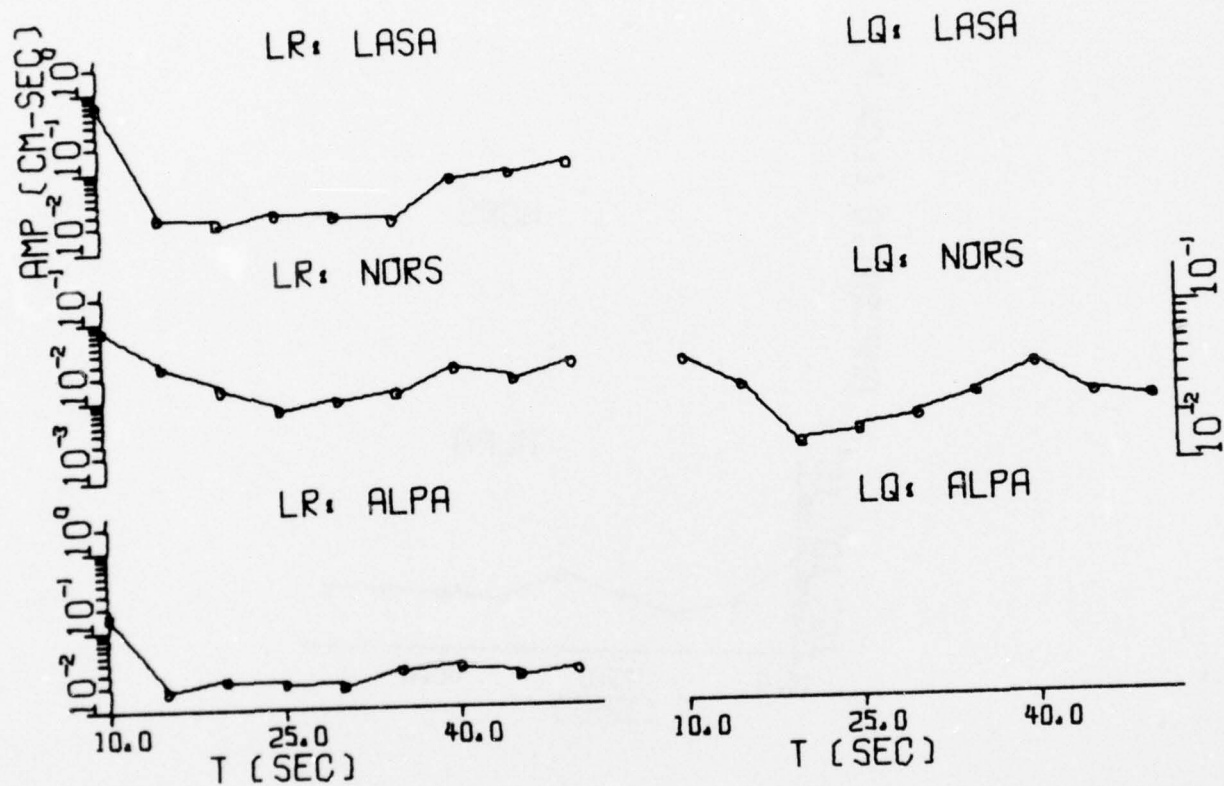


FIGURE III-28
OBSERVED SURFACE WAVE SPECTRA: EKZ/220/75
(PAGE 1 OF 2)

(b) LQ/LR Amplitude Spectral Ratio

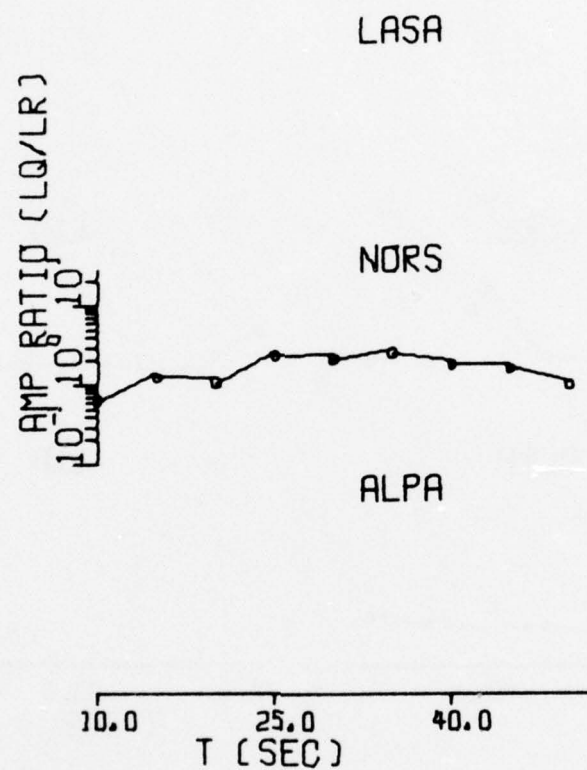


FIGURE III-28
OBSERVED SURFACE WAVE SPECTRA: EKZ/220/75
(PAGE 2 OF 2)

(a) Amplitude Spectra

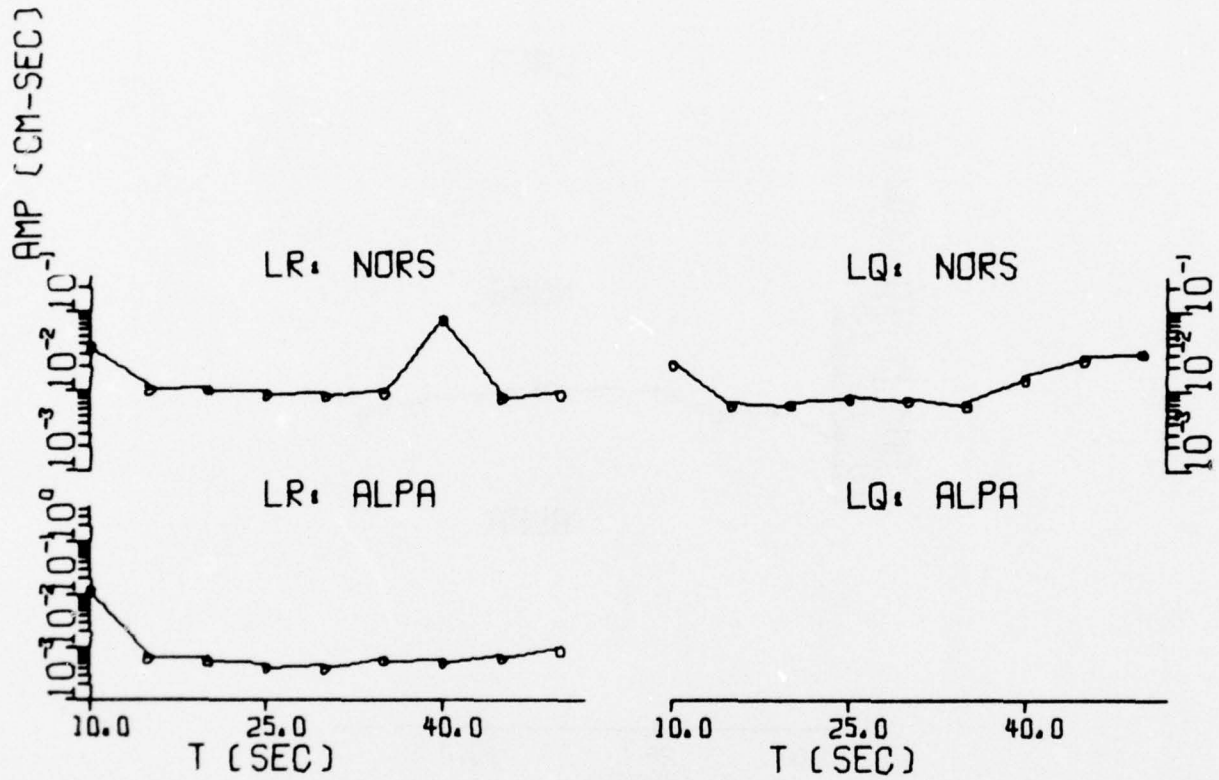


FIGURE III-29
OBSERVED SURFACE WAVE SPECTRA: EKZ/311/75
(PAGE 1 OF 2)

(b) LQ/LR Amplitude Spectral Ratio

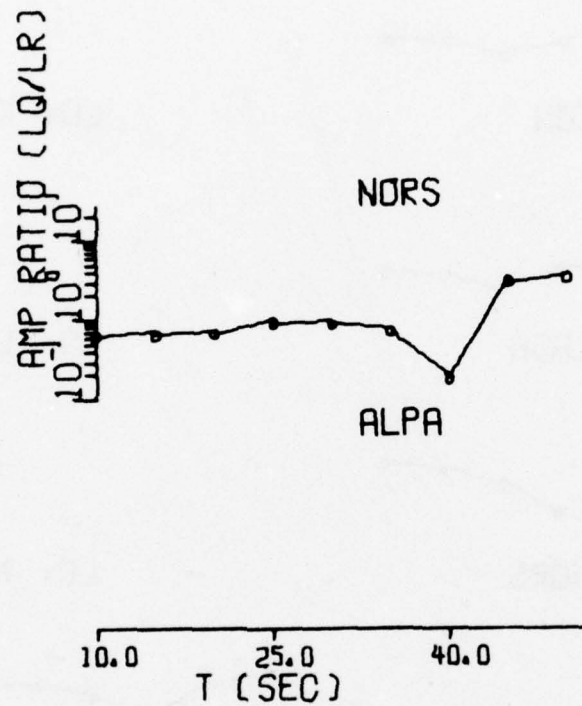


FIGURE III-29
OBSERVED SURFACE WAVE SPECTRA: EKZ/311/75
(PAGE 2 OF 2)

(a) Amplitude Spectra

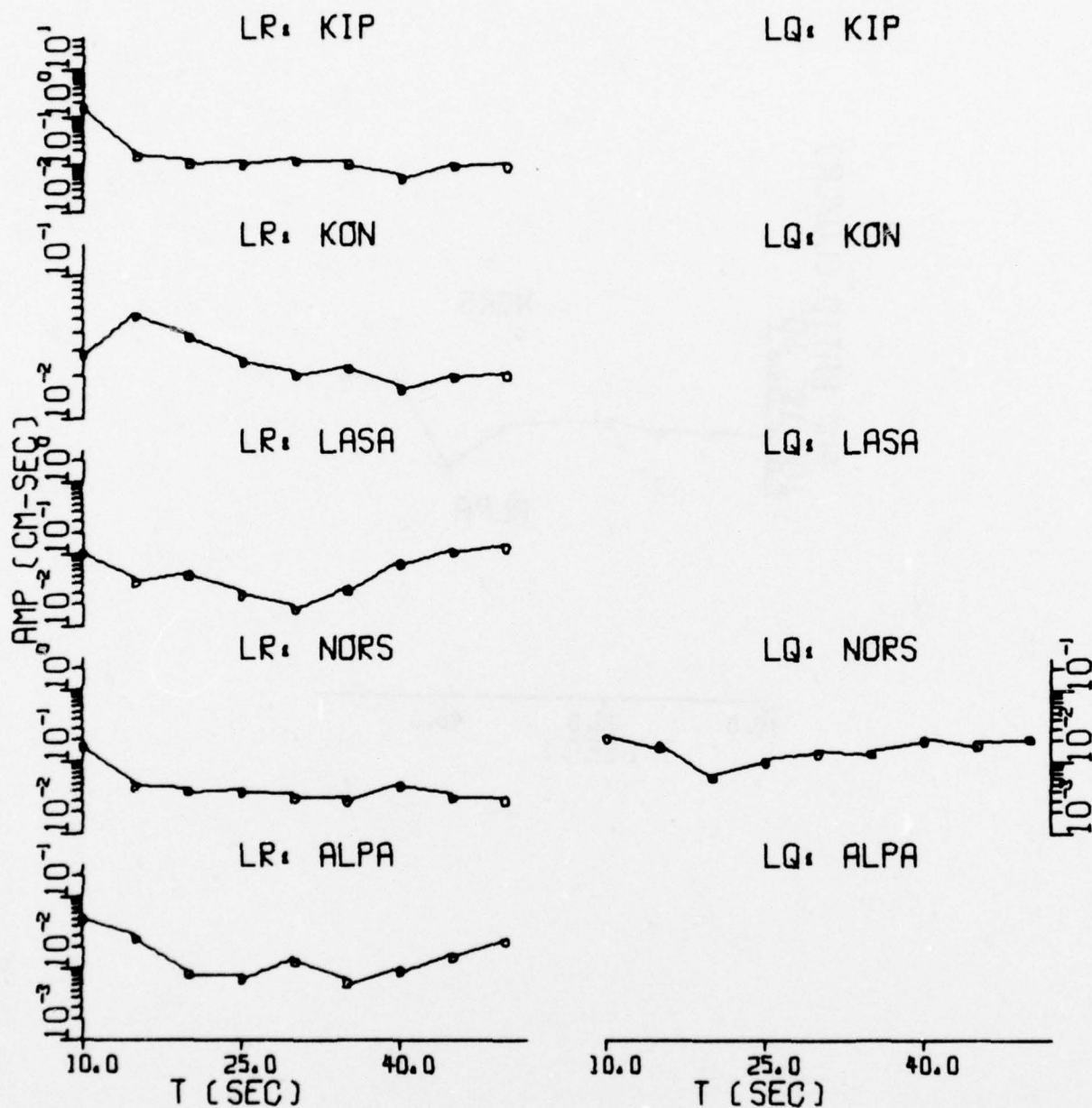


FIGURE III-30
OBSERVED SURFACE WAVE SPECTRA: EKZ/427/75
(PAGE 1 OF 3)

(a) Amplitude Spectra

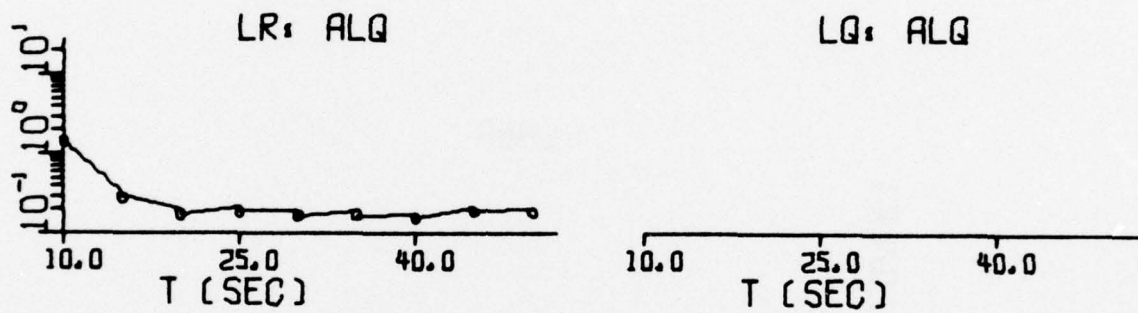


FIGURE III-30
OBSERVED SURFACE WAVE SPECTRA: EKZ/427/75
(PAGE 2 OF 3)

(b) LQ/LR Amplitude Spectral Ratio

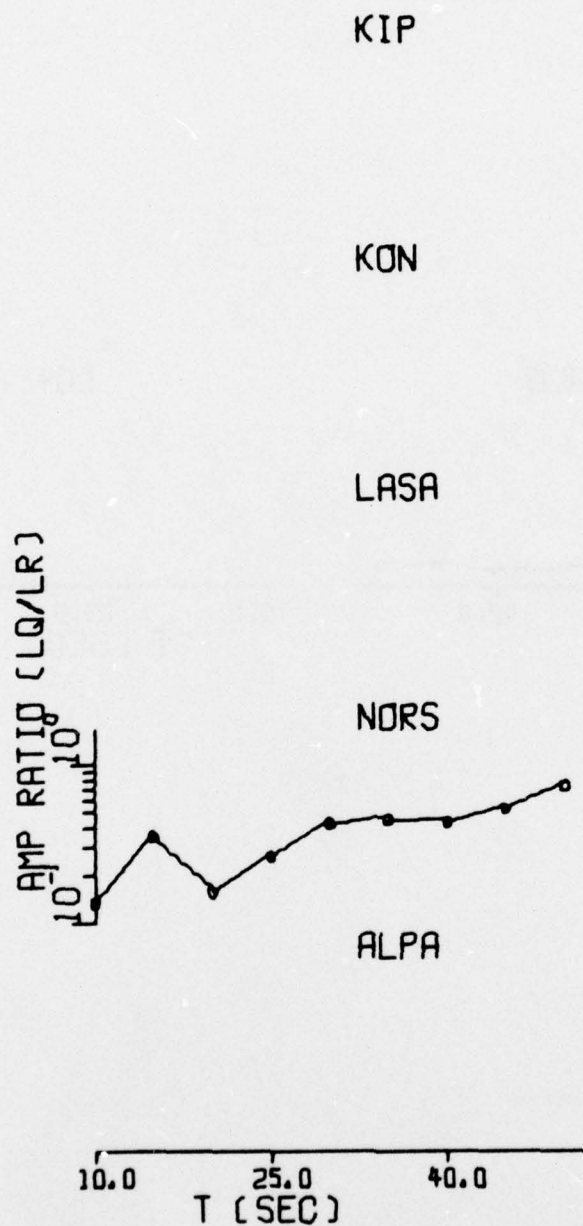


FIGURE III-30
OBSERVED SURFACE WAVE SPECTRA: EKZ/427/75
(PAGE 3 OF 3)

(a) Amplitude Spectra

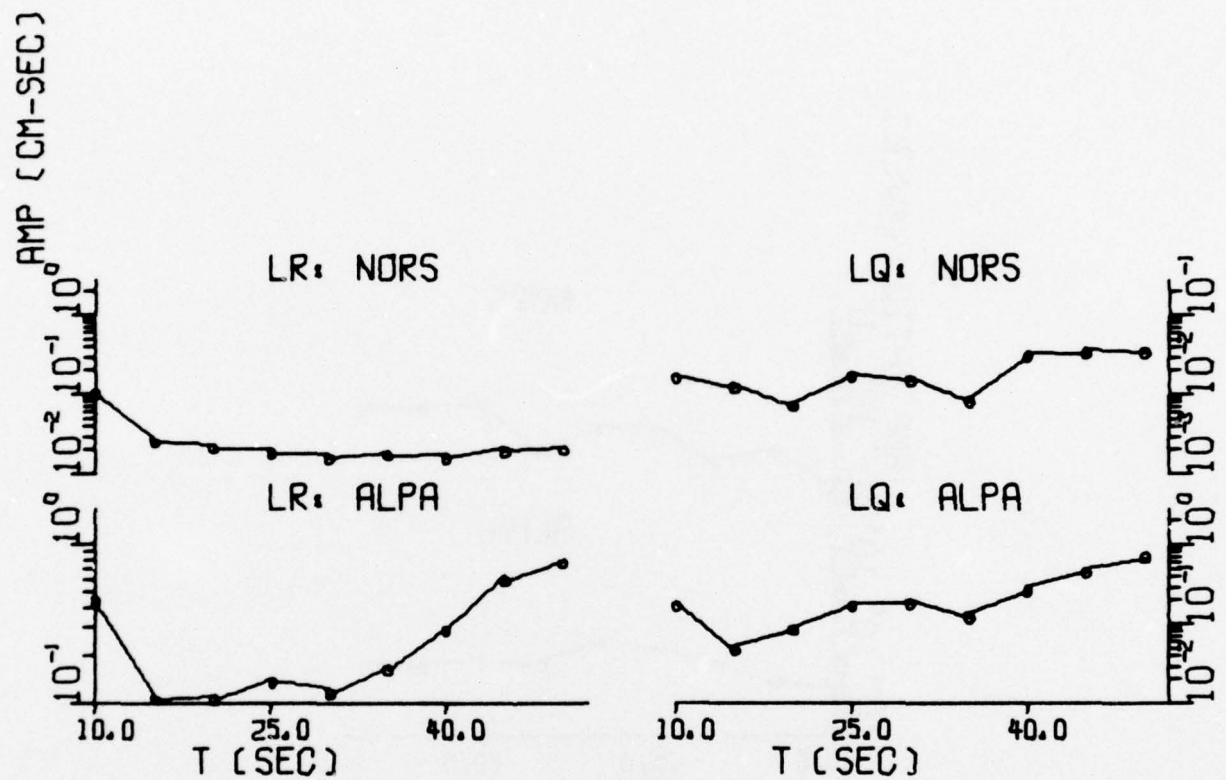


FIGURE III-31
OBSERVED SURFACE WAVE SPECTRA: EKZ/1029/5
(PAGE 1 OF 2)

(b) LQ/LR Amplitude Spectral Ratio

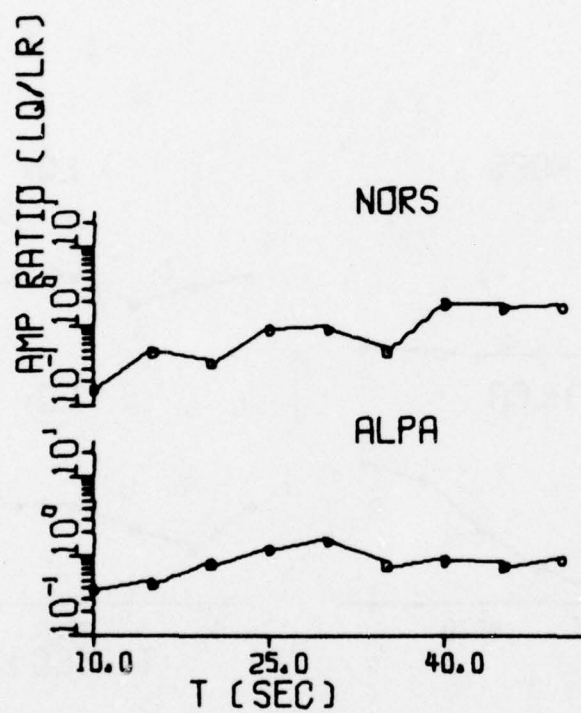


FIGURE III-31
OBSERVED SURFACE WAVE SPECTRA: EKZ/1029/5
(PAGE 2 OF 2)

(a) Amplitude Spectra

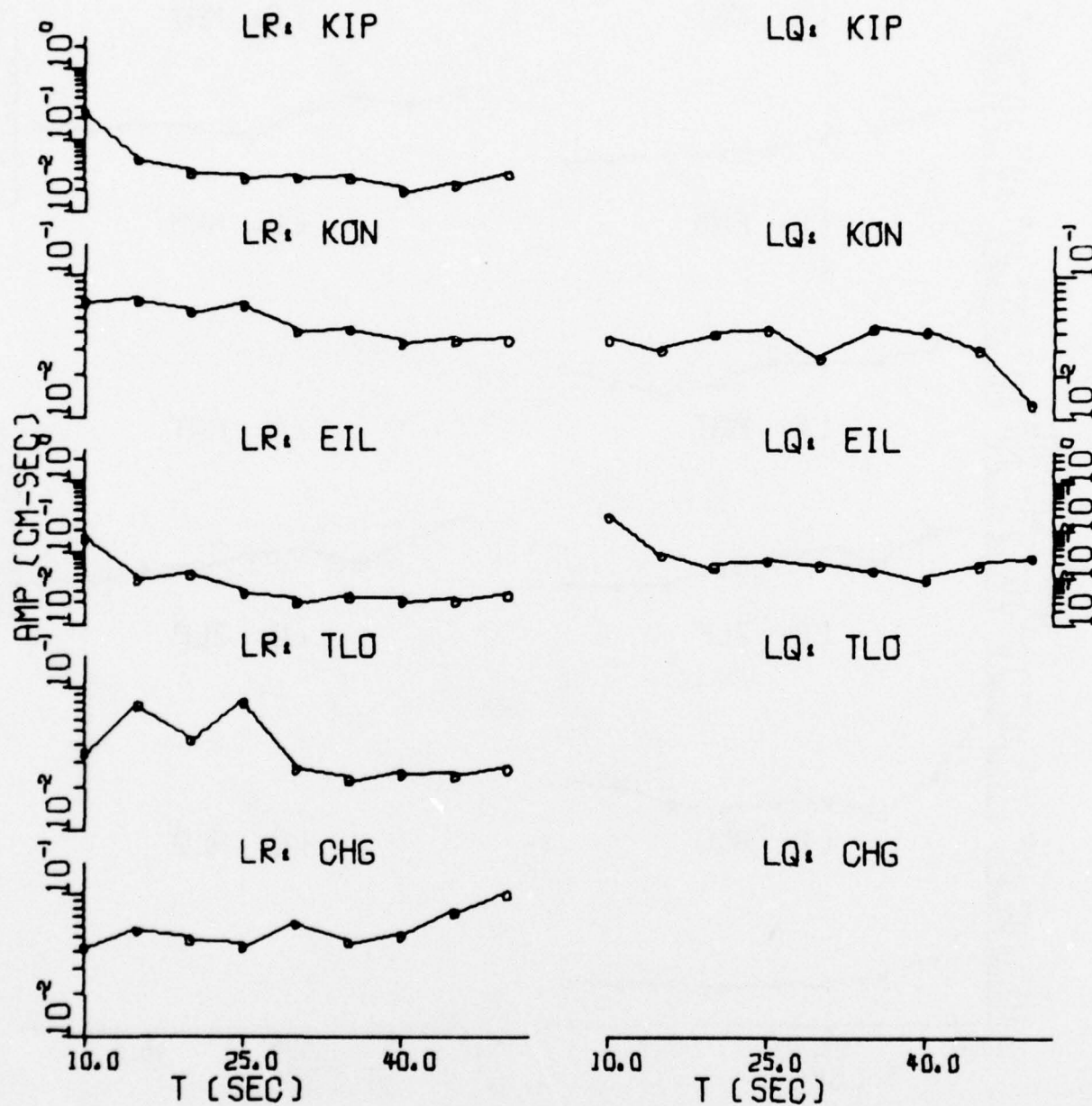


FIGURE III-32
OBSERVED SURFACE WAVE SPECTRA: EKZ/704/76
(PAGE 1 OF 4)

(a) Amplitude Spectra

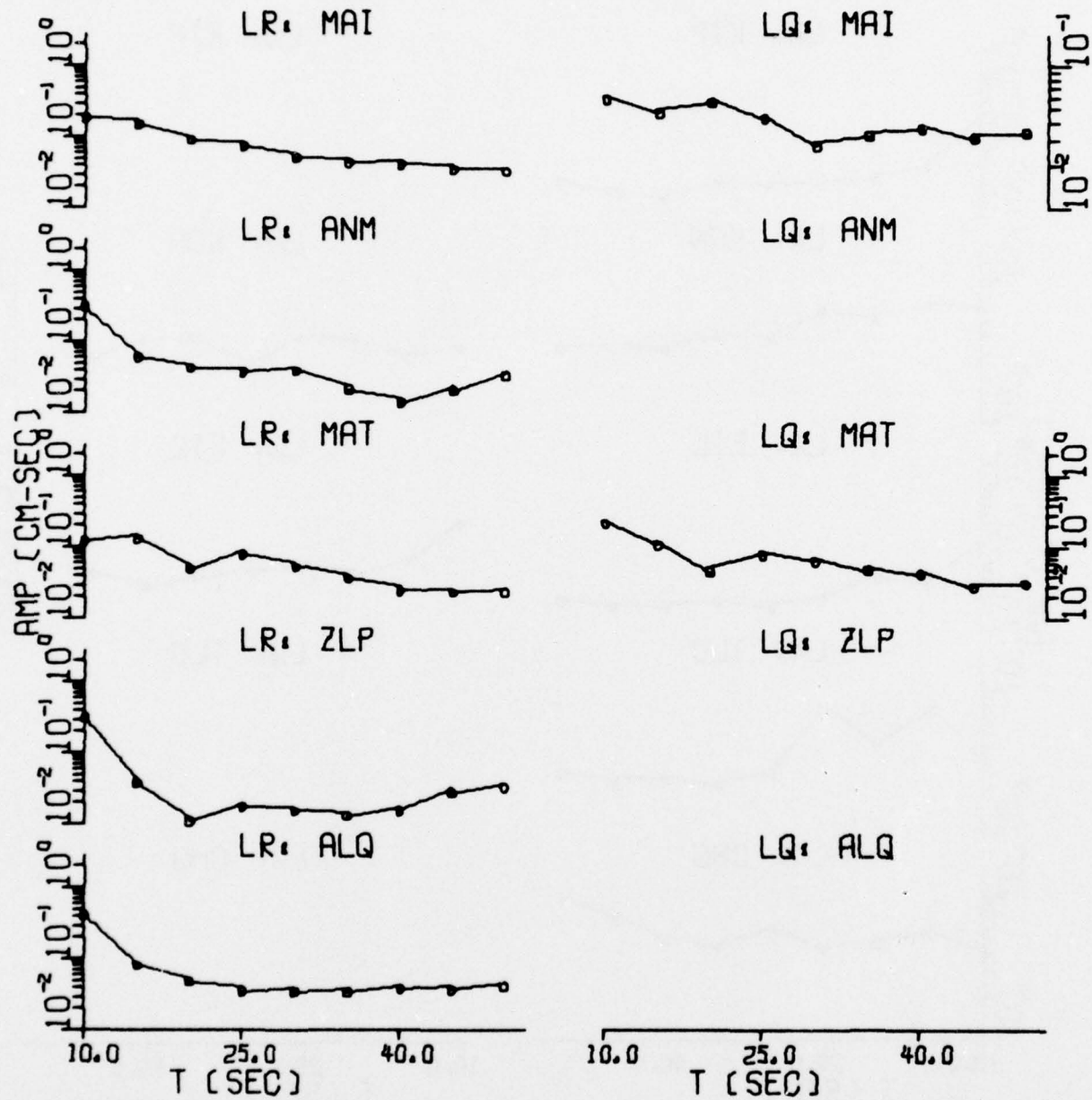


FIGURE III-32
OBSERVED SURFACE WAVE SPECTRA: EKZ/704/76
(PAGE 2 OF 4)

(b) LQ/LR Amplitude Spectral Ratio

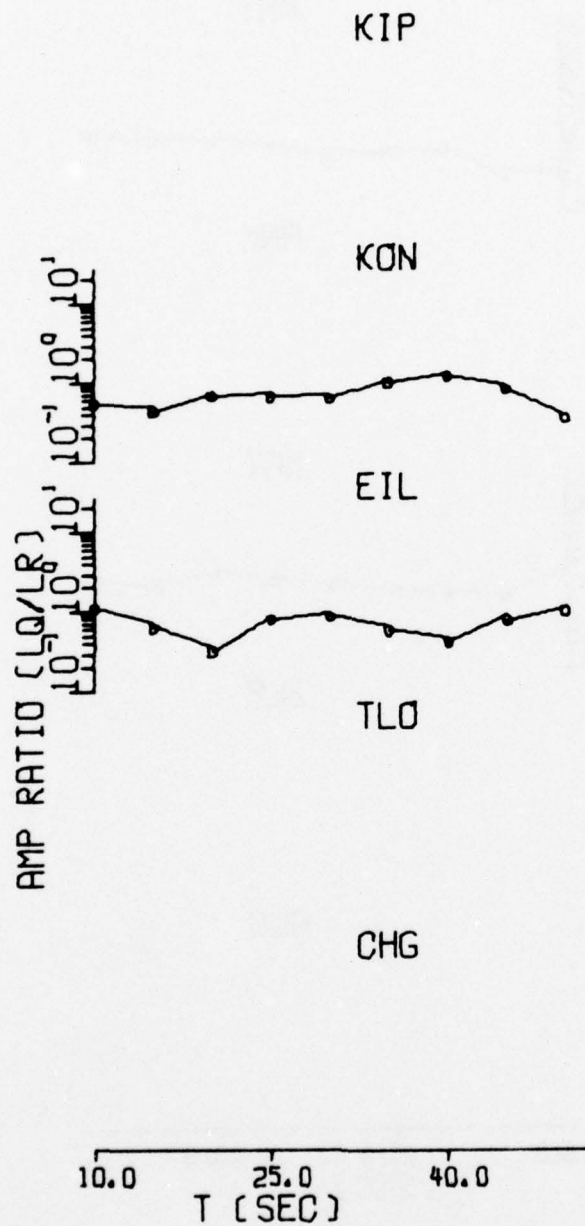


FIGURE III-32
OBSERVED SURFACE WAVE SPECTRA: EKZ/704/76
(PAGE 3 OF 4)

(b) LQ/LR Amplitude Spectral Ratio

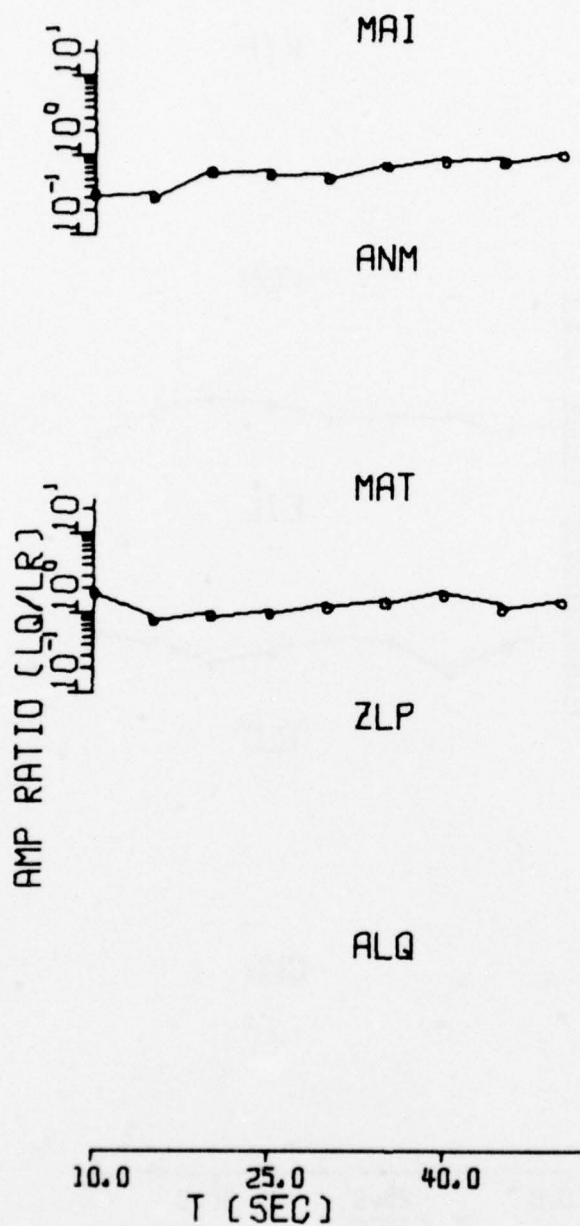


FIGURE III-32

OBSERVED SURFACE WAVE SPECTRA: EKZ/704/76
(PAGE 4 OF 4)

(a) Amplitude Spectra

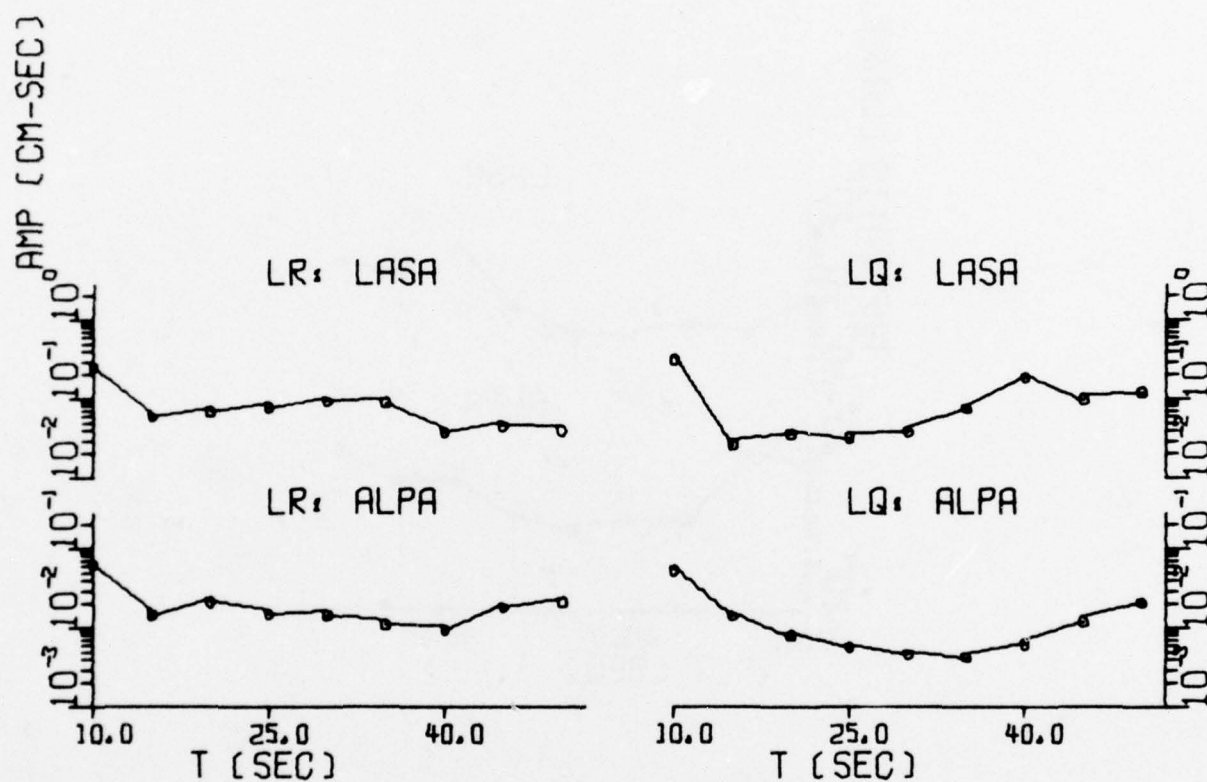


FIGURE III-33
OBSERVED SURFACE WAVE SPECTRA: PNE/1222/1
(PAGE 1 OF 2)

(b) LQ/LR Amplitude Spectral Ratio

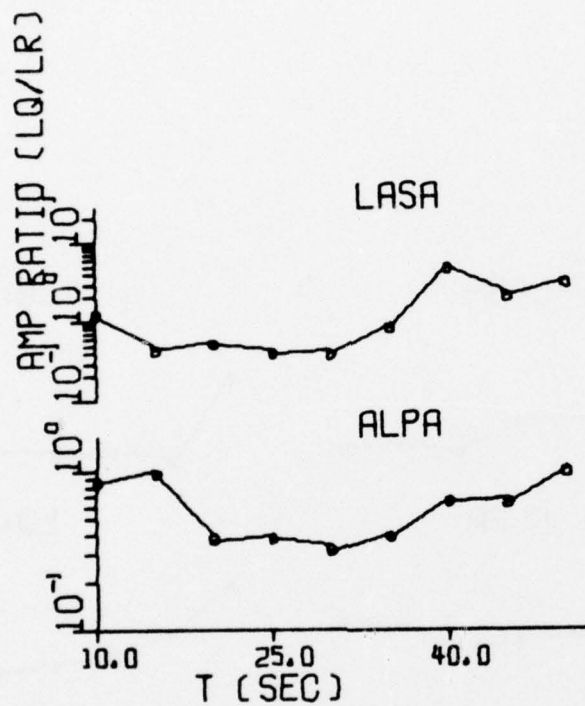


FIGURE III-33
OBSERVED SURFACE WAVE SPECTRA: PNE/1222/1
(PAGE 2 OF 2)

(a) Amplitude Spectra

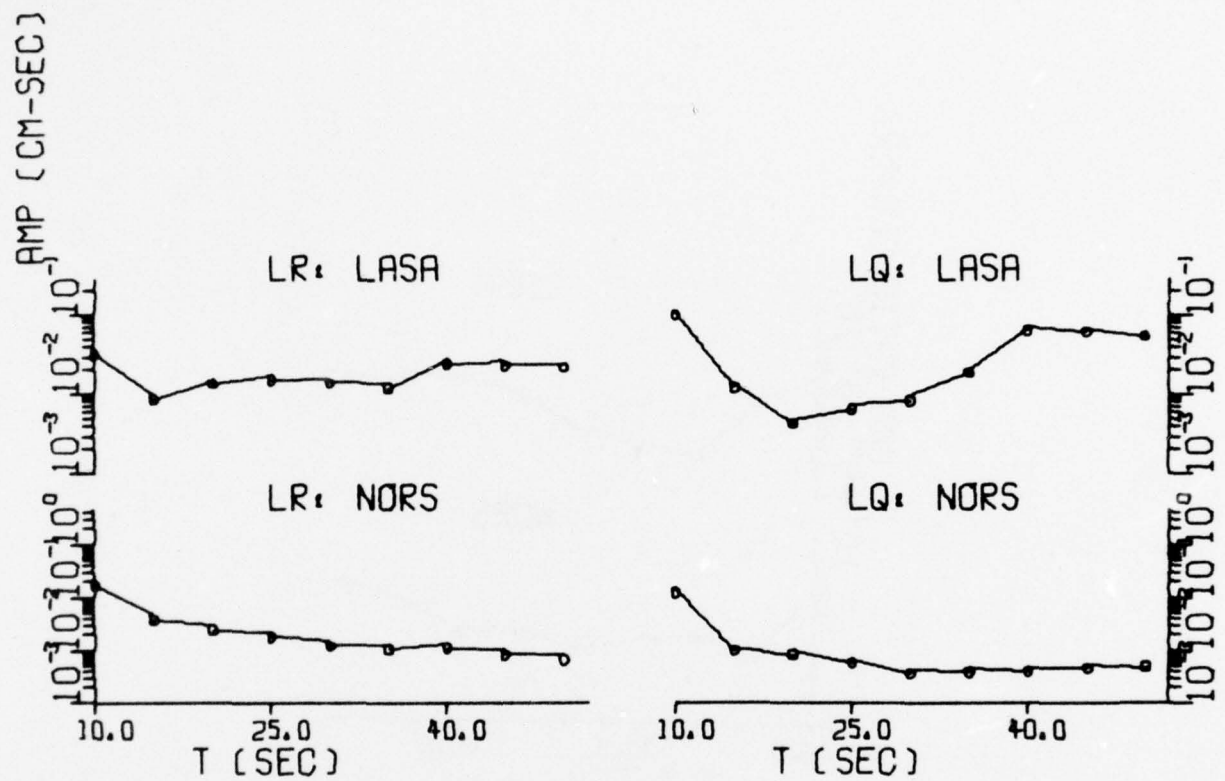


FIGURE III-34
OBSERVED SURFACE WAVE SPECTRA: PNE/820/72
(PAGE 1 OF 2)

(b) LQ/LR Amplitude Spectral Ratio

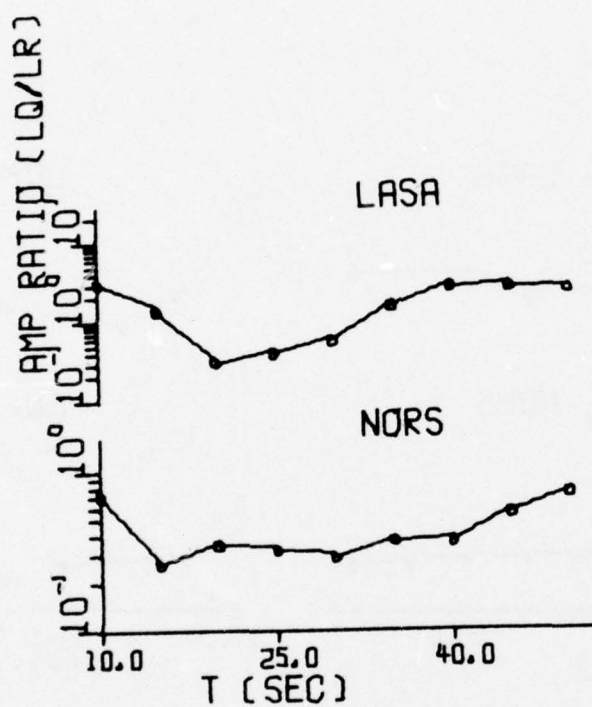


FIGURE III-34
OBSERVED SURFACE WAVE SPECTRA: PNE/820/72
(PAGE 2 OF 2)

(a) Amplitude Spectra

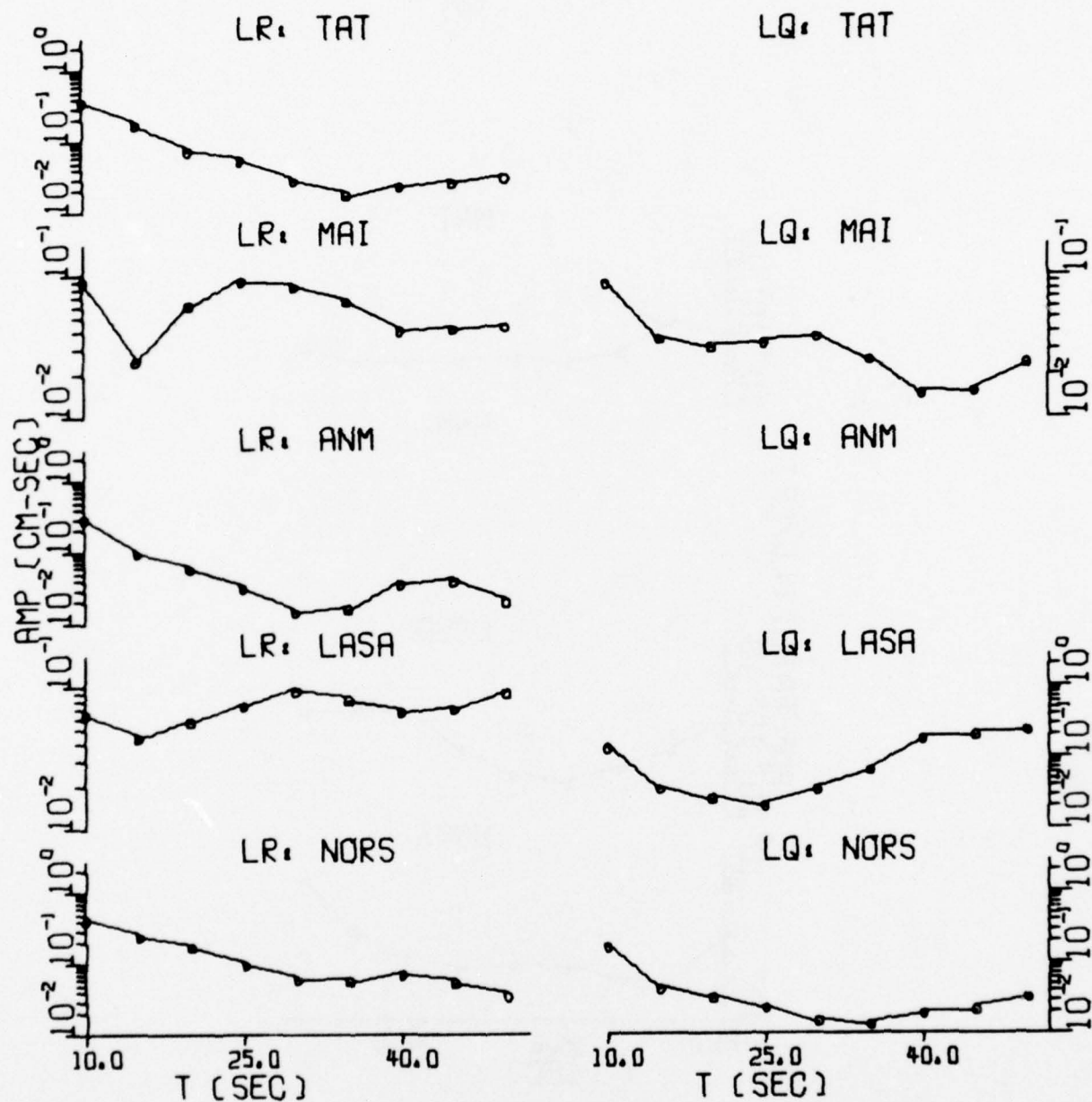


FIGURE III-35
OBSERVED SURFACE WAVE SPECTRA: PNE/729/76
(PAGE 1 OF 2)

(b) LQ/LR Amplitude Spectral Ratio

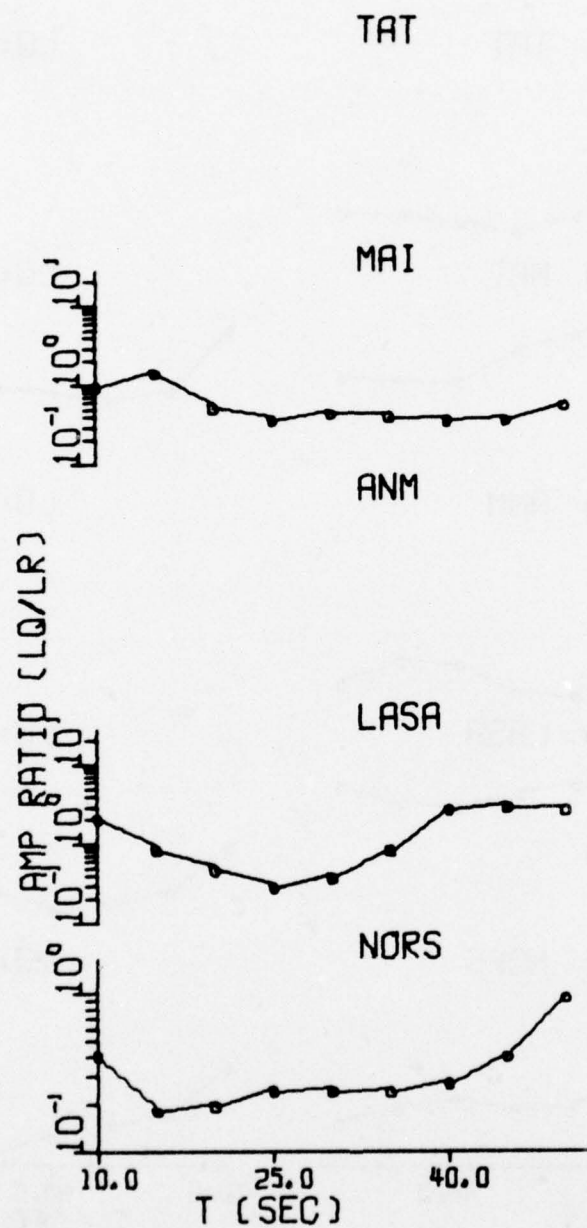


FIGURE III-35
OBSERVED SURFACE WAVE SPECTRA: PNE/729/76
(PAGE 2 OF 2)

observation station of a given event. The Love wave to Rayleigh wave amplitude ratios (LQ/LR), if available, are given in part (b). It is noticed that these observed spectra are represented by spectral values at nine discrete periods, namely 10 to 50 seconds at 5 second increments, and can be considered as the straight-line-interpolated version of the continuous spectra for the period range from 10 to 50 seconds.

a. The NTS events

Figures III-9 through III-24 show the observed surface wave amplitude spectra and LQ/LR spectral ratios for the selected NTS events. The results of examining these spectra and LQ/LR spectral ratios can be summarized as follows:

- For all events, most of the observation stations indicate Love wave motion, although, theoretically, an explosive source in a horizontally layered homogeneous isotropic medium should not generate Love waves. These observations of the Love waves from an explosion event can be best explained by the tectonic strain release associated with the explosion (Toksöz, et al., 1965). However, we have not observed the situation that the Love wave amplitude is always smaller than the corresponding Rayleigh wave amplitude at a given observation station as Lambert et al. (1972) observed. This is thought to be reasonable since, at some observation stations, Rayleigh waves generated from a point explosion source might destructively interfere with the Rayleigh waves radiated from the tectonic strain release, while the Love wave radiated from the tectonic strain release might be at the maximum of its radiation pattern.
- The shapes of the observed spectra vary from event to event for any given observation station. It is not apparent from

visual inspection whether these events have similar source mechanisms. However, there is a common feature in these spectra with a few exceptions. The common feature is that the average spectral amplitude is higher at short periods and decreases toward longer periods. From knowledge of the theoretical spectral variation with respect to focal depth for the explosive and double-couple source, this kind of spectral behavior is a definite indication of very shallow focal depth. This conjecture of very shallow focal depth, that will be shown later in the source parameter estimations of these events in Section V, justifies the assumption made by Lambert et al. (1972), Toksöz et al. (1964, 1965) and Mitchell (1975) that the double-couple source modeling the explosion-associated tectonic strain release is at the shot depth of the explosion.

- For any given event, the level of the observed spectra varies from observation station to observation station. This azimuthal variation of the observed spectra can be seen more clearly when the observed radiation patterns are plotted in Subsection V-C for several events with good azimuthal coverage. This variation of the spectral level among the various observation stations indicates that surface wave radiation from these events is not isotropic, i. e., the radiation pattern is non-circular. In addition to the observation of Love waves, this is another indication of possible tectonic strain release associated with these events. It is also noticed that, for any given observation station, the spectral level of the observed spectra varies from event to event. This is definitely, although not entirely, due to the fact that these events have different sizes, as indicated by their m_b . However, this also might be an indication that double-couple sources modeling the possible tectonic

strain release associated with these explosion events might not all have the same strike directions. This conjecture of different strike directions, that will be shown later in the source parameter estimations of these events in Section V, does not quite agree with the assumption made by some authors (Lambert, et al., 1972; Toksöz, et al., 1964, 1965) that the double-couple source modeling of the explosion-associated tectonic strain release has the same strike direction as that of the local earthquakes in the same region.

- For some events, it is noticed that the spectral level of the observed spectra at the SDCS stations is two to three times higher than that at other stations. There is no known physical explanation for this difference, although it is suspected that this relatively high spectral level is spurious and probably due to the miscalibration of the instruments in the field recordings or in the analog-to-digital (A/D) conversion. The reason for this suspicion is based on the examination of the signal calibration value ($m\mu/cc$) which shows abnormally large variation from event to event and from trace to trace, ranging from 1 $m\mu/cc$ to 20 $m\mu/cc$. However, the spectral shapes of the observed spectra at the SDCS stations seem comparable to those at other stations. Therefore, in the source parameter estimations of these events in Section V, the observed spectra from the SDCS stations are only used for those events for which no other data are available.
- The LQ/LR spectral ratios, as shown in part (b) of Figures III-9 through III-24, range from 0, if we assign $LQ/LR = 0$ for those observation stations which do not have useable Love wave recordings, to about 10, taking into account all events,

stations, and periods. These LQ/LR spectral ratios are compatible with the average fundamental mode LQ/LR spectral ratios for the shallow earthquakes theoretically modeled by the double-couple sources with all possible source mechanisms, i. e., dip angle ranging from 10 to 90 degrees, slip angle ranging from -90 to +90 degrees, and strike angle ranging from 0 to 180 degrees (Turnbull, 1976). This does not quite agree with the observations made by Lambert et al. (1972) that LQ/LR spectral ratios for explosions are less than one and are much less than those for earthquakes. Also, it is noticed that, on the average, the LQ/LR spectral ratios increase, although not significantly, from 10 seconds toward 50 seconds. This is somewhat different from the theoretical results for earthquakes given by Turnbull (1976) where the average fundamental mode LQ/LR spectral ratios increase very noticeably from 10 seconds toward 50 seconds. However, this difference is not thought significant enough to be used as the discrimination feature between the earthquake and the explosion as implicitly suggested by Lambert et al. (1972).

- In order to make possible comparison of the LQ/LR spectral ratios among the selected events, it is helpful to tabulate the values of the LQ/LR spectral ratios for all selected events observed at the same station. Referring to Table II-1, it is noticed that stations KON and ALPA have both Rayleigh and Love wave recordings for most of the selected events. Therefore, in Table III-1, the LQ/LR spectral ratios observed at KON and ALPA are given with the events ordered in decreasing event m_b . These values in Table III-1 are thought to be representative for the LQ/LR spectral ratios of the selected

TABLE III-1
TYPICAL LQ/LR SPECTRAL RATIOS FOR THE SELECTED NTS EVENTS

Event I. D.	m_b	Period (sec)								
		50	45	40	35	30	25	20	15	10
<u>Station: KON</u>										
NTS/212/76	6.3	1.34	1.37	1.14	0.85	0.82	0.89	0.67	0.39	1.15
NTS/626/75	6.2	1.56	1.35	1.07	0.75	0.54	0.81	0.59	0.65	1.83
NTS/619/75	6.1	1.53	1.23	1.08	0.77	0.48	0.77	0.54	0.71	1.52
NT1/317/76	6.1	5.11	4.56	2.92	1.78	1.55	0.36	0.32	0.67	0.65
NTS/514/75	6.0	0.92	0.89	0.89	0.66	0.66	0.94	0.55	0.32	0.54
NT1/603/75	5.9	1.05	1.04	0.86	0.81	0.61	0.92	0.55	0.34	0.38
NT2/317/76	5.8	2.07	2.46	1.99	0.81	0.53	0.69	0.64	1.03	2.11
NT2/603/75	5.7	0.89	0.87	0.86	0.62	0.47	1.01	0.57	0.68	4.92
NTS/430/75	5.2	0.74	0.80	0.89	1.50	1.64	2.24	2.04	0.61	4.67
<u>Station: ALPA</u>										
NTS/1028/5	6.4	0.89	1.14	1.55	1.92	1.45	1.30	1.19	0.54	0.38
NTS/626/75	6.2	0.86	0.96	1.27	1.33	1.10	0.97	0.90	0.48	0.21
NTS/103/76	6.2	1.12	1.35	1.81	2.02	1.74	1.49	1.35	0.90	0.61
NTS/619/75	6.1	0.55	0.66	0.92	1.04	0.92	0.84	0.77	0.60	0.35
NTS/514/75	6.0	0.61	0.81	1.14	1.35	1.10	0.87	0.81	0.20	0.27
NT1/603/75	5.9	0.32	0.45	0.60	0.62	0.56	0.59	0.57	0.25	0.18
NT2/603/75	5.7	0.61	0.51	0.84	0.77	1.11	0.09	0.56	0.28	0.37
NTS/926/74	5.6	0.46	0.36	0.51	0.46	0.45	0.40	0.64	0.44	0.91
NTS/430/75	5.2	1.20	1.02	1.01	0.67	0.62	0.58	0.47	0.38	0.38

events. Theoretically, if two events have the same or very similar focal depth, dip, slip and strike angle, and F value, their LQ/LR spectral ratios observed at the same observation station should be very similar. Referring to Table III-1, although no exactly identical LQ/LR spectral ratios are observed among these events, it is noticed that the events NTS/514/75, NT1/603/75, and NTS/619/75 have similar LQ/LR spectral ratios. Also, the events NTS/1028/5 and NTS/626/75 have similar LQ/LR spectral ratios. There is no apparent correlation between the event m_b and the LQ/LR spectral ratio. This is expected, since the difference in the event m_b should disappear in the process of taking the Love wave to the Rayleigh wave amplitude spectral ratio.

b. The EKZ events

Figures III-25 through III-32 show the observed surface wave amplitude spectra and the LQ/LR spectral ratios for the selected EKZ events. The spectral quality of these EKZ events is not as good as that of the NTS events. There are fewer stations where good surface wave recordings are available. An exception to this is the event EKZ/704/76. Also, Love wave recordings are not as frequently available as for NTS events. Nevertheless, for all selected EKZ events, Love wave recordings do exist at least for one observation station. Whenever they are available, their amplitude spectra seem compatible with the corresponding Rayleigh wave amplitude spectra.

In general, results similar to those stated previously for the NTS events about the variation of the spectral shape and the spectral level are found for the selected EKZ events. Again, as for the selected NTS events, the shape of the observed amplitude spectra varies from event to event for any given observation station, yet the spectral shape indicates a very shallow

event depth. Although Love wave motions are observed only at a few observation stations, variation of the spectral level of observed Rayleigh wave amplitude spectra does exist among the observation stations for a given event. This azimuthal variation of the observed Rayleigh wave amplitude suggests that the selected EKZ events do contain some double-couple component.

The LQ/LR spectral ratios, as shown in part (b) of Figures III-25 through III-32, range from 0 to 5. In general, these LQ/LR spectral ratios seem slightly lower than those for the NTS events; however, the difference is not thought to be significant enough to make a distinction between the explosions at EKZ and NTS. The typical values of the LQ/LR spectral ratios observed at stations ALPA and NORS are given in Table III-2. As with the NTS events, no obvious correlations are observed between these values and the event m_b . No noticeable similarity in the LQ/LR spectral ratios among the events is observed.

c. The PNE events

Figures III-33 through III-35 show the observed surface wave amplitude spectra and the LQ/LR spectral ratios for the selected PNE events. Also the typical values of the LQ/LR spectral ratios observed at stations NORS and LASA are shown in Table III-3. Love wave motion is observed at most of the stations for these three PNE events. As observed in the NTS and the EKZ events, the general shapes of the observed amplitude spectra suggest that these events took place at very shallow depths. Although there are only two observation stations involved in the events PNE/1222/1 and PNE/820/72, variation in the observed surface wave amplitude spectra is noticeable among observation stations for all three events. This anisotropic radiation of the surface waves together with the observation of the Love wave motion is again indicative of tectonic strain release associated with these explosions. The range of the variation of the LQ/LR spectral ratios

TABLE III-2
TYPICAL LQ/LR SPECTRAL RATIOS FOR THE SELECTED EKZ EVENTS

Event I. D.	m_b	Period (sec)								
		50	45	40	35	30	25	20	15	10
<u>Station: NORS</u>										
EKZ/723/73	6.3	1.80	1.59	0.82	0.30	0.47	0.58	0.25	0.32	0.23
EKZ/1029/5	5.8	1.75	1.73	1.92	0.48	0.94	0.93	0.34	0.48	0.16
EKZ/220/75	5.7	1.00	1.67	1.85	2.05	2.21	2.37	1.07	1.30	0.65
EKZ/427/75	5.6	0.73	0.52	0.43	0.44	0.42	0.76	0.16	0.35	0.13
EKZ/311/75	5.4	3.31	2.97	0.18	0.69	0.91	0.92	0.66	0.65	0.62
EKZ/1026/3	5.3	1.27	1.81	1.96	1.94	1.28	1.34	2.65	1.33	0.83
<u>Station: ALPA</u>										
EKZ/723/73	6.3	2.70	1.90	1.36	1.42	1.47	0.79	0.69	0.48	0.88
EKZ/1214/3	6.0	0.50	0.54	0.48	0.41	0.93	0.53	0.29	0.45	1.79
EKZ/1029/5	5.8	0.89	0.75	0.89	0.75	1.58	1.22	0.79	0.45	0.38
EKZ/1026/3	5.3	0.65	0.90	0.87	1.07	2.18	0.82	0.59	1.29	1.49

TABLE III-3
TYPICAL LQ/LR SPECTRAL RATIOS FOR THE SELECTED PNE EVENTS

Event I. D.	m_b	Period (sec)								
		50	45	40	35	30	25	20	15	10
<u>Station: NORS</u>										
PNE/729/76	5.9	0.92	0.40	0.27	0.24	0.24	0.29	0.19	0.18	0.40
PNE/820/72	5.7	0.73	0.55	0.36	0.33	0.29	0.32	0.35	0.26	0.71
<u>Station: LASA</u>										
PNE/1222/1	6.0	3.02	2.10	4.83	0.84	0.39	0.40	0.57	0.43	1.20
PNE/729/76	5.9	2.55	2.84	2.67	0.79	0.37	0.28	0.46	0.83	2.05
PNE/820/72	5.7	2.51	2.69	2.69	1.05	0.31	0.41	0.31	1.37	3.09

is very much the same as that for the EKZ events, from 0 to about 5. Referring to Table III-3, the LQ/LR spectral ratios for the event PNE/820/72 are quite similar to those for the event PNE/729/76, indicating that these two events very likely have similar source parameters in terms of depth, dip, slip and strike angle, and the F value.

2. Relative Love Wave Excitation from a Suite of NTS Events

As discussed in Subsection III-B-1-a, Love wave motion is observed for all selected NTS events at most observation stations. However, at any given observation station, no apparent correlation between the level of the observed Love wave amplitude spectra and the event m_b is observed. This is thought to be reasonable, since at any given observation station the observed spectral level of the Love wave amplitude spectra not only depends on the event m_b but also depends (even more heavily) on the F value, which is the indication of the amount of the tectonic strain release associated with the explosion, and the strike direction of the double-couple source which models the explosion-associated tectonic strain release. For example, even assuming that two explosion events have the same amount of tectonic strain release, the Love wave amplitude spectral levels for these two events observed at the same station can be very different just due to the different orientations of the Love wave radiation patterns caused by the different strike directions.

To examine the relative Love wave excitation from a suite of NTS events, two approaches are taken. In the first approach, one NTS event is taken as a reference event and the relative Love wave excitation is determined from the ratios of the observed Love wave amplitude spectra of a given event to those of the reference event. These ratios are calculated for all available common observation stations where they are compared among selected NTS events. In the second approach, the seismic moment of the tectonic

strain release associated with the explosion is estimated for each NTS event and these estimated seismic moments are then compared among the selected events.

For the first approach, the event NTS/619/75, which has observed Love wave amplitude spectra at all six observation stations, is chosen as the reference event. The Love wave amplitude ratios of the other NTS events to the reference event NTS/619/75 are shown in Table III-4 for the observation stations ALPA and KON. In Table III-4, the events are arranged in the order of decreasing m_b . Theoretically, if these events have identical or very similar source parameters, then their Love wave ratios should be very similar at any observation station and these ratios can be conveniently used as a measure of the relative Love wave excitations (Lambert, et al., 1972). However, without knowledge of the source parameters of these events, the direct comparisons of these Love wave ratios can be very misleading. Referring to Table III-4, it is obvious that quite different conclusions about the relative Love wave excitation from these events can be drawn by examining the Love wave ratios observed at station KON or by examining those observed at station ALPA. For example, for event NTS/430/75, the Love wave ratios observed at ALPA indicate that this event should have much less Love wave excitation than event NTS/619/75; while the Love wave ratios observed at station KON suggest that the Love wave excitation from event NTS/430/75 should be about 1.5 times larger than that from event NTS/619/75. These differences in Love wave ratios for the same event observed at different observation stations can not be explained by the m_b differences between event NTS/430/75 and the reference event NTS/619/75. Moreover, the Love wave ratios observed at the same observation stations for events with comparable m_b , such as the events NTS/626/75 and NTS/103/76, show drastic differences. No apparent correlation between the Love wave ratios and the event m_b are observed, i. e., the larger m_b does not necessarily imply the larger Love

TABLE III-4

LOVE WAVE AMPLITUDE RATIOS OF THE SELECTED NTS EVENTS:
REFERENCE EVENT NTS/619/75 $m_b = 6.1$

Event I. D.	m_b	Period (sec)								
		50	45	40	35	30	25	20	15	10
<u>Station: KON</u>										
NTS/212/76	6.3	2.59	3.40	2.85	2.96	3.84	3.62	2.58	2.25	1.20
NTS/626/75	6.2	1.76	1.87	1.70	1.69	1.78	1.67	1.55	1.55	0.57
NT1/317/76	6.1	0.75	0.84	0.65	0.60	0.50	0.16	0.23	0.47	0.09
NTS/514/75	6.0	0.56	0.62	0.63	0.68	1.05	0.96	0.96	0.52	0.36
NT1/603/75	5.9	0.36	0.44	0.39	0.48	0.66	0.58	0.52	0.31	0.09
NT2/317/76	5.8	0.32	0.37	0.35	0.24	0.22	0.29	0.41	0.47	0.16
NT2/603/76	5.7	0.20	0.22	0.21	0.21	0.27	0.29	0.42	0.31	0.14
NTS/430/75	5.2	1.09	1.33	1.21	1.56	2.03	1.50	2.16	1.46	1.15
<u>Station: ALPA</u>										
NTS/1028/5	6.4	5.02	5.38	5.02	4.57	4.37	4.23	4.51	2.27	2.71
NTS/626/75	6.2	2.87	2.88	2.72	2.50	2.43	2.41	2.58	2.08	1.13
NTS/103/76	6.2	9.64	9.51	8.86	8.33	7.88	7.29	8.13	4.92	5.11
NTS/514/75	6.0	0.69	0.79	0.76	0.74	0.71	0.64	0.69	0.28	0.62
NT1/603/75	5.9	0.23	0.27	0.28	0.26	0.26	0.29	0.27	0.21	0.29
NT2/603/75	5.7	0.12	0.09	0.10	0.09	0.09	0.08	0.13	0.09	0.12
NTS/926/74	5.6	0.05	0.03	0.03	0.02	0.02	0.03	0.06	0.04	0.12
NTS/430/75	5.2	0.18	0.07	0.05	0.03	0.03	0.03	0.03	0.04	0.04

wave ratios. It is believed that these large differences in the observed Love wave ratios are probably caused by the differences in the F values and the source parameters among the selected NTS events. Therefore, it seems not too plausible to obtain reliable information about the relative Love wave excitation by direct comparison of amplitude spectra or amplitude ratios observed at a number of common observation stations.

For the second approach, Table III-5 presents the estimated seismic moments of the tectonic strain releases associated with the selected NTS events, their locations, and event m_b . The details of how these seismic moments were estimated will be given in Section V where the source parameter estimations of all selected NTS, EKZ, and PNE events are discussed. In Table III-5, the events are ordered in decreasing seismic moment. Thus, Table III-5 actually gives the rankings of the selected NTS events in terms of their associated tectonic strain release. The seismic moment is estimated from the observed surface wave amplitude spectra recorded at all observation stations. Since it is a constant for a given event, the seismic moment, which measures tectonic strain release associated with an explosion, is thought to be a more stable and useful quantity than direct observations of surface wave amplitude spectra or Love wave spectral ratios. Referring to Table III-5, for the NTS PAHUTE events, there is an apparent trend between the estimated seismic moments of the explosion-associated tectonic strain releases and the event m_b . For those events which took place in hard rock, i. e., shot location indicated by NTS PAHUTE, the trend indicates that the seismic moment of the explosion-associated tectonic strain release decreases with decreasing m_b . This trend is thought to be reasonable, if the source of the tectonic strain energy released by an explosion is by relaxation of the cavity (Toksöz, et al., 1965; Press and Archambeau, 1962). One event which deviates drastically from the rest of the events is NTS/430/75. The m_b of this event is 5.2 and yet the estimated seismic moment associated with this

TABLE III-5
ESTIMATED SEISMIC MOMENTS OF THE TECTONIC STRAIN RELEASES
ASSOCIATED WITH THE SELECTED NTS EVENTS

Event I. D.	m_b	$M_E \times 10^{25}$ dyne-cm	Location*
NTS/1028/5	6.4	0.243	NTS PAHUTE
NTS/626/75	6.2	0.127	NTS PAHUTE
NTS/103/76	6.2	0.111	NTS PAHUTE
NTS/212/76	6.3	0.105	NTS PAHUTE
NTS/314/76	6.3	0.0975	NTS PAHUTE
NT1/317/76	6.1	0.0428	NTS PAHUTE
NTS/309/76	6.0	0.0332	NTS PAHUTE
NTS/430/75	5.2	0.0212	NTS
NTS/619/75	6.1	0.0192	NTS PAHUTE
NT2/317/76	5.8	0.0180	NTS
NTS/514/75	6.0	0.0170	NTS PAHUTE
NT1/603/75	5.9	0.00864	NTS PAHUTE
NT2/603/75	5.7	0.00302	NTS
NTS/926/74	5.6	0.00163	NTS

*This information is obtained from the announced United States Nuclear Test Statistics given by Nevada Operation Office, Energy Research and Administration (30 June 1976)

explosion is what is expected of the events with m_b 's around 6.0. The real physical reason for this large deviation is not known at the present time. One possible explanation for this situation is that a real earthquake was triggered by this explosion. In that case, the size of the triggered earthquake is not directly dependent on the size of the explosion (Brune and Pomeroy, 1963; Aki, 1964).

SECTION IV

TRAVEL PATH ATTENUATION

Several factors affect the spectral level and shape of the far-field surface wave amplitude spectra of a seismic event. These factors can be conveniently lumped into three groups: the source parameters of the event, travel path effects, and the instrument response of the observation station. Therefore, in order to estimate the seismic source parameters using the observed far-field surface wave spectra, some appropriate corrections to the observed spectra must be made. The corrections for the instrument response and geometric spreading are trivial, while the correction for the energy attenuation, which is the other part of the travel path effect, generally is not well known due to limited knowledge of the surface wave energy dissipation.

The travel path attenuation correction is important in the estimation of the seismic source parameters by spectral fitting of observed far-field surface wave data. The level of the attenuation curve can affect the estimation of the seismic moment, and the general shape of the curve can affect the estimation of the focal depth and the source mechanism. So far, when no reliable knowledge of energy attenuation along the travel paths of interest is available, Tryggvason's energy attenuation curve (Tryggvason, 1965) has been used. The general shape of Tryggvason's curve is believed to be reasonable, although the level of the curve seems a little low (Tryggvason, 1965; Anderson, 1964). Nevertheless, in the past, using Tryggvason's attenuation correction, the seismic moment estimates of numerous Eurasian seismic events have fitted very well with the seismic moment-versus-bodywave magnitude curve determined from the revised ω^2 -model given by Tsai (1972b).

It is the purpose of this section to obtain the surface wave attenuation curves for several travel paths of interest and to find out how applicable Tryggvason's curve is.

Two methods to determine the surface wave attenuation coefficients will be derived and discussed in Subsection A. In Subsection B, these methods are applied to the observed surface wave data available for the selected NTS and EKZ events.

A. METHODS

The term 'energy dissipation' or 'energy attenuation' used throughout this report is chosen to indicate all energy lost along the travel path including absorption, reflected energy, and scattered energy.

In the following derivation, it is assumed that there is no energy transferred from one frequency to another along the travel path and that the observed amplitude spectra have been corrected for the station instrument response. Two methods will be described below: the two-station method which is suitable for two stations along the same event-station travel path, and the isotropic-source method which can be employed for the explosion data.

1. Two-Station Method

The observed surface wave amplitude spectra of a given seismic event recorded at two stations can be related as follows:

$$\frac{A_1(f)}{A_2(f)} = R(O_1, O_2, f) \left(\frac{\sin \Delta_2}{\sin \Delta_1} \right)^{\frac{1}{2}} e^{-k_{A1}(f) D_1 + k_{A2}(f) D_2} \quad (IV-1)$$

where

$A_i(f)$ is the observed amplitude spectrum for frequency f at station i ,

$k_{Ai}(f)$ is the amplitude attenuation coefficient for frequency f along the travel path i (great circle path between the seismic event and station i),
 D_i is the epicentral distance in km to station i ,
 Δ_i is the epicentral distance in degrees to station i ,
 O_i is the source azimuthal angle to station i , and
 $R(O_1, O_2, f)$ is the ratio of the source excitation at O_1 to that at O_2 , for frequency f .

In equation (IV-1) the term $R(O_1, O_2, f)$ accounts for the non-circular radiation pattern of the source. For an isotropic source, $R(O_1, O_2, f) = 1.0$. For an anisotropic source, such as an earthquake, in general $R(O_1, O_2, f) \neq 1$. However, in the special case, $O_1 = O_2$, $R(O_1, O_2, f) = 1$ regardless of source type. That is, when two observation stations are on the same great circle path between the seismic event and the station and have the same azimuthal angle, equation (IV-1) can be reduced to

$$\frac{A_1(f)}{A_2(f)} = \left(\frac{\sin \Delta_2}{\sin \Delta_1} \right)^{\frac{1}{2}} e^{-k_A(f)(D_1 - D_2)} \quad (\text{IV-2})$$

where k_A now is the amplitude attenuation coefficient for frequency f along the travel path between stations 1 and 2. Therefore, equation (IV-2) can be applied to the surface wave data recorded at two stations along the same travel path to calculate the travel path attenuation as follows:

$$k_A(f) = \frac{\ln \left[\frac{A_1(f)}{A_2(f)} \right] + \frac{1}{2} \ln \left(\frac{\sin \Delta_1}{\sin \Delta_2} \right)}{D_2 - D_1} \quad (\text{IV-3})$$

Estimates of observational errors inherent in the two-station method might be inferred in the following way. Hermann (1974), in his studies of source spectra of earthquakes and anelastic attenuation of surface waves,

found that the source spectra could be estimated within a factor of 1.5 at 95% confidence level from a good data set. As a consequence of this error estimate, one can state that in such a case the individual spectral amplitudes at a recording station can be determined within a factor of 1.5 accuracy, at the same confidence level. Using this estimate of the variation in the observed spectra, an estimate can be made of the inherent error in the attenuation coefficient determinations by the two-station method. That is, in the worst possible case (the amplitude A_1 could be 1.5 times larger than the average and A_2 could be 1.5 times smaller than the average; or A_1 could be 1.5 times smaller and A_2 could be 1.5 times larger), the variation of the calculated $k_A(f)$ may be estimated as:

$$\left| \Delta k_A(f) \right| = \frac{2 \ln(1.5)}{D_2 - D_1} . \quad (\text{IV-4})$$

2. Isotropic-Source Method

When data from more than two stations are available, two approaches other than the two-station method can be used. One method outlined by Tsai and Aki (1969) assumes that the source characteristics (focal depth, source mechanism, and average structure of the medium) are known; while the other method used by Tryggvason (1965) assumes that the surface wave radiation is isotropic. There are advantages and disadvantages in using these methods. Tsai and Aki's approach can take into account possible variations in the observed spectral amplitudes at each station and, hence, can be applied to the observed data from any source type as long as the exact source characteristics are known a priori, which is the shortcoming of this method. On the other hand, Tryggvason's approach is more straight forward since no prior knowledge about the source characteristics is required. However, Tryggvason's method can only be applied to observed data from an isotropic source. Also, in both methods, the estimated k_A value represents a regional average rather than a value characteristic of a particular travel path as that obtained through the two-station method.

Here, Tryggvason's method is chosen to be employed by the observed surface wave data from the selected NTS and EKZ events. The main reason for choosing Tryggvason's method is that the source characteristics of these events are not known, and explosion events are closer to an isotropic source than are earthquake events. The original Tryggvason's method only applies to surface wave data from one explosion event. In the following, Tryggvason's method will be extended in order to use the surface wave data from many explosion events from the same area. Also, the variance of the estimated k_A value will be derived.

In Tryggvason's method, the surface wave amplitude attenuation coefficient can be estimated from the following equation by using the far-field observed surface wave amplitude spectra at several observation stations for one explosion:

$$\ln A_i(f) + \frac{1}{2} \ln \sin \Delta_i = C_2(f) - D_i k_A(f) \quad i = 1, \text{NSITE} \quad (\text{IV-5})$$

where A_i , Δ_i , and D_i were previously defined. $k_A(f)$ is now the average amplitude attenuation coefficient for travel paths between the event and all NSITE available observation stations at frequency f . C_2 is a constant depending on frequency and the given explosion event. In equation (IV-5), k_A and C_2 are two unknown parameters to be estimated. Hence, when NSITE is greater than two, k_A and C_2 can be estimated by linear regression; i. e., minimizing the following quantity

$$\epsilon = \sum_{i=1}^{\text{NSITE}} \left[\left(\ln A_i + \frac{1}{2} \ln \sin \Delta_i \right) - (C_2 - D_i k_A) \right]^2. \quad (\text{IV-6})$$

The estimated k_A will be as follows:

$$k_A(f) = \frac{\text{NSITE} \sum_i \left[\left(\ln A_i + \frac{1}{2} \ln \sin \Delta_i \right) D_i \right] - \left(\sum_i D_i \right) \left[\sum_i \left(\ln A_i + \frac{1}{2} \ln \sin \Delta_i \right) \right]}{\left(\sum_i D_i \right)^2 - \text{NSITE} \sum_i D_i^2} \quad (\text{IV-7})$$

where \sum_i stands for $\sum_{i=1}^{NSITE}$. It can be easily shown that equation (IV-7) will be reduced to equation (IV-3) when NSITE is equal to two, as expected. By regression analysis, the standard error S of the estimated k_A values can be estimated from the sample as

$$S^2 = \frac{NSITE}{NSITE-2} \frac{\epsilon}{\left| \left(\sum_i D_i \right)^2 - NSITE \sum_i D_i^2 \right|} \quad (IV-8)$$

We have discussed the method for obtaining the average amplitude attenuation coefficient k_A together with its error estimate S . This process can be performed with data from each of the selected events in the same area so that independent estimates of k_A can be made for each event. The result is that a mean k_A value can be obtained together with its error estimate. Now each k_{Aj} has been determined from the observed data at $NSITE_j$ stations with a corresponding variance S_j^2 , where j refers to the particular estimate made from the j^{th} explosion. The mean k_A value and its error estimate can be obtained from k_{Aj} and S_j^2 as follows (Hoel, 1972; Herrmann and Mitchell, 1975):

$$\bar{k}_A = \sum_{j=1}^{NEXP} k_{Aj} / NEXP \quad (IV-9)$$

$$\bar{S}^2 = \sum_{j=1}^{NEXP} S_j^2 / NEXP \quad (IV-10)$$

where $NEXP$ is the number of available explosions in the same area.

B. RESULTS

To calculate the surface wave amplitude attenuation coefficients for the travel path of interest, the methods discussed in the previous subsection are applied to the Rayleigh wave data from two groups of events, namely

the selected NTS and EKZ events as listed in Table II-1. The observed Rayleigh wave amplitude spectra with appropriate instrument response correction are obtained in the manner described in Section II. In the following, the results will be presented in terms of two groups of travel paths, i. e., the travel paths from the NTS to the observation stations available to the selected NTS events and the travel paths from EKZ to the observation stations available to the EKZ events.

1. Travel Paths From the NTS to the Observation Stations

Referring to Figure III-1 which shows the travel paths encountered from the NTS to the observation stations, these travel paths can be logically divided into two groups: (1) mostly oceanic paths from the NTS to stations in the Pacific Ocean and (2) mostly continental or mixed (i. e., partially continental and partially oceanic) paths from the NTS to the rest of the observation stations. Therefore, two sets of Rayleigh wave attenuation coefficients are estimated for two groups of travel paths. The travel paths in the first group are those from the NTS to stations CTA, KIP, and MAT. The travel paths in the second group include those from the NTS to stations ALPA, NORS, LASA, CHG, TLO, KON, OGD, ALQ, ZLP, and MAI. The travel paths from the NTS to the SDCS Stations are purposely excluded due to the non-uniform data quality at those stations as discussed in Section III. For the first group of travel paths, it is noticed from Figure II-1 that the stations KIP and CTA are almost on the same event-station great circle path. Referring to Table II-3a, the azimuthal angles at the source for these two stations differ by only 1 degree, and there are four events (NTS/103/76, NTS/314/76, NT1/317/76, and NT2/317/76) which have Rayleigh wave recordings at these two stations. Therefore, in addition to obtaining the average Rayleigh wave attenuation coefficients by the isotropic-source method for the first group of travel paths, the two-station method is used to obtain the Rayleigh wave attenuation coefficients particularly for the travel path between stations KIP and CTA.

Figure IV-1 shows the Rayleigh wave amplitude attenuation coefficients from 10 to 50 seconds calculated at 5 second increments, and obtained for the first group of travel paths. In this figure, the average Rayleigh wave amplitude attenuation coefficients \bar{k}_A are obtained by the isotropic-source method for the travel paths between the NTS and the stations CTA, KIP, and MAT. These are indicated by the solid dot (●) with the vertical bar showing the standard error $\pm \bar{S}$ of the estimated \bar{k}_A value. The Rayleigh wave amplitude attenuation coefficients obtained by the two-station method for the travel path between the stations KIP and CTA are indicated by the cross (x). For comparison purposes, the average Rayleigh wave attenuation coefficients obtained by Mitchell et al. (1976) for the travel paths within the Pacific Ocean are indicated by the solid square (■). The values of Mitchell et al. (1976) agree quite well with our values, except that their value at 15 seconds is significantly higher. Nevertheless, all their values lie well within the standard error of our values. Also, the agreement between the values for the travel path from the station KIP to the station CTA and the average values for the travel paths from the NTS to the stations CTA, KIP, and MAT is good. Compared to the values of Mitchell et al. (1976), our values exhibit larger scatter at the short periods. This probably is due to our using fewer observation stations (3 stations versus 20 stations). Also, some of the scatter is due to variations of the observed station spectral amplitudes from anisotropic surface wave radiation caused by not accounting for tectonic strain releases of the NTS events in using the isotropic source method. The above facts are also thought to be responsible for the larger standard error ($\bar{S} \approx 1.5 \times 10^{-4} \text{ km}^{-1}$) as compared to the variation $|\Delta k_A|$ of the calculated k_A value by the two-station method, given by equation (IV-4) ($|\Delta k_A| \approx 1.0 \times 10^{-4} \text{ km}^{-1}$ for $D_2 - D_1 = 7610 \text{ km}$ between KIP and CTA).

Figure IV-2 shows the average Rayleigh wave amplitude attenuation coefficients from 10 to 50 seconds at 5 second increments. These were obtained from the second group of travel paths. These values are

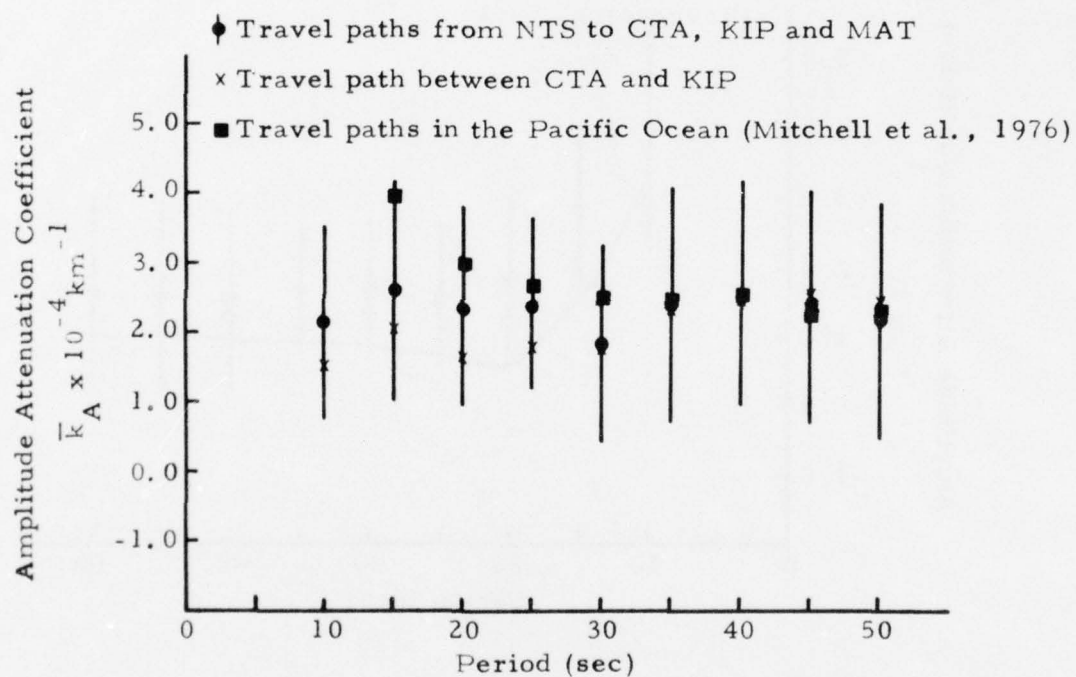


FIGURE IV-1
 AVERAGE RAYLEIGH WAVE AMPLITUDE ATTENUATION
 FOR TRAVEL PATHS IN THE PACIFIC OCEAN

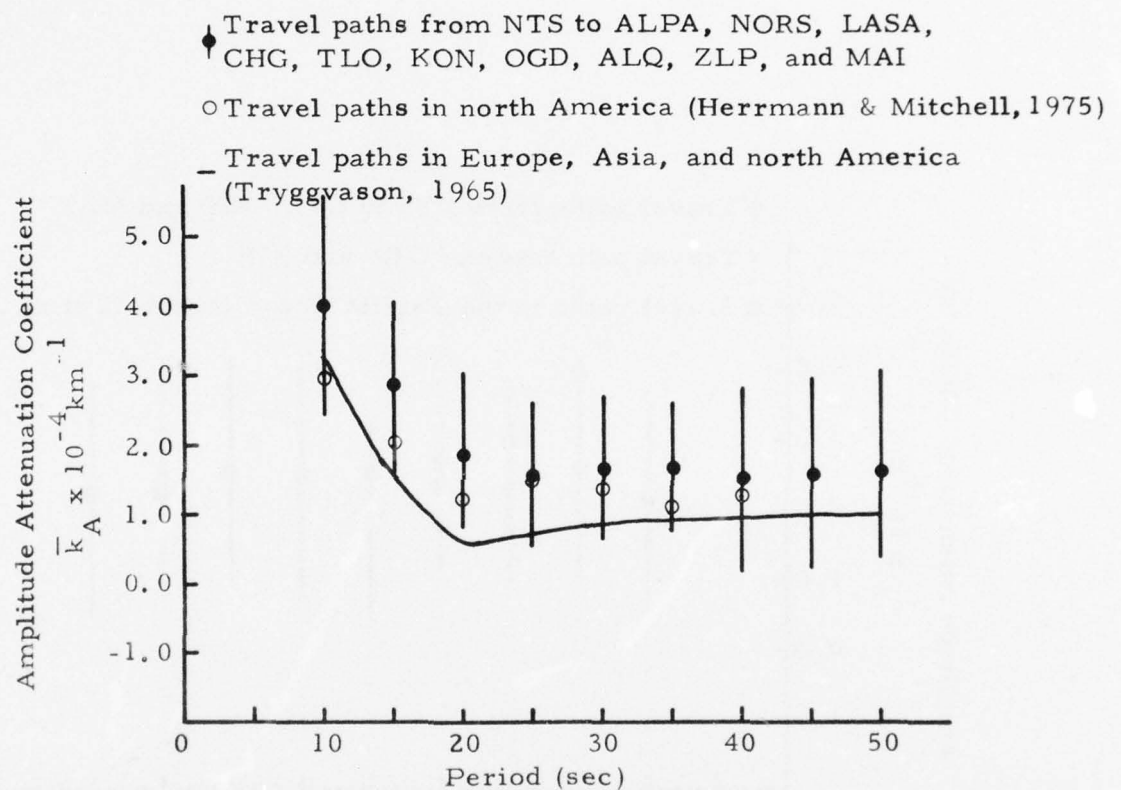


FIGURE IV-2

AVERAGE RAYLEIGH WAVE AMPLITUDE ATTENUATION FOR TRAVEL PATHS FROM THE NTS TO OBSERVATION STATIONS

indicated by the solid dot (●) with the vertical bar showing the standard error. These values indicate that the average Rayleigh wave amplitude attenuation for the second group of travel paths decreases rapidly from $4.1 \times 10^{-4} \text{ km}^{-1}$ at 10 seconds to $1.8 \times 10^{-4} \text{ km}^{-1}$ at 20 seconds and stays at a lower value (about $1.6 \times 10^{-4} \text{ km}^{-1}$) between 25 seconds and 50 seconds. For comparison purposes, this figure shows the average Rayleigh wave attenuation coefficients obtained by Herrmann and Mitchell (1975) for the travel paths within North America, and the Rayleigh wave attenuation curve given by Tryggvason (1965) for travel paths from Novaya Zemlya to stations in Europe, Asia, and North America. Herrmann and Mitchell's values are shown as open circles (o) while Tryggvason's values are given by the solid curve. Results from the comparison among these three sets of Rayleigh wave attenuation values can be summarized as follows:

- The variations of the \bar{k}_A values with respect to period are very similar among these three sets. They all indicate that the attenuation is highest at 10 seconds, decreases rapidly to a low value at about 20 to 25 seconds, and maintains a low value with very little change between 25 and 50 seconds.
- In general, among these three sets of attenuation values, our values are the highest and Tryggvason's are the lowest. However, this difference is thought not to be significant, because: (1) all Herrmann and Mitchell's values fall well within the standard error of our values and most of Tryggvason's values also lie within our standard error, and (2) the standard errors of these three sets of \bar{k}_A values overlap.
- In the period range from 10 to 50 seconds, the standard error of our values is about $1.35 \times 10^{-4} \text{ km}^{-1}$ and those of Tryggvason's, and Herrmann and Mitchell's are about $0.8 \times 10^{-4} \text{ km}^{-1}$ and $2.1 \times 10^{-4} \text{ km}^{-1}$, respectively. The smaller standard

error of Tryggvason's values, as compared to the standard error of our, can probably be attributed to the fact that (1) Tryggvason used a much larger number of stations (14 stations versus our 10 stations), and (2) the travel paths involved in Tryggvason's estimation are more uniform. However, the larger standard error of Herrmann and Mitchell's values, as compared to the standard error of ours, seems unreasonable since Herrmann and Mitchell used a much larger number of stations than we did in the estimation of \bar{k}_A values (about 35 stations versus our 10 stations), and their method did account for the spectral amplitude variation among various stations due to anisotropic surface wave radiation. Several possible explanations for their larger standard error are: (1) the source parameters which they assumed for their events might not be correct, while accurate prior knowledge of the event source parameters is quite critical to their method, and (2) the quality of their data might not be uniformly good for various observation stations.

2. Travel Paths from EKZ to the Observation Stations

Referring to Figure III-2, it can be observed that almost all of the travel paths encountered from EKZ to the observation stations are continental or mixed. Referring to Table II-1b for the observation stations available to the selected EKZ events, the travel paths which are included in the estimation of the Rayleigh wave amplitude attenuation are those from EKZ to stations ALPA, NORS, LASA, TLO, EIL, KON, KIP, ALQ, ZLP, MAT, GUM, and MAI. The travel path from EKZ to station CHG is intentionally excluded since surface waves traveling along this path exhibit an abnormal group delay (as discussed in Subsection III-A) and abnormal absorption (as observed by Turnbull, et al., 1973). The isotropic-source method is used to

estimate the average Rayleigh wave amplitude attenuation coefficients from 10 to 50 seconds at 5 second increments. It is noticed from Figure III-2 that stations KON and ZLP almost have the same event-station great circle path from EKZ. Referring to Table II-3b, the azimuthal angles at the source for these two stations differ by 2.1 degrees. Therefore, the two-station method is applied to event EKZ/704/76, which had Rayleigh wave recordings at these two stations, to calculate the Rayleigh wave attenuation coefficients along the travel path between stations KON and ZLP. This travel path is mostly oceanic, across the Atlantic Ocean.

Figure IV-3 presents the obtained Rayleigh wave amplitude attenuation coefficients for the travel path between stations KON and ZLP. They are shown by solid dots (●). Also included in this figure are the Rayleigh wave amplitude attenuation coefficients previously obtained for the travel path between stations TLO and ZLP (Sun, 1976) and those obtained by Tsai and Aki (1969) for the travel path between station BEC in Bermuda and station SDB in South Africa. They are shown by crosses (x) and by solid squares (■), respectively. These three travel paths are mostly oceanic, across various parts of the Atlantic Ocean, and their Rayleigh wave attenuation coefficients shown in Figure IV-3 are all obtained by the two-station method. The variations among these three sets of attenuation coefficients are small, except that Tsai and Aki's (1969) values show larger scattering and a higher attenuation at 15 seconds.

Figure IV-4 shows the average Rayleigh wave amplitude attenuation coefficients for the travel paths from EKZ to the observation stations. These values are indicated by the solid dots (●) with vertical bars showing the standard error. These values indicate that the average Rayleigh wave amplitude attenuation for these travel paths decreases rapidly from $4.2 \times 10^{-4} \text{ km}^{-1}$ at 10 seconds to $1.6 \times 10^{-4} \text{ km}^{-1}$ at 20 seconds and decreases gradually with small variations from 25 to 50 seconds. In this figure, again

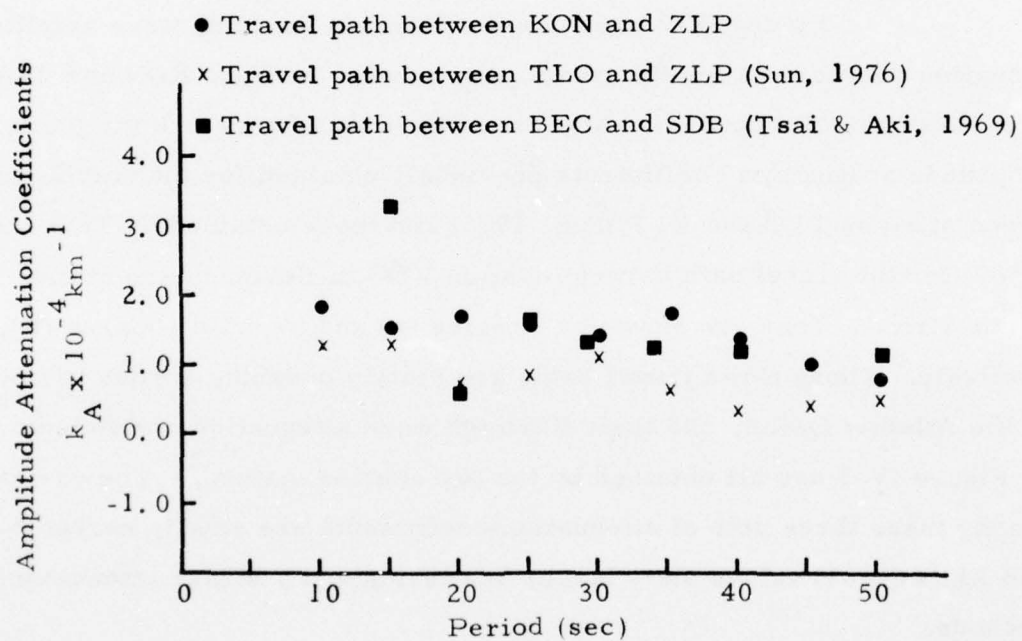


FIGURE IV-3
 RAYLEIGH WAVE AMPLITUDE ATTENUATION FOR
 TRAVEL PATHS IN THE ATLANTIC OCEAN

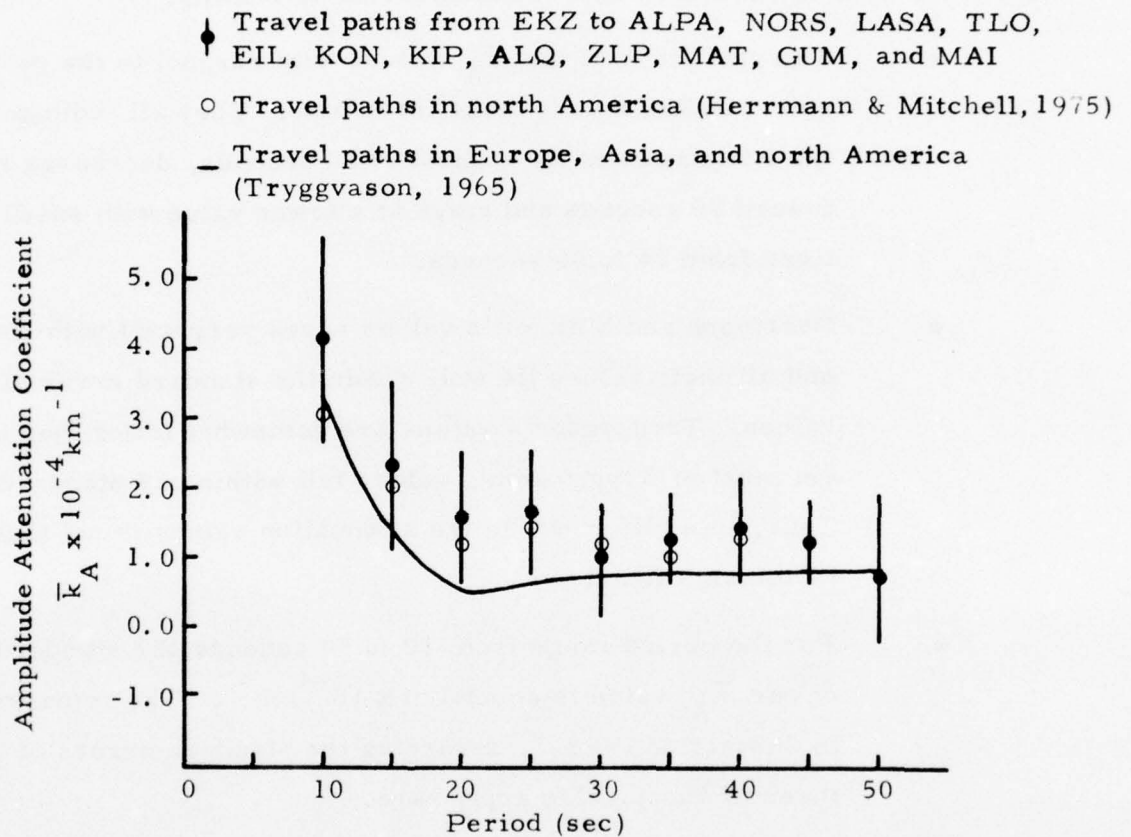


FIGURE IV-4
 AVERAGE RAYLEIGH WAVE AMPLITUDE ATTENUATION FOR
 TRAVEL PATH FROM THE EKZ TO OBSERVATION STATIONS

for comparison purposes, the average Rayleigh wave amplitude attenuation coefficients obtained by Herrmann and Mitchell (1975) and those given by Tryggvason (1965) are shown by open circles (o) and solid curves, respectively. Results from the comparison among these three sets of Rayleigh wave amplitude attenuation values can be summarized as follows:

- The variations of the $\bar{\kappa}_A$ values with respect to the period are quite similar among these three sets. They all indicate that the attenuation is the highest at 10 seconds, decreases rapidly toward 20 seconds and stays at a lower value with small variations from 25 to 50 seconds.
- Herrmann and Mitchell's values agree very well with our values and all their values lie well within the standard error of our values. Tryggvason's values are somewhat lower than ours, yet most of Tryggvason's values fall within our standard error. Thus, this difference in the attenuation values is not thought to be too significant.
- For the period range from 10 to 50 seconds, the standard error of our $\bar{\kappa}_A$ value is about $1.0 \times 10^{-4} \text{ km}^{-1}$. The remarks made in Subsection IV-B-1, regarding the standard errors of the three methods, also apply here.

SECTION V
SOURCE PARAMETER ESTIMATES OF THE SELECTED
NTS, EKZ, AND PNE EVENTS

Many underground nuclear explosions generate horizontally polarized seismic shear waves (SH and Love) along with P, SV, and Rayleigh waves. Theoretically, an explosive source in a horizontally layered, homogeneous, isotropic medium should not generate SH or Love waves. The significance of the magnitude of the SH and Love waves radiated from explosions has been demonstrated by many investigators (Press and Archambeau, 1962; Brune and Pomeroy, 1963; Toksöz, et al., 1965; and Lambert, et al., 1972). The possible mechanisms which might be responsible for these SH and Love waves have also been discussed by them. These mechanisms are wave type conversion, near-source irregularity, and tectonic strain release. The first two mechanisms have been ruled out by simple comparison of various observations from different explosions in the same area (Brune and Pomeroy, 1963; and Toksöz, et al., 1965). The tectonic strain release associated with the explosion is thought to be the most plausible mechanism for the generation of the SH and Love waves by the explosion event (Toksöz, et al., 1965).

A nuclear explosion is not an ideal point source. The shock wave generated vaporizes, melts, crushes, and cracks the rocks out to some distance, depending on the yield of the explosion and the strength of the medium. The cracks caused by the explosion would not generate any SH or Love waves unless there were differential movement along them. In a medium which is not pre-stressed the cracks and the movement along cracks would be distributed uniformly, with radial symmetry around the point of explosion. Therefore, one would not expect an SH or Love wave radiation pattern which could be represented by a dipole or a double-couple source. In a pre-stressed

medium, an explosion may release a part of the existing strain energy by one or more of the following three mechanisms. First, the intense stress waves near the explosion may trigger an earthquake; second, the strain energy may be released by directional cracking; and third, the strain energy may be released by the creation of a cavity.

In this section, our goal is not to verify the existence of the SH and Love waves from the explosion nor to demonstrate the possible mechanisms which generate these shear waves. Rather, in this section, our spectral fitting technique is designed to take into account any possible tectonic strain release associated with an explosion. The technique is applied to selected NTS, EKZ, and PNE explosion events (as listed in Table II-1). Source parameters of these events will be determined from the observed far-field surface wave spectra. Hopefully, source parameter estimates of these events will lead to a better understanding of the physics of the explosions from NTS and EKZ.

If there is tectonic strain release, P, SV, SH, Love, and Rayleigh waves are radiated. These will be added to the explosion-generated P, SV, and Rayleigh waves. Although the SH and Love waves will be due to the tectonic strain release only, the P, SV, and Rayleigh waves will contain fractions due to both sources. It is not possible to separate the fraction of energy due to the explosion alone unless the space and time functions of both sources are known exactly. Since this information is not available, we resort to some indirect techniques and make certain assumptions, which will be discussed later on.

In the following, a procedure of source parameter estimation using far-field surface wave data will be described briefly in Subsection A. Subsection B will present the layered half-space earth models used to analyze the NTS, EKZ, and PNE events. In Subsection C, the source parameter estimates of the selected NTS, EKZ, and PNE events will be presented and the results from the examination of these source parameter estimates will be given.

A. A PROCEDURE OF SOURCE PARAMETER ESTIMATION USING FAR-FIELD SURFACE WAVE DATA

A procedure to obtain the seismic source parameter estimation using far-field surface wave data is schematically shown in Figure V-1. The field tapes from observation stations are edited to obtain the surface wave time traces for a particular event. The edited time traces are analyzed using the ISPS to obtain the demultipathed surface wave spectra, as discussed by Sun and Shaub (1977). The observed spectra are corrected for instrument response, geometric spreading, and travel path attenuation. Finally, the corrected spectra are input to an amplitude spectral fitting process to obtain estimates of the source parameters. The first three blocks in Figure V-1 are pertinent to the data handling and have been discussed in Sections II and III. In the following, the amplitude spectral fitting process will be briefly described.

The amplitude spectra fitting process employs the modified Tsai's method for the estimation of seismic source parameters (Tsai and Aki, 1970; Tsai and Shen, 1972; Turnbull, et al., 1973). The modified Tsai's method is an exhaustive searching scheme to find the best fit between the observed and the theoretically calculated surface wave amplitude spectra. Originally, the modified Tsai's method was developed to obtain a source parameter estimate of an earthquake modeled by a double-couple source. The model yields five source parameters; seismic moment (M), focal depth (h), dip (δ), slip (λ), and strike (ϕ) angle. For an explosion event with associated tectonic strain release, the theoretical source model which is used here combines a point explosive source and a point double-couple source. Theoretical surface wave spectra are generated by this combined source in a layered half-space earth (Harkrider, 1964; Ben-Menahem and Harkrider, 1964; Toksöz, et al., 1965). A point explosive source models an ideal explosion and radiates only isotropic Rayleigh waves, while a point double-couple source models the explosion-associated tectonic strain release and radiates anisotropic Rayleigh

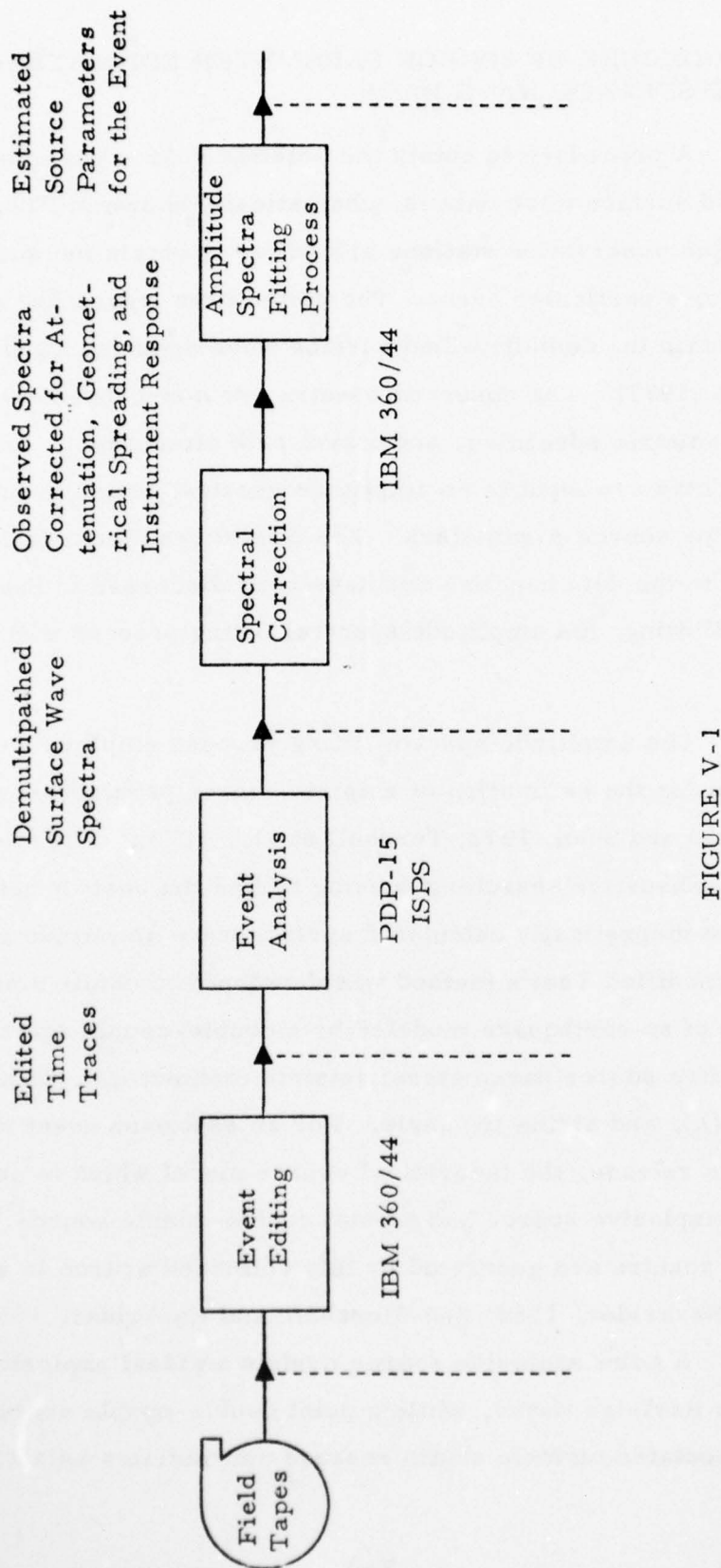


FIGURE V-1
SCHEMATIC DIAGRAM SHOWING A PROCEDURE TO OBTAIN THE SEISMIC
SOURCE PARAMETER ESTIMATION USING FAR-FIELD SURFACE WAVE DATA

and Love waves. Therefore, the resultant Rayleigh wave radiated from the combined source is the vector sum of the Rayleigh wave from the point explosion source and that from the point double-couple source. The resultant Love wave from the combined source comes entirely from the point double-couple source. The resultant amplitude spectra can be expressed as follows:

$$\begin{aligned}
 Y_{ij}^R &= \left| M_E LR_E(h, \delta, \lambda, \phi) + M_X LR_X(h) \right|_{ij} \\
 &= M_E \left| LR_E + F LR_X \right|_{ij} \\
 Y_{ij}^L &= M_E \left| LQ_E(h, \delta, \lambda, \phi) \right|_{ij} \quad (V-1)
 \end{aligned}$$

where

Y_{ij}^R and Y_{ij}^L are the theoretical Rayleigh and Love wave amplitude spectra of the combined source, respectively, for the i -th period at the j -th station,
 LR_E and LQ_E are the theoretical Rayleigh and Love wave spectra of the double-couple source, respectively, for a seismic moment of one dyne-cm,
 LR_X is the theoretical Rayleigh wave spectrum of the point explosive source for a seismic moment of one dyne-cm,
 M_E and M_X are the moments of the double-couple source and the explosive source, respectively, and
 F is the relative strength of the explosive source with respect to the double-couple source, i. e.,
 $F = M_X / M_E$.

It is assumed here that the explosion-associated tectonic strain release takes place in the vicinity of the explosion, i. e., the depths of the explosive source and the double-couple source are the same. Therefore, for an explosion with tectonic strain release, there are six parameters involved in the theoretical source model. These are focal depth (h), dip angle (δ), slip angle (λ), strike angle (ϕ), seismic moment of the double-couple source (M_E), and the relative strength of the explosion (F). The geometry of the double-couple source which models the explosion-associated tectonic strain release is shown in Figure V-2.

Let $s_p(\delta, \lambda, \phi, h, F)$ be a member in a predefined set of source parameters $S(\delta, \lambda, \phi, h, F)$. The exhaustive search in the amplitude spectral fitting process tests each member in S and obtains the member which yields the best fit between the observed and the theoretically calculated surface wave amplitude spectra. The entire set of the source parameters S can be conveniently defined by the upper and lower bounds of each source parameter with discrete increment; that is

$$h_1 \leq h \leq h_m \quad \text{with increment of } \Delta h$$

$$\delta_1 \leq \delta \leq \delta_k \quad \text{with increment of } \Delta \delta$$

$$\lambda_1 \leq \lambda \leq \lambda_l \quad \text{with increment of } \Delta \lambda$$

$$\phi_1 \leq \phi \leq \phi_n \quad \text{with increment of } \Delta \phi$$

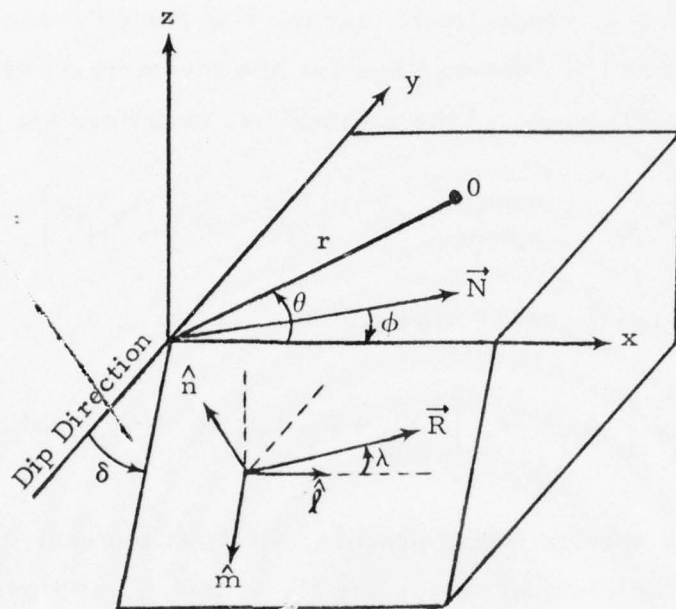
$$F_1 \leq F \leq F_q \quad \text{with increment of } \Delta F$$

where m , k , l , n , and q are positive integers. Thus, the entire set S is a discrete set consisting of $m \cdot k \cdot l \cdot n \cdot q$ members. In the amplitude spectral fitting process which is applied here, the following values of the source parameters are used:

$$h = 0.5, 1.5, 2.5, 4.0, 6.0, 8.0, 10.0 \text{ km};$$

$$30^\circ \leq \delta \leq 90^\circ, \Delta \delta = 10^\circ; -90^\circ \leq \lambda \leq 90^\circ, \Delta \lambda = 30^\circ;$$

$$0^\circ \leq \phi \leq 175^\circ, \Delta \phi = 5^\circ; 0.25 \leq F \leq 3.0, \Delta F = 0.25.$$



- δ = Dip angle
- λ = Slip angle
- ϕ = Strike angle
- θ = Azimuth angle with respect to strike direction
- \hat{n} = Surface normal
- \hat{m}, \hat{p} = Orthogonal vectors on the surface of fault plane
- \vec{R} = One force vector of double-couple force on the surface of fault plane
- O = Arbitrary observation station
- \vec{N} = Geographical north

FIGURE V-2
GEOMETRY OF THE DOUBLE-COUPLE SOURCE WHICH MODELS
THE EXPLOSION-ASSOCIATED TECTONIC STRAIN RELEASE

The non-uniform increment in h is dictated by the individual layer thickness of the layered half-space earth model which is chosen for the source region.

Let X_{ij}^R and X_{ij}^L denote the observed Rayleigh and Love wave spectral amplitudes, respectively, for the i -th period at the j -th station. The difference between the observed spectra and the corresponding theoretical spectra, which will be called the residual ϵ , is defined as:

$$\epsilon(s_p) = \sum_j \sum_i \left[(X_{ij}^R - Y_{ij}^R)^2 + (X_{ij}^L - Y_{ij}^L)^2 \right]. \quad (V-2)$$

Substituting (V-1) into (V-2), we have

$$\epsilon(s_p) = \sum_j \sum_i \left[(X_{ij}^R - M_E |LR_E + FLR_X|_{ij})^2 + (X_{ij}^L - M_E |LQ_E|_{ij})^2 \right]. \quad (V-2a)$$

In the amplitude spectra fitting process, first the moment M_E is estimated by minimizing the residual $\epsilon(s_p)$ for all i and j , or explicitly:

$$M_E(s_p) = \frac{\sum_j \sum_i \left[X_{ij}^R |LR_E + FLR_X|_{ij} + X_{ij}^L |LQ_E|_{ij} \right]}{\sum_j \sum_i \left[|LR_E + FLR_X|_{ij}^2 + |LQ_E|_{ij}^2 \right]}. \quad (V-3)$$

In other words, for a particular member s_p in the set of source parameters S , the optimum moment is first found from equation (V-3). Then, the resultant $M_E(s_p)$ is used in equation (V-2a) to compute the minimum residual $\epsilon(s_p)$ for this particular member s_p . The minimum residual $\epsilon(s_p)$ is computed for each of the members in S . This ϵ value is used as a convenient criterion for judging the goodness of the fit between the observed and the theoretically calculated spectra for each member s_p . In the end, the source parameter estimation of a given event will be the member s_p^{optimal} whose theoretical surface wave spectra fits most closely the observed spectra; that is:

$$\epsilon_{\min}^{\text{all}}(s_p^{\text{optimal}}) = \text{Minimum} [\epsilon(s_p)] \quad \text{for all } s_p \text{ in } S. \quad (\text{V-4})$$

In order to attain a greater degree of confidence in using the source parameter estimation based on the minimum residual criterion, a detailed knowledge of the residual distribution about the absolute minimum given by equation (V-4) would be helpful to guard against a possible spurious minimum generated by poor quality data. Therefore, in the amplitude spectral fitting process used here, the distributions of $\epsilon(s_p)$ with respect to the source parameters are generated as follows.

In the fitting process, the focal depth is varied last, because the focal depth (h) will affect the shape of the theoretical surface wave amplitude spectra the most, especially for Rayleigh waves (Turnbull, et al., 1974). There is one $\epsilon_{\min}^{h_i}$ at one focal depth h_i , that is

$$\epsilon_{\min}^{h_i} = \text{Minimum} \left\{ \epsilon[s_p(\delta, \lambda, \phi, h_i, F)] \right\} \quad \text{for all } \delta, \lambda, \phi \text{ and } F \text{ at depth } h_i. \quad (\text{V-5})$$

The variation of $\epsilon_{\min}^{h_i}$ with respect to the focal depth is obtained and a standard value ϵ , say $[\epsilon_{\min}^{h_i}]_{\text{standard}}$, is determined from those $\epsilon_{\min}^{h_i}$ for the purpose of picking appropriate members in the set of source parameters S to form a sample set S_d . In the entire set of source parameters S , those members whose $\epsilon(s_p)$'s are less than $[\epsilon_{\min}^{h_i}]_{\text{standard}}$ are included in the sample set S_d . These form the distributions of $\epsilon(s_p)$ with respect to the source parameters. These residual distributions for the various source parameters will be more easily understood from the results which will be presented later on for the source parameter estimations of the selected NTS, EKZ, and PNE events.

B. EARTH MODELS

In order to generate the theoretical surface wave spectra which are needed in the amplitude spectral fitting process, a layered half-space, which models the source region earth structure, has to be obtained first. Three earth models are used for the selected NTS, EKZ, and PNE events, respectively.

For the NTS events, two structures appear to be appropriate for the source mechanism study. One is the 35CM2 earth model of Alexander (1963) for the events occurring near (37°N , 116°W), and the other is the modified Eaton's model (Toksöz, et al., 1965) for the events near (39°N , 118°W). Since our selected NTS events all took place near (37°N , 116°W), the layered half-space earth model for our selected NTS events was constructed from the 35CM2 model. Basically, the 35CM2 model is a simple structure consisting of about 2-3 km of 'sedimentary' material overlaying a rather uniform section of 'granite' material about 23 km thick, which in turn overlies an intermediate section about 25 km thick. A maximum propagation velocity occurs at a depth of about 50 km with a gradual decrease in velocity at greater depth corresponding to the beginning of the Gutenberg low-velocity zone centered at a depth of around 125-150 km. To estimate source parameters from long-period surface waves, we need the structure profile of the earth model down to a depth of around 400-500 km. Since the 35CM2 model has a similar structure profile as the Gutenberg model for any depth greater than about 50 km, our NTS earth model merges the 35CM2 model with the Gutenberg model at a depth of 150 km. The structure profile of our NTS earth model is given in Table V-1, and theoretical dispersions for the Rayleigh and the Love wave are given in Table V-2.

For the selected EKZ and PNE events, the earth models are constructed from the information given by Rodriguez (1969). The locations of our selected EKZ and PNE events are shown on Figure V-3, in relation to

TABLE V-1
STRUCTURE PROFILE OF THE NTS EARTH MODEL (37°N, 116°W)

Thickness (km)	V _p (km/sec)	V _s (km/sec)	ρ(g/cm ³)
2	3.80	1.75	2.20
13	6.10	3.60	2.80
10	6.20	3.70	2.80
11	7.62	4.07	3.20
14	7.62	4.07	3.25
16	8.10	4.62	3.32
20	8.00	4.53	3.40
20	7.94	4.46	3.40
45	7.80	4.40	3.40
25	7.89	4.35	3.43
25	7.98	4.38	3.46
25	8.10	4.42	3.48
25	8.21	4.46	3.50
50	8.38	4.54	3.53
50	8.62	4.68	3.58
50	8.87	4.85	3.62
50	9.15	5.04	3.69
50	9.45	5.21	3.82
50	9.88	5.45	4.01

TABLE V-2
SURFACE WAVE DISPERSION FOR THE NTS EARTH MODEL
(37°N, 116°W)

	T (sec)	C (km/sec)	V (km/sec)	k (km ⁻¹)
Love Wave (LQ)	60	4.351	4.107	0.0241
	55	4.328	4.069	0.0264
	50	4.300	4.018	0.0292
	45	4.266	3.948	0.0327
	40	4.222	3.856	0.0372
	35	4.165	3.747	0.0431
	30	4.089	3.632	0.0512
	25	3.993	3.527	0.0629
	20	3.878	3.436	0.0810
	15	3.742	3.342	0.112
	10	3.564	3.161	0.176
Rayleigh Wave (LR)	60	3.981	3.877	0.0263
	55	3.971	3.855	0.0288
	50	3.959	3.817	0.0318
	45	3.941	3.755	0.0354
	40	3.914	3.661	0.0401
	35	3.871	3.526	0.0464
	30	3.802	3.353	0.0551
	25	3.698	3.170	0.0680
	20	3.557	3.020	0.0883
	15	3.386	2.916	0.124
	10	3.203	2.886	0.196

T: Period, C: Phase Velocity, V: Group Velocity, k: Wavenumber

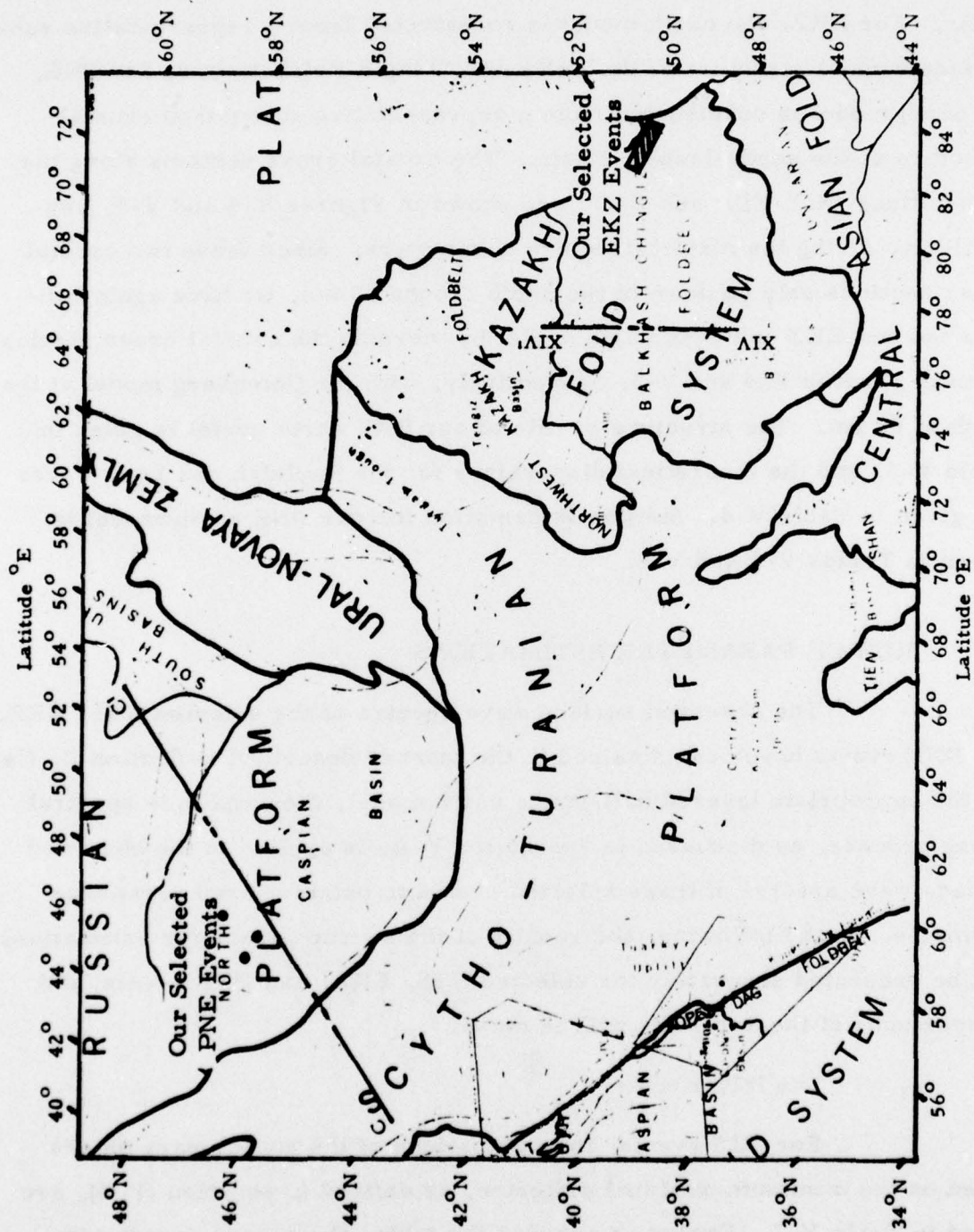


FIGURE V-3

LOCATIONS OF THE SELECTED EKZ AND PNE EVENTS, AND LOCAL GEOLOGY

major geological features. The selected EKZ events are in the Balkhash-Chingiz Foldbelt, while the selected PNE events are in the north Caspian Basin. For EKZ, the earth model is constructed from a representative subsurface crustal structure of the Balkhash-Chingiz Foldbelt; and, for PNE, the earth model is constructed from a representative subsurface crustal structure of the north Caspian Basin. The crustal cross sections along the broken lines XIV-XIV' and C-C' are shown in Figures V-4 and V-5, respectively, giving the major structure parameters. Since these two crustal cross sections only go down to the depth around 50 km, we have again constructed our EKZ and PNE earth model by merging the crustal cross sections, given in Figures V-4 and V-5, respectively, with the Gutenberg model at the depth of 50 km. The structure profile of our EKZ earth model is given in Table V-3, and the theoretical dispersions for the Rayleigh and Love waves are given in Table V-4. Similar information for our PNE earth model is given in Tables V-5 and V-6.

C. SOURCE PARAMETER ESTIMATIONS

The observed surface wave spectra of the selected NTS, EKZ, and PNE events have been obtained in the manner described in Section II. Using the appropriate layered half-space earth model, the amplitude spectral fitting process, as discussed in Subsection V-A, is applied to the observed surface wave spectra of these selected events to obtain source parameter estimates. In the following, the results of the source parameter estimations will be presented separately for selected NTS, EKZ, and PNE events, and comparisons of these results will be made.

1. The NTS Events

For NTS events, the estimations of the source parameters based on the minimum-residual criterion, as defined in equation (V-4), are listed in Table V-7. Except as noted in the table, the source parameter

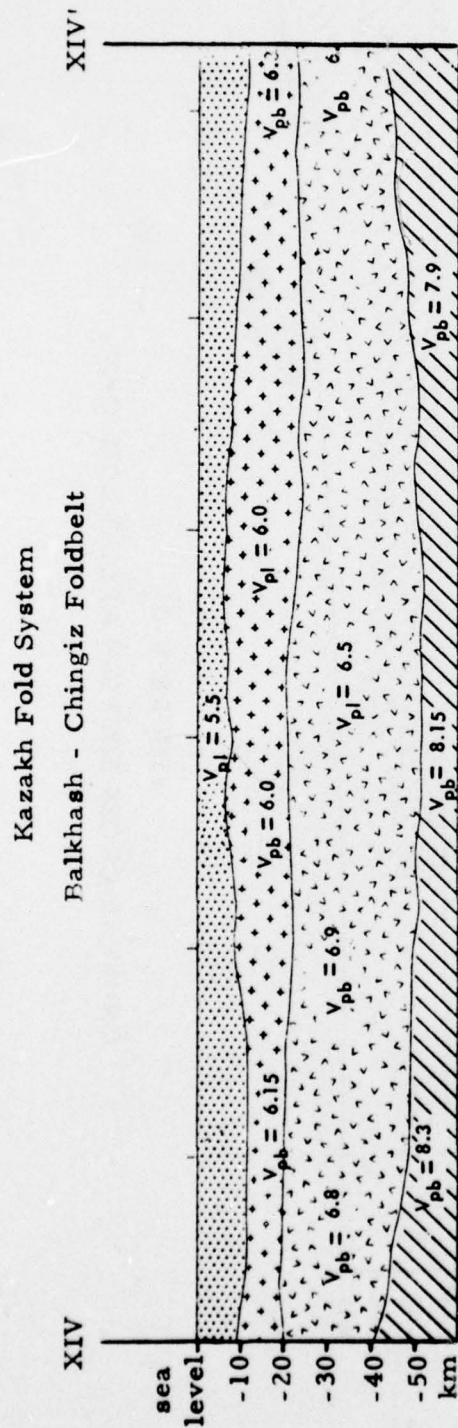


FIGURE V-4
CRUSTAL CROSS SECTION ALONG LINE XIV-XIV'

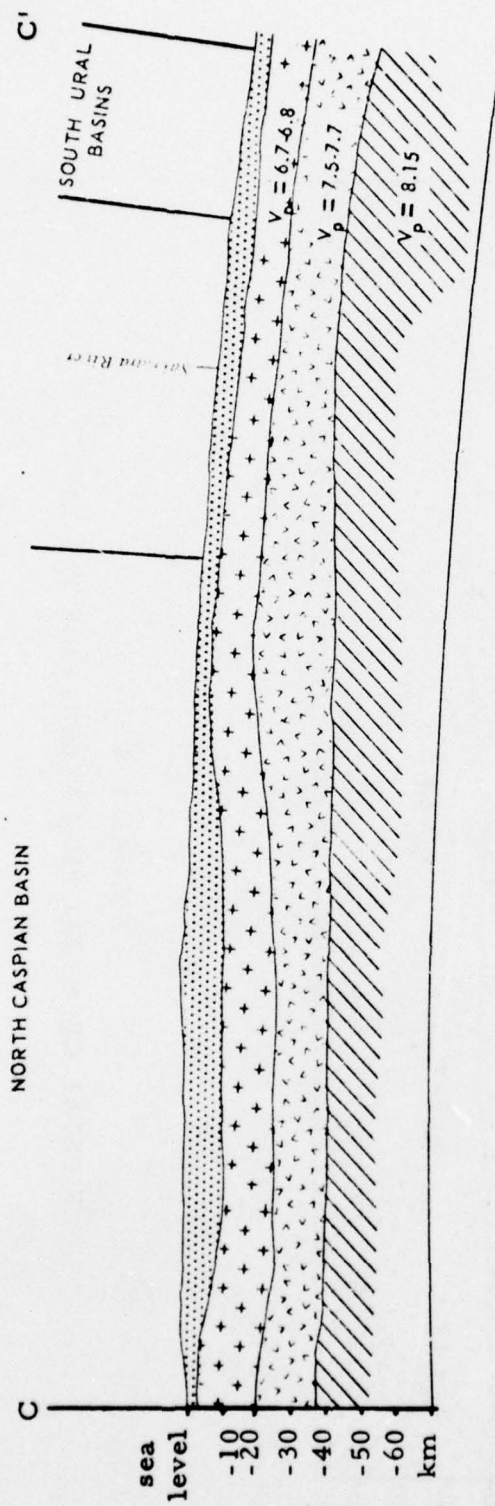


FIGURE V-5
CRUSTAL CROSS SECTION ALONG LINE C-C'

TABLE V-3
STRUCTURE PROFILE OF THE EKZ EARTH MODEL
(BALKHASH-CHINGIZ FOLDBELT)

Thickness (km)	V _p (km/sec)	V _s (km/sec)	ρ (g/cm ³)
10	5.50	3.18	2.65
12	6.15	3.55	2.74
22	6.70	3.87	3.05
6	8.20	4.65	3.32
10	8.17	4.62	3.34
10	8.14	4.57	3.35
10	8.10	4.51	3.36
10	8.07	4.46	3.37
10	8.02	4.41	3.38
25	7.93	4.37	3.39
25	7.85	4.35	3.41
25	7.89	4.35	3.43
25	7.98	4.38	3.46
25	8.10	4.42	3.48
25	8.21	4.46	3.50
50	8.38	4.54	3.53
50	8.62	4.68	3.58
50	8.87	4.85	3.62
50	9.15	5.04	3.69
50	9.45	5.21	3.82
50	9.88	5.45	4.01

TABLE V-4
SURFACE WAVE DISPERSION FOR THE EKZ EARTH MODEL
(BELKHASH-CHINGIZ FOLDBELT)

	T (sec)	C (km/sec)	V (km/sec)	k (km ⁻¹)
Love Wave (LQ)	60	4.297	4.010	0.0244
	55	4.270	3.960	0.0268
	50	4.236	3.892	0.0297
	45	4.193	3.801	0.0333
	40	4.138	3.687	0.0380
	35	4.065	3.558	0.0442
	30	3.972	3.434	0.0527
	25	3.859	3.335	0.0651
	20	3.732	3.271	0.0842
	15	3.597	3.227	0.116
	10	3.455	3.182	0.182
Rayleigh Wave (LR)	60	3.929	3.809	0.0267
	55	3.918	3.793	0.0292
	50	3.905	3.762	0.0322
	45	3.888	3.708	0.0359
	40	3.862	3.617	0.0407
	35	3.819	3.477	0.047
	30	3.749	3.281	0.0559
	25	3.637	3.072	0.0691
	20	3.487	2.940	0.0901
	15	3.321	2.884	0.126
	10	3.147	2.816	0.200

T: Period, C: Phase Velocity, V: Group Velocity, k: Wavenumber

TABLE V-5
STRUCTURE PROFILE OF THE PNE EARTH MODEL
(NORTH CASPIAN BASIN)

Thickness (km)	V_p (km/sec)	V_s (km/sec)	ρ (g/cm ³)
8	6.14	3.55	2.74
16	6.75	3.90	3.05
16	7.60	4.40	3.05
10	8.20	4.65	3.32
10	8.17	4.62	3.34
10	8.14	4.57	3.35
10	8.10	4.51	3.36
10	8.07	4.46	3.37
10	8.02	4.41	3.38
25	7.93	4.37	3.39
25	7.85	4.35	3.41
25	7.98	4.38	3.43
25	8.10	4.42	3.48
25	8.21	4.46	3.50
50	8.38	4.54	3.53
50	8.62	4.68	3.58
50	8.87	4.85	3.62
50	9.15	5.04	3.69
50	9.45	5.21	3.82
50	9.88	5.45	4.01

TABLE V-6
SURFACE WAVE DISPERSION FOR THE PNE EARTH MODEL
(NORTH CASPIAN BASIN)

	T (sec)	C (km/sec)	V (km/sec)	k (km ⁻¹)
Love Wave (LQ)	60	4.434	4.291	0.0236
	55	4.421	4.286	0.0258
	50	4.408	4.277	0.0285
	45	4.394	4.263	0.0318
	40	4.378	4.237	0.0359
	35	4.357	4.191	0.0412
	30	4.326	4.106	0.048
	25	4.275	3.967	0.0588
	20	4.189	3.806	0.0750
	15	4.065	3.683	0.103
	10	3.912	3.611	0.161
Rayleigh Wave (LR)	60	4.022	3.990	0.026
	55	4.019	4.000	0.028
	50	4.018	4.005	0.0313
	45	4.017	4.000	0.0348
	40	4.014	3.980	0.0391
	35	4.007	3.937	0.0448
	30	3.991	3.854	0.0525
	25	3.955	3.713	0.0636
	20	3.880	3.514	0.0810
	15	3.750	3.372	0.112
	10	3.581	3.267	0.175

T: Period, C: Phase Velocity, V: Group Velocity, k: Wavenumber

TABLE V-7
ESTIMATIONS OF SOURCE PARAMETERS OBTAINED BY AMPLITUDE
SPECTRAL FITTING BASED ON THE MINIMUM-RESIDUAL
CRITERION: SELECTED NTS EVENTS
(PAGE 1 OF 2)

Event I. D.	Optimal Solution					
	Depth h km	Dip Angle δ°	Slip Angle λ°	Strike $N\phi^\circ E$	Moment M_F 10^{25} dyne-cm	M_X
NTS/430/75	0.5	40	-90	55	0.212×10^{-1}	0.212×10^{-1}
NTS/514/75	0.5	60	30	10	0.170×10^{-1}	0.212×10^{-1}
NT1/603/75	0.5	80	0	10	0.864×10^{-2}	0.129×10^{-1}
NT2/603/75	0.5	70	30	40	0.302×10^{-2}	0.377×10^{-2}
NTS/619/75	0.5	80	30	10	0.192×10^{-1}	0.240×10^{-1}
NTS/626/75	0.5	40	-90	125	0.127	0.191
NTS/1028/5	0.5	50	-90	150	0.243	0.243
NTS/926/74	0.5	80	30	160	0.163×10^{-2}	0.244×10^{-2}
						1.00
						1.25
						1.50
						1.25
						1.25
						1.50
						1.00
						1.50

TABLE V-7

ESTIMATIONS OF SOURCE PARAMETERS OBTAINED BY AMPLITUDE
SPECTRAL FITTING BASED ON THE MINIMUM-RESIDUAL
CRITERION: SELECTED NTS EVENTS
(PAGE 2 OF 2)

Event I. D.	Optimal Solution					
	Depth h km	Dip Angle δ_o°	Slip Angle λ_o°	Strike $N\phi_o^\circ E$	Moment M_E 10^{25} dyne-cm	M_X
NTS/103/76	0.5	70	0	170	0.111	0.111
NTS/212/76	0.5	90	30	175	0.105	0.105
NTS/309/76	0.5	80	-30	120	0.332×10^{-1}	0.415×10^{-1}
NTS/314/76	0.5	90	-60	170	0.975×10^{-1}	0.975×10^{-1}
NT1/317/76	0.5	40	-90	95	0.428×10^{-1}	0.428×10^{-1}
NT2/317/76	0.5	50	-90	130	0.180×10^{-1}	0.270×10^{-1}
NT1/204/76*	0.5	70	30	100	0.772×10^{-2}	0.135×10^{-1}
NT2/204/76*	2.5	30	-90	30	0.372×10^{-1}	0.464×10^{-1}
						1.00
						1.00
						1.25
						1.00
						1.00
						1.50
						1.75
						1.25

*The source parameter estimates of these two events are obtained by using the observation spectra at the SDCS stations.

estimates of these events are obtained without including the observed spectra at the SDCS stations. This is due to the non-uniform data quality observed at the SDCS stations as discussed in Subsection III-B. The depth estimates of these events are all very shallow; 0.5 km except 2.5 km for the event NT2/204/76. The very shallow depths of these events are to be expected, since these events are presumed underground explosions. The dip and slip angle estimates of the tectonic strain releases associated with these events can be generally grouped into two kinds: nearly strike-slip for 10 events and purely dip-slip for 6 events. These dip and slip angle estimates are quite different from the assumption made by other investigators (Toksöz, et al., 1965; Lambert, et al., 1972; Mitchell, 1975) that the tectonic strain release associated with the NTS explosion has the vertical strike-slip type of mechanism ($\delta = 90^\circ, \lambda = 0^\circ$). Even for those 10 events with nearly strike-slip type of mechanism for their associated tectonic strain releases, there are variations in their dip and slip angle estimates ($\delta = 60^\circ$ to $90^\circ, \lambda = -30^\circ$ to 30°). However, with just a few exceptions, the strike angle estimates are quite close to the N-S direction as assumed by some authors (Toksöz, et al., 1965; Lambert, et al., 1972). The estimates of the relative strength of the explosive source and the double-couple source, i. e., the F values (M_X/M_E), vary from 1.00 to 1.75 among these events.

Among these 16 selected NTS events, there are six events which can be grouped into three pairs, based on their similar locations and times of detonations (see Table II-1). These three pairs are NT1/603/75 and NT2/603/75, NT1/317/76 and NT2/317/76, and NT1/204/76 and NT2/204/76. The locations of two events in each pair were very close and their detonations were about 20 to 30 minutes apart. The source parameter estimates of tectonic strain releases associated with two events in the first two pairs are very similar. The larger event (in terms of its m_b) of each pair releases a larger amount of tectonic strain energy (in terms of the estimated seismic moment of the tectonic strain release). This probably

indicates that the two events in each of the first two pairs had similar mechanisms in releasing the tectonic strain energy. However, the source parameter estimates of the tectonic strain releases associated with the two events in the last pair, i. e., NT1/204/76 and NT2/204/76, indicate quite a different situation. The depth estimate of the event NT2/204/76 is 2.5 km which is quite unusual for an explosion with an m_b of 5.7. The dip and slip estimates of the tectonic strain releases associated with these two events are quite different and the event NT2/204/76 has a much larger seismic moment estimate of the tectonic strain release. These differences in source parameter estimates well might have been caused by a problem with the observed spectra, since they were only available at SDCS stations whose observed spectra are questionable as discussed in Subsection III-B. Alternatively, these differences might be due to a real physical reason if NT2/204/76 released the tectonic strain energy by actually triggering an earthquake at a depth greater than the shot depth.

The residual distributions with respect to the estimated depth, dip angle, slip angle, and strike angle are shown in Figures V-6 through Figure V-21, together with the spectral fit for each event. The residual distribution for one particular source parameter, say depth, consists of the variation of the minimum residual values with respect to the depths tested in the spectral fitting process and the percentage of occurrences at the various tested depths. For each event, the residual distributions are given in part (a) of each figure. The best spectral fits of Rayleigh and Love waves (as defined by equation (V-4)) are shown in part (b). In these figures, the residual values are normalized with respect to $\epsilon_{\min}^{\text{all}}(s_p^{\text{optimal}})$ and are indicated as the relative minimum residuals (R. M. R.). The observed spectra are indicated by crosses (x) and the best fit theoretical spectra are represented by open circles (o) connected by straight lines. When there are no observed spectra for either the Rayleigh or Love wave, the crosses are plotted on top of the corresponding open circles. In general, the agreement between

(a) Residual Distributions

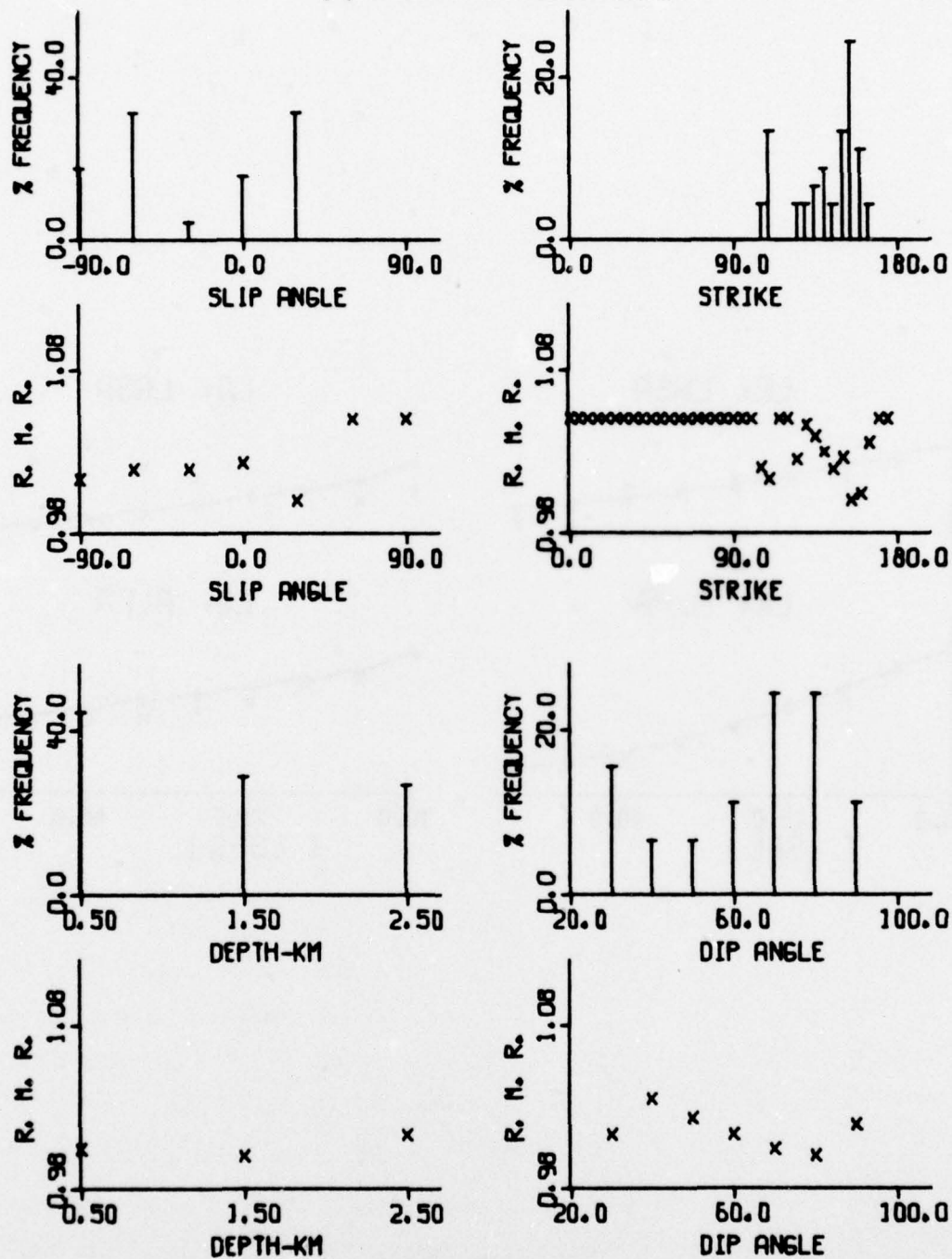


FIGURE V-6

RESULTS FROM AMPLITUDE SPECTRAL FITTING: NTS/926/74
(PAGE 1 OF 2)

(b) Spectral Fits

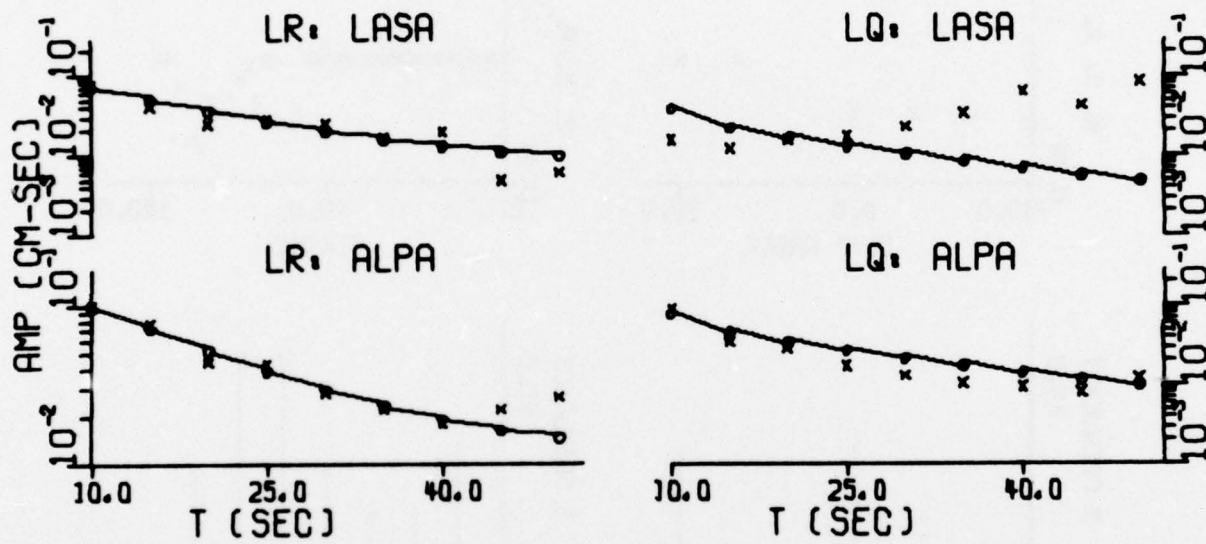


FIGURE V-6
RESULTS FROM AMPLITUDE SPECTRAL FITTING: NTS/926/74
(PAGE 2 OF 2)

(a) Residual Distributions

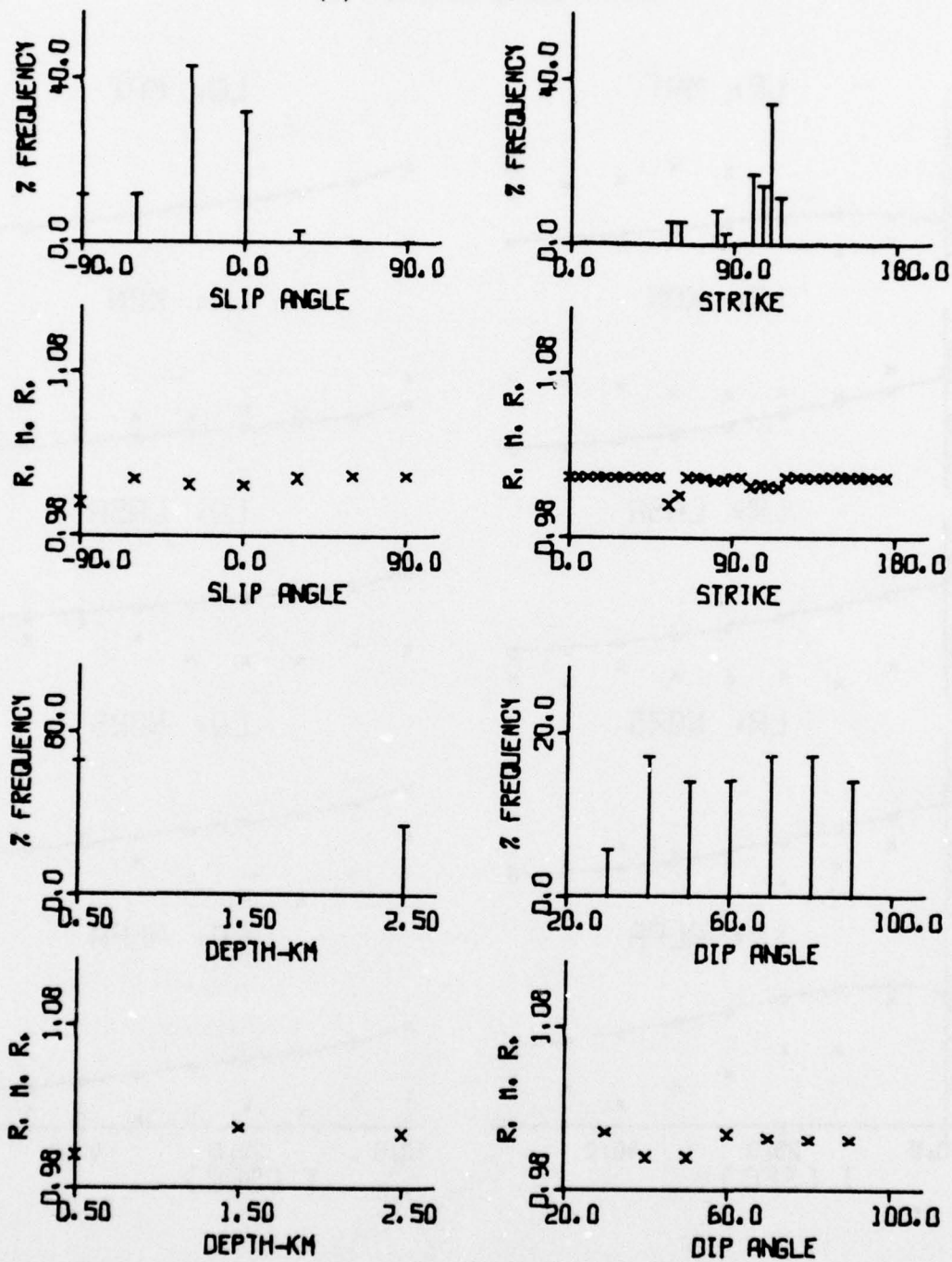


FIGURE V-7

RESULTS FROM AMPLITUDE SPECTRAL FITTING: NTS/430/75
(PAGE 1 OF 2)

(b) Spectral Fits

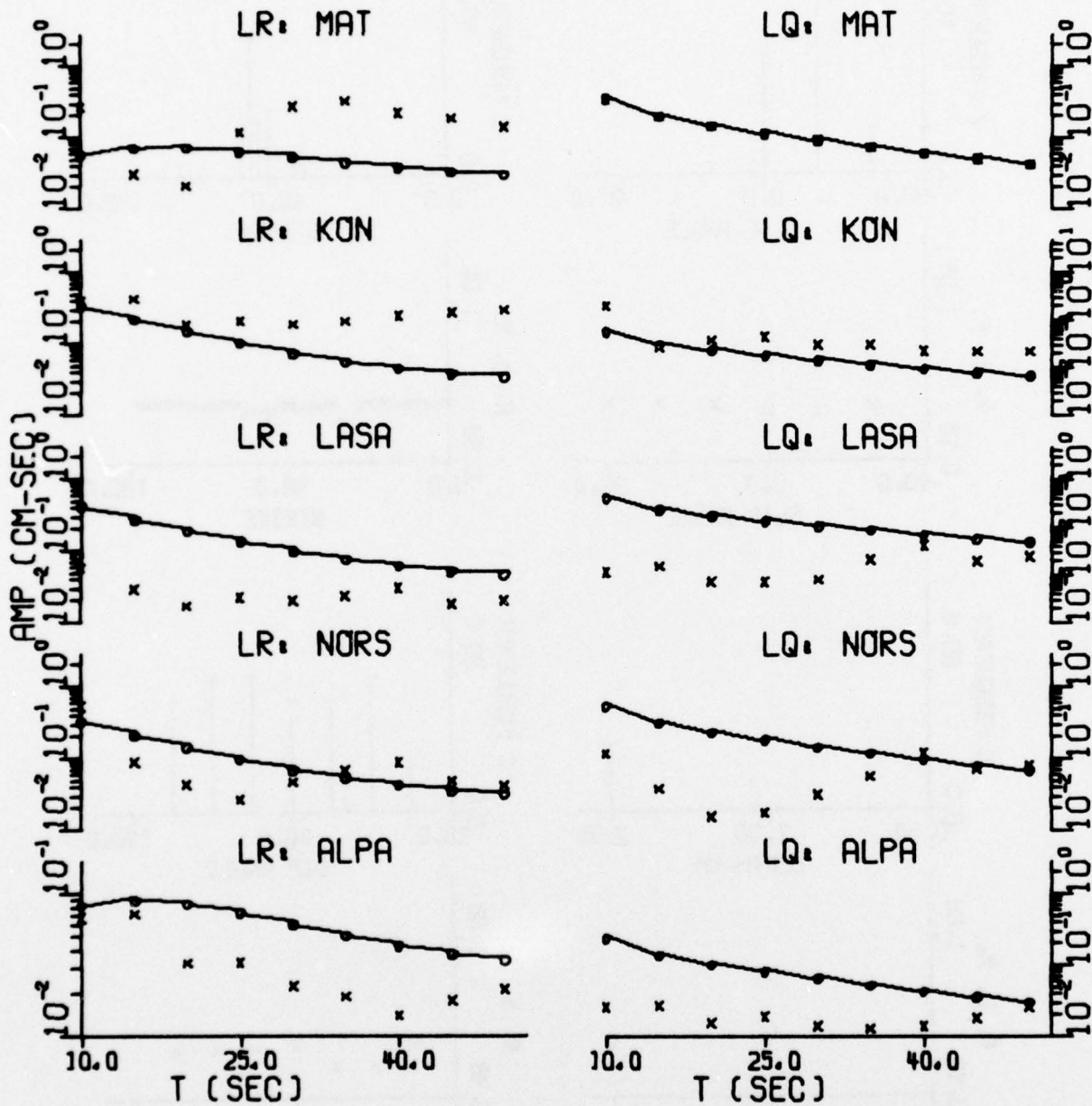


FIGURE V-7
RESULTS FROM AMPLITUDE SPECTRAL FITTING: NTS/430/75
(PAGE 2 OF 2)

(a) Residual Distributions

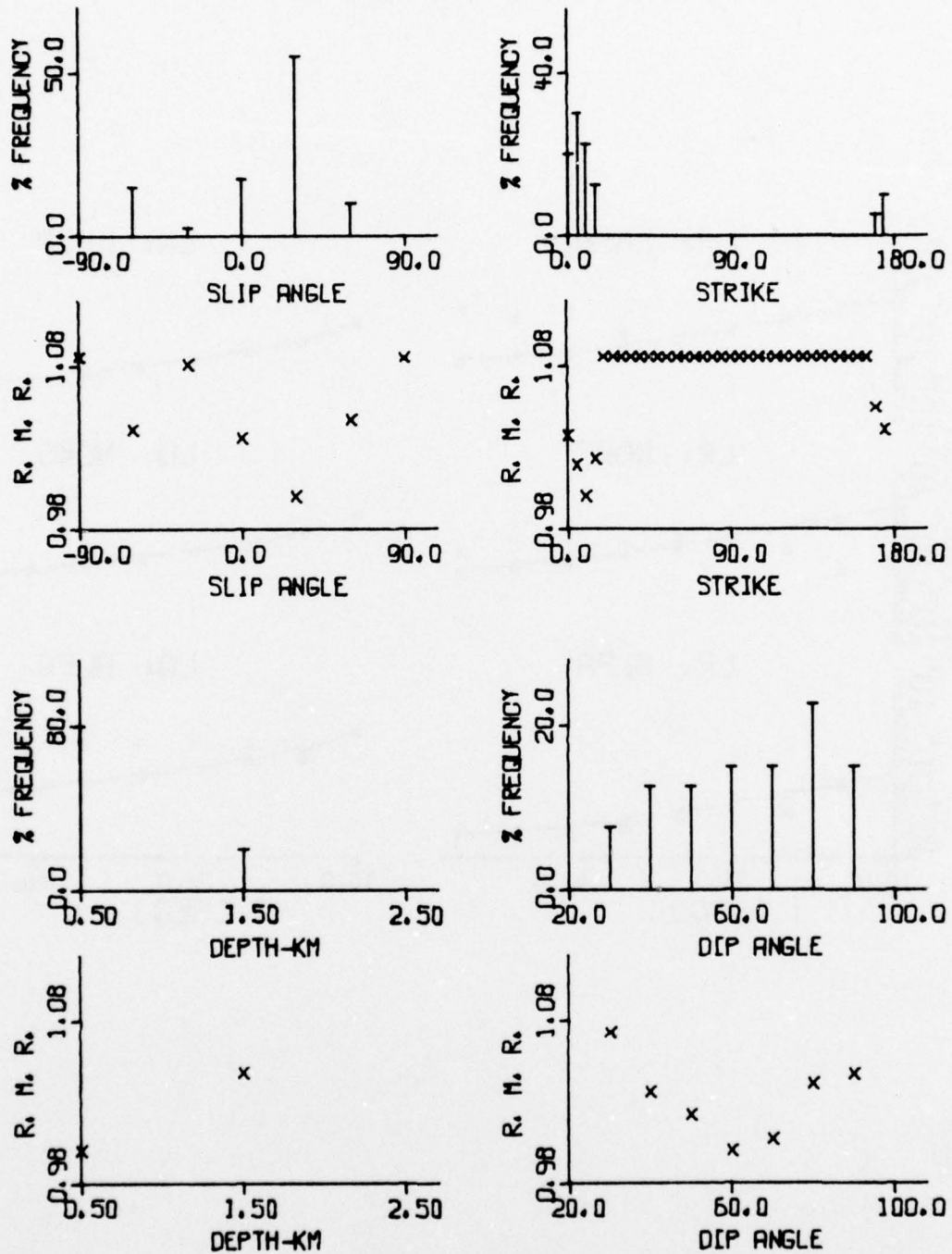


FIGURE V-8

RESULTS FROM AMPLITUDE SPECTRAL FITTING: NTS/514/75
(PAGE 1 OF 3)

(b) Spectral Fits

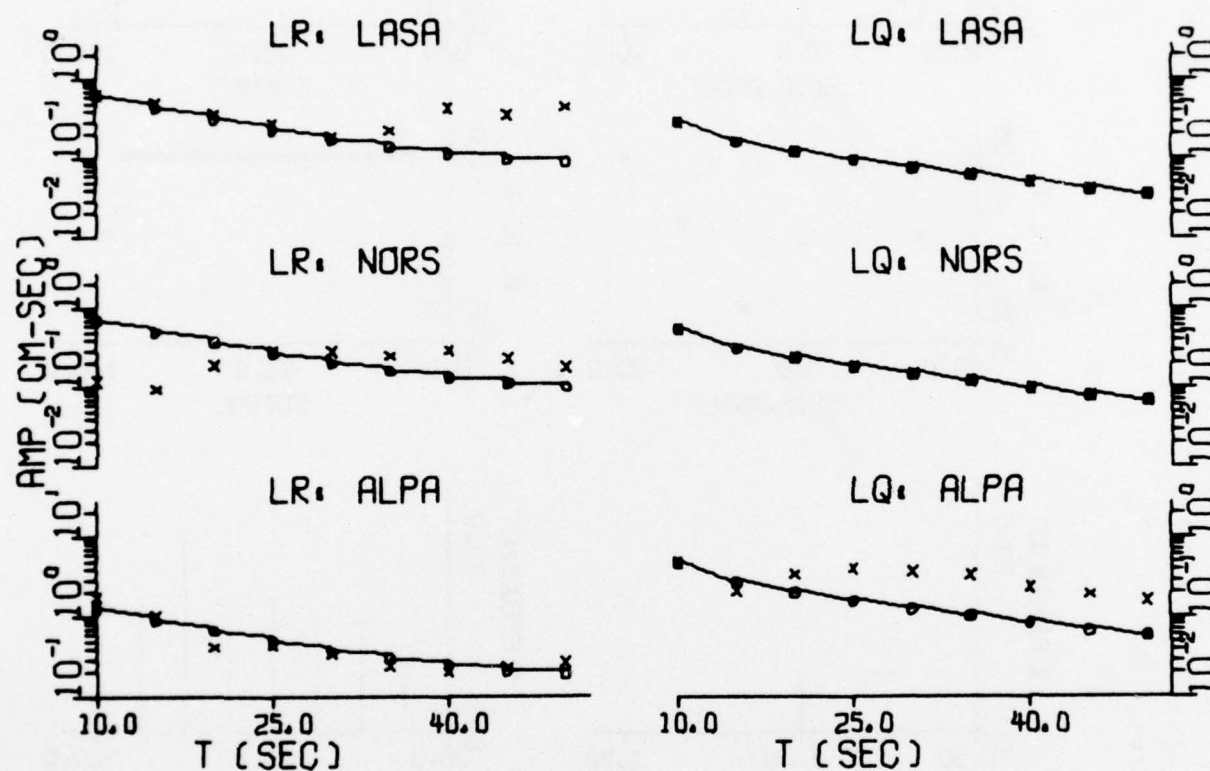


FIGURE V-8
RESULTS FROM AMPLITUDE SPECTRAL FITTING: NTS/514/75
(PAGE 2 OF 3)

(b) Spectral Fits

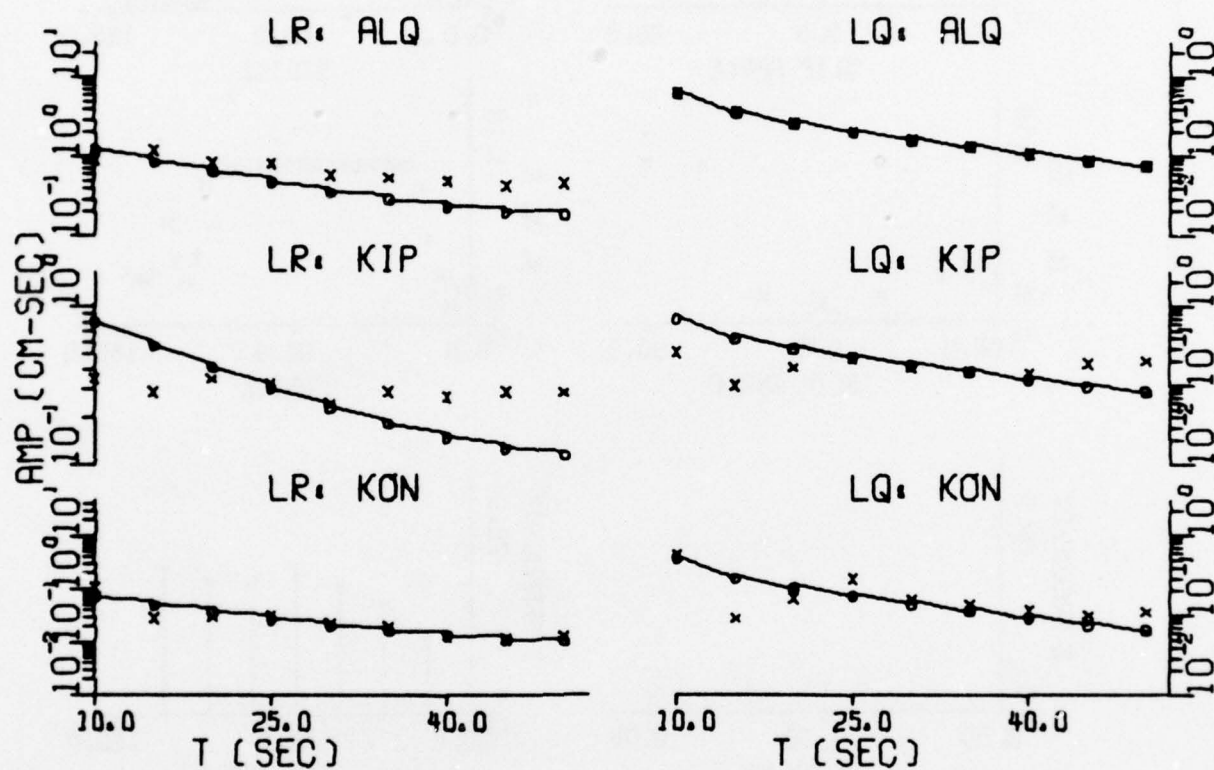


FIGURE V-8
RESULTS FROM AMPLITUDE SPECTRAL FITTING: NTS/514/75
(PAGE 3 OF 3)

(a) Residual Distributions

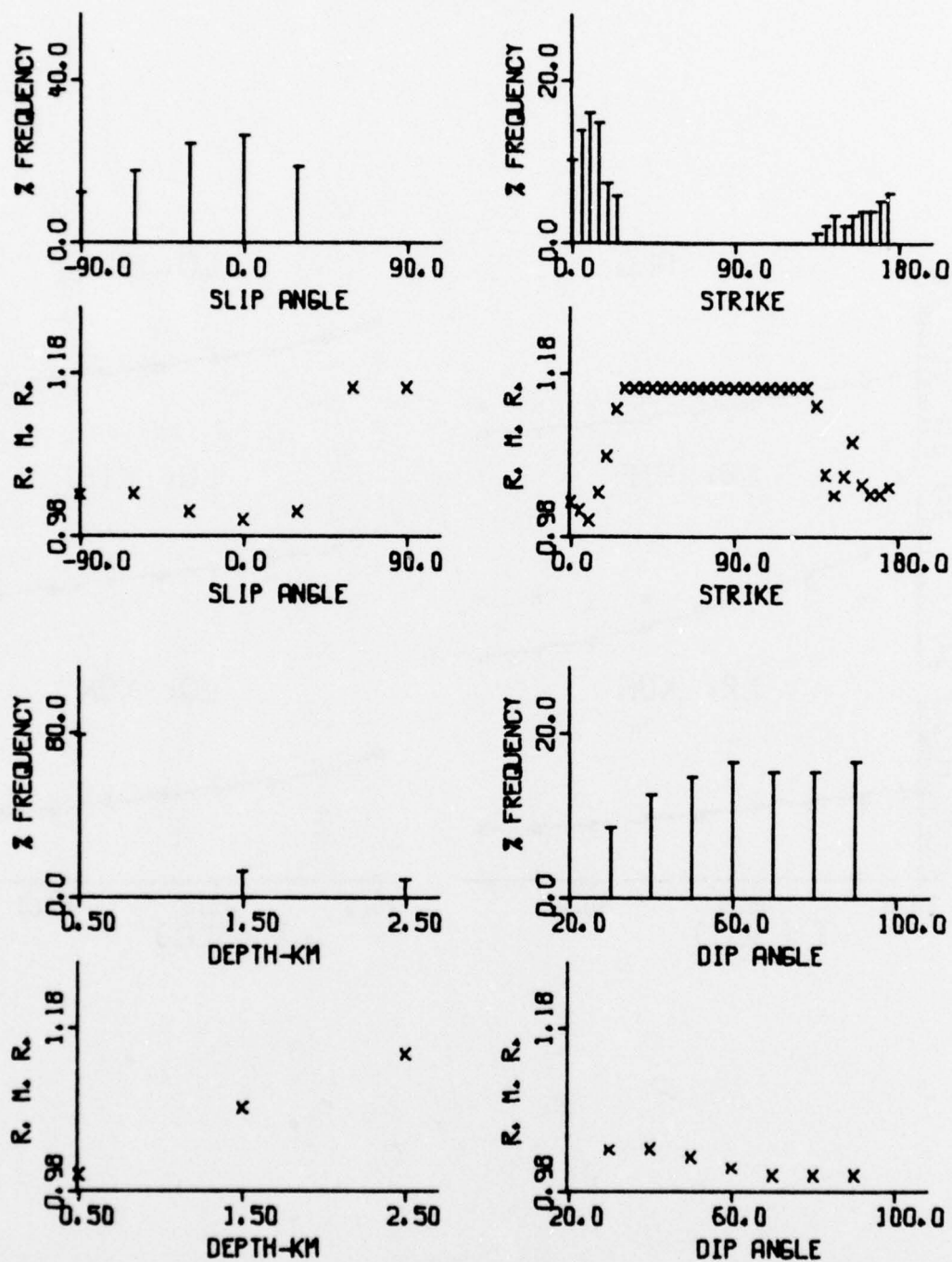


FIGURE V-9

RESULTS FROM AMPLITUDE SPECTRAL FITTING: NT1/603/75
(PAGE 1 OF 2)

(b) Spectral Fits

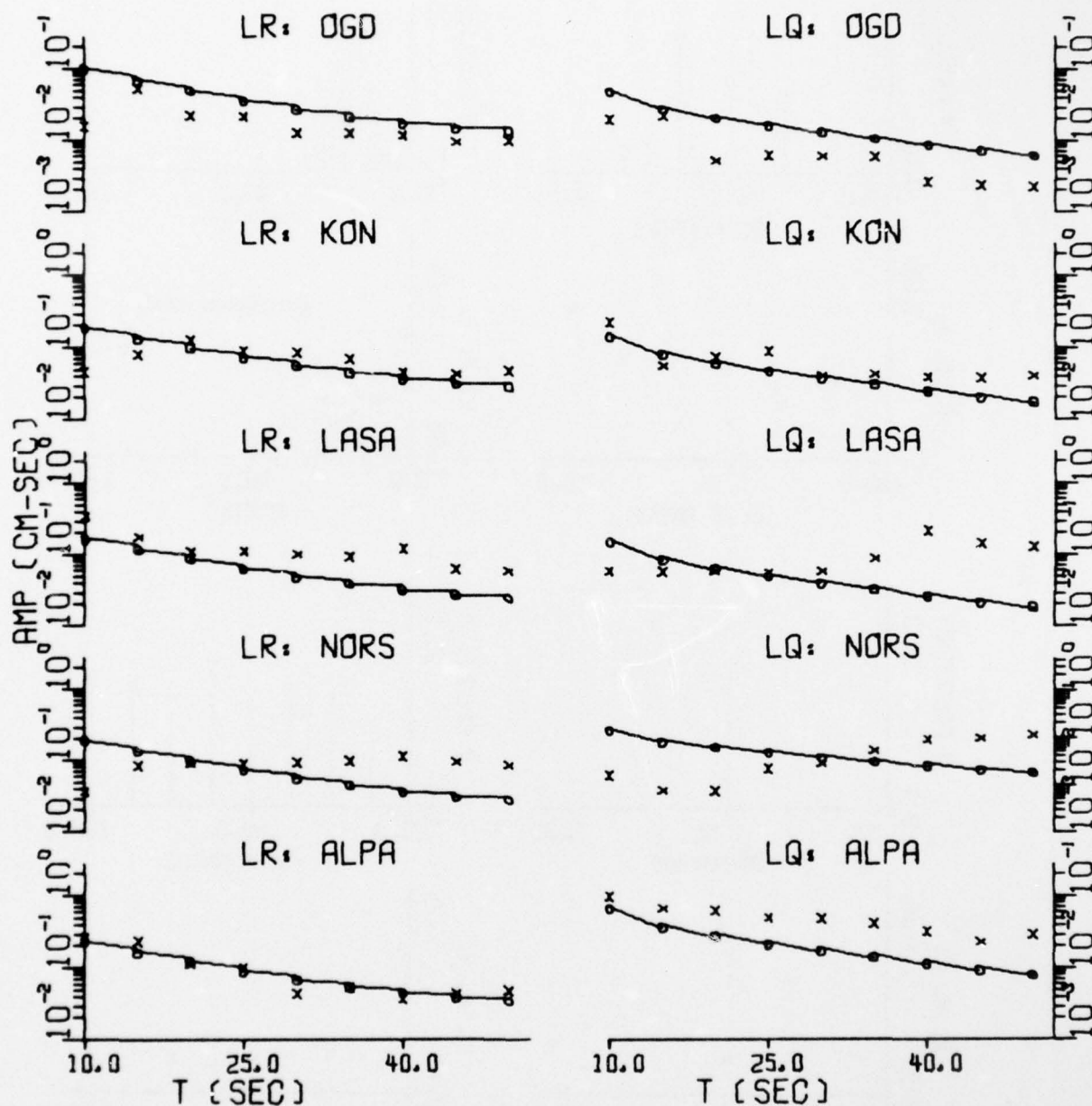


FIGURE V-9
RESULTS FROM AMPLITUDE SPECTRAL FITTING: NT1/603/75
(PAGE 2 OF 2)

(a) Residual Distributions

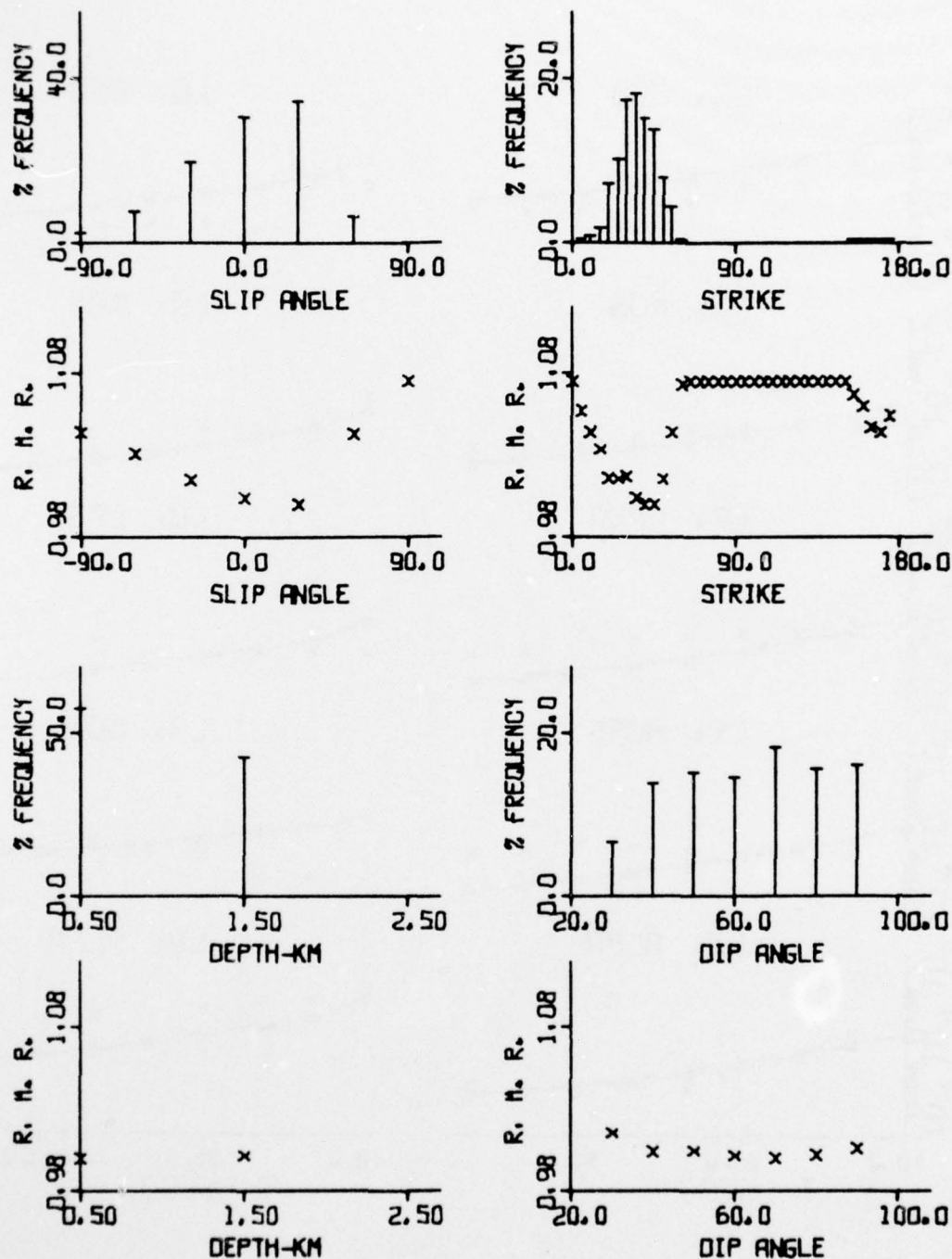


FIGURE V-10

RESULTS FROM AMPLITUDE SPECTRAL FITTING: NT2/603/75
(PAGE 1 OF 2)

(b) Spectral Fits

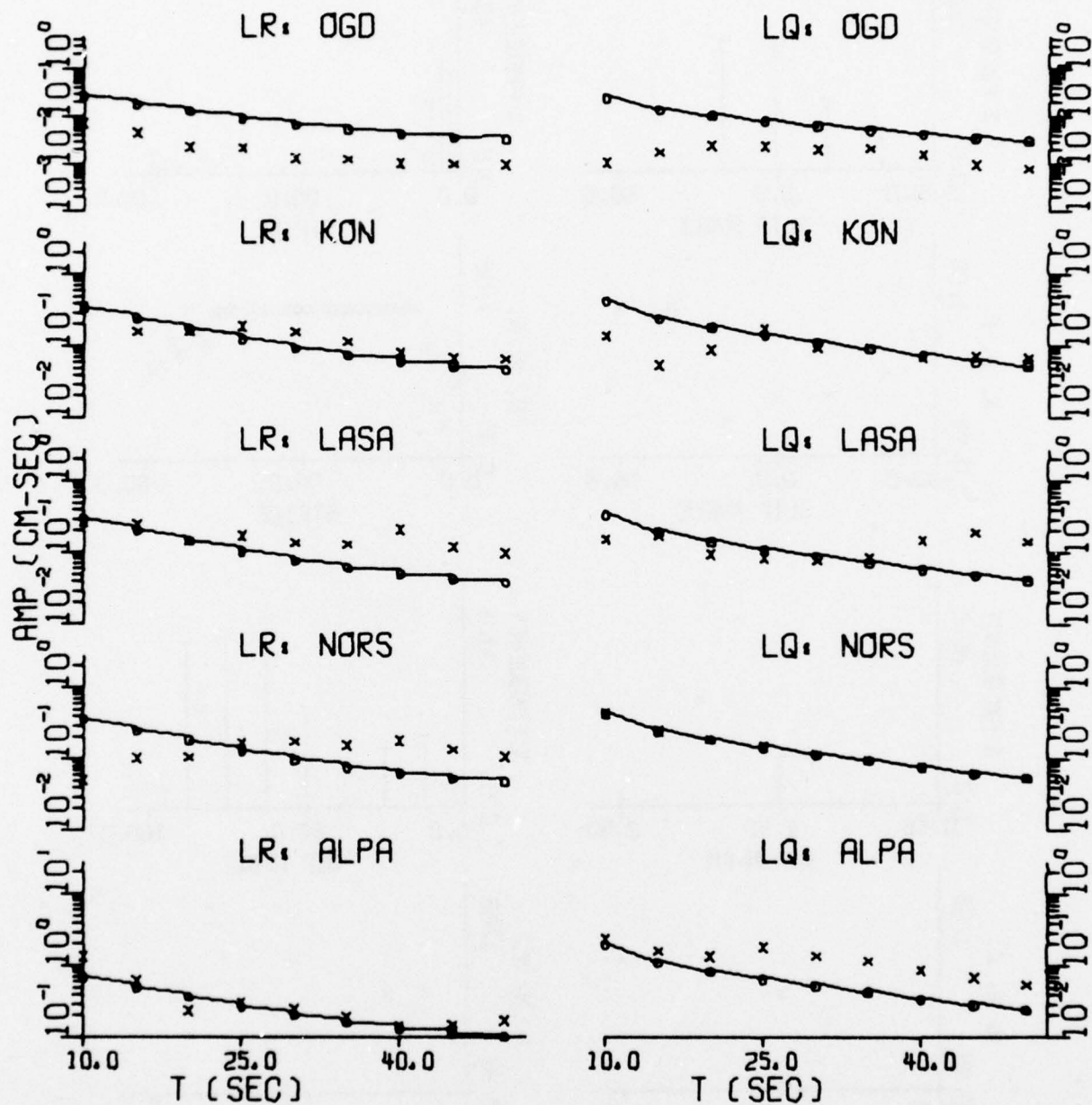


FIGURE V-10
RESULTS FROM AMPLITUDE SPECTRAL FITTING: NT2/603/75
(PAGE 2 OF 2)

(a) Residual Distributions

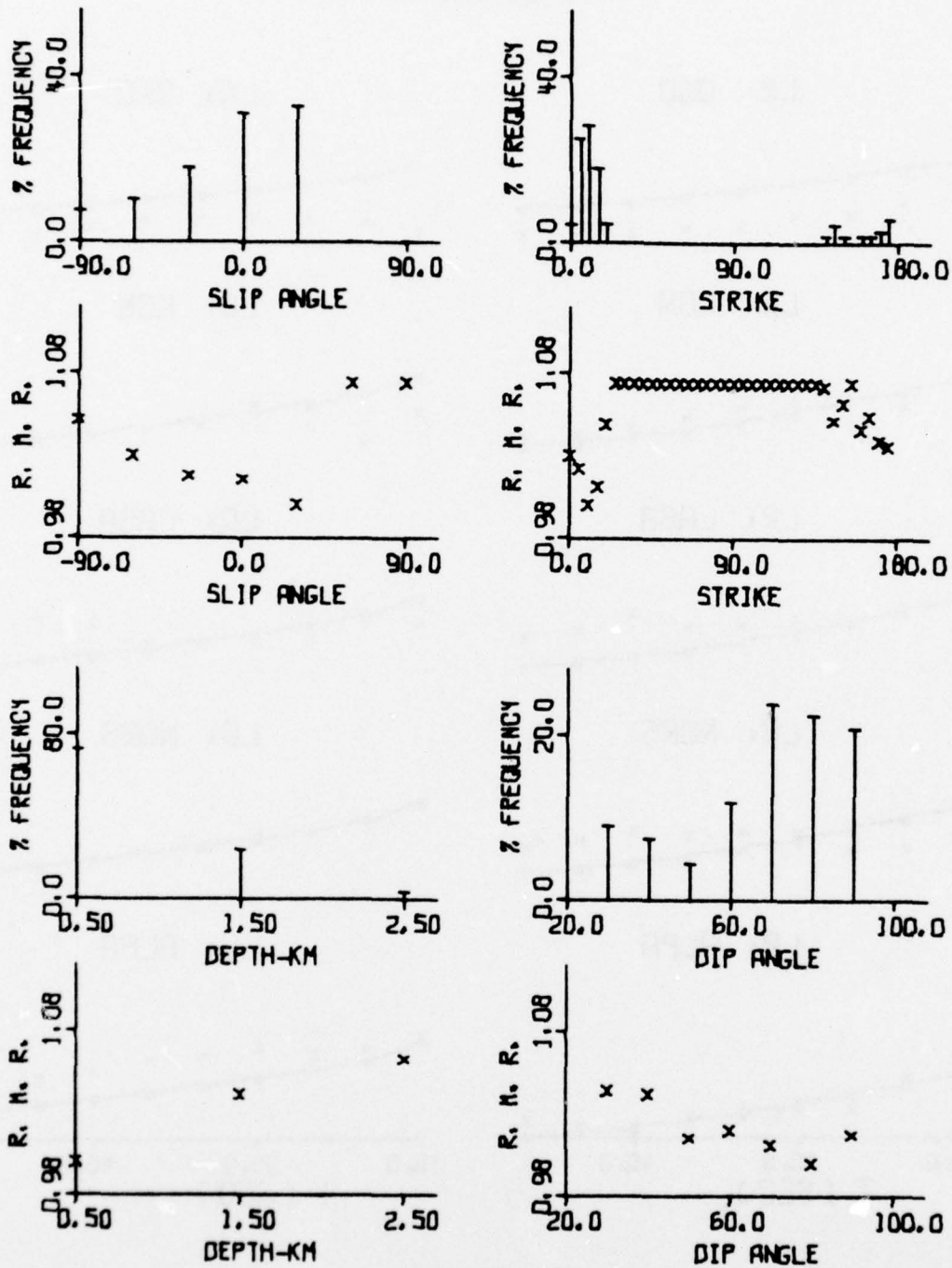


FIGURE V-11

RESULTS FROM AMPLITUDE SPECTRAL FITTING: NTS/619/75
(PAGE 1 OF 3)

(b) Spectral Fits

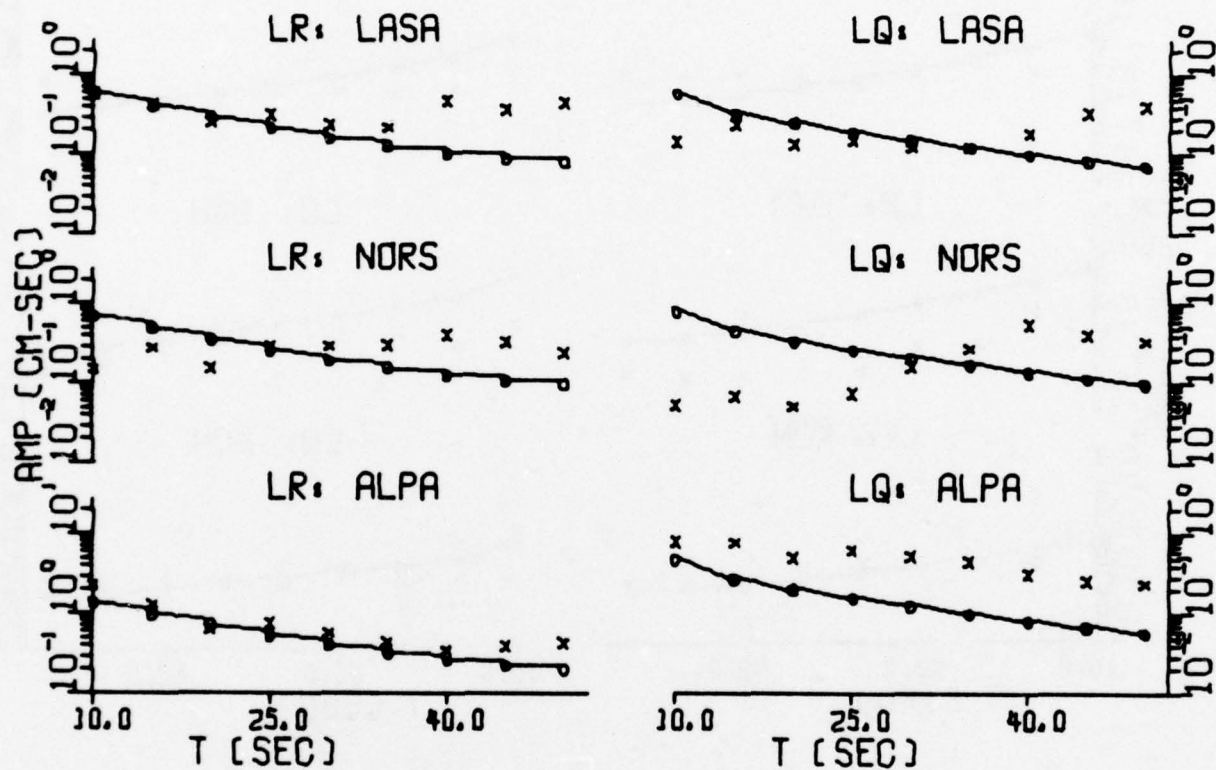


FIGURE V-11

RESULTS FROM AMPLITUDE SPECTRAL FITTING: NTS/619/75
(PAGE 2 OF 3)

(b) Spectral Fits

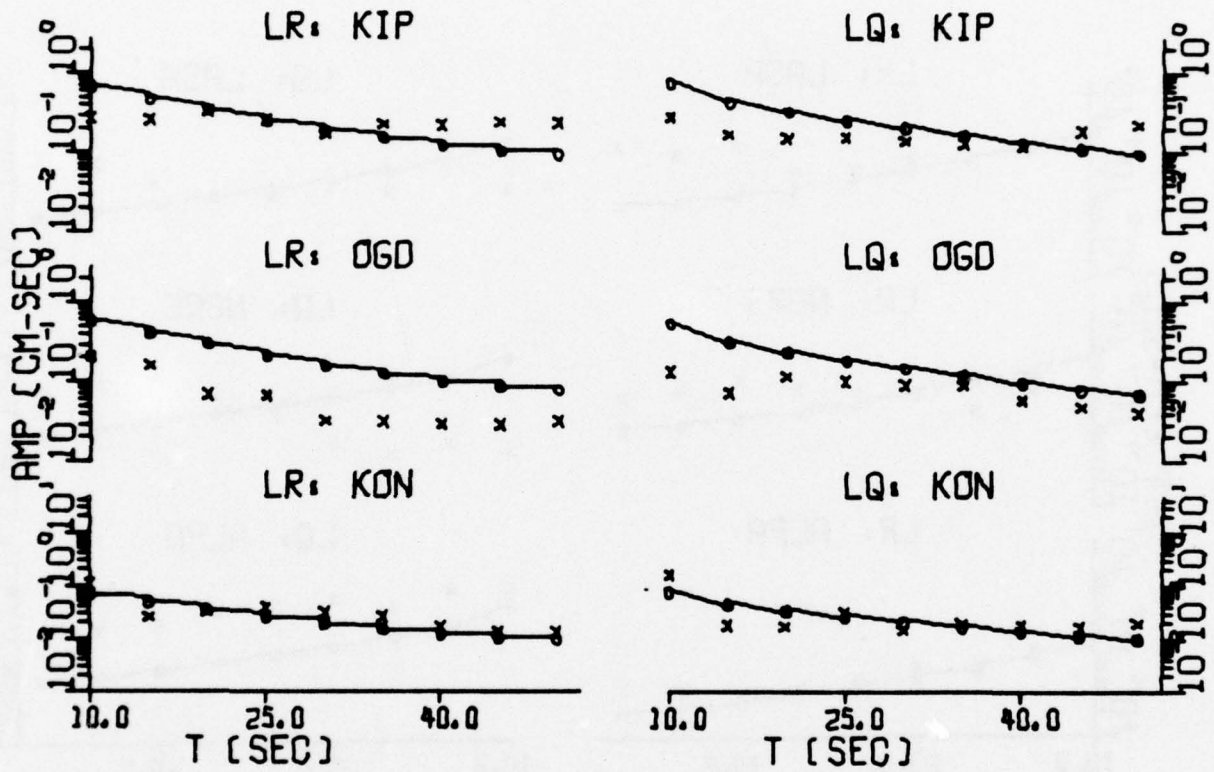


FIGURE V-11

RESULTS FROM AMPLITUDE SPECTRAL FITTING: NTS/619/75
(PAGE 3 OF 3)

(a) Residual Distributions

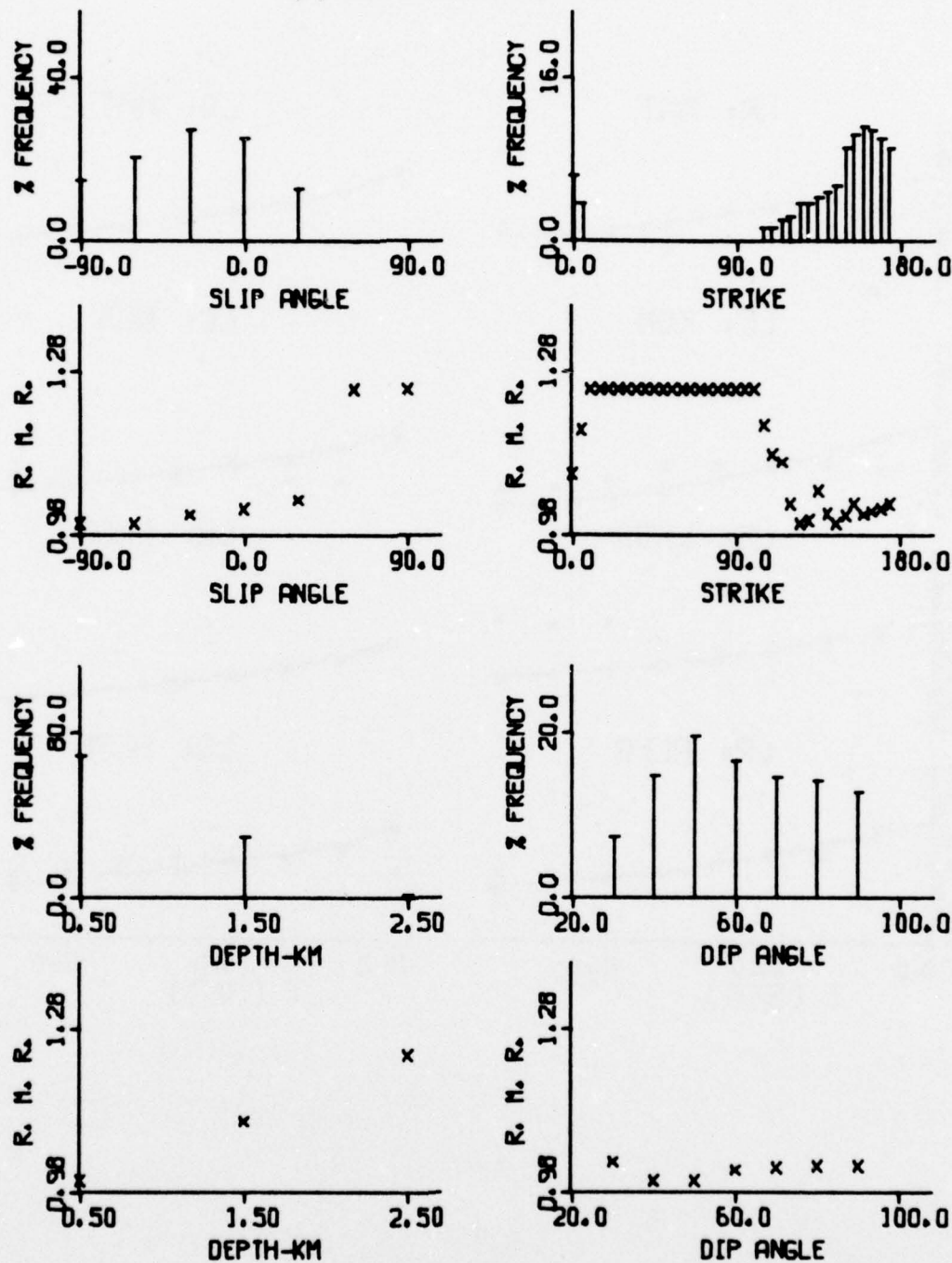


FIGURE V-12

RESULTS FROM AMPLITUDE SPECTRAL FITTING: NTS/626/75
(PAGE 1 OF 2)

(b) Spectral Fits

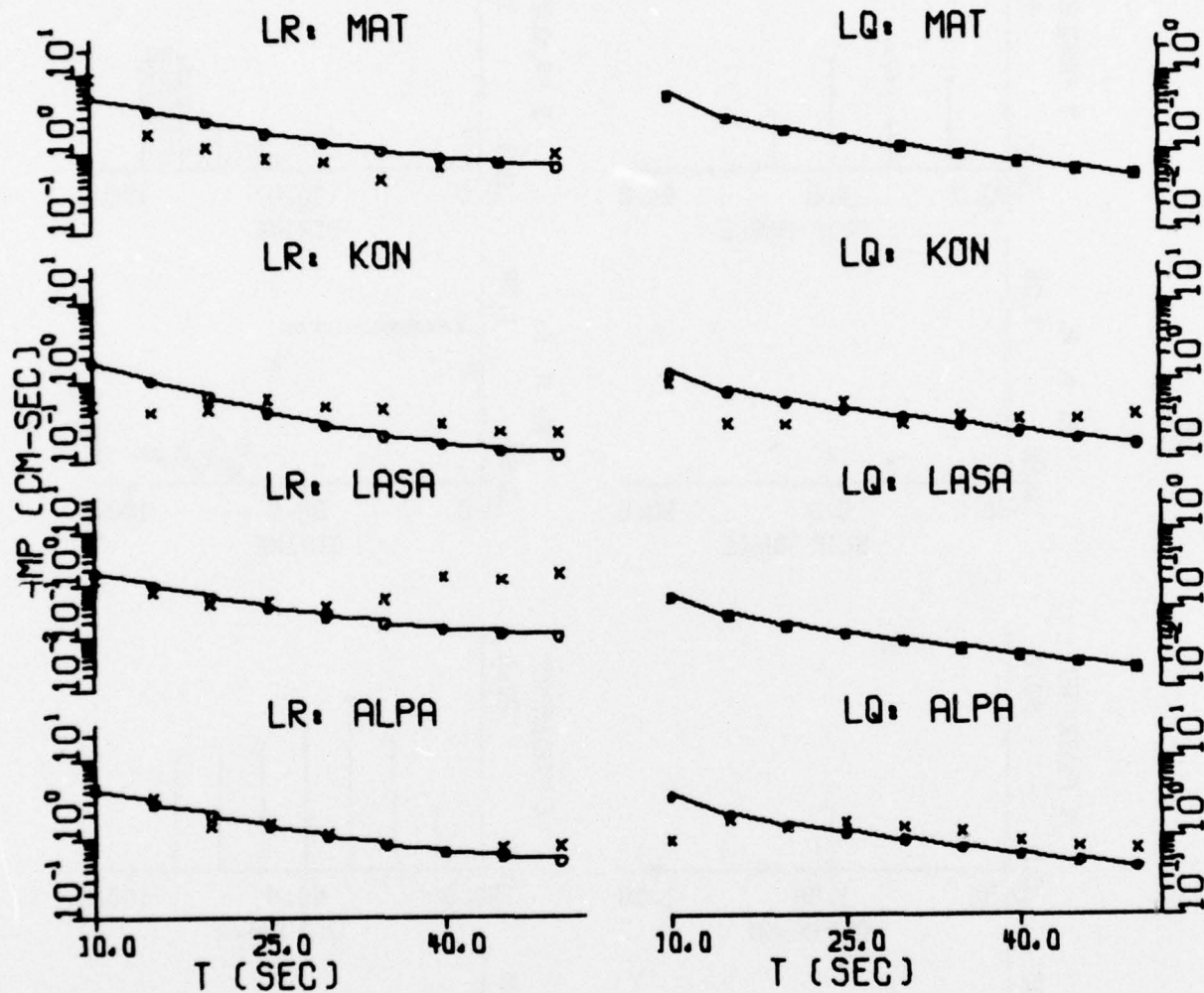


FIGURE V-12

RESULTS FROM AMPLITUDE SPECTRAL FITTING: NTS/626/75
(PAGE 2 OF 2)

(a) Residual Distributions

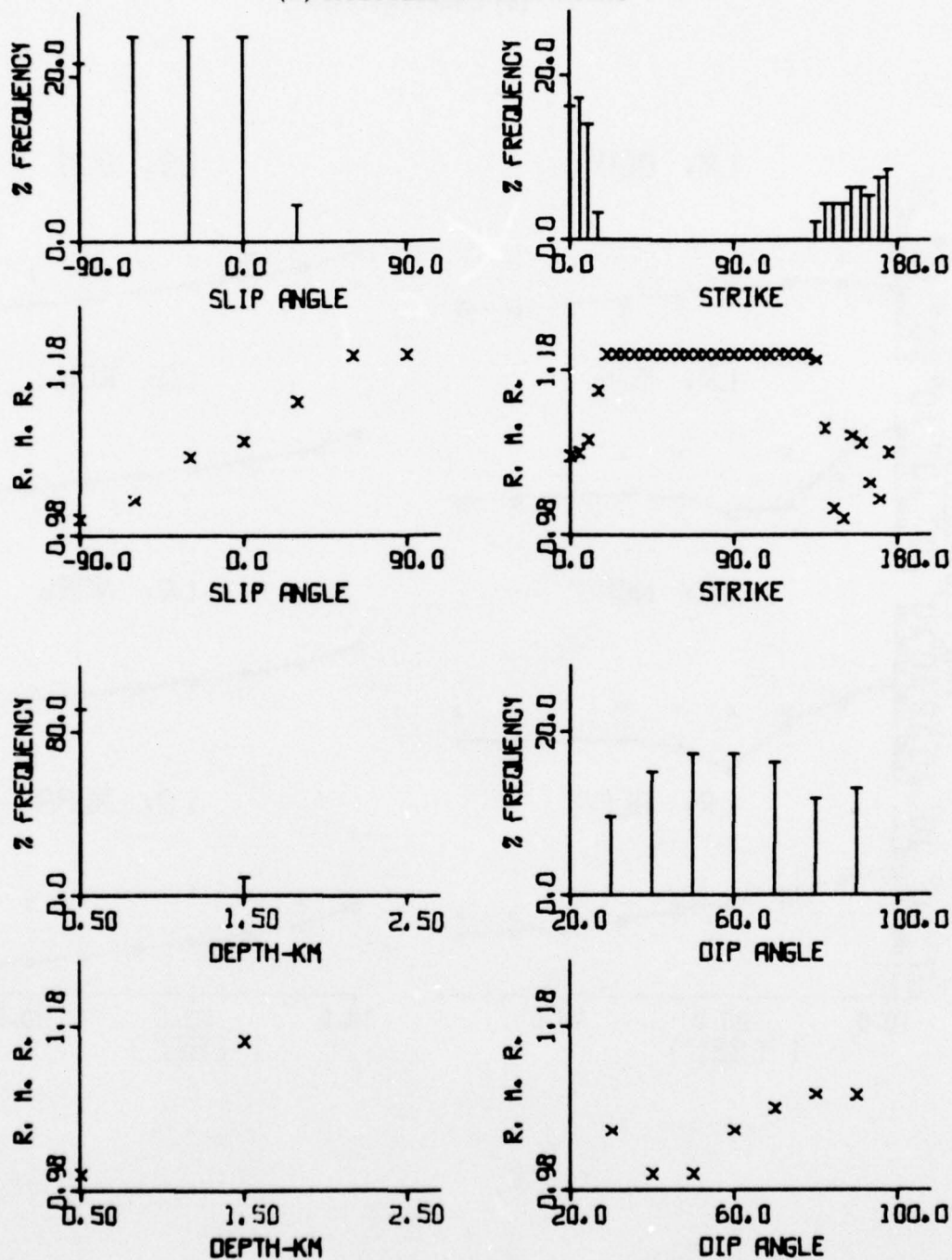


FIGURE V-13

RESULTS FROM AMPLITUDE SPECTRAL FITTING: NTS/1028/5
(PAGE 1 OF 3)

(b) Spectral Fits

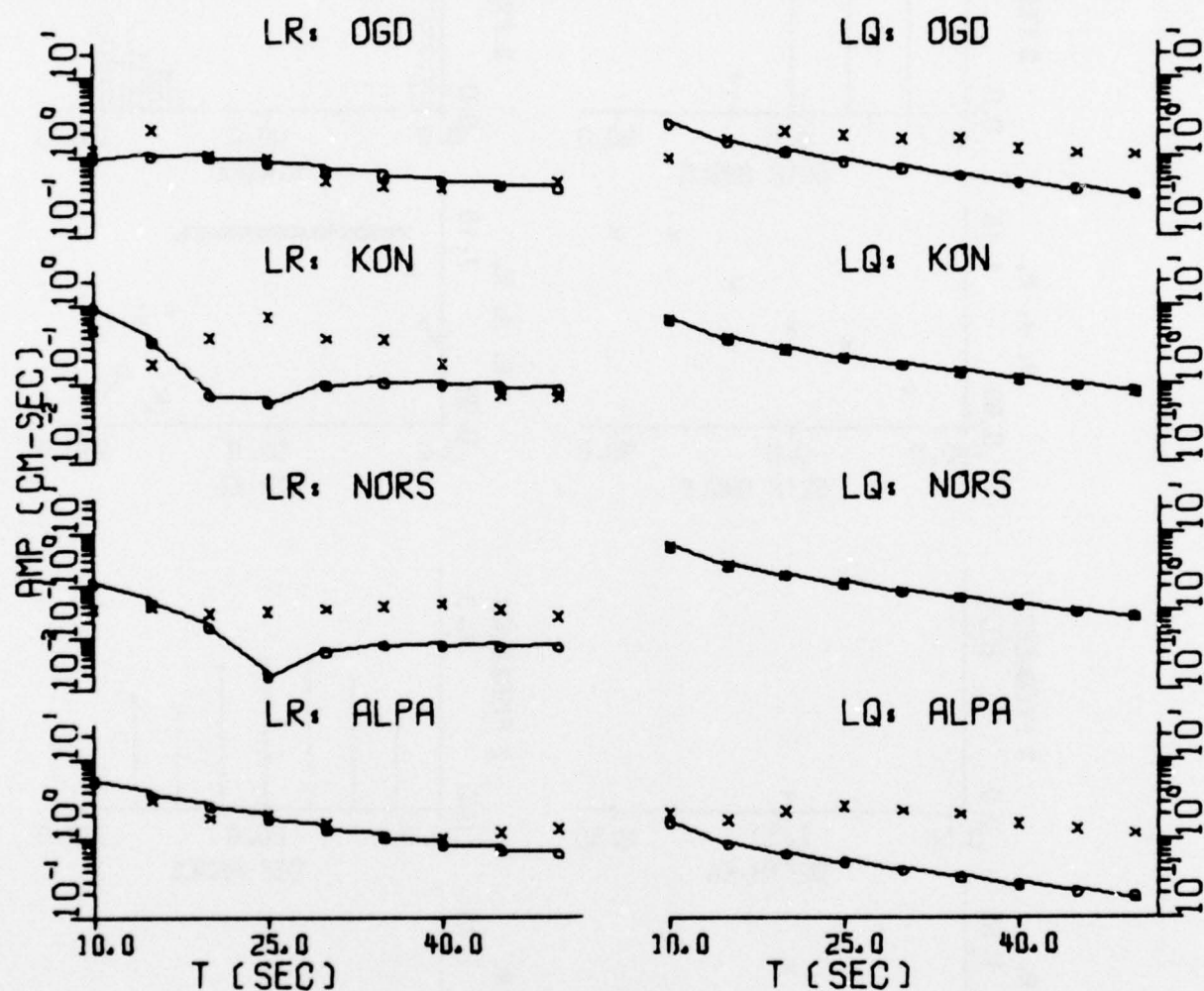


FIGURE V-13
RESULTS FROM AMPLITUDE SPECTRAL FITTING: NTS/1028/5
(PAGE 2 OF 3)

(b) Spectral Fits

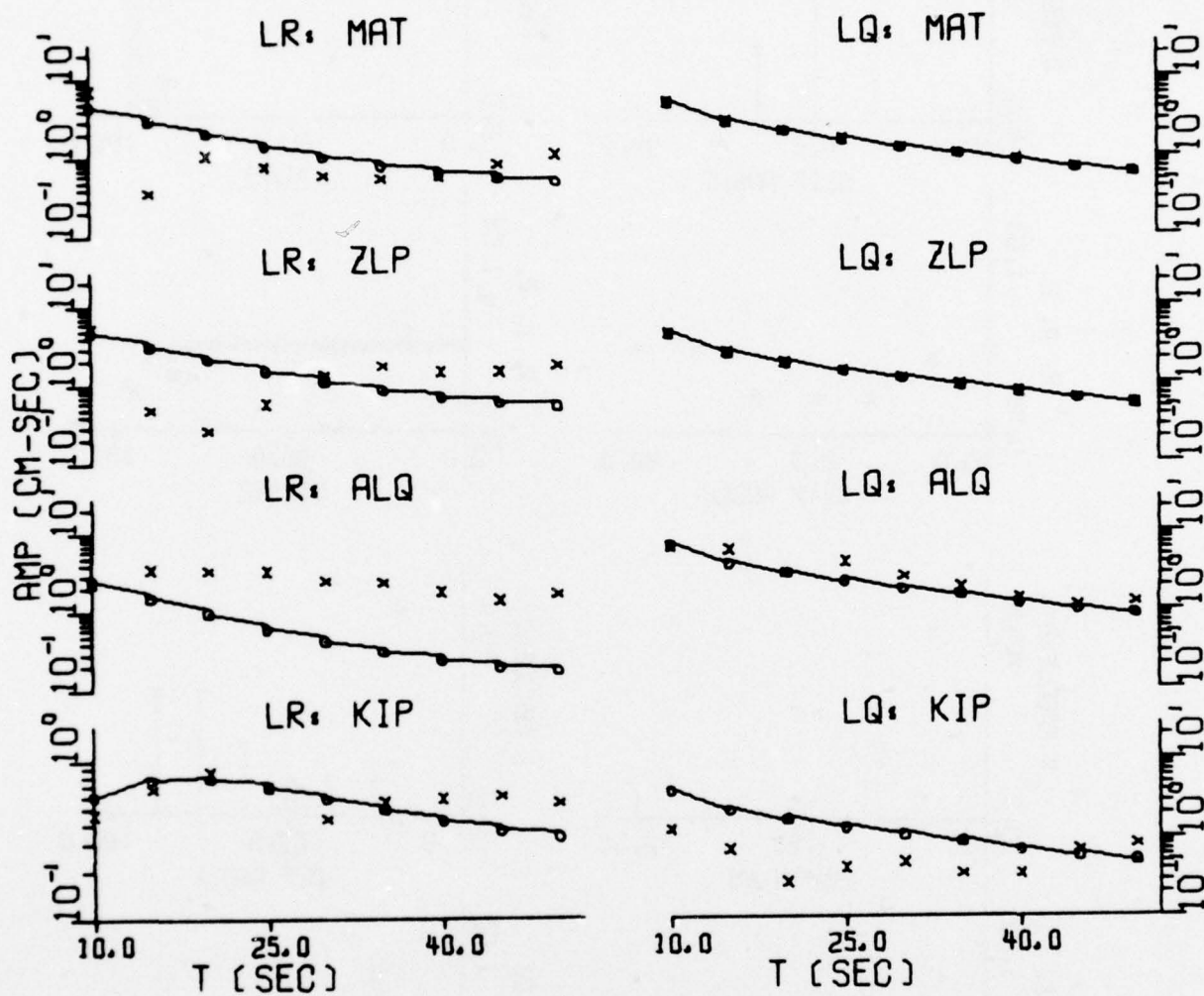


FIGURE V-13

RESULTS FROM AMPLITUDE SPECTRAL FITTING: NTS/1028/5
(PAGE 3 OF 3)

(a) Residual Distributions

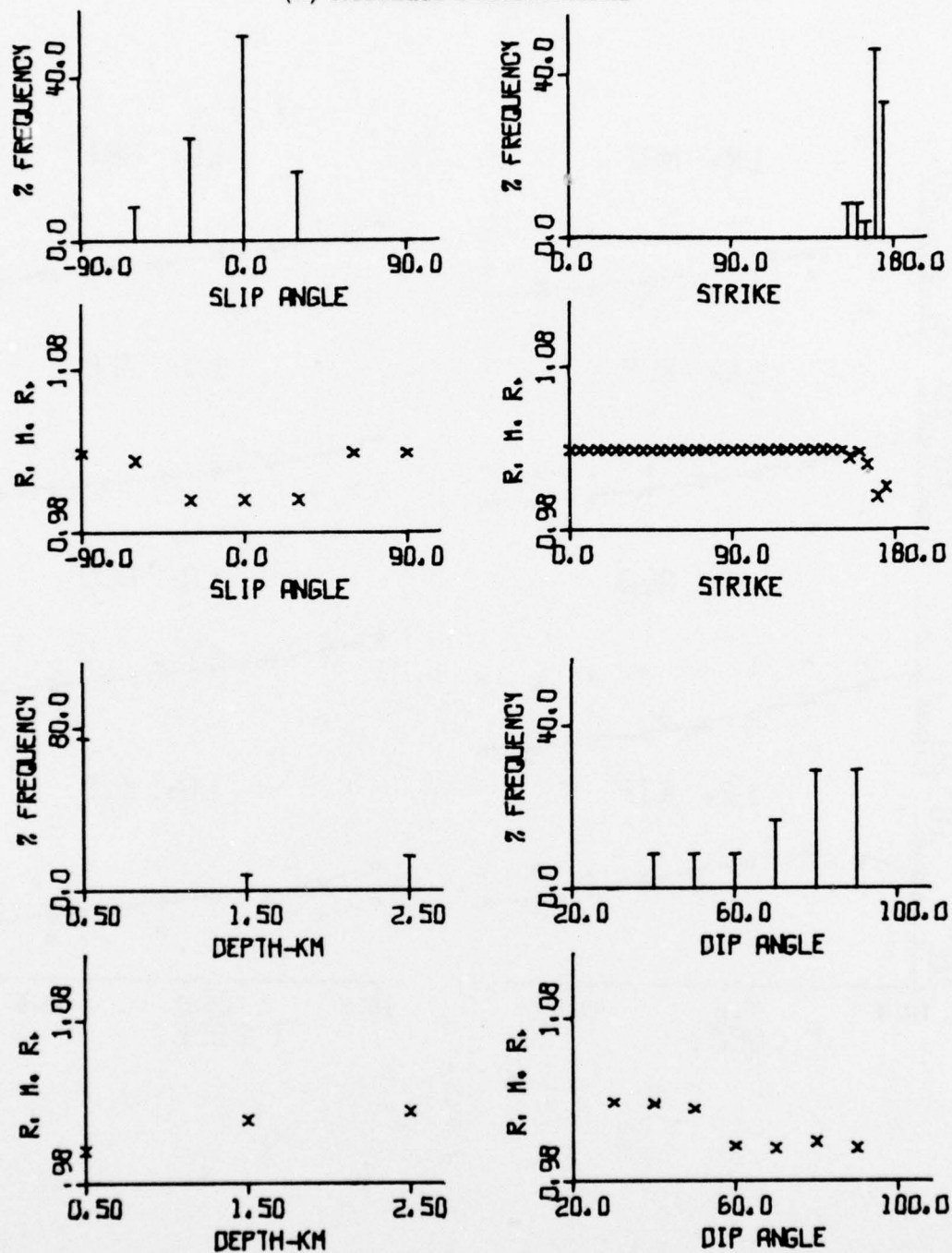


FIGURE V-14

RESULTS FROM AMPLITUDE SPECTRAL FITTING: NTS/103/76
(PAGE 1 OF 2)

(b) Spectral Fits

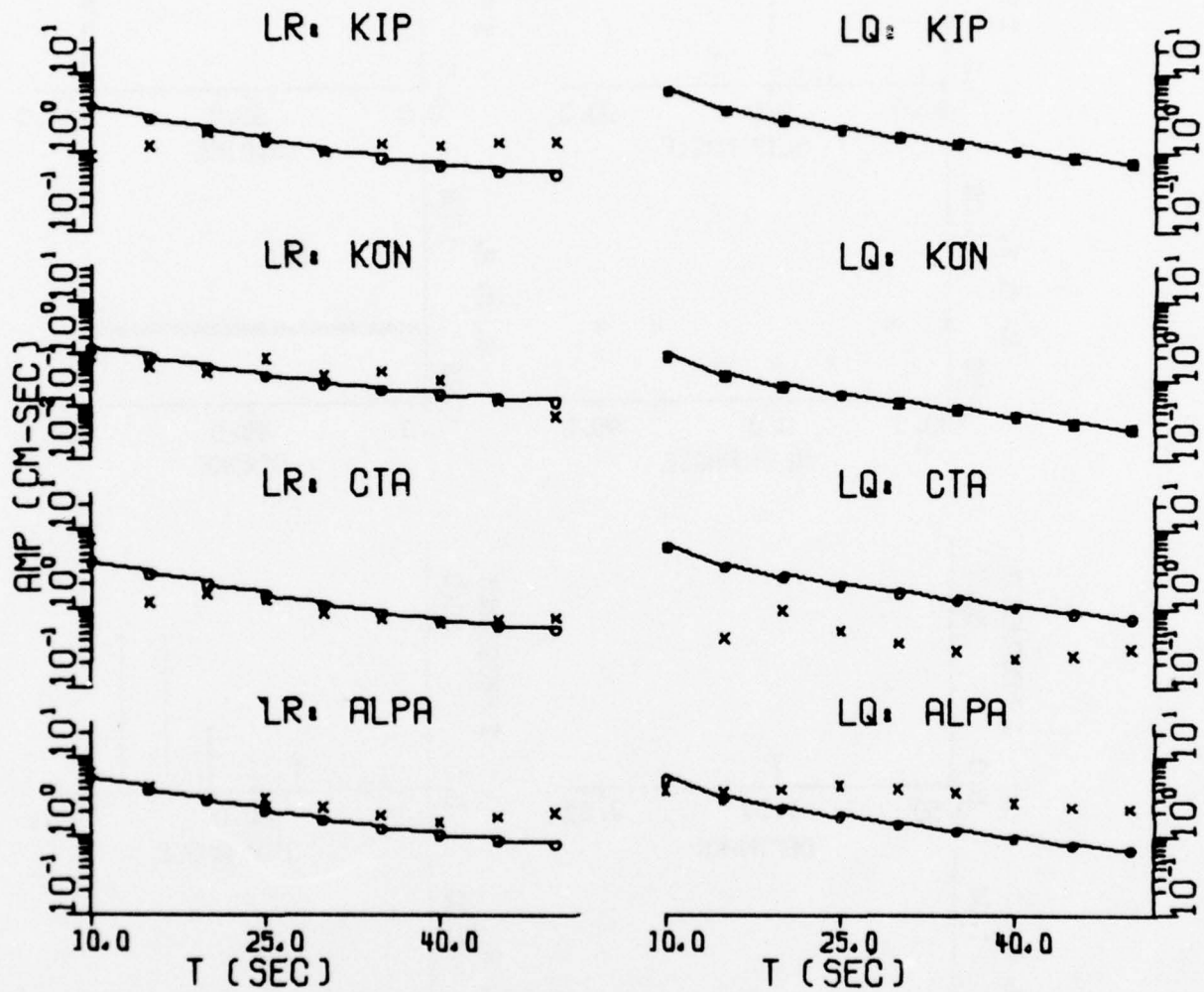


FIGURE V-14
RESULTS FROM AMPLITUDE SPECTRAL FITTING: NTS/103/76
(PAGE 2 OF 2)

(a) Residual Distributions

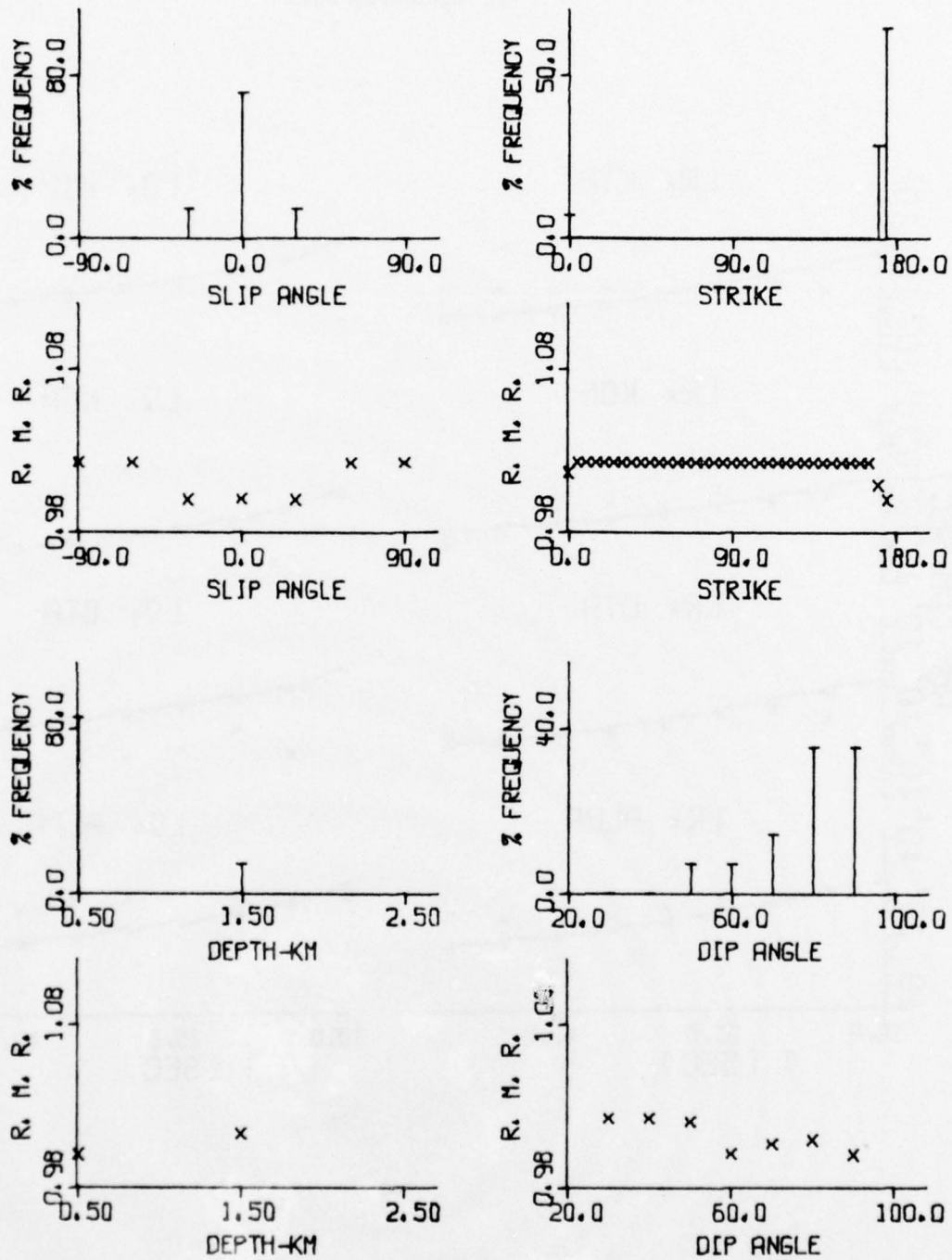


FIGURE V-15

RESULTS FROM AMPLITUDE SPECTRAL FITTING: NTS/212/76
(PAGE 1 OF 2)

(b) Spectral Fits

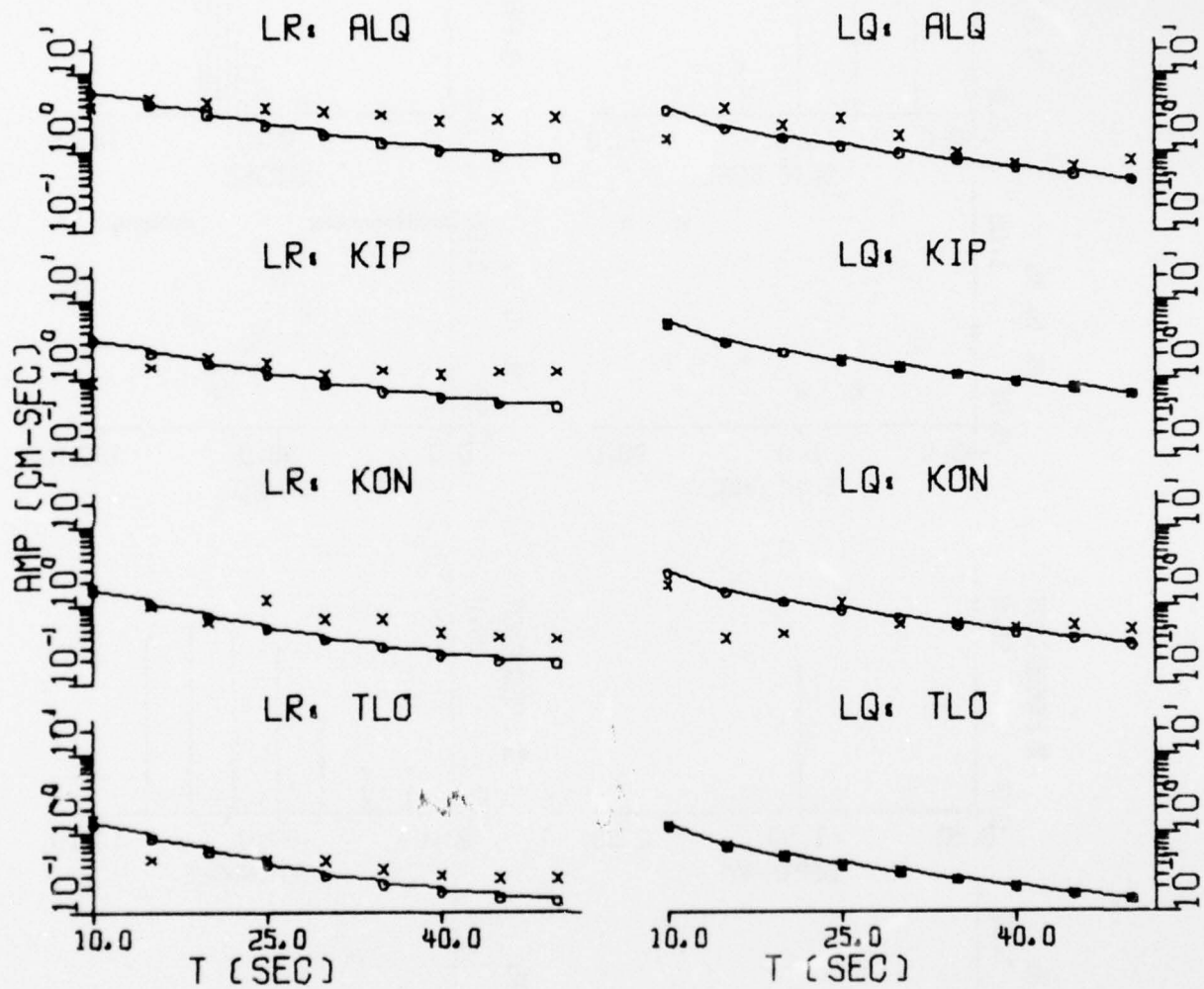


FIGURE V-15
RESULTS FROM AMPLITUDE SPECTRAL FITTING: NTS/212/76
(PAGE 2 OF 2)

(a) Residual Distributions

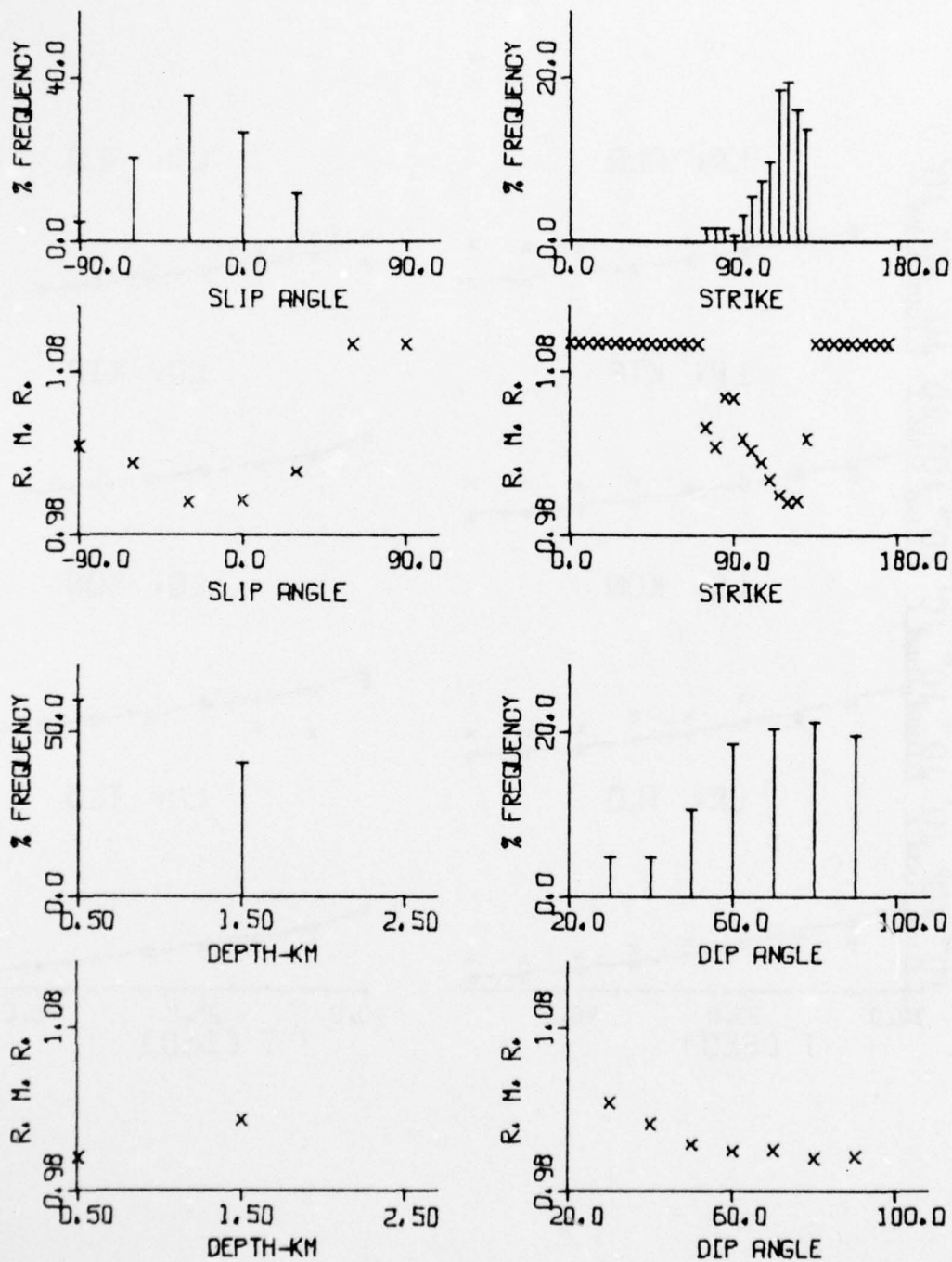


FIGURE V-16

RESULTS FROM AMPLITUDE SPECTRAL FITTING: NTS/309/76
(PAGE 1 OF 3)

(b) Spectral Fits

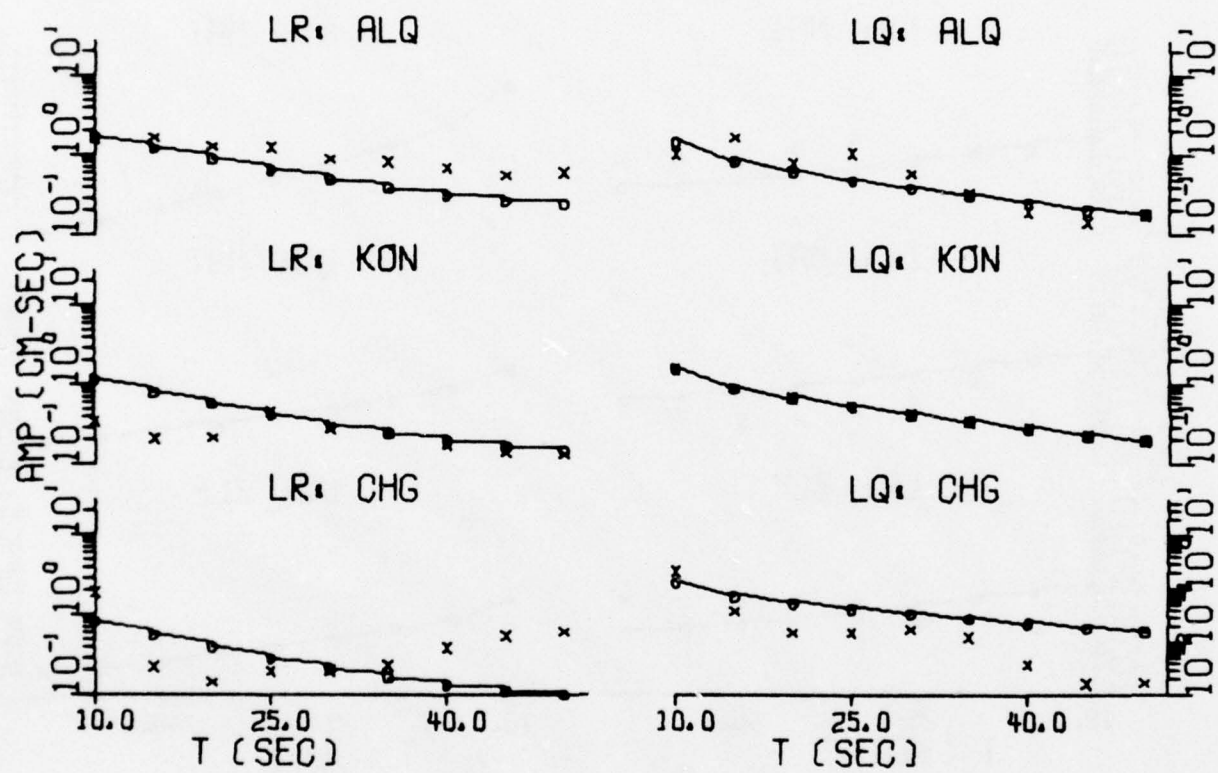


FIGURE V-16

RESULTS FROM AMPLITUDE SPECTRAL FITTING: NTS/309/76
(PAGE 2 OF 3)

(b) Spectral Fits

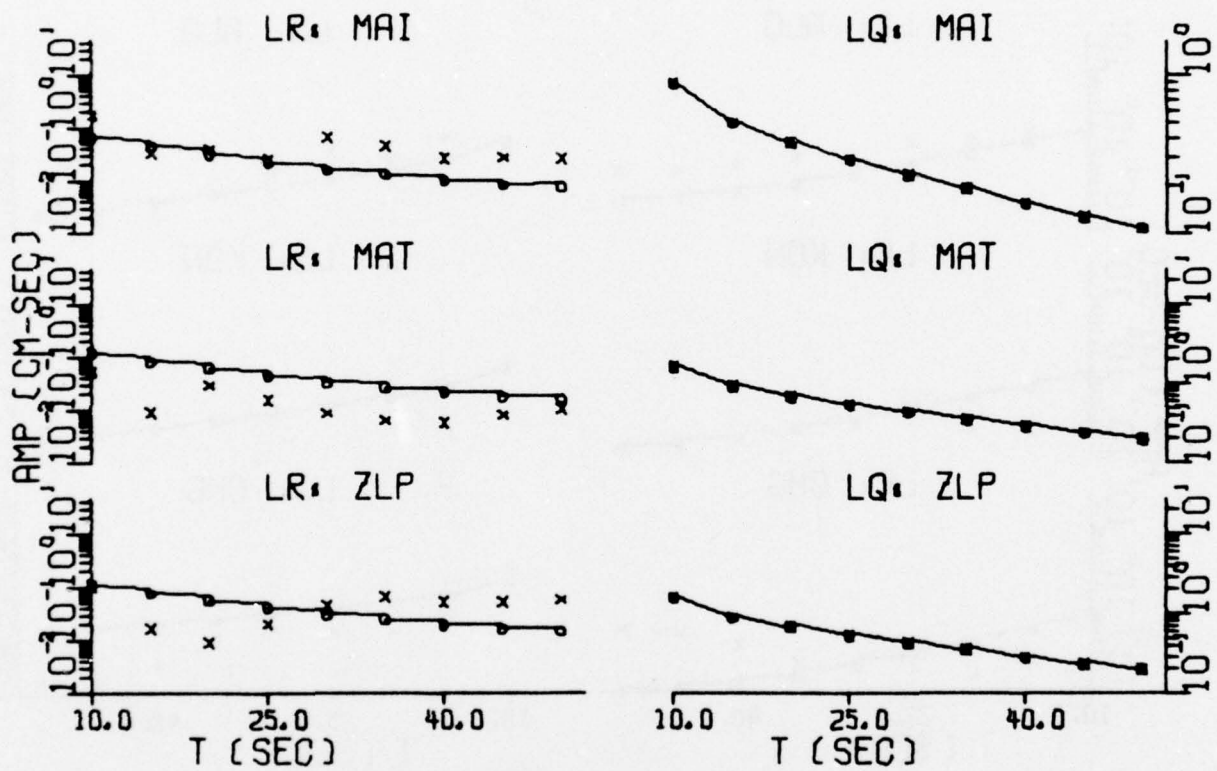


FIGURE V-16
RESULTS FROM AMPLITUDE SPECTRAL FITTING: NTS/309/76
(PAGE 3 OF 3)

(a) Residual Distributions

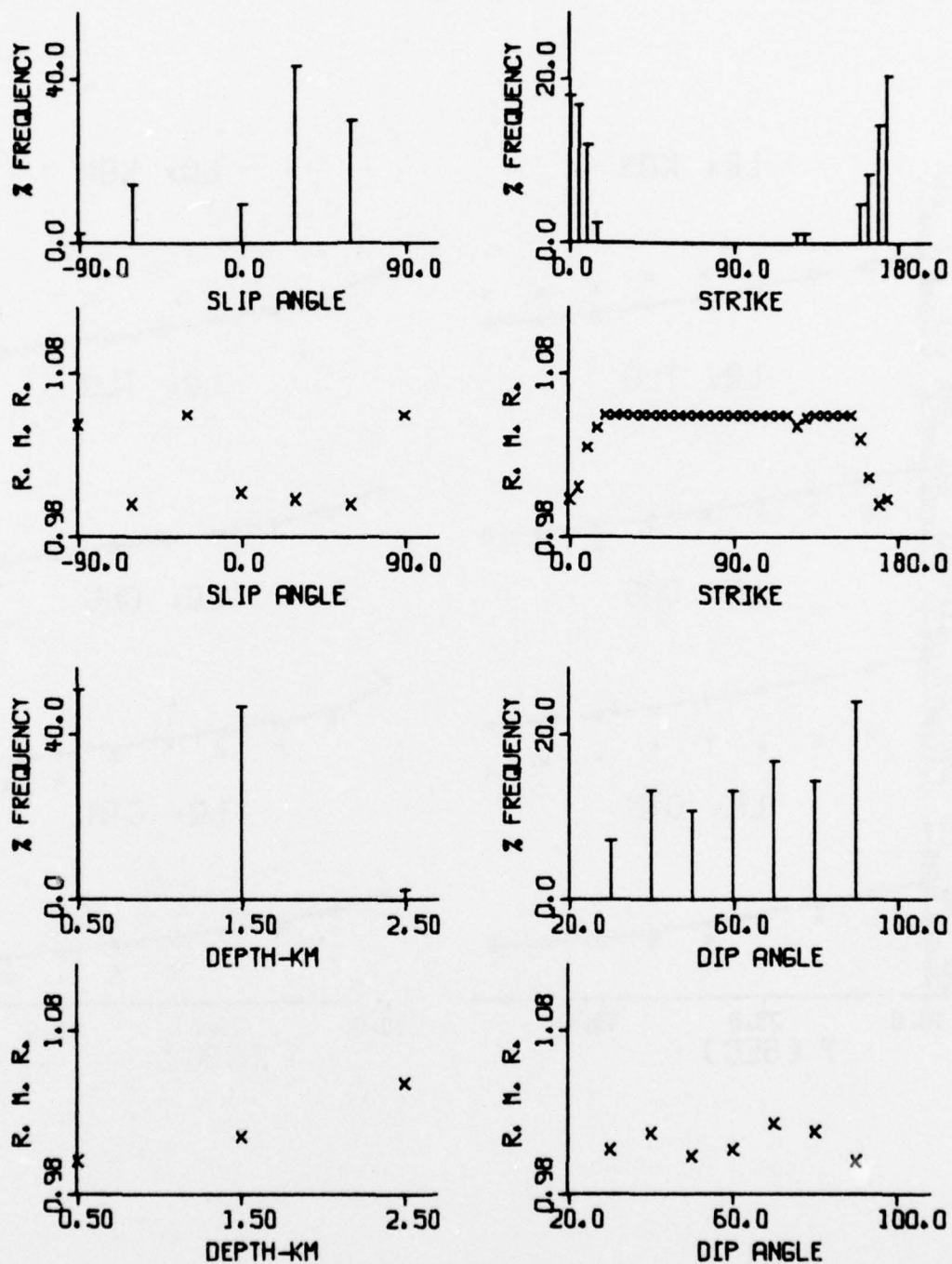


FIGURE V-17

RESULTS FROM AMPLITUDE SPECTRAL FITTING: NTS/314/76
(PAGE 1 OF 3)

(b) Spectral Fits

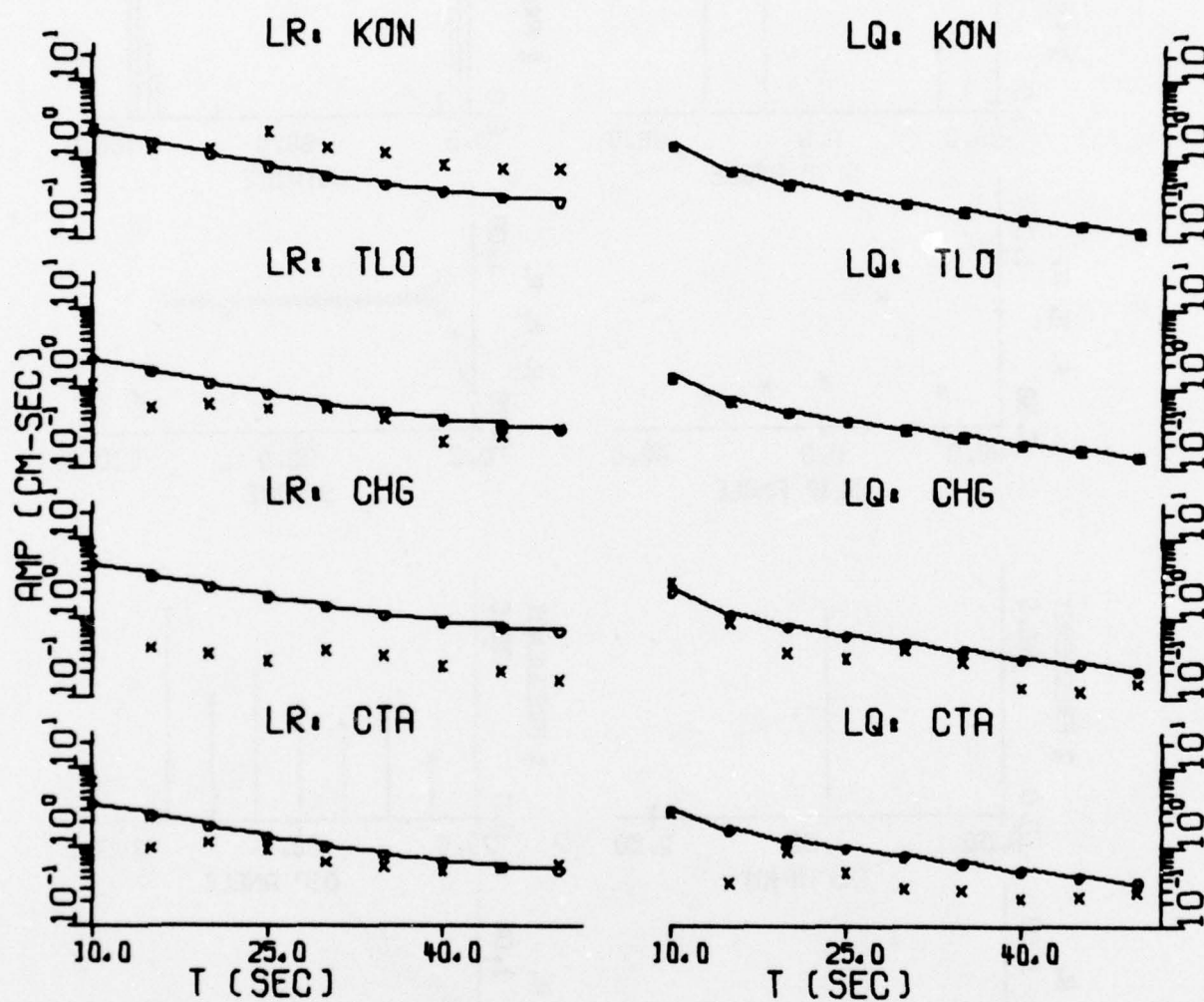


FIGURE V-17

RESULTS FROM AMPLITUDE SPECTRAL FITTING: NTS/314/76
(PAGE 2 OF 3)

(b) Spectral Fits

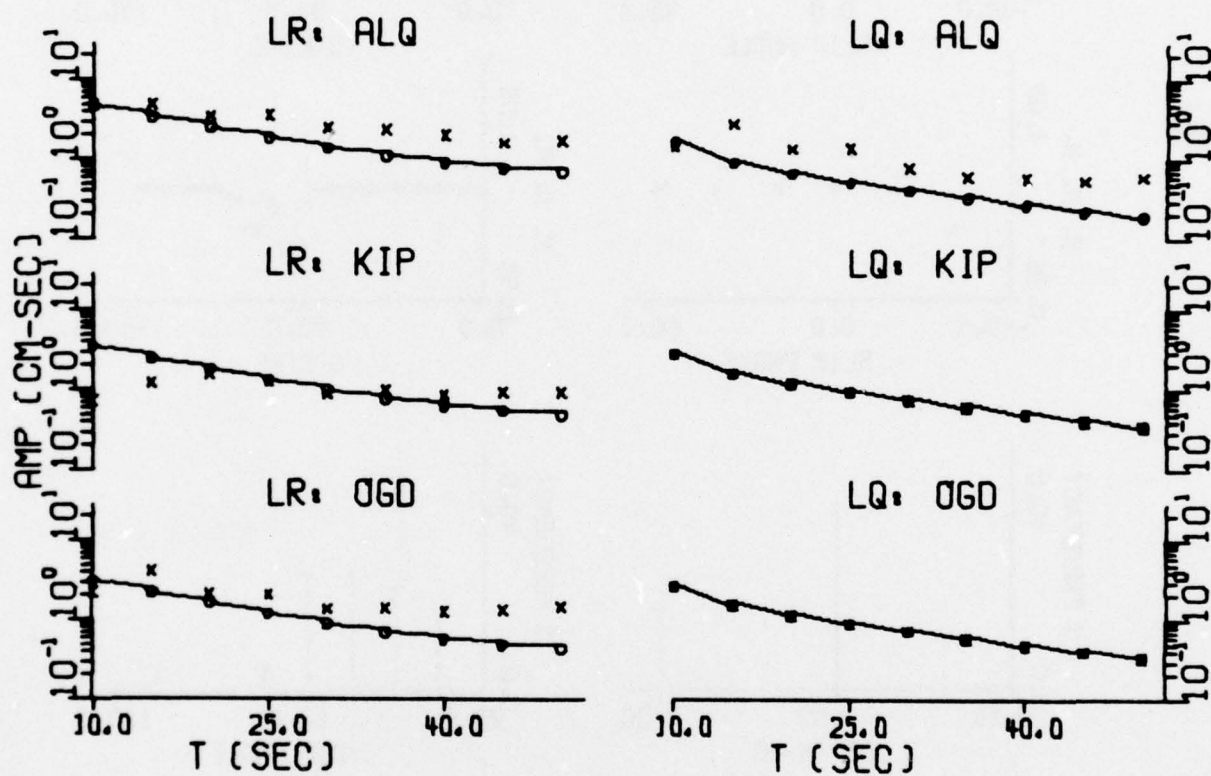


FIGURE V-17
RESULTS FROM AMPLITUDE SPECTRAL FITTING: NTS/314/76
(PAGE 3 OF 3)

(a) Residual Distributions

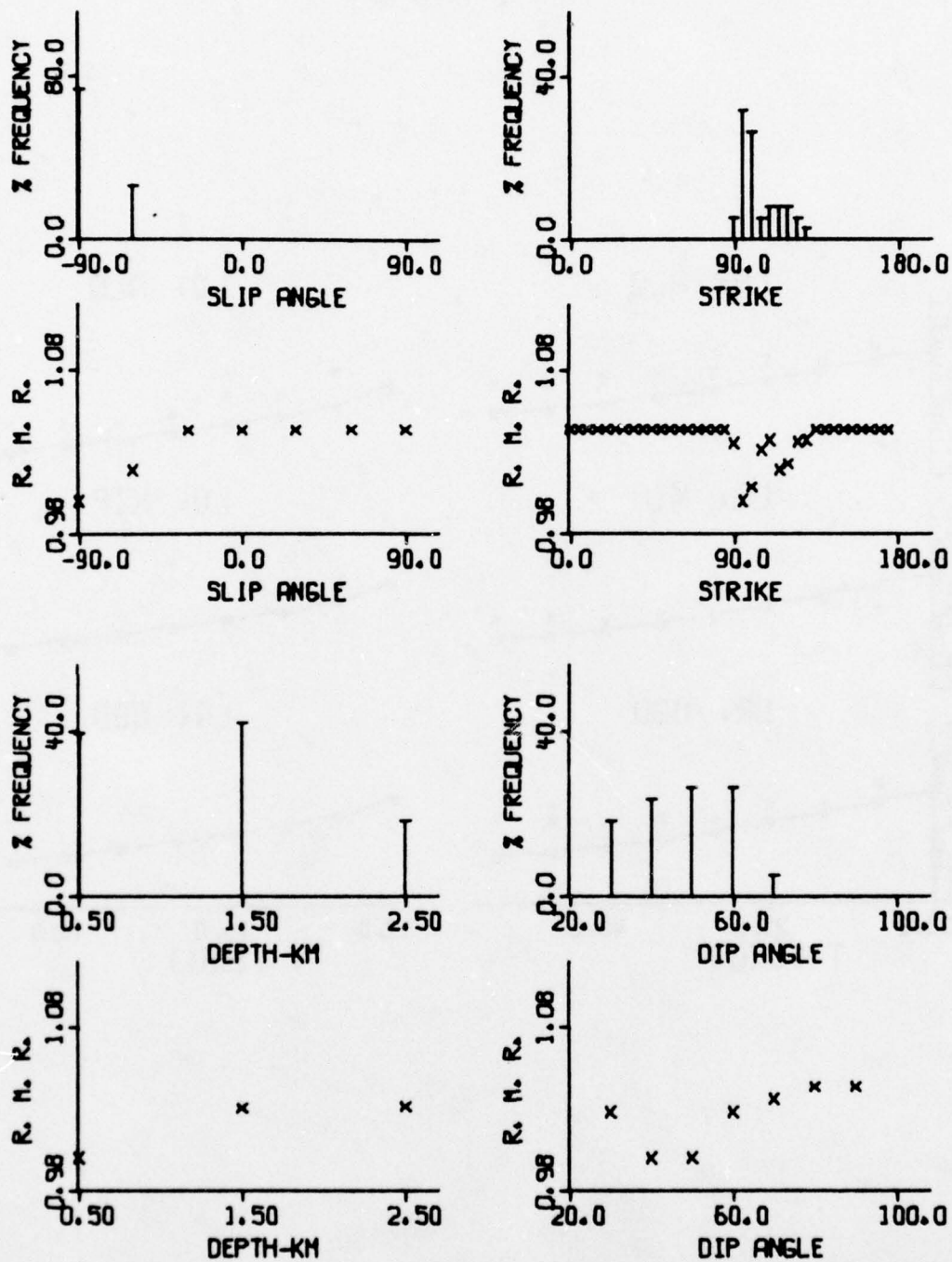


FIGURE V-18

RESULTS FROM AMPLITUDE SPECTRAL FITTING: NT1/317/76
(PAGE 1 OF 3)

(b) Spectral Fits

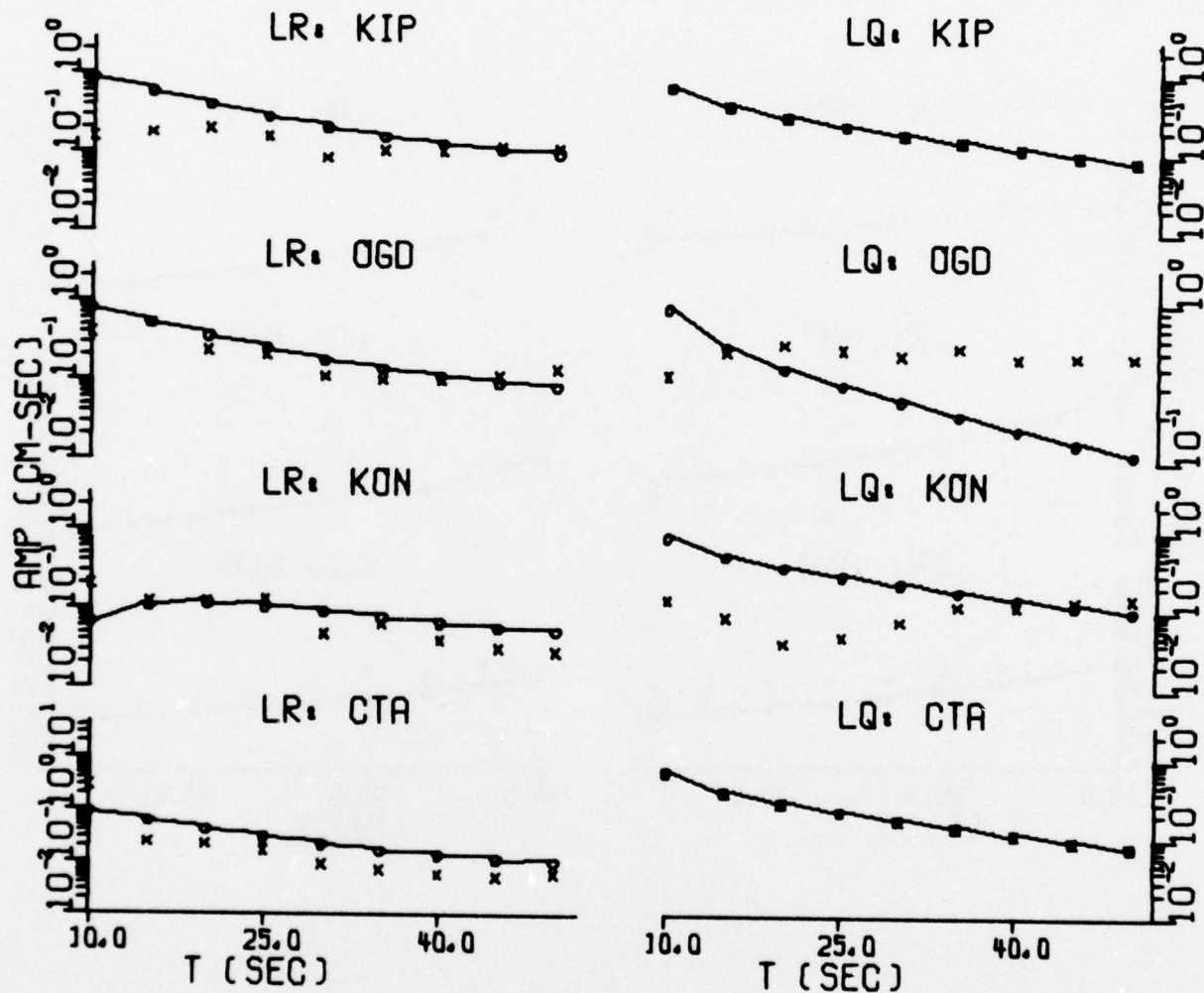


FIGURE V-18
RESULTS FROM AMPLITUDE SPECTRAL FITTING: NT1/317/76
(PAGE 2 OF 3)

(b) Spectral Fits

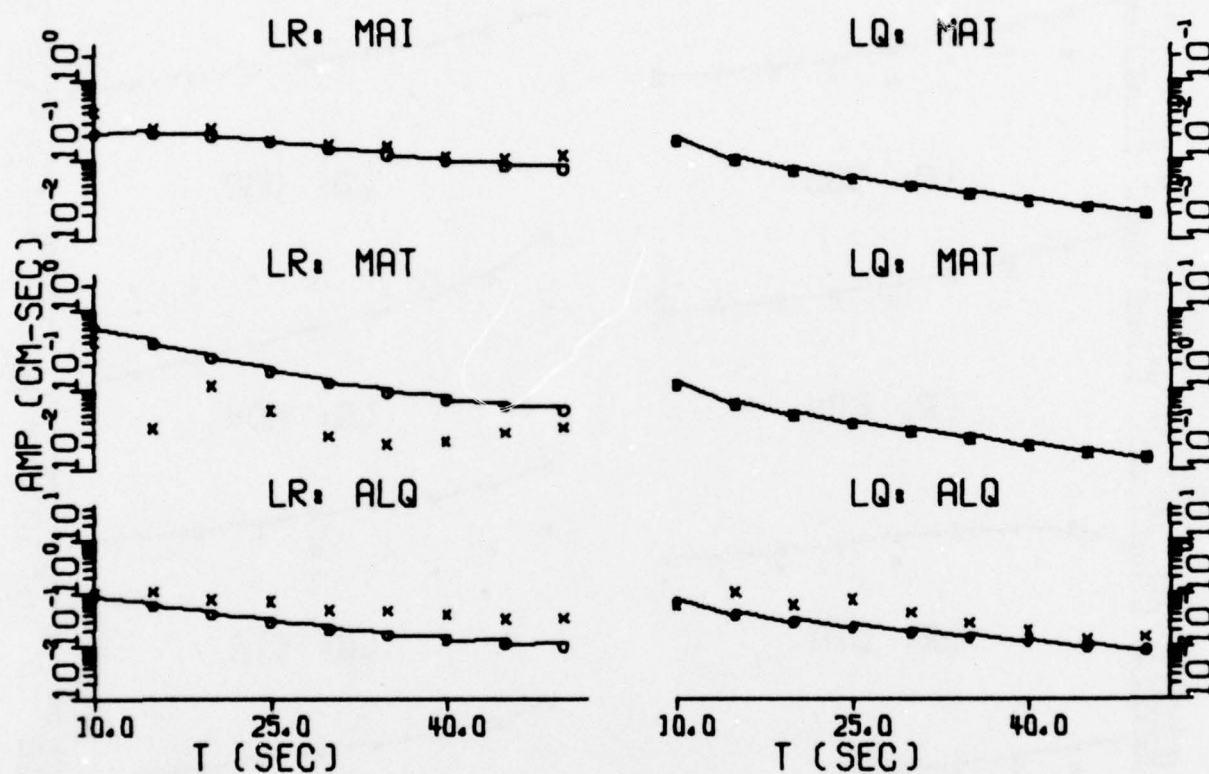


FIGURE V-18

RESULTS FROM AMPLITUDE SPECTRAL FITTING: NT1/317/76
(PAGE 3 OF 3)

(a) Residual Distributions

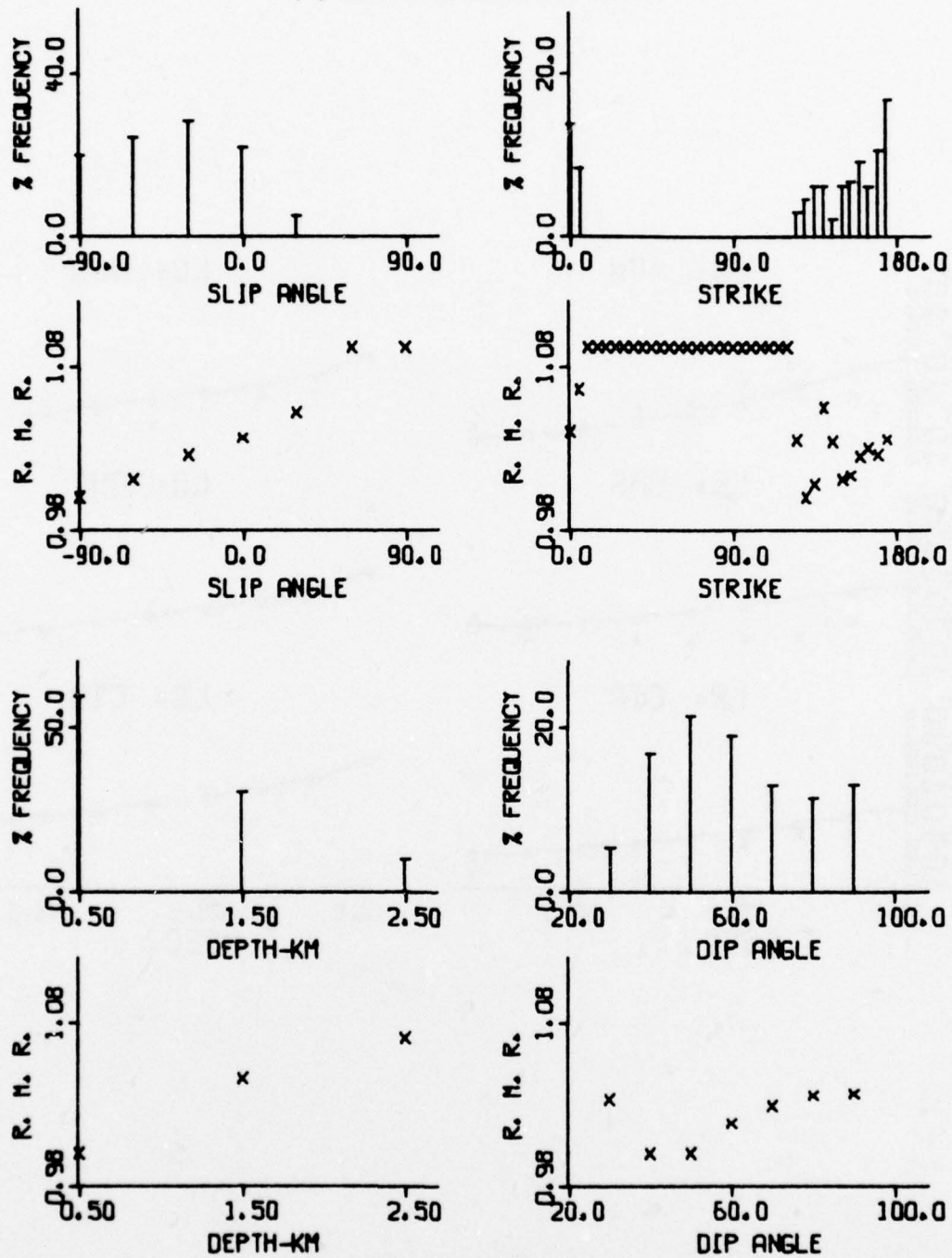


FIGURE V-19

RESULTS FROM AMPLITUDE SPECTRAL FITTING: NT2/317/76
(PAGE 1 OF 3)

(b) Spectral Fits

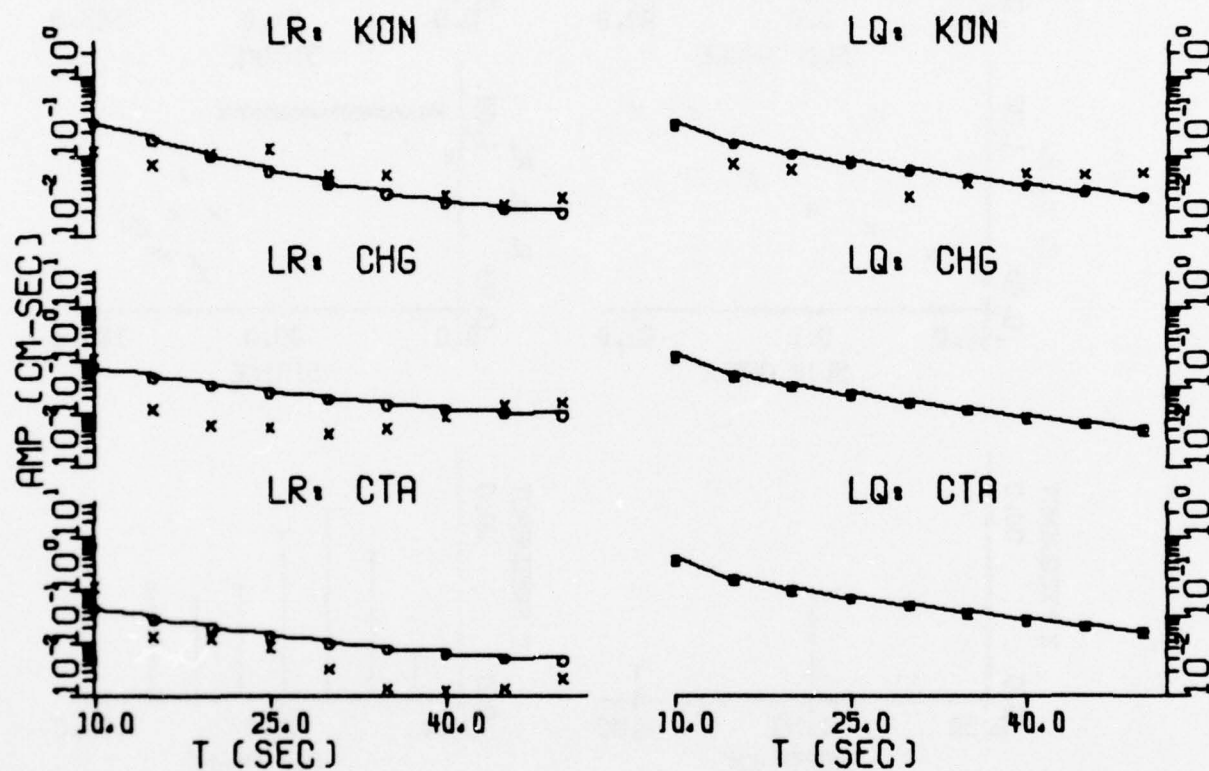


FIGURE V-19
RESULTS FROM AMPLITUDE SPECTRAL FITTING: NT2/317/76
(PAGE 2 OF 3)

(b) Spectral Fits

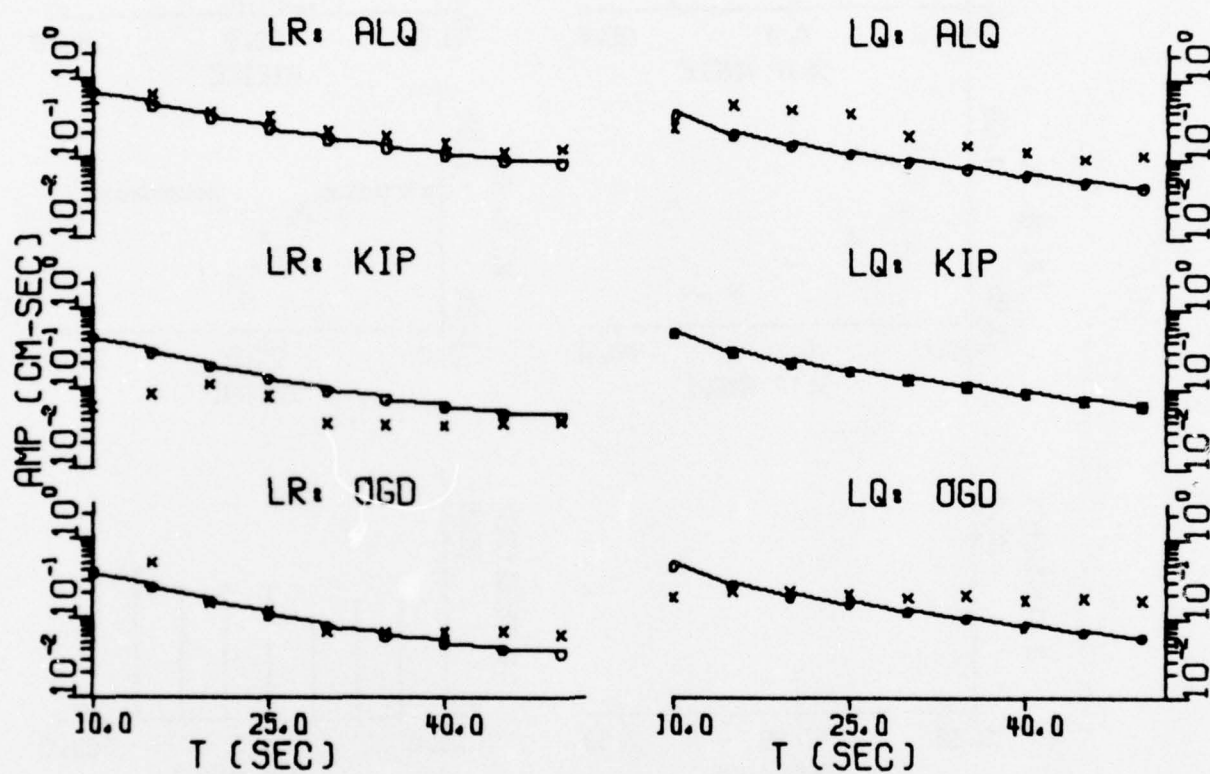


FIGURE V-19
RESULTS FROM AMPLITUDE SPECTRAL FITTING: NT2/317/76
(PAGE 3 OF 3)

(a) Residual Distributions

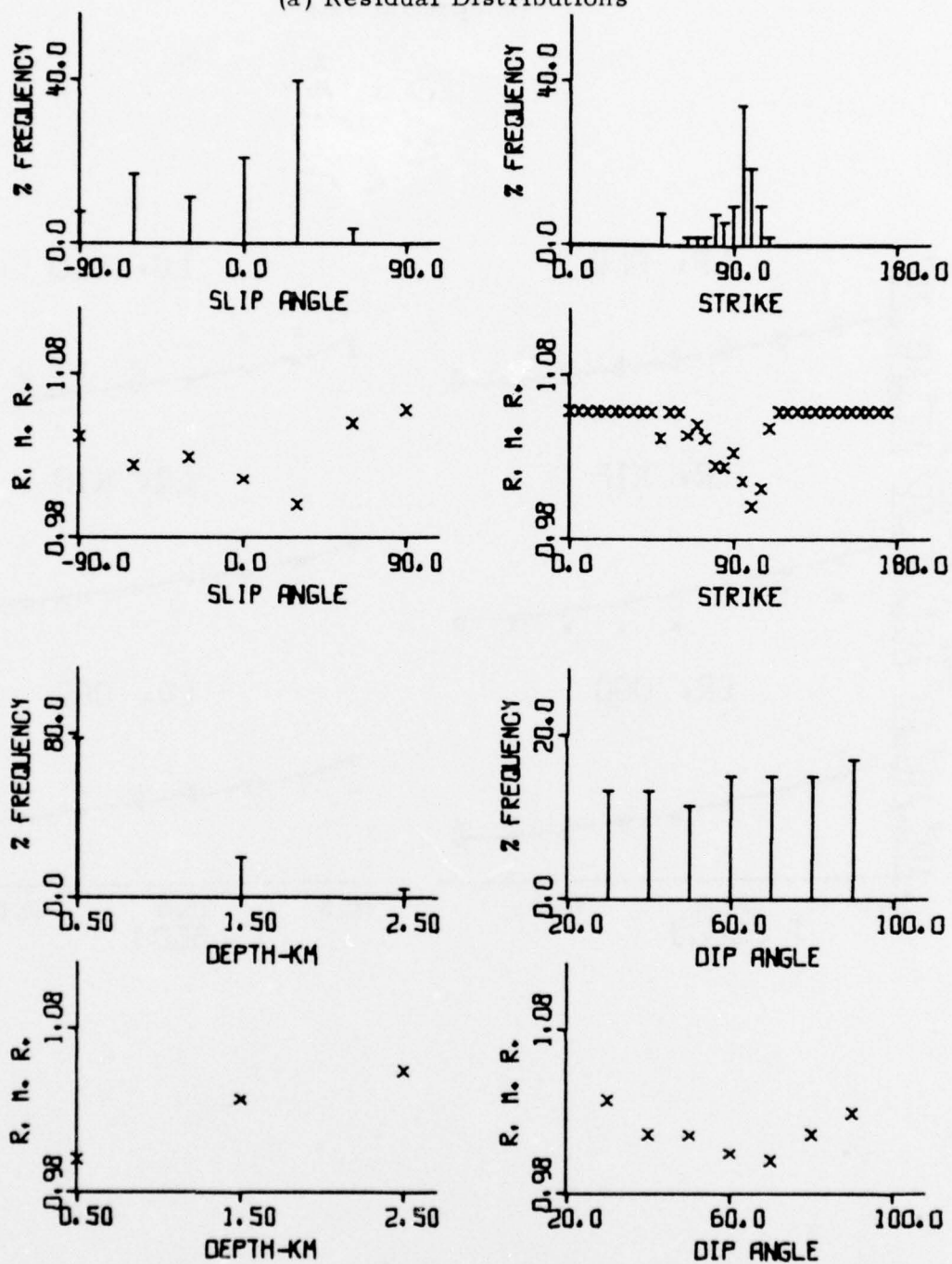


FIGURE V-20

RESULTS FROM AMPLITUDE SPECTRAL FITTING: NT1/204/76
(PAGE 1 OF 2)

(b) Spectral Fits

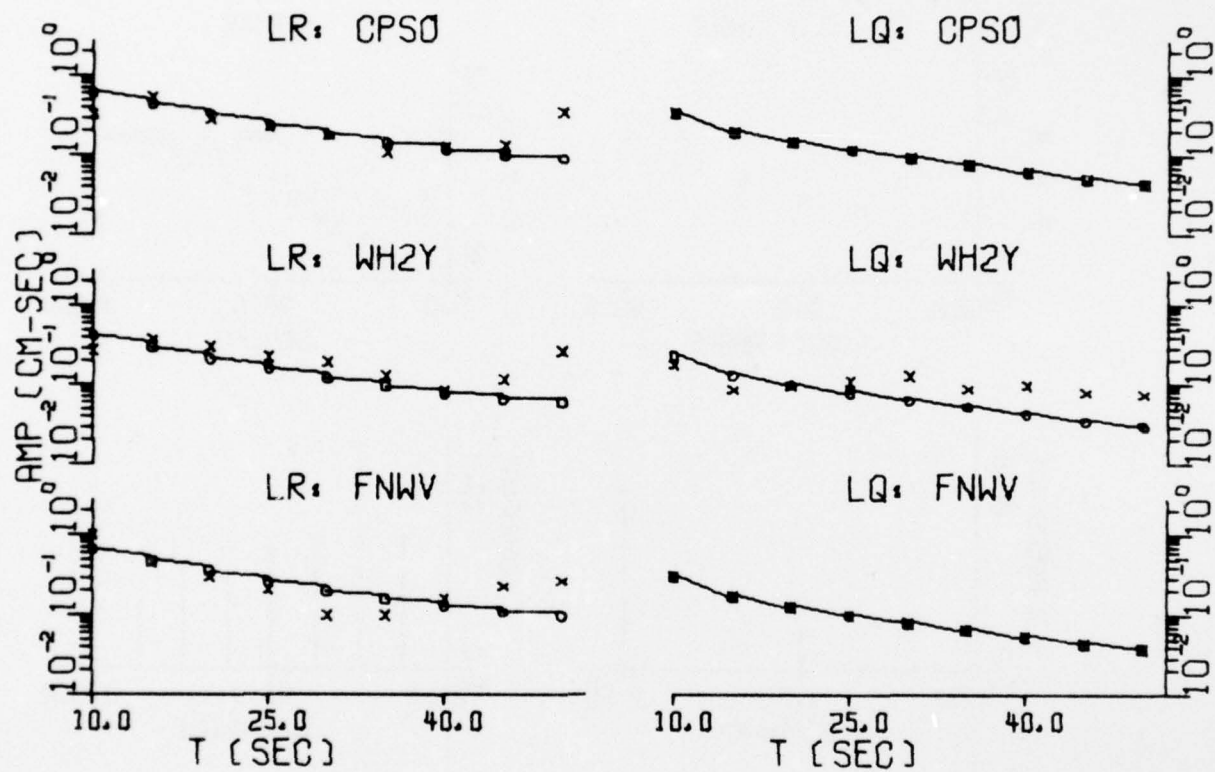


FIGURE V-20
RESULTS FROM AMPLITUDE SPECTRAL FITTING: NT1/204/76
(PAGE 2 OF 2)

(a) Residual Distributions

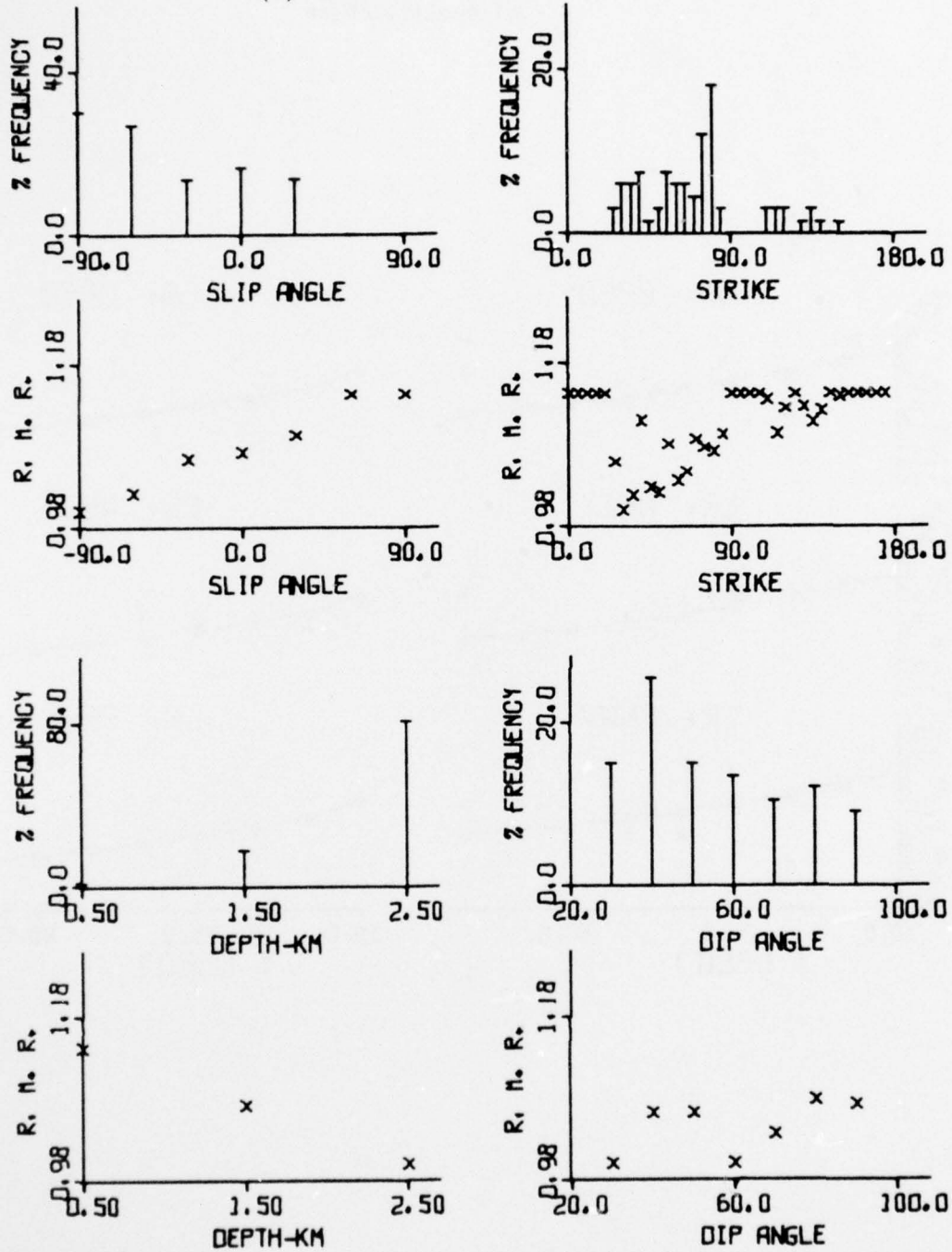


FIGURE V-21

RESULTS FROM AMPLITUDE SPECTRAL FITTING: NT2/204/76
(PAGE 1 OF 2)

(b) Spectral Fits

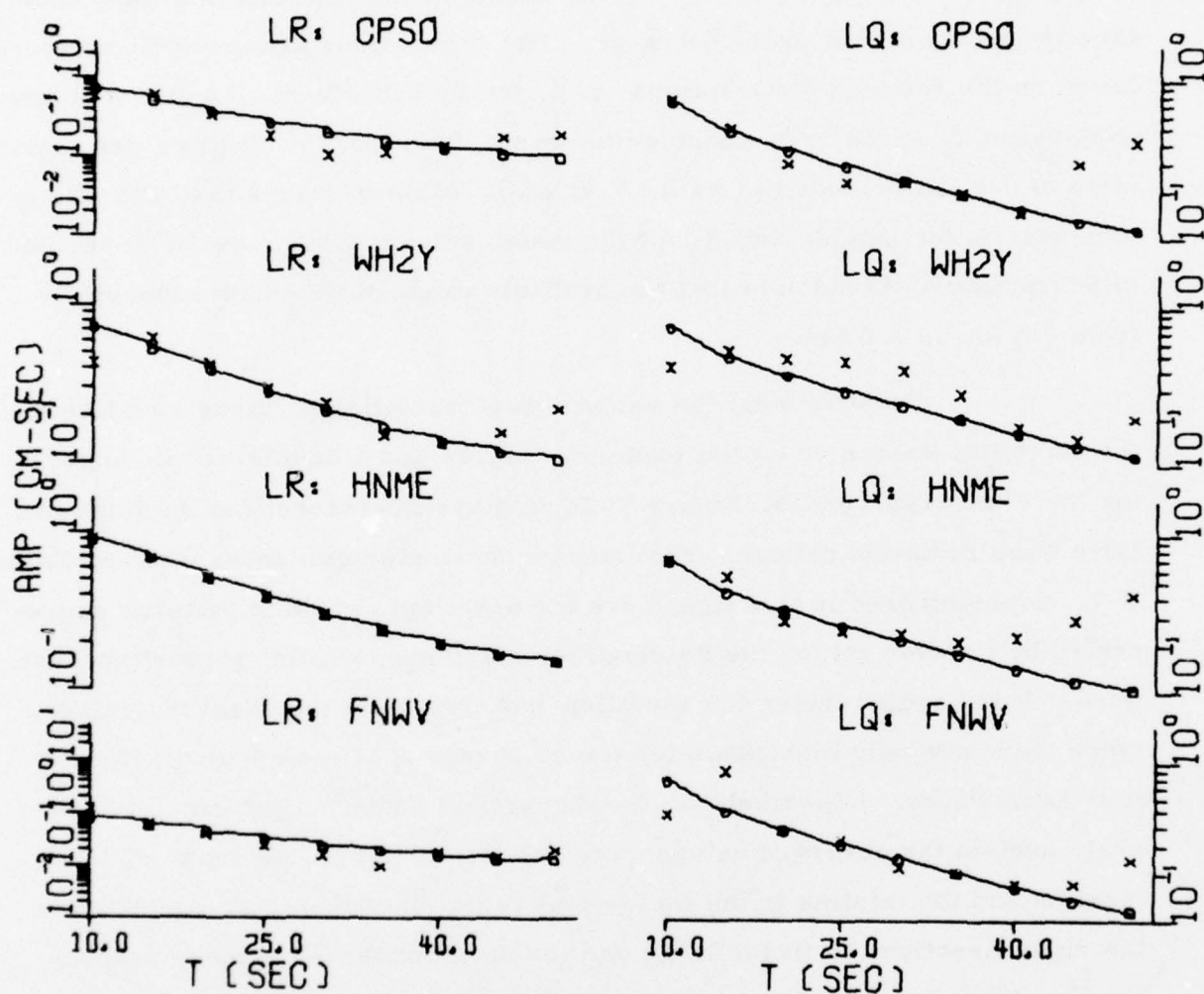


FIGURE V-21
RESULTS FROM AMPLITUDE SPECTRAL FITTING; NT2/204/76
(PAGE 2 OF 2)

the observed spectra and the best fit theoretical spectra is fairly good, especially for the Rayleigh waves. From the residual distributions shown in Figures V-6 to V-21, the estimates of the source parameters of each event can be represented in terms of the probable range of the estimate and the percentage frequency of that probable range. The estimations of source parameters based on the residual distributions are listed in Table V-8. To give a clearer explanation of Table V-8, consider the event NT1/603/75. It has a depth estimate of 0.5 km indicated in Table V-7; while Table V-8 says that 91% of the members in the sample set S_d of the tested source parameter (as described in Subsection V-A) indicate that the probable range of the depth estimate is from 0.5 km to 1.5 km.

To show what the surface wave radiation patterns look like for the combined source of a point explosive source and a double-couple source, for the event NTS/1028/5, Figure V-22 displays the theoretical Rayleigh and Love wave radiation patterns from source parameter estimates given in Table V-7. Superimposed in this figure are the observed radiation patterns represented by crosses (x) for the Rayleigh wave and open circles (o) for the Love wave. It is hard to determine radiation patterns from the observed values, since there are only eight Rayleigh waves observed at each period and only four Love waves. Nevertheless, the theoretical radiation patterns, in general, explain the observed values quite satisfactorily, in the sense that the maxima and the minima in the theoretical radiation patterns are oriented in the right directions to fit the large and the small observed values, respectively. Also shown in this figure are radiation patterns of the Love-to-Rayleigh (LQ/LR) ratios. The theoretical LQ/LR radiation pattern agrees quite well with the four observed values at most of the periods. This indicates that the travel path attenuation correction using Tryggvason's attenuation curve probably is fairly reasonable.

TABLE V-8
ESTIMATIONS OF SOURCE PARAMETERS OBTAINED BY AMPLITUDE
SPECTRAL FITTING BASED ON THE RESIDUAL DISTRIBUTIONS:
SELECTED NTS EVENTS
(PAGE 1 OF 2)

Event I. D.	Source Parameters							
	Depth h km		Dip Angle δ°		Slip Angle λ°		Strike $N\phi^\circ E$	
	Probable Range	% Frequency	Probable Range	% Frequency	Probable Range	% Frequency	Probable Range	% Frequency
NTS/430/75	0.5	66	40 ~ 90	97	0 ~ -90	98	100 ~ 115	78
NTS/514/75	0.5	80	50 ~ 90	80	0 ~ +30	75	0 ~ 15	85
NT1/603/75	0.5 ~ 1.5	91	40 ~ 90	91	-60 ~ +30	87	-10 ~ 25	73
NT2/603/75	0.5 ~ 1.5	100	40 ~ 90	95	-30 ~ +30	84	25 ~ 45	77
NTS/619/75	0.5 ~ 1.5	98	60 ~ 90	80	-30 ~ +30	82	-5 ~ 15	82
NTS/626/75	0.5 ~ 1.5	98	40 ~ 90	93	0 ~ -90	87	125 ~ 185	93
NTS/1028/5	0.5	91	40 ~ 90	90	0 ~ -90	96	-40 ~ 10	97
NTS/926/74	0.5 ~ 1.5	75	60 ~ 90	73	30	31	135 ~ 160	70
					-60	31		
					-90	18		

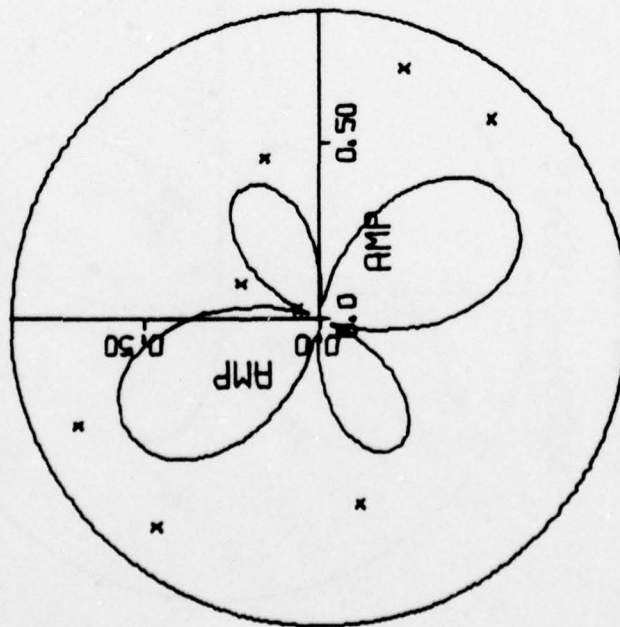
TABLE V-8

ESTIMATIONS OF SOURCE PARAMETERS OBTAINED BY AMPLITUDE
SPECTRAL FITTING BASED ON THE RESIDUAL DISTRIBUTIONS:
SELECTED NTS EVENTS
(PAGE 2 OF 2)

Event I. D.	Source Parameter							
	Depth h km		Dip Angle δ °		Slip Angle λ °		Strike $N\phi^{\circ}E$	
	Probable Range	% Frequency	Probable Range	% Frequency	Probable Range	% Frequency	Probable Range	% Frequency
NTS/103/76	0.5 ~ 1.5	84	70 ~ 90	78	-30 ~ +30	92	170 ~ 175	80
NTS/212/76	0.5	86	70 ~ 90	86	0	72	170 ~ 175	93
NTS/309/76	0.5 ~ 1.5	100	60 ~ 90	82	-30 ~ +30	75	110 ~ 130	80
NTS/314/76	0.5 ~ 1.5	98	60 ~ 90	70	-60 30 ~ 60	15 74	-15 ~ 10	90
NT1/317/76	0.5 ~ 1.5	82	30 ~ 60	95	-60 ~ -90	100	95 ~ 120	87
NT2/317/76	0.5 ~ 1.5	90	40 ~ 90	95	0 ~ -90	95	130 ~ 140 150 ~ 185	14 81
NT1/204/76*	0.5 ~ 1.5	96	50 ~ 90	74	30 ~ -60	89	90 ~ 105	80
NT2/204/76*	1.5 ~ 2.5	99	30 ~ 60	70	0 ~ -90	87	30 ~ 40 55 ~ 80	19 53

* The source parameter estimates of these two events are obtained by using the observation spectra at the SDCS stations.

NTS/1028/5
 DOUBLE COUPLE EXPLOSION
 LR--PERIOD=50.0
 NORTH--0 DEGREE



NTS/1028/5
 DOUBLE COUPLE EXPLOSION
 LQ--PERIOD=50.0
 NORTH--0 DEGREE

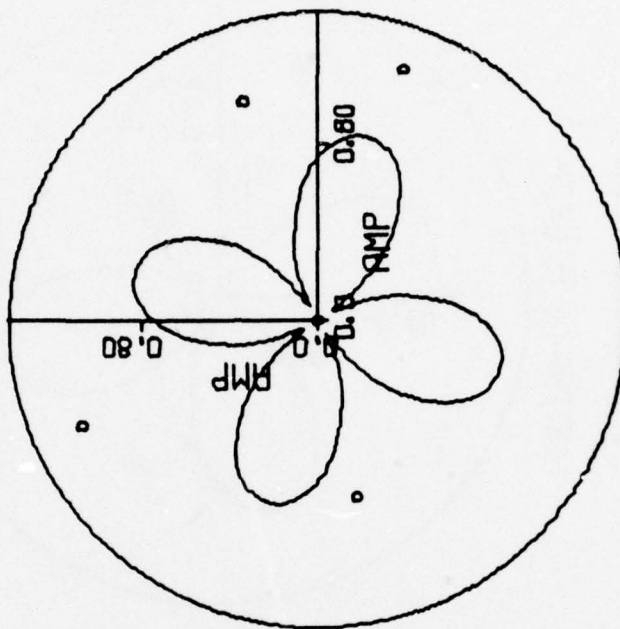
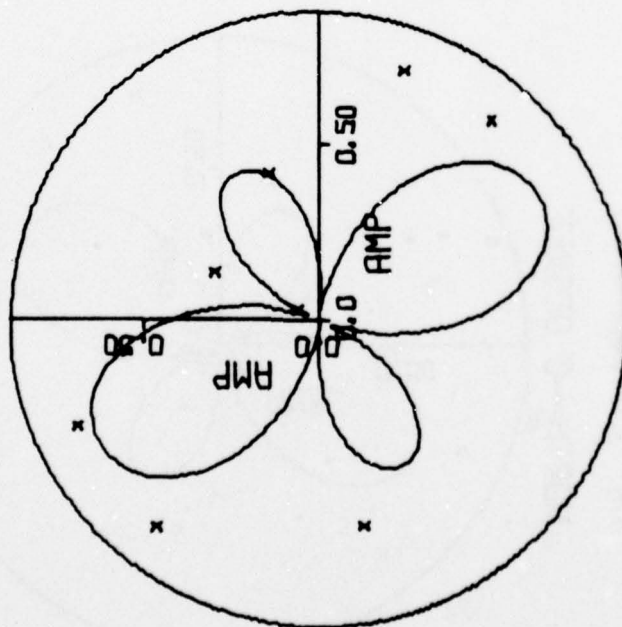


FIGURE V-22
 SURFACE WAVE RADIATION PATTERNS FOR EVENT NTS/1028/5
 (PAGE 1 OF 18)

NTS/1028/5
 DOUBLE COUPLE
 LR--PERIOD=45.0
 NORTH--0 DEGREE



NTS/1028/5
 DOUBLE COUPLE
 LQ--PERIOD=45.0
 NORTH--0 DEGREE

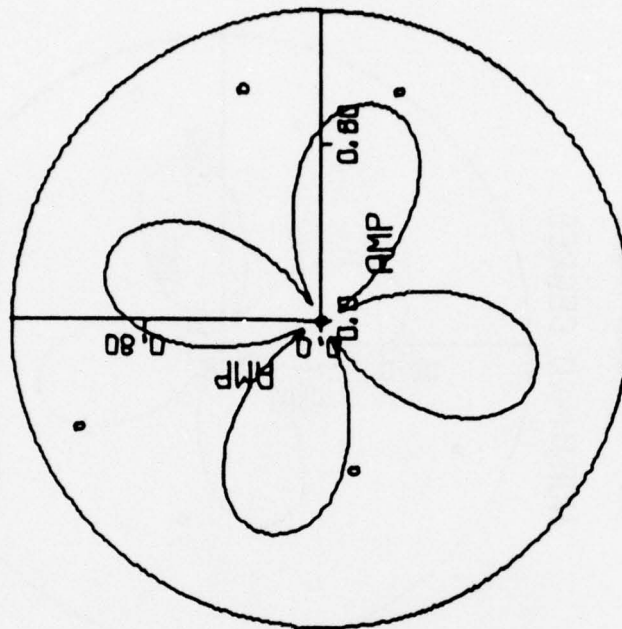
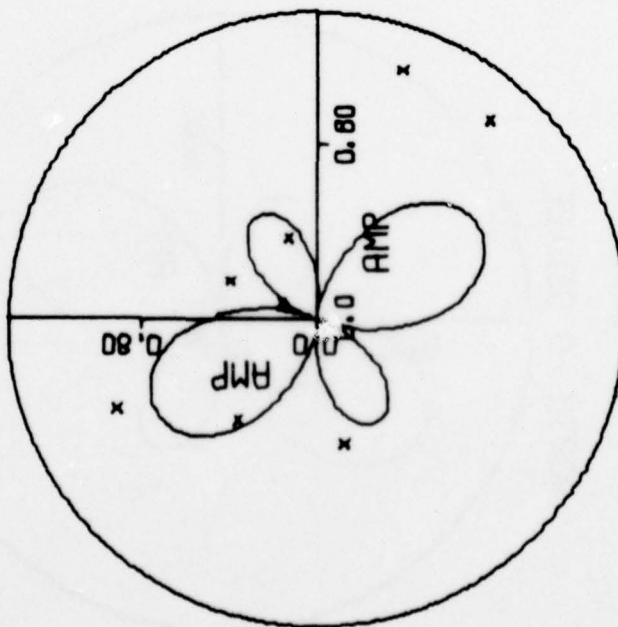


FIGURE V-22
 SURFACE WAVE RADIATION PATTERNS FOR EVENT NTS/1028/5
 (PAGE 2 OF 18)

NTS/1028/5
 DOUBLE COUPLE EXPLOSION
 LR--PERIOD=40.0
 NORTH--0 DEGREE



NTS/1028/5
 DOUBLE COUPLE EXPLOSION
 LQ--PERIOD=40.0
 NORTH--0 DEGREE

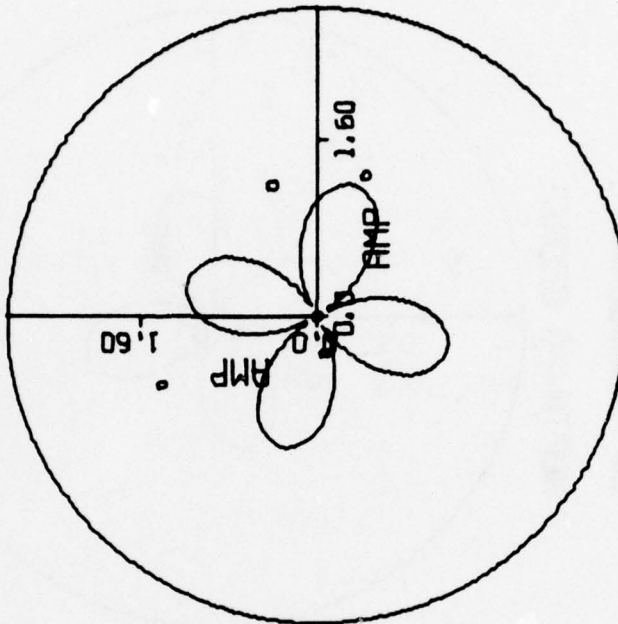
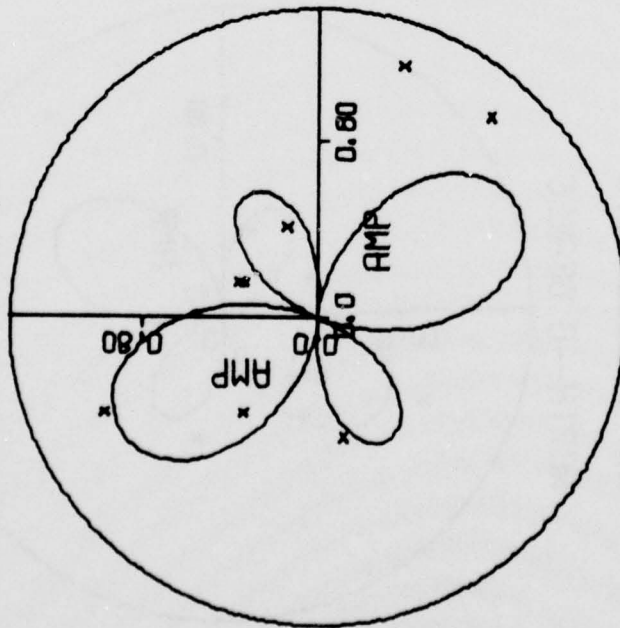


FIGURE V-22
 SURFACE WAVE RADIATION PATTERNS FOR EVENT NTS/1028/5
 (PAGE 3 OF 18)

NTS/1028/5
 DOUBLE COUPLE EXPLOSION
 LR--PERIOD=35.0
 NORTH--0 DEGREE



NTS/1028/5
 DOUBLE COUPLE EXPLOSION
 LQ--PERIOD=35.0
 NORTH--0 DEGREE

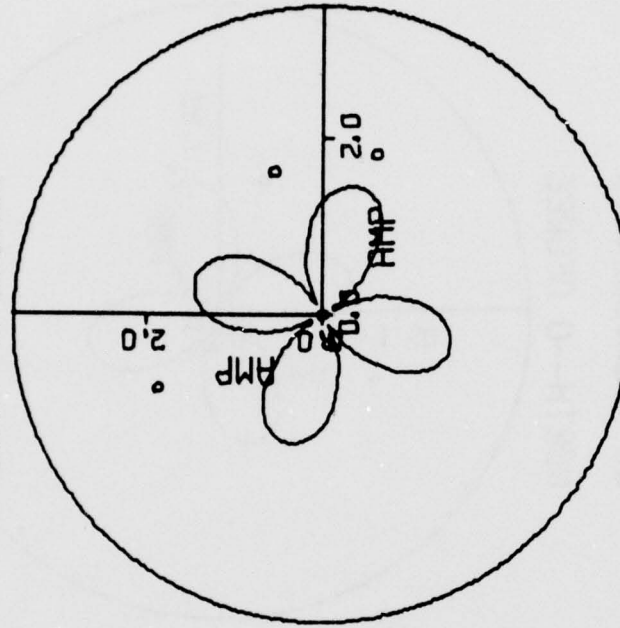
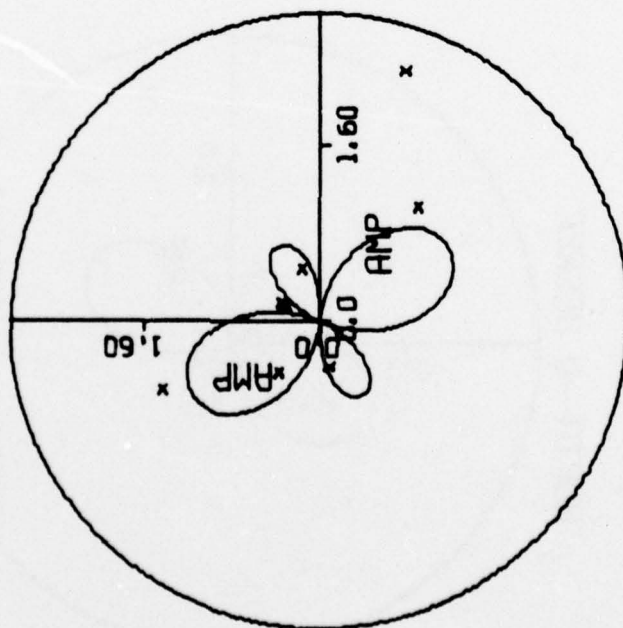


FIGURE V-22
 SURFACE WAVE RADIATION PATTERNS FOR EVENT NTS/1028/5
 (PAGE 4 OF 18)

NTS/1028/5
 DOUBLE COUPLE EXPLOSION
 LR--PERIOD=30.0
 NORTH--0 DEGREE



NTS/1028/5
 DOUBLE COUPLE EXPLOSION
 LQ--PERIOD=30.0
 NORTH--0 DEGREE

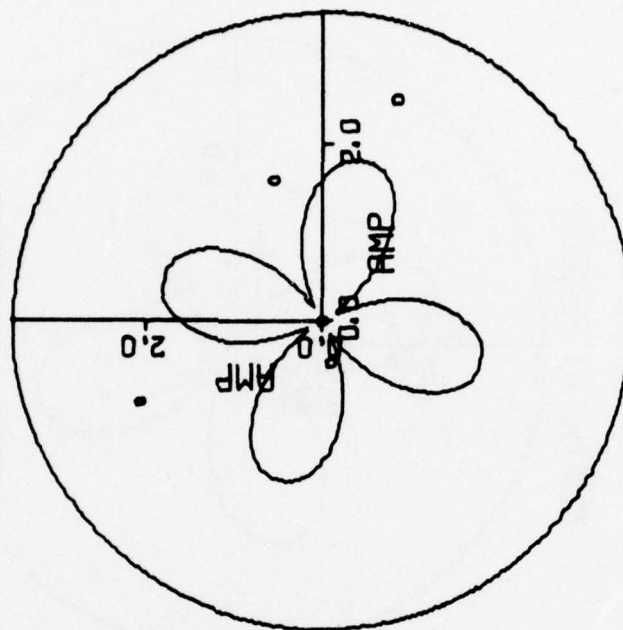
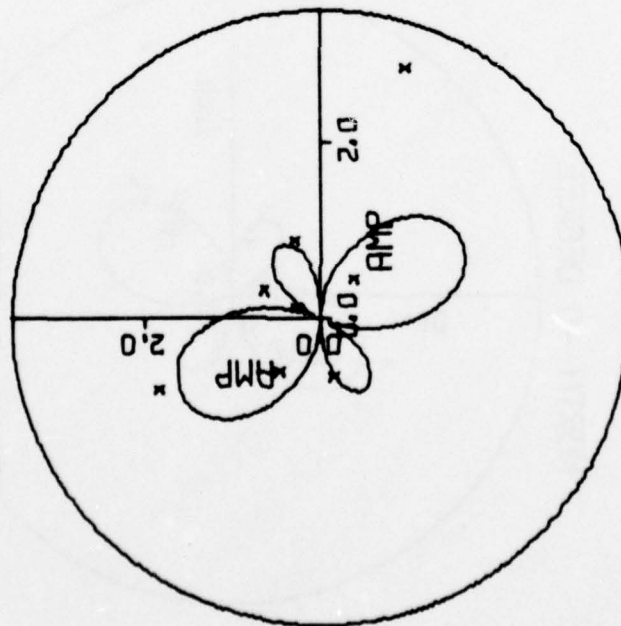


FIGURE V-22
 SURFACE WAVE RADIATION PATTERNS FOR EVENT NTS/1028/5
 (PAGE 5 OF 18)

NTS/1028/5
 DOUBLE COUPLE EXPLOSION
 LR--PERIOD=25.0
 NORTH--0 DEGREE



NTS/1028/5
 DOUBLE COUPLE EXPLOSION
 LQ--PERIOD=25.0
 NORTH--0 DEGREE

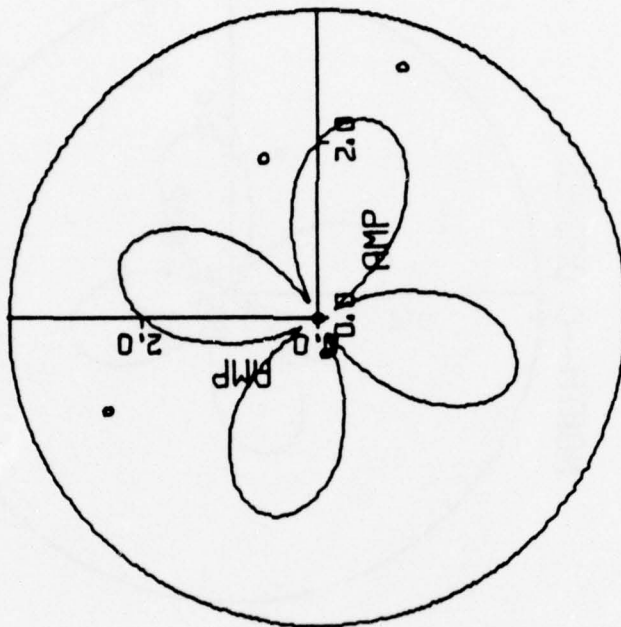
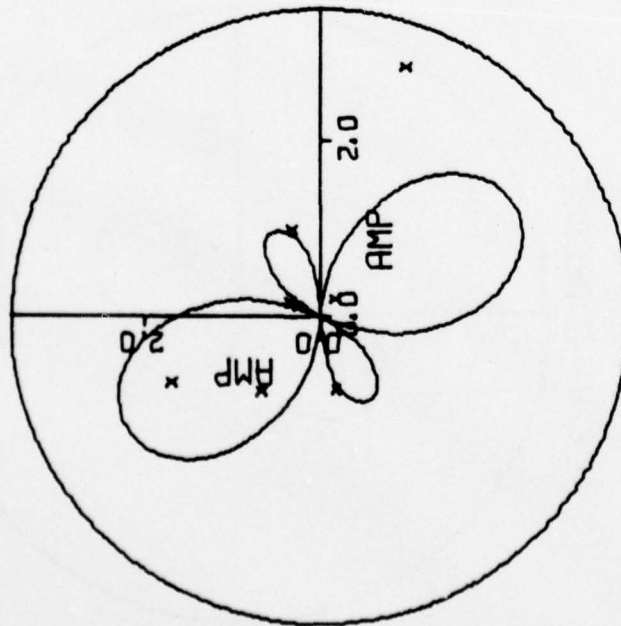


FIGURE V-22

SURFACE WAVE RADIATION PATTERNS FOR EVENT NTS/1028/5
 (PAGE 6 OF 18)

NTS/1028/5
 DOUBLE COUPLE EXPLOSION
 LR--PERIOD=20.0
 NORTH--0 DEGREE



NTS/1028/5
 DOUBLE COUPLE EXPLOSION
 LQ--PERIOD=20.0
 NORTH--0 DEGREE

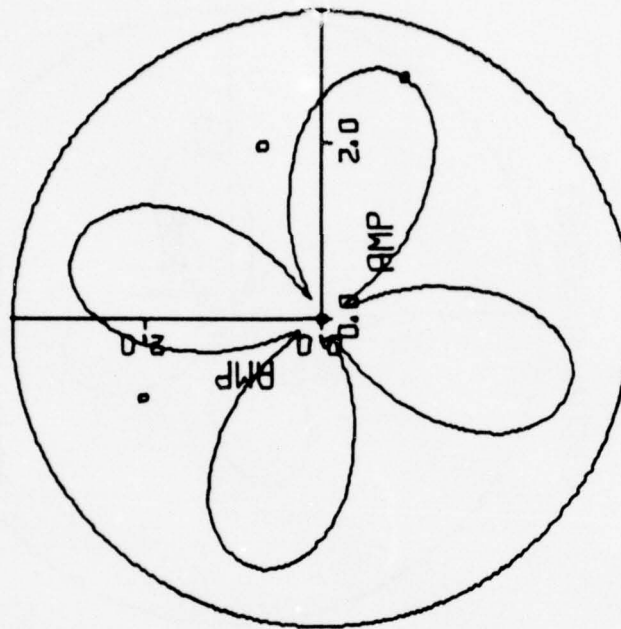
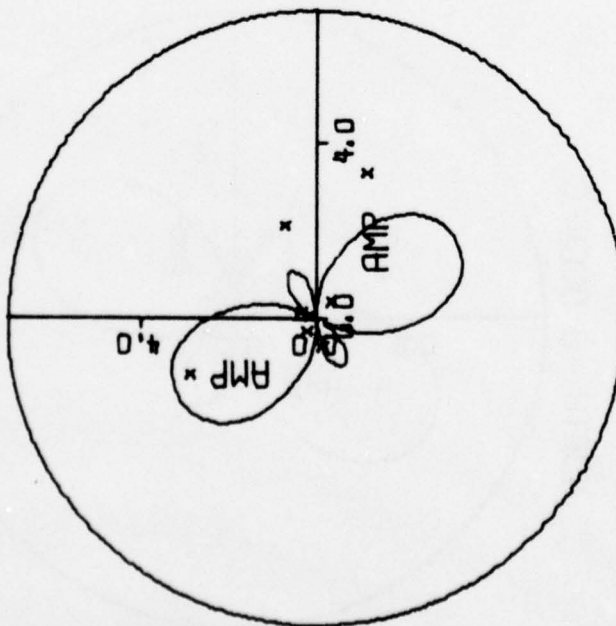


FIGURE V-22
 SURFACE WAVE RADIATION PATTERNS FOR EVENT NTS/1028/5
 (PAGE 7 OF 18)

NTS/1028/5
 DOUBLE COUPLE EXPLOSION
 LR--PERIOD=15.0
 NORTH--0 DEGREE



NTS/1028/5
 DOUBLE COUPLE EXPLOSION
 LQ--PERIOD=15.0
 NORTH--0 DEGREE

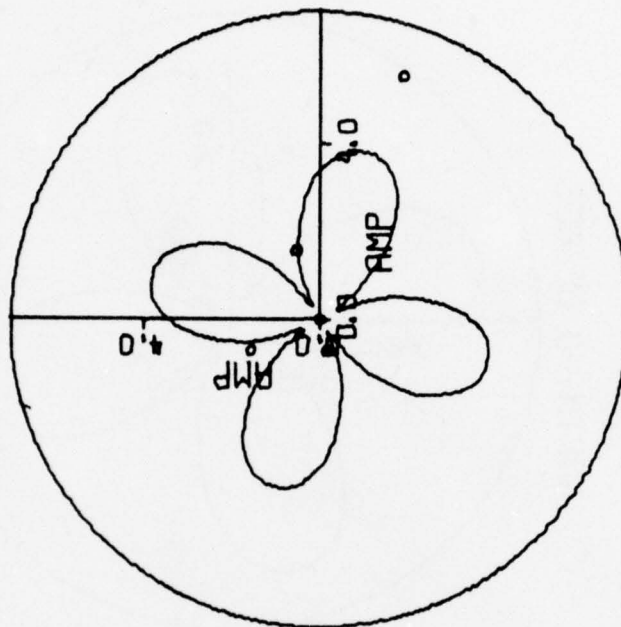
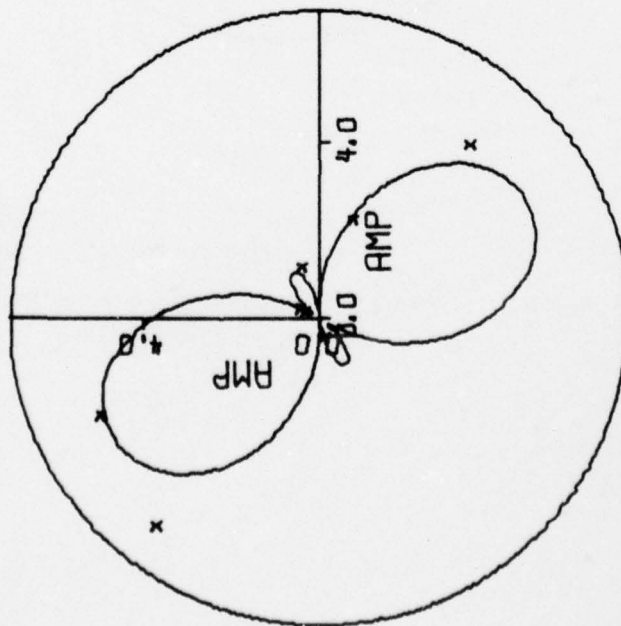


FIGURE V-22

SURFACE WAVE RADIATION PATTERNS FOR EVENT NTS/1028/5
 (PAGE 8 OF 18)

NTS/1028/5
 DOUBLE COUPLE EXPLOSION
 LR--PERIOD=10.0
 NORTH--0 DEGREE



NTS/1028/5
 DOUBLE COUPLE EXPLOSION
 LQ--PERIOD=10.0
 NORTH--0 DEGREE

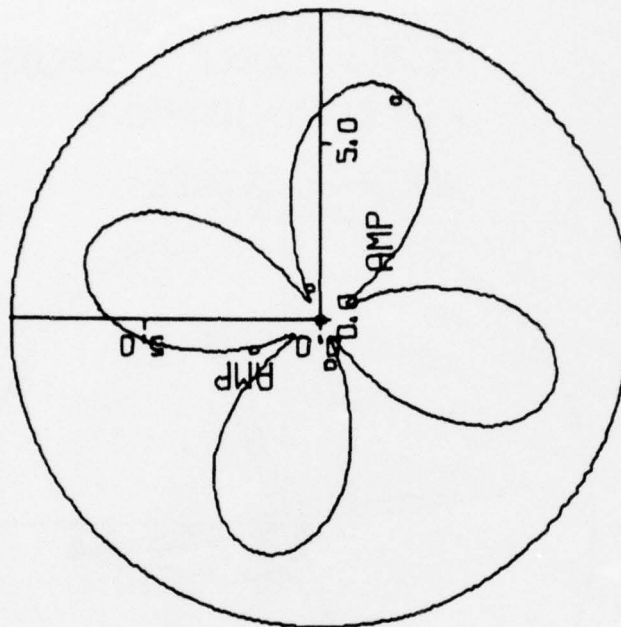


FIGURE V-22
 SURFACE WAVE RADIATION PATTERNS FOR EVENT NTS/1028/5
 (PAGE 9 OF 18)

NTS/1028/5
DOUBLE COUPLE EXPLOSION
LQ/LR--PERIOD=50.0
NORTH--0 DEGREE

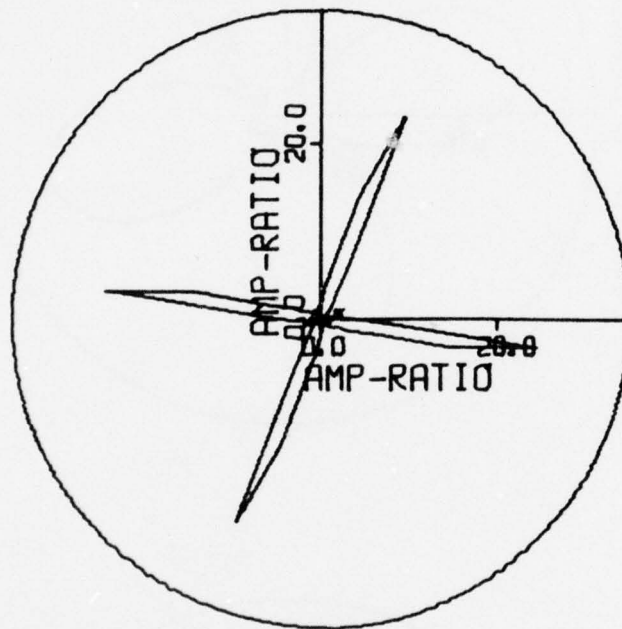


FIGURE V-22
SURFACE WAVE RADIATION PATTERNS FOR EVENT NTS/1028/5
(PAGE 10 OF 18)

NTS/1028/5
DOUBLE COUPLE EXPLOSION
LQ/LR--PERIOD=45.0
NORTH--0 DEGREE

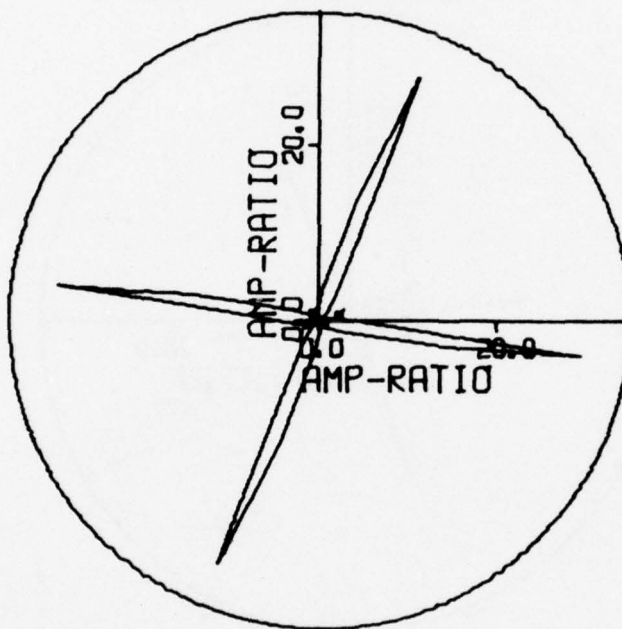


FIGURE V-22
SURFACE WAVE RADIATION PATTERNS FOR EVENT NTS/1028/5
(PAGE 11 OF 18)

NTS/1028/5
DOUBLE COUPLE EXPLOSION
LQ/LR--PERIOD=40.0
NORTH--0 DEGREE

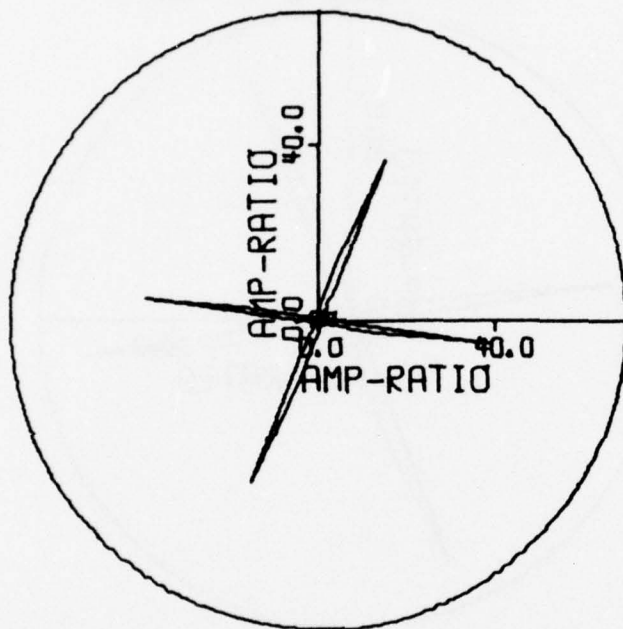


FIGURE V-22
SURFACE WAVE RADIATION PATTERNS FOR EVENT NTS/1028/5
(PAGE 12 OF 18)

NTS/1028/5
DOUBLE COUPLE EXPLOSION

LQ/LR--PERIOD=35.0

NORTH--0 DEGREE

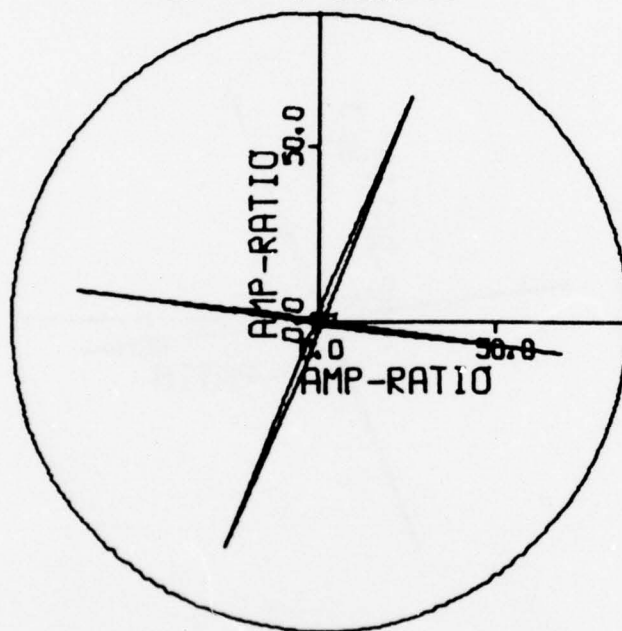


FIGURE V-22

SURFACE WAVE RADIATION PATTERNS FOR EVENT NTS/1028/5
(PAGE 13 OF 18)

NTS/1028/5
DOUBLE COUPLE EXPLOSION

LQ/LR--PERIOD=30.0

NORTH--0 DEGREE

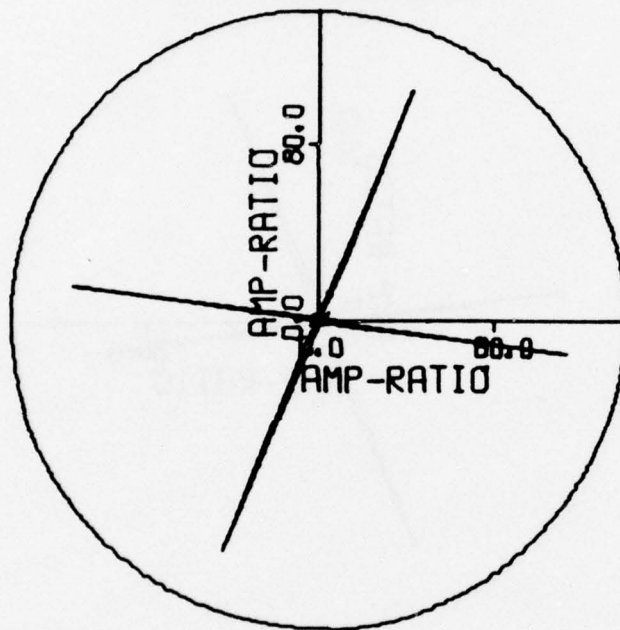


FIGURE V-22

SURFACE WAVE RADIATION PATTERNS FOR EVENT NTS/1028/5
(PAGE 14 OF 18)

NTS/1028/5
DOUBLE COUPLE EXPLOSION
LQ/LR--PERIOD=25.0

NORTH--0 DEGREE

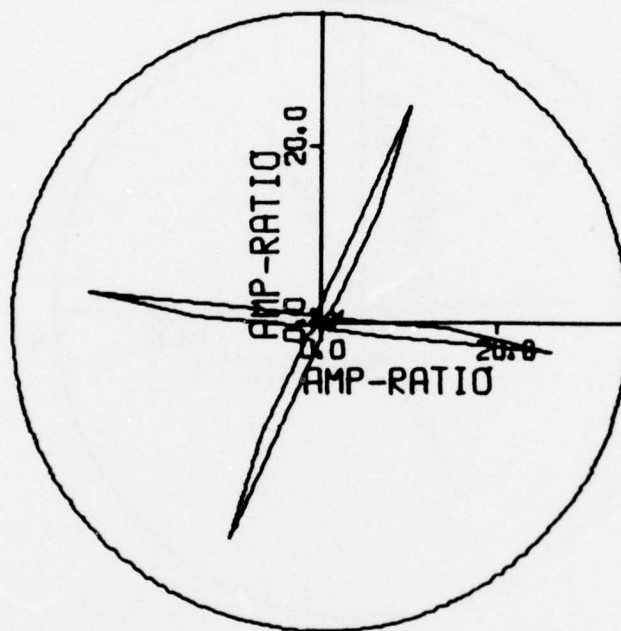


FIGURE V-22
SURFACE WAVE RADIATION PATTERNS FOR EVENT NTS/1028/5
(PAGE 15 OF 18)

NTS/1028/5
DOUBLE COUPLE EXPLOSION
LQ/LR--PERIOD=20.0
NORTH--0 DEGREE

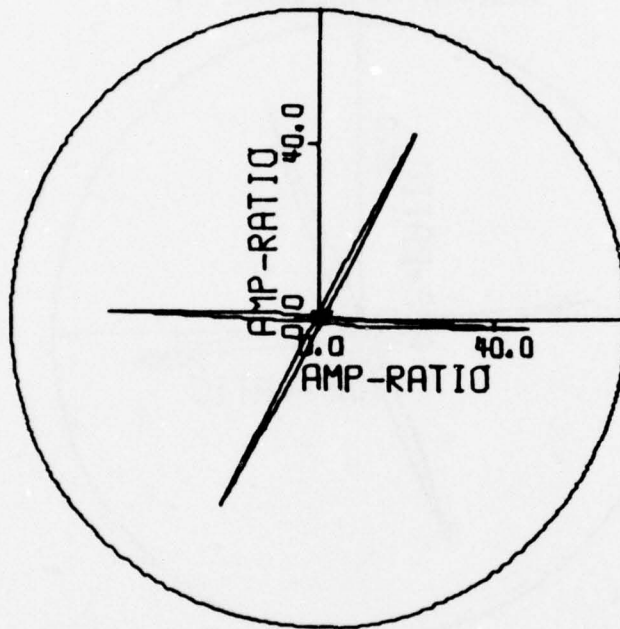


FIGURE V-22
SURFACE WAVE RADIATION PATTERNS FOR EVENT NTS/1028/5
(PAGE 16 OF 18)

NTS/1028/5
DOUBLE COUPLE EXPLOSION
LQ/LR--PERIOD=15.0
NORTH--0 DEGREE

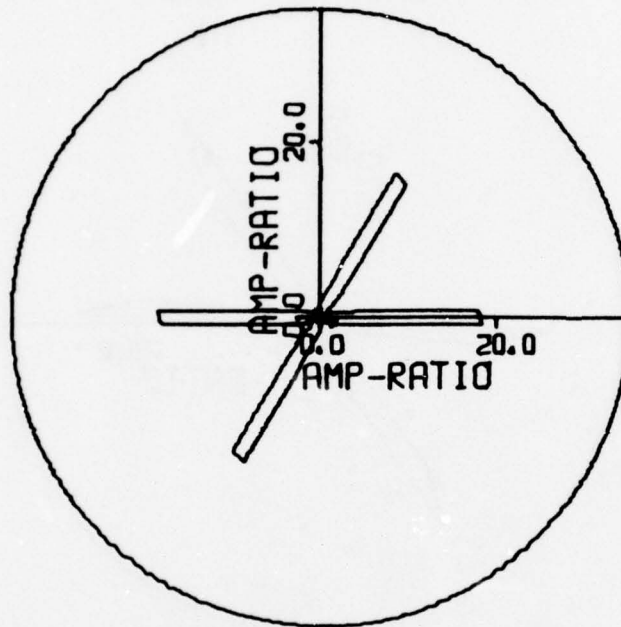


FIGURE V-22
SURFACE WAVE RADIATION PATTERNS FOR EVENT NTS/1028/5
(PAGE 17 OF 18)

NTS/1028/5
DOUBLE COUPLE EXPLOSION
LQ/LR--PERIOD=10.0
NORTH--0 DEGREE

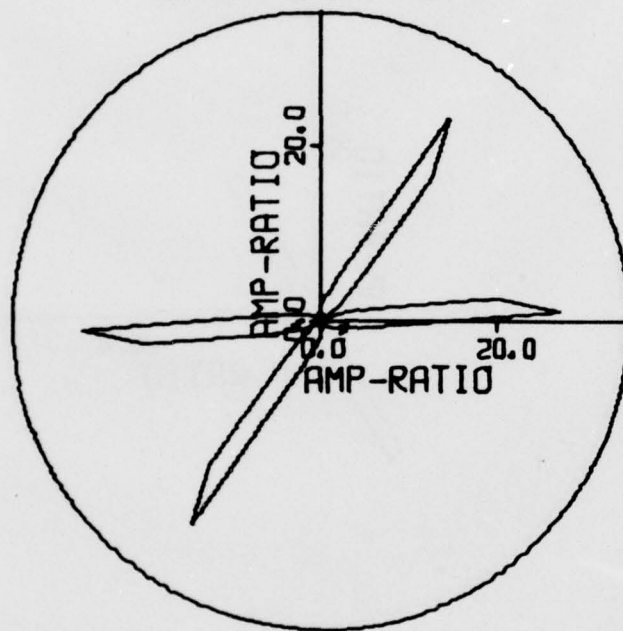


FIGURE V-22
SURFACE WAVE RADIATION PATTERNS FOR EVENT NTS/1028/5
(PAGE 18 OF 18)

2. The EKZ Events

For the selected EKZ events, estimations of source parameters based on the minimum-residual criterion are listed in Table V-9. Those based on the residual distributions are listed in Table V-10. The residual distributions with respect to the estimated depth, dip angle, slip angle, and strike angle are shown in Figures V-23 to V-30, together with the spectral fit for each event. Except for the events EKZ/1214/3 and EKZ/1029/5, the source parameter estimates of the selected EKZ events suggest that the depths of these events are all very shallow, 0.5 km. The double-couple sources which model tectonic strain releases associated with these events have a purely dip-slip type of mechanism, and the strike directions vary among these events. The F values vary from 1.0 to 1.5 among these events. Judging from the estimated F values of these EKZ events, the double-couple source is partially responsible for the observed surface waves of these events, although the exact mechanisms (earthquake triggering, directional cracking, or cavity distortion) which release the tectonic strain energy associated with these events are not known.

The theoretical surface wave radiation patterns, together with the observed values (indicated by the crosses (x)), generated by using the source parameter estimates listed in Table V-9, are shown in Figure V-31 for the event EKZ/704/76. This event has the largest number of observed values among these selected EKZ events. Again, as for the event NTS/1028/5, it is hard to form the observed radiation patterns from only 10 observed values of the Rayleigh wave and 4 observed values of the Love wave at each period. Nevertheless, the theoretical radiation patterns fit most of the observations. The theoretical LQ/LR radiation patterns explain the observed values very well. Again, this indicates that Tryggvason's attenuation curve is fairly representative for the average surface wave attenuation along the travel paths from EKZ to the available stations.

TABLE V-9

ESTIMATIONS OF SOURCE PARAMETERS OBTAINED BY AMPLITUDE
SPECTRAL FITTING BASED ON THE MINIMUM-RESIDUAL
CRITERION: SELECTED EKZ EVENTS

Event I. D.	Optimal Solution						
	Depth h km	Dip Angle δ°	Slip Angle λ°	Strike N ϕ° E	Moment M_E 10 ²⁵ dyne-cm	M_X	F
EKZ/723/73	0.5	60	-90	120	0.220 x 10 ⁻¹	0.220 x 10 ⁻¹	1.00
EKZ/1026/3	0.5	40	-90	175	0.214 x 10 ⁻²	0.321 x 10 ⁻²	1.50
EKZ/1214/3	2.5	80	60	110	0.731 x 10 ⁻²	0.731 x 10 ⁻²	1.00
EKZ/220/75	0.5	40	-90	15	0.527 x 10 ⁻²	0.791 x 10 ⁻²	1.50
EKZ/311/75	0.5	30	-90	60	0.189 x 10 ⁻²	0.284 x 10 ⁻²	1.50
EKZ/427/75	0.5	40	-90	50	0.198 x 10 ⁻¹	0.248 x 10 ⁻¹	1.25
EKZ/1029/5	1.5	90	0	85	0.113 x 10 ⁻¹	0.113 x 10 ⁻¹	1.00
EKZ/704/76	0.5	60	-90	25	0.557 x 10 ⁻²	0.835 x 10 ⁻²	1.50

TABLE V-10

ESTIMATIONS OF SOURCE PARAMETERS OBTAINED BY AMPLITUDE
SPECTRAL FITTING BASED ON THE RESIDUAL DISTRIBUTIONS:
SELECTED EKZ EVENTS

Event I. D.	Source Parameters							
	Depth h km		Dip Angle δ°		Slip Angle λ°		Strike $N\phi^\circ E$	
	Probable Range	% Frequency	Probable Range	% Frequency	Probable Range	% Frequency	Probable Range	% Frequency
EKZ/723/73	0.5 ~ 1.5	100	40 ~ 80	80	-90 ~ 0	85	140 ~ 170	68
EKZ/1026/3	0.5 ~ 1.5	98	30 ~ 70	80	-90 ~ 0	89	-5 ~ 55	91
EKZ/1214/3	1.5 ~ 2.5	77	-	-	-60 ~ +60	92	-	-
EKZ/220/75	0.5	84	30 ~ 70	79	-90 ~ 0	82	-	-
EKZ/311/75	0.5	82	30 ~ 70	88	-90 ~ 0	92	-	-
EKZ/427/75	0.5 ~ 1.5	98	30 ~ 70	83	-90 ~ 0	93	50 ~ 100	90
EKZ/1029/5	1.5 ~ 2.5	79	50 ~ 90	95	-30 ~ +30	96	75 ~ 95	95
EKZ/704/76	0.5 ~ 1.5	97	30 ~ 70	88	-90 ~ -60	81	20 ~ 60	88

(a) Residual Distributions

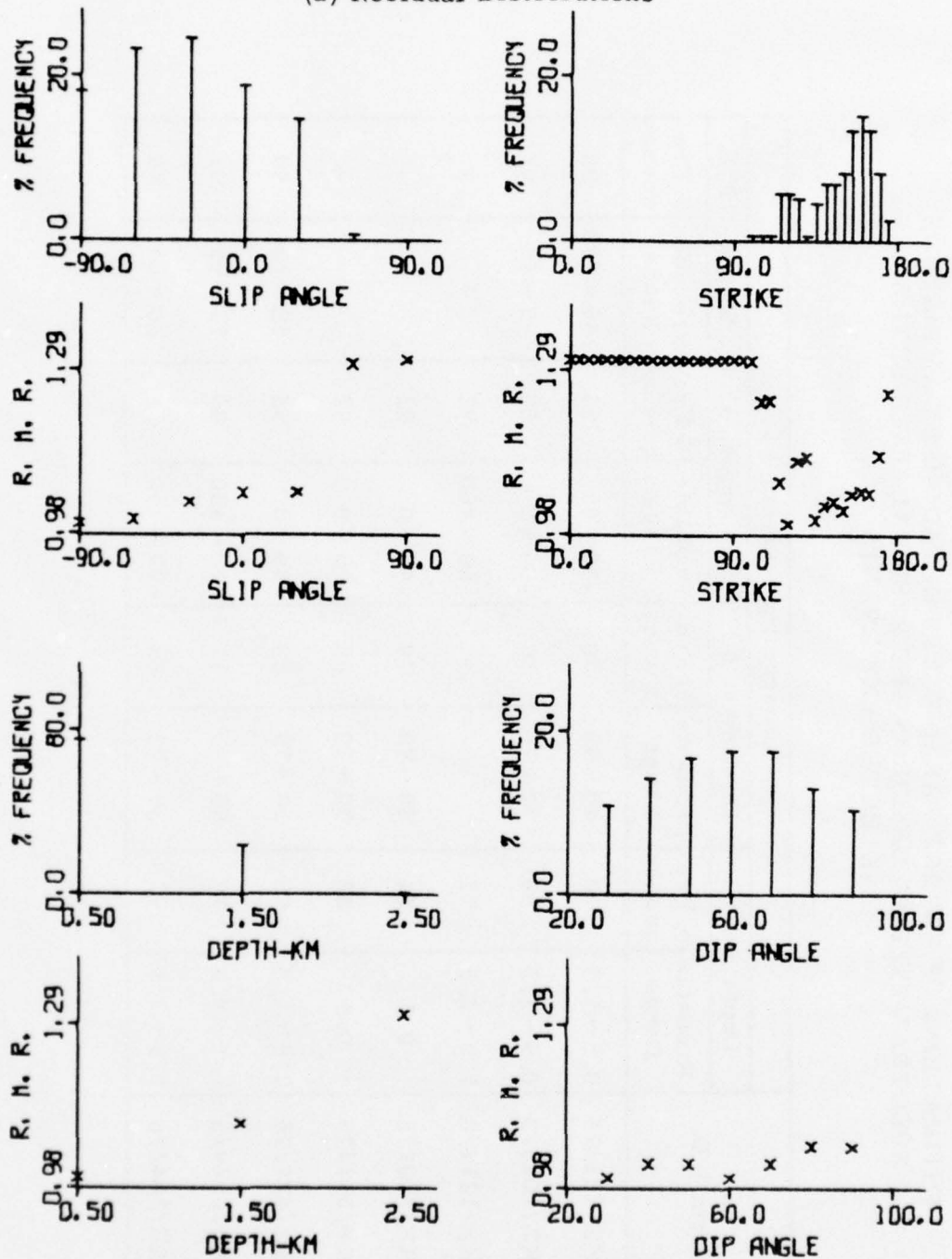


FIGURE V-23

RESULTS FROM AMPLITUDE SPECTRAL FITTING: EKZ/723/73
(PAGE 1 OF 2)

(b) Spectral Fits

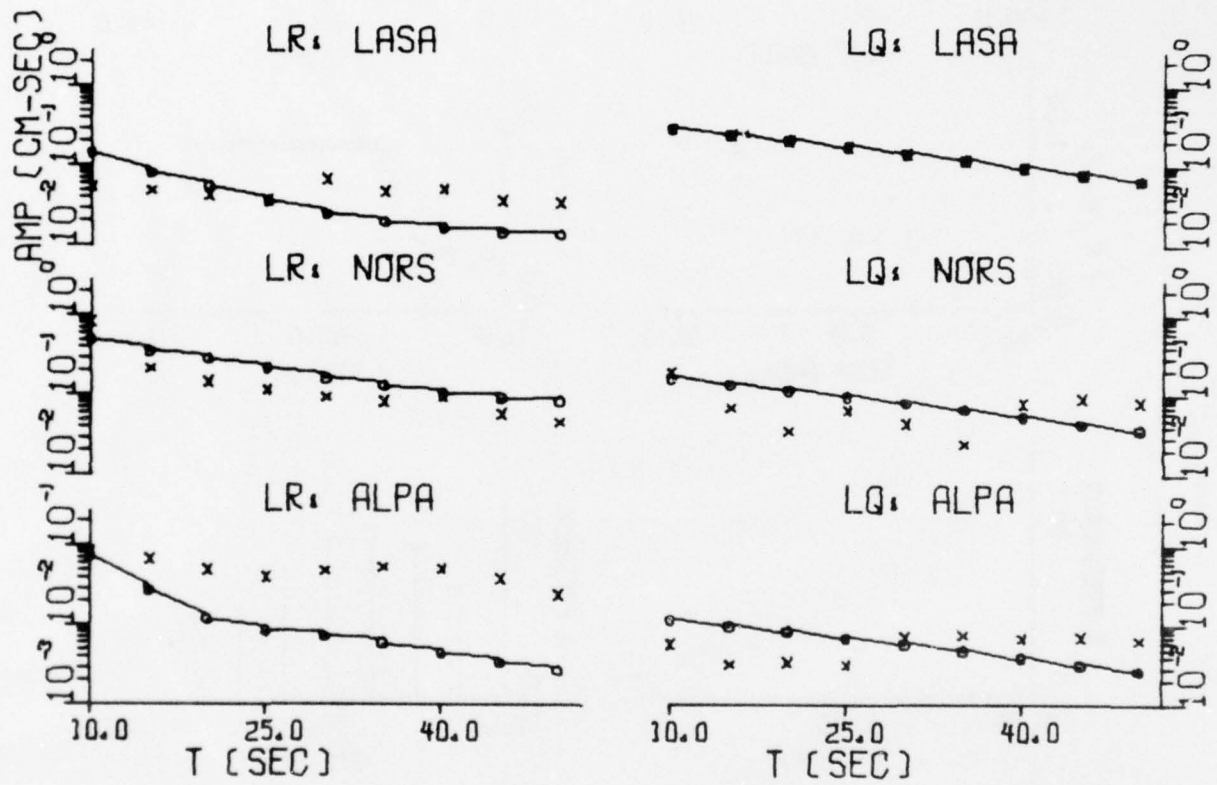


FIGURE V-23
RESULTS FROM AMPLITUDE SPECTRAL FITTING: EKZ/723/73
(PAGE 2 OF 2)

(a) Residual Distributions

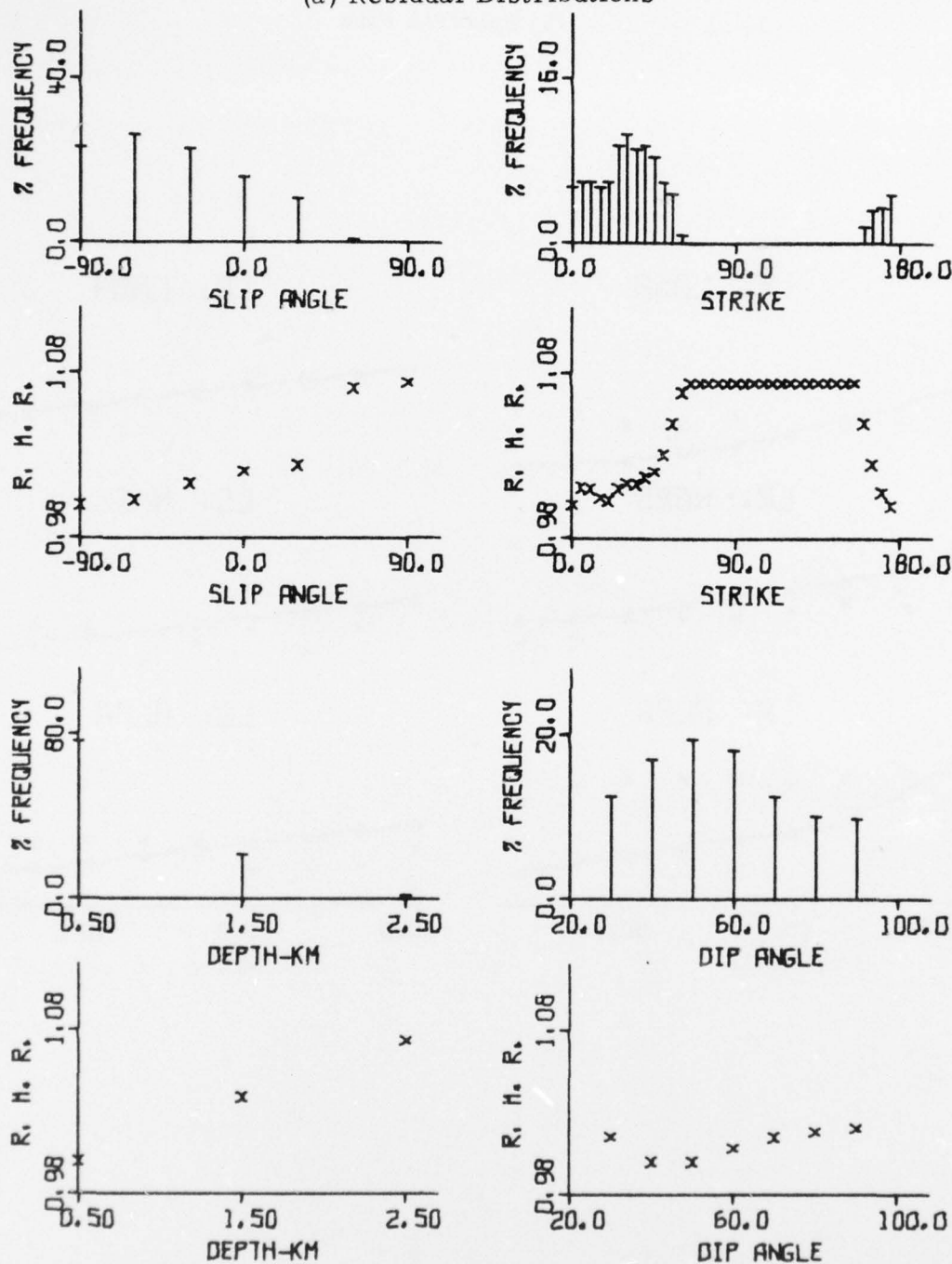


FIGURE V-24

RESULTS FROM AMPLITUDE SPECTRAL FITTING: EKZ/1026/3
(PAGE 1 OF 2)

(b) Spectral Fits

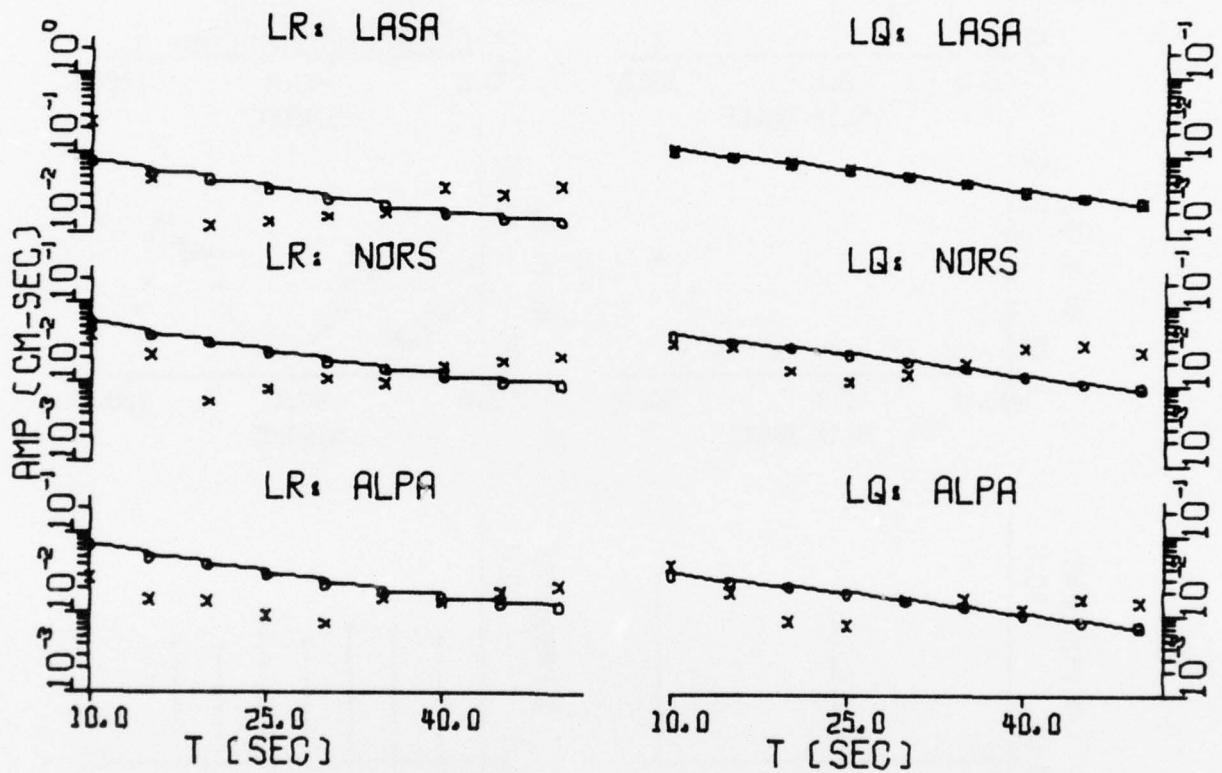


FIGURE V-24
RESULTS FROM AMPLITUDE SPECTRAL FITTING: EKZ/1026/3
(PAGE 2 OF 2)

(a) Residual Distributions

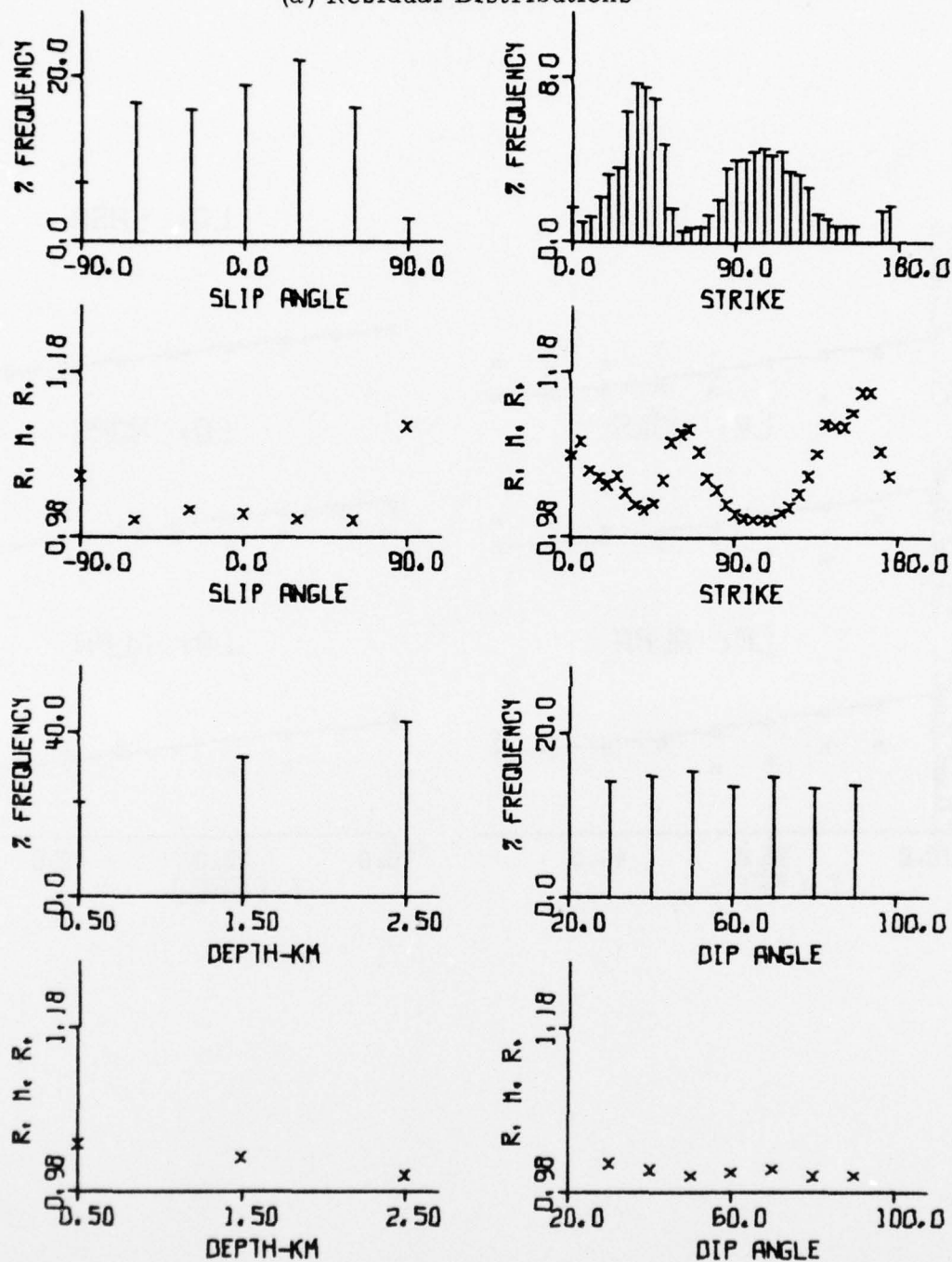


FIGURE V-25

RESULTS FROM AMPLITUDE SPECTRAL FITTING: EKZ/1214/3
(PAGE 1 OF 2)

(b) Spectral Fits

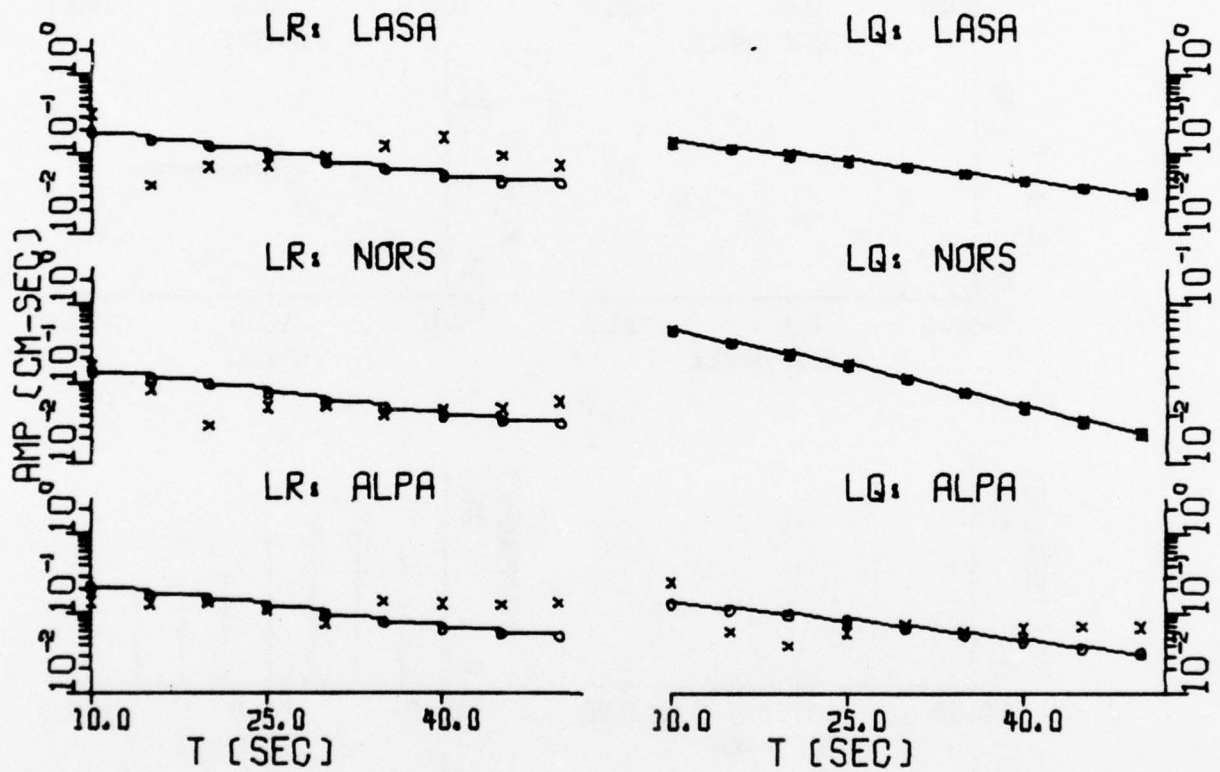


FIGURE V-25
RESULTS FROM AMPLITUDE SPECTRAL FITTING: EKZ/1214/3
(PAGE 2 OF 2)

(a) Residual Distributions

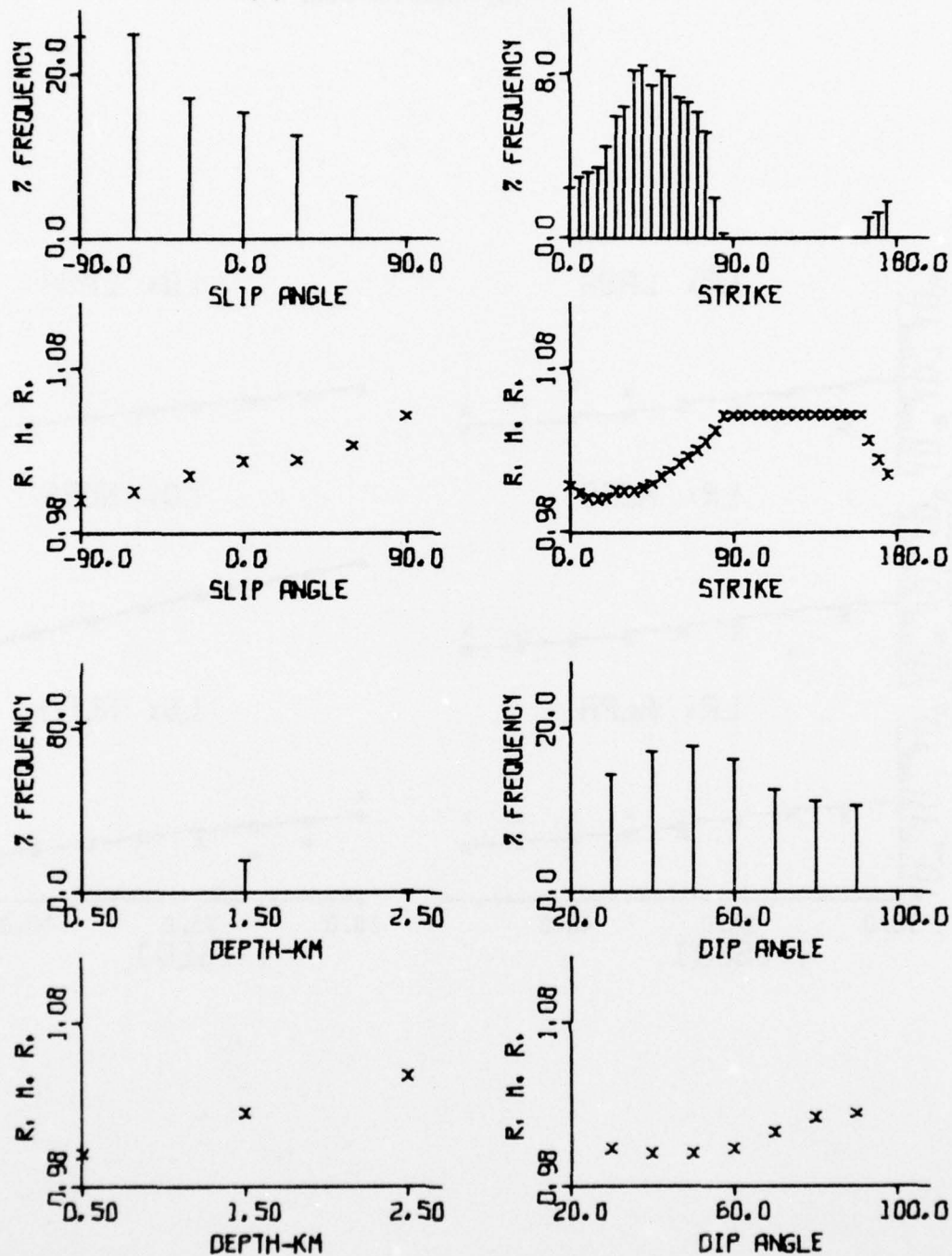


FIGURE V-26

RESULTS FROM AMPLITUDE SPECTRAL FITTING: EKZ/220/75
(PAGE 1 OF 2)

(b) Spectral Fits

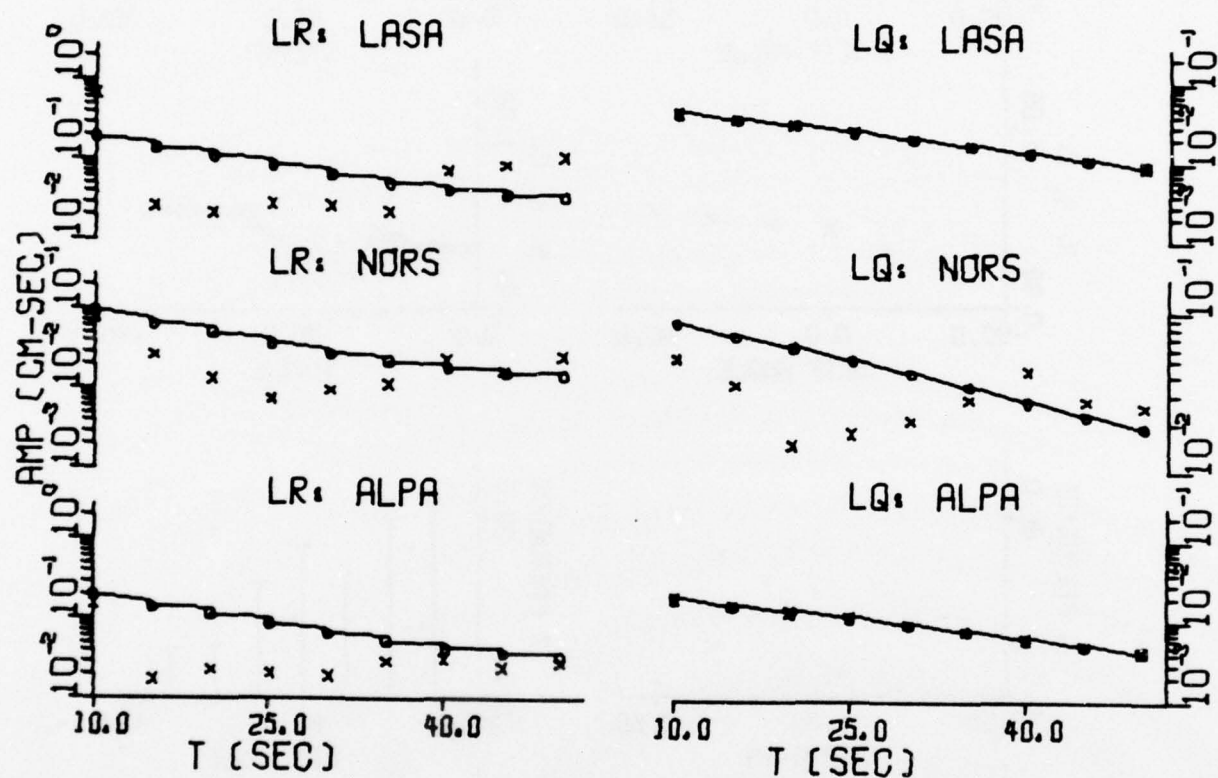


FIGURE V-26
RESULTS FROM AMPLITUDE SPECTRAL FITTING: EKZ/220/75
(PAGE 2 OF 2)

(a) Residual Distributions

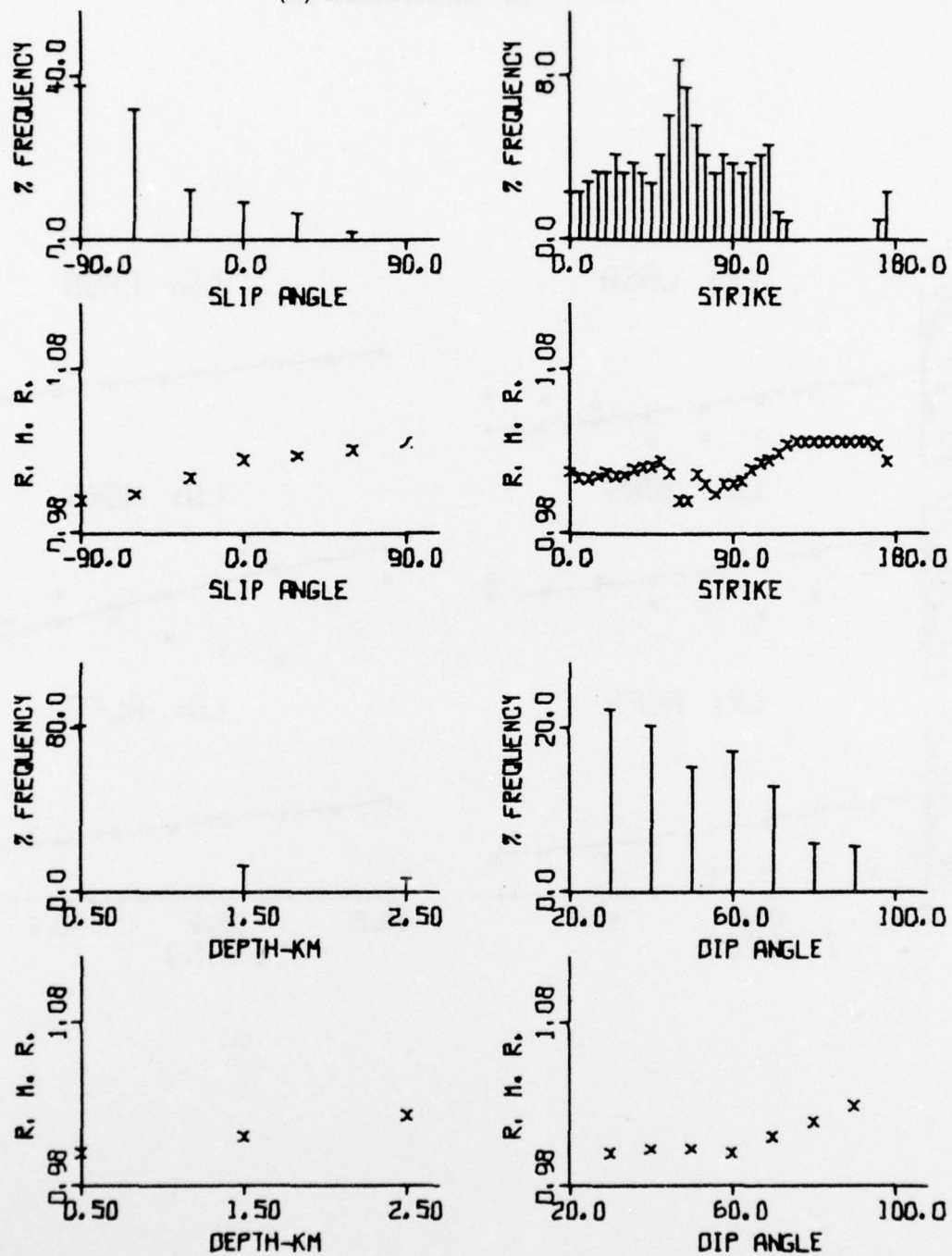


FIGURE V-27

RESULTS FROM AMPLITUDE SPECTRAL FITTING: EKZ/311/75
(PAGE 1 OF 2)

(b) Spectral Fits

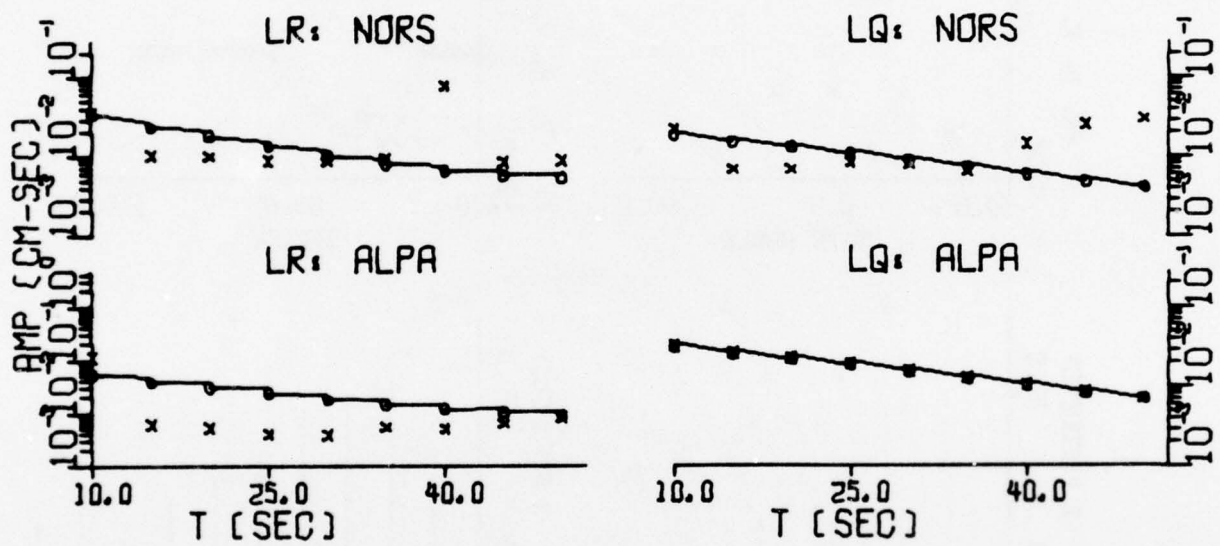


FIGURE V-27

RESULTS FROM AMPLITUDE SPECTRAL FITTING: EKZ/311/75
(PAGE 2 OF 2)

(a) Residual Distributions

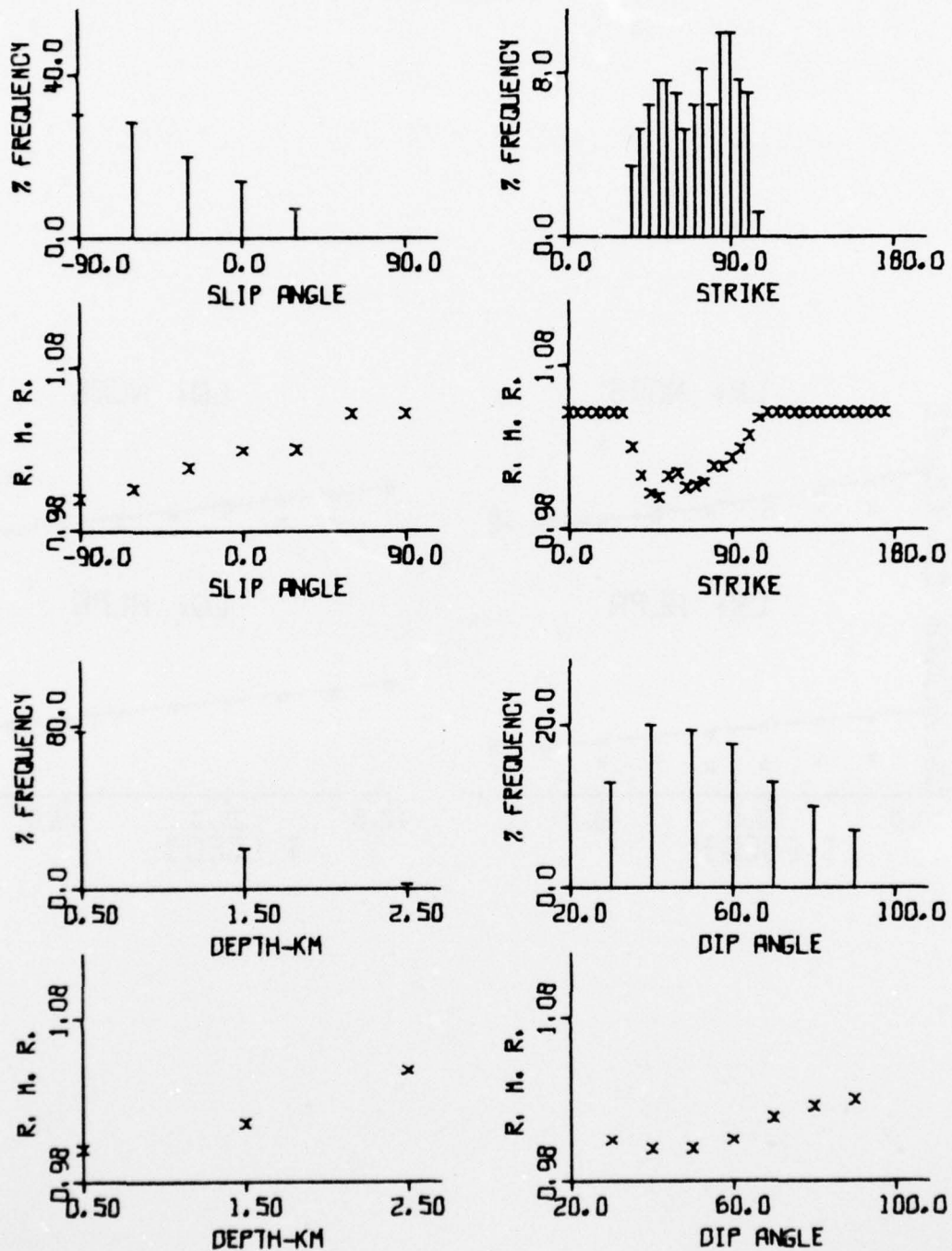


FIGURE V-28

RESULTS FROM AMPLITUDE SPECTRAL FITTING: EKZ/427/75
(PAGE 1 OF 3)

(b) Spectral Fits

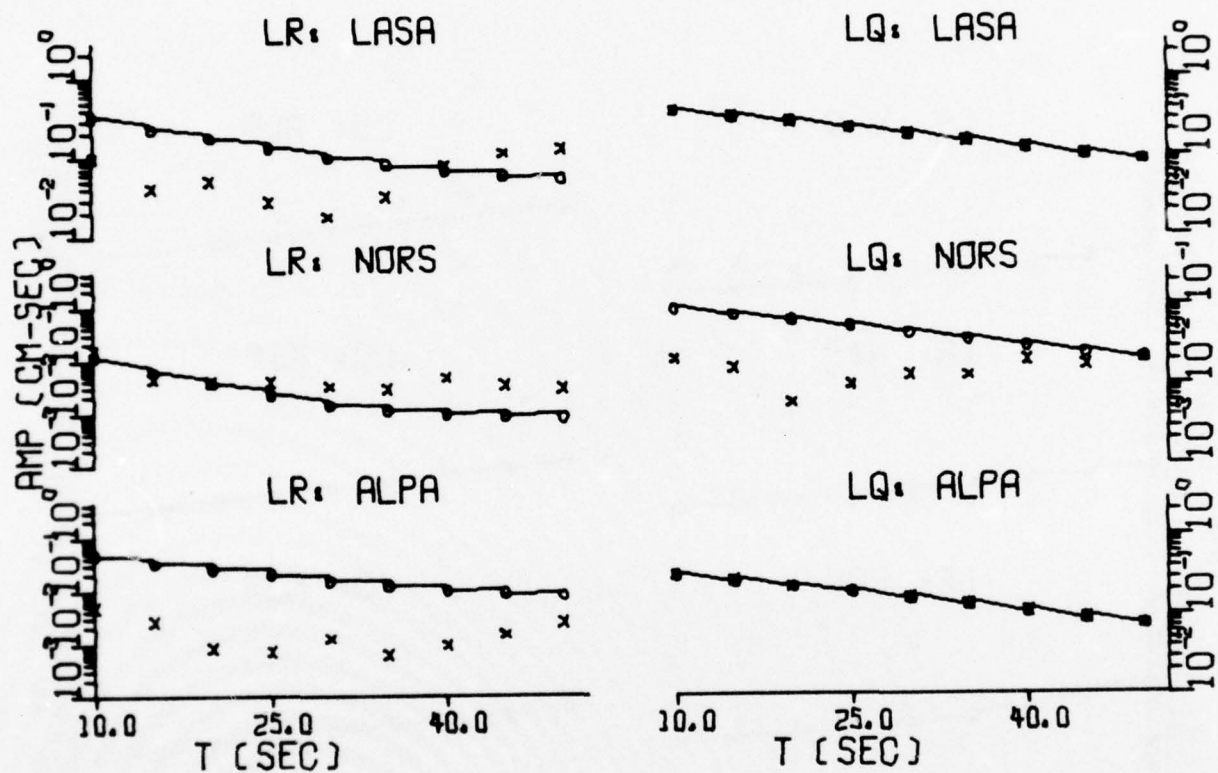


FIGURE V-28
RESULTS FROM AMPLITUDE SPECTRAL FITTING: EKZ/427/75
(PAGE 2 OF 3)

(b) Spectral Fits

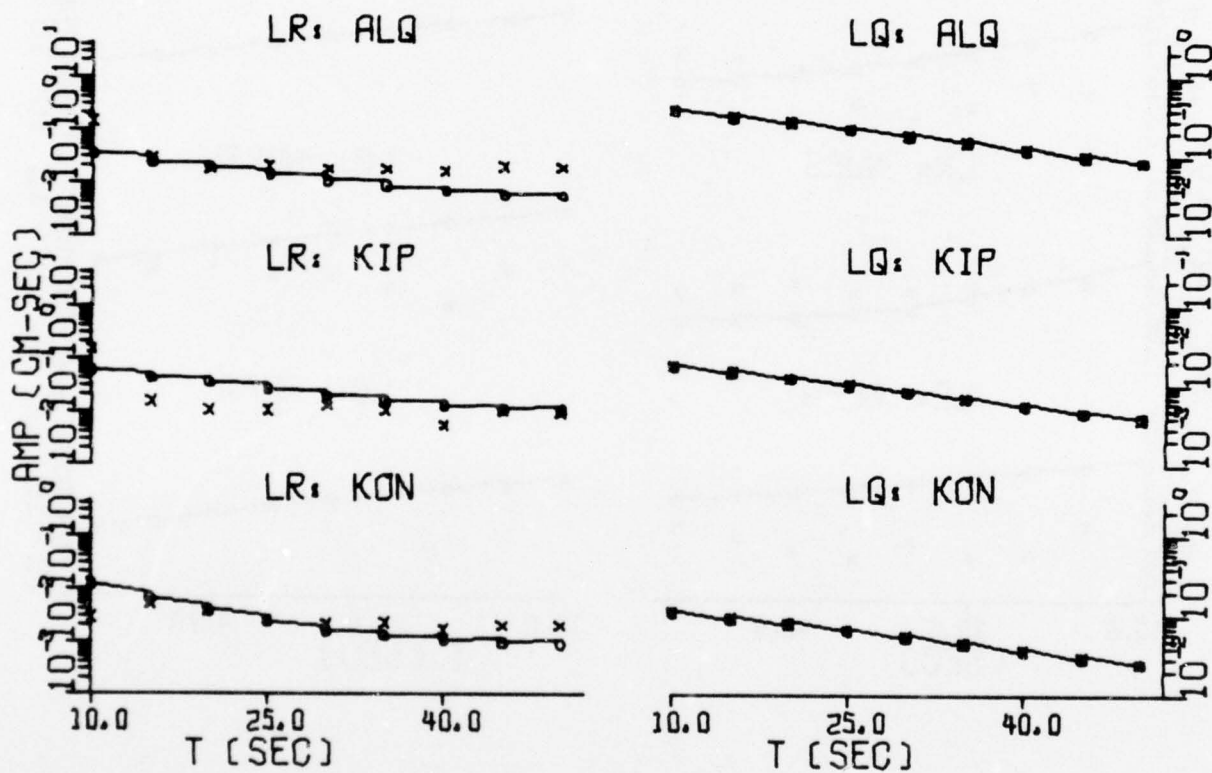


FIGURE V-28

RESULTS FROM AMPLITUDE SPECTRAL FITTING: EKZ/427/75
(PAGE 3 OF 3)

(a) Residual Distributions

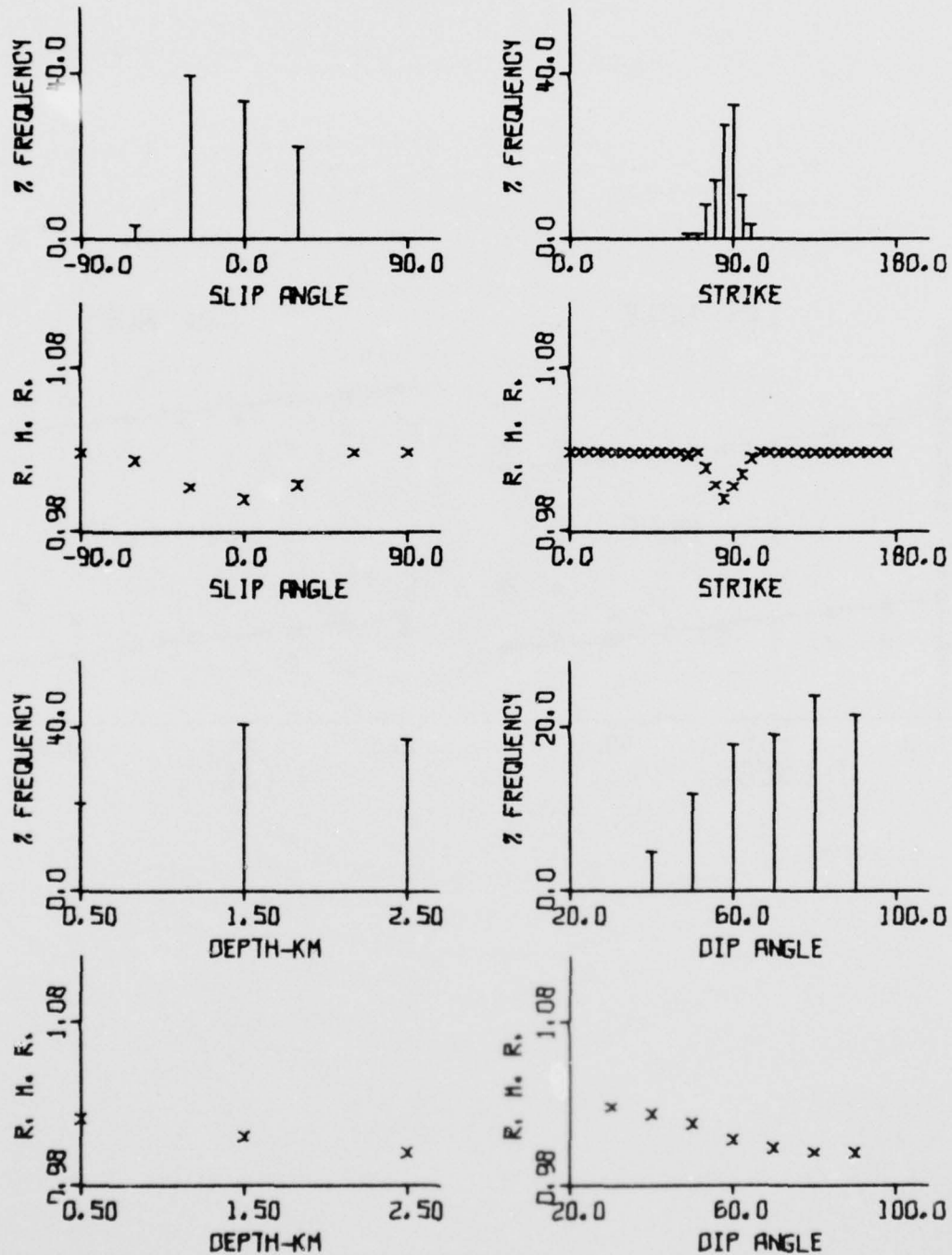


FIGURE V-29

RESULTS FROM AMPLITUDE SPECTRAL FITTING: EKZ/1029/5
(PAGE 1 OF 2)

(b) Spectral Fits

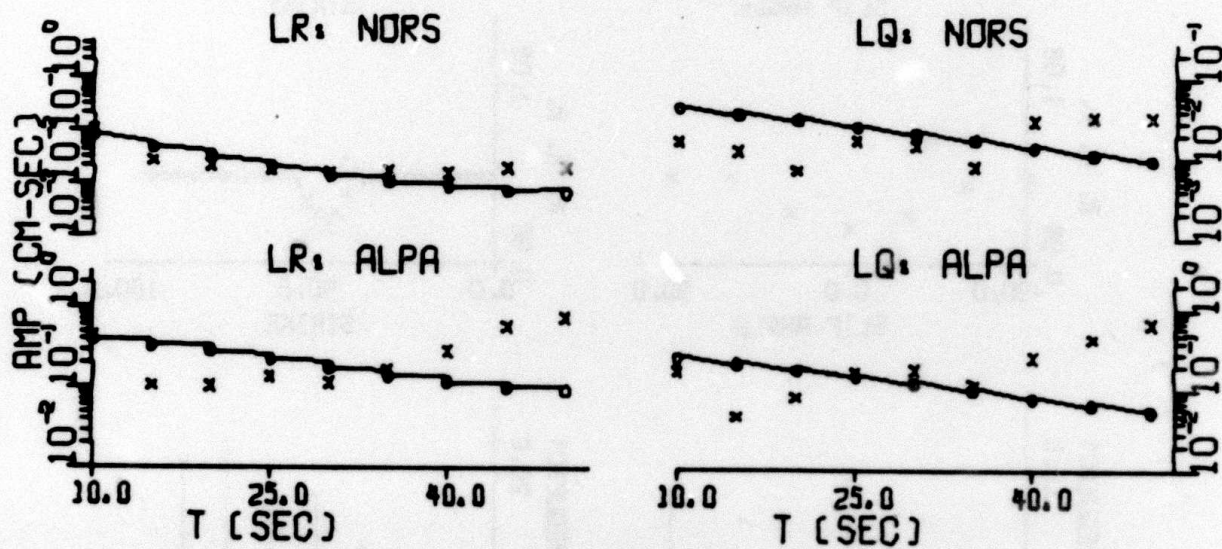


FIGURE V-29

RESULTS FROM AMPLITUDE SPECTRAL FITTING: EKZ/1029/5
(PAGE 2 OF 2)

(a) Residual Distributions

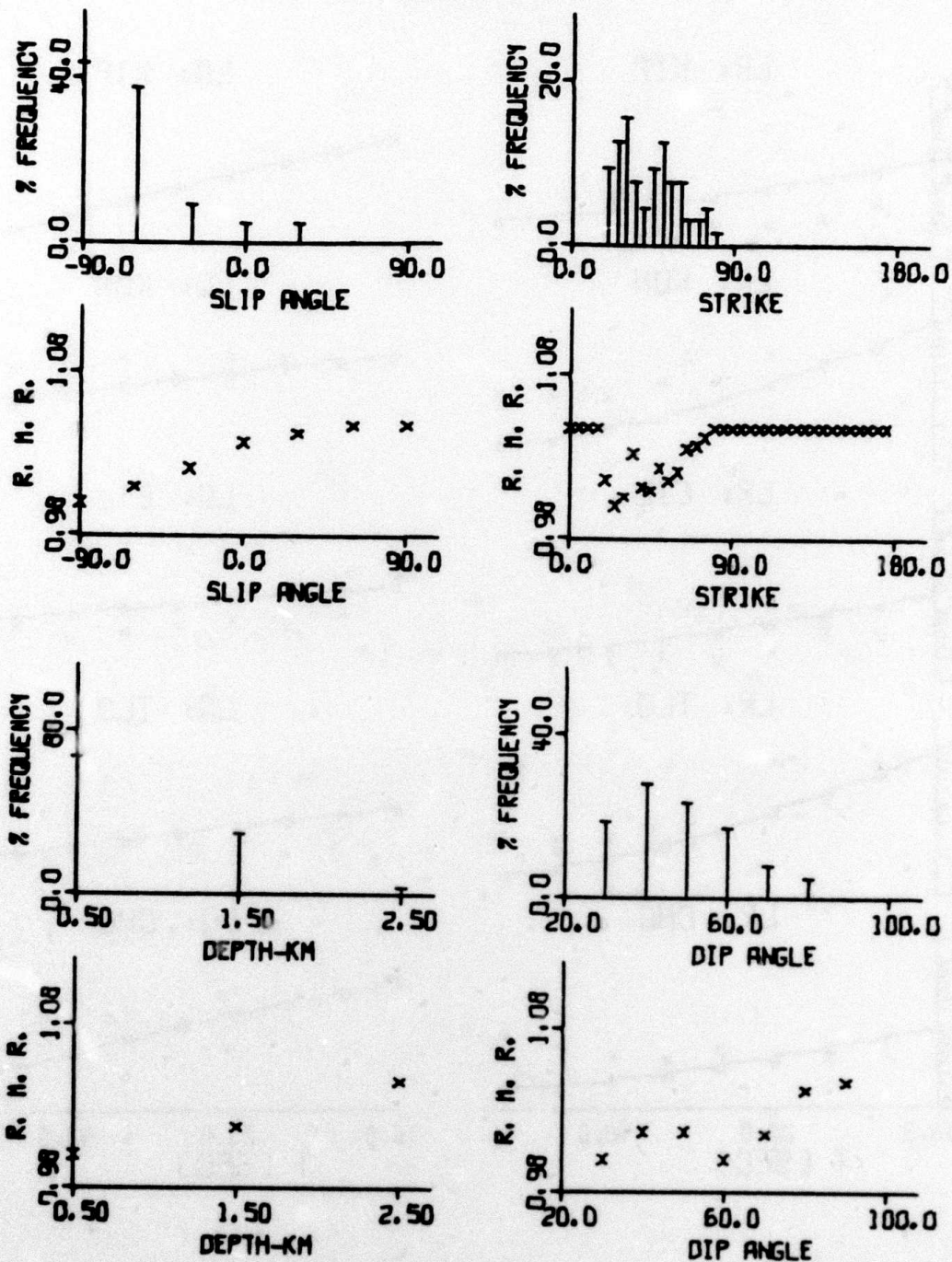


FIGURE V-30

RESULTS FROM AMPLITUDE SPECTRAL FITTING: EKZ/704/76
(PAGE 1 OF 3)

(b) Spectral Fits

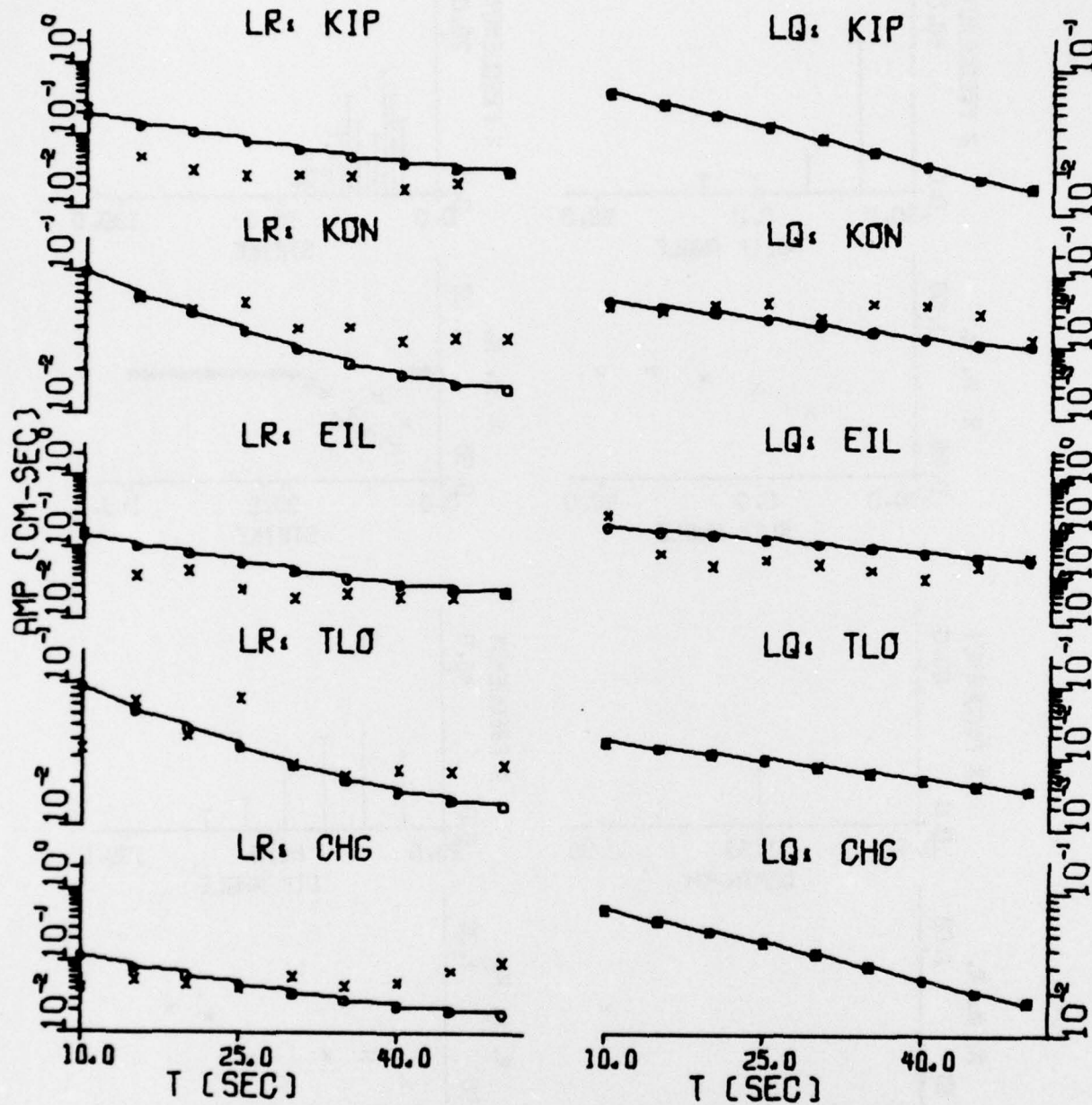


FIGURE V-30

RESULTS FROM AMPLITUDE SPECTRAL FITTING: EKZ/704/76
(PAGE 2 OF 3)

(b) Spectral Fits

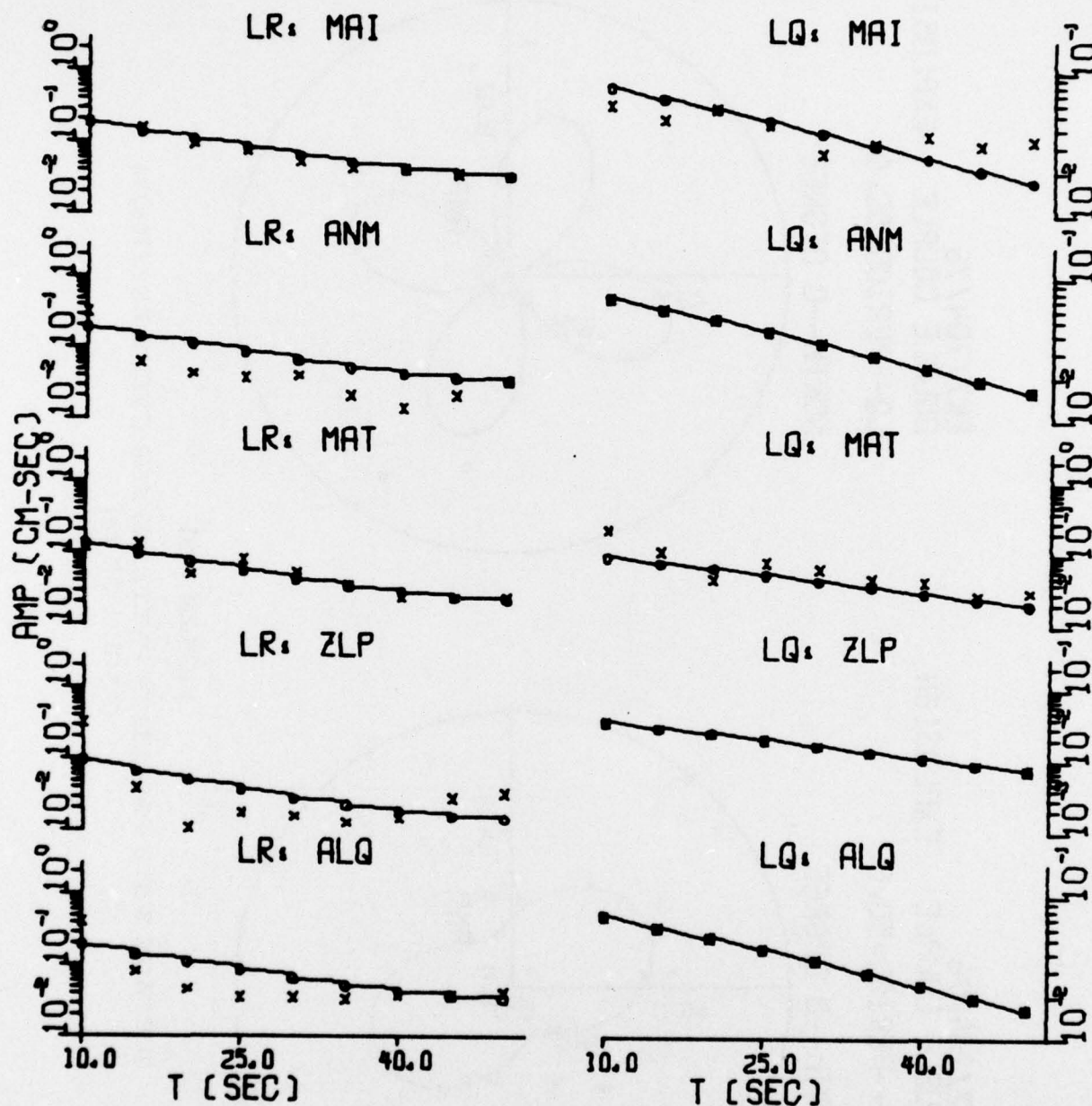
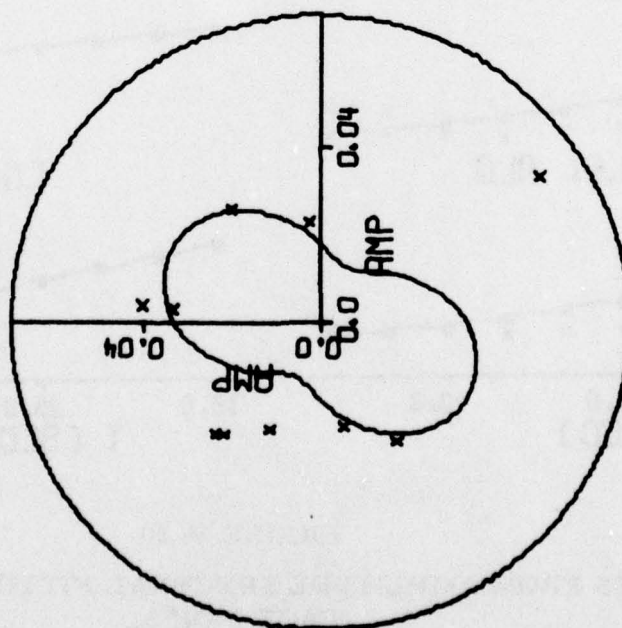


FIGURE V-30

RESULTS FROM AMPLITUDE SPECTRAL FITTING: EKZ/704/76
(PAGE 3 OF 3)

EKZ/704/76
 DOUBLE COUPLE EXPLOSION
 LR--PERIOD=50.0
 NORTH--0 DEGREE



EKZ/704/76
 DOUBLE COUPLE EXPLOSION
 LQ--PERIOD=50.0
 NORTH--0 DEGREE

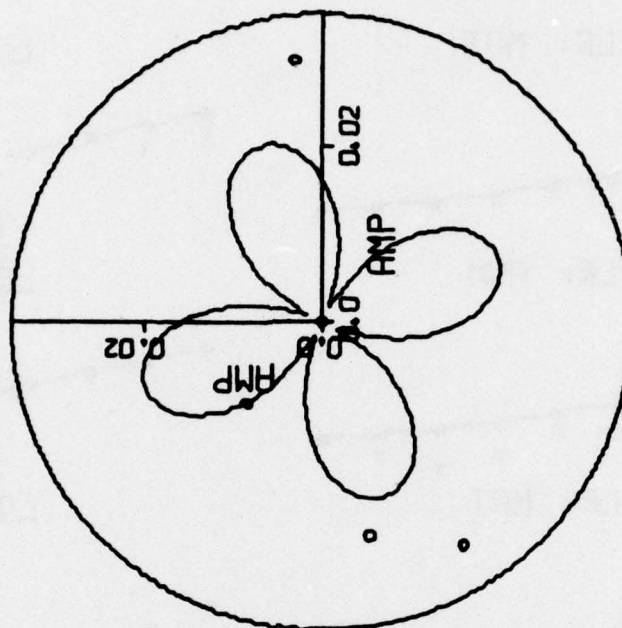
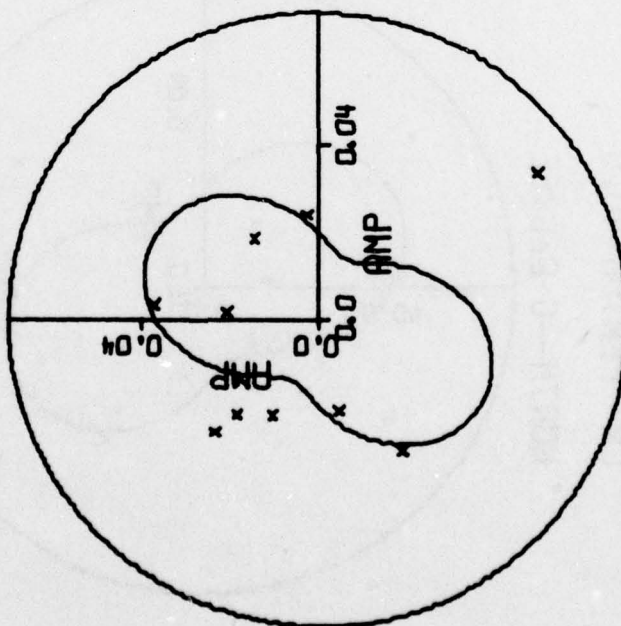


FIGURE V-31
 SURFACE WAVE RADIATION PATTERNS FOR EVENT EKZ/704/76
 (PAGE 1 OF 18)

EKZ/704/76
 DOUBLE COUPLE EXPLOSION
 LR--PERIOD=45.0
 NORTH--0 DEGREE



EKZ/704/76
 DOUBLE COUPLE EXPLOSION
 LQ--PERIOD=45.0
 NORTH--0 DEGREE

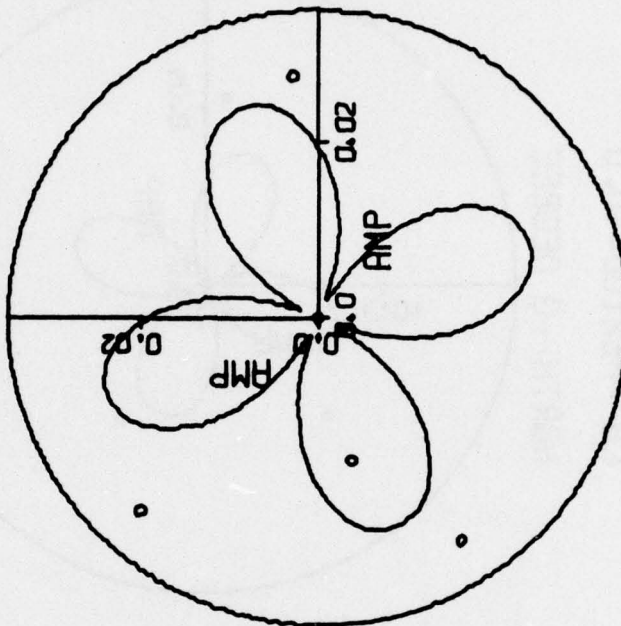
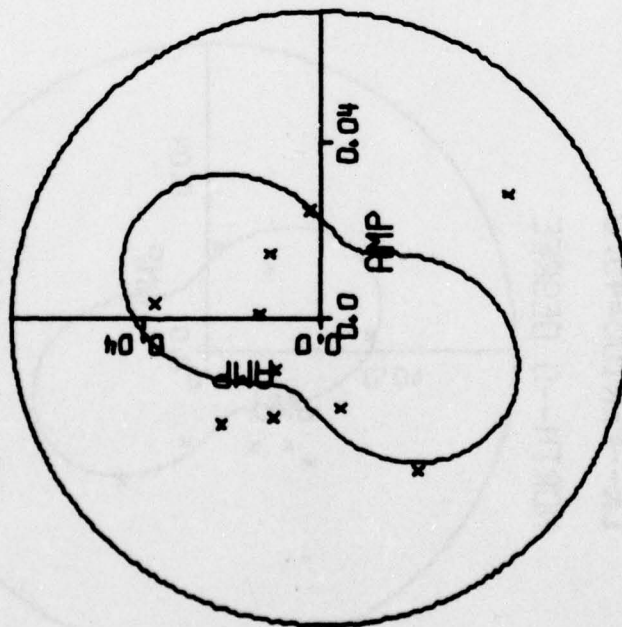


FIGURE V-31
 SURFACE WAVE RADIATION PATTERNS FOR EVENT EKZ/704/76
 (PAGE 2 OF 18)

EKZ/704/76
 DOUBLE COUPLE EXPLOSION
 LR--PERIOD=40.0
 NORTH--0 DEGREE



EKZ/704/76
 DOUBLE COUPLE EXPLOSION
 LQ--PERIOD=40.0
 NORTH--0 DEGREE

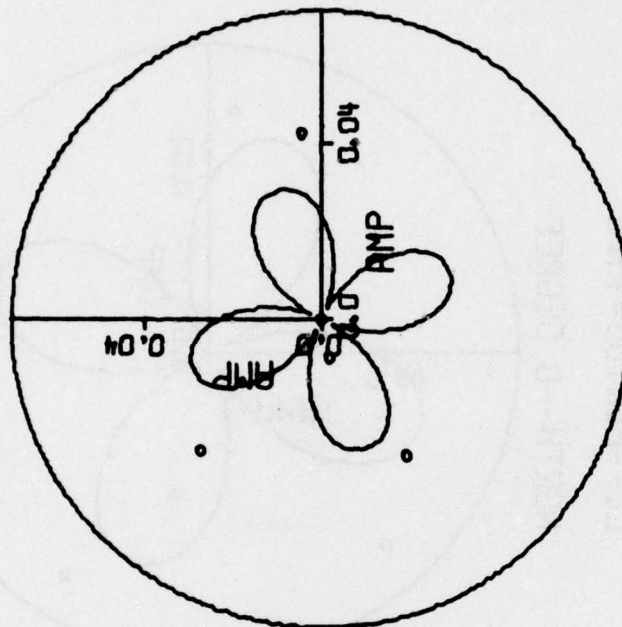
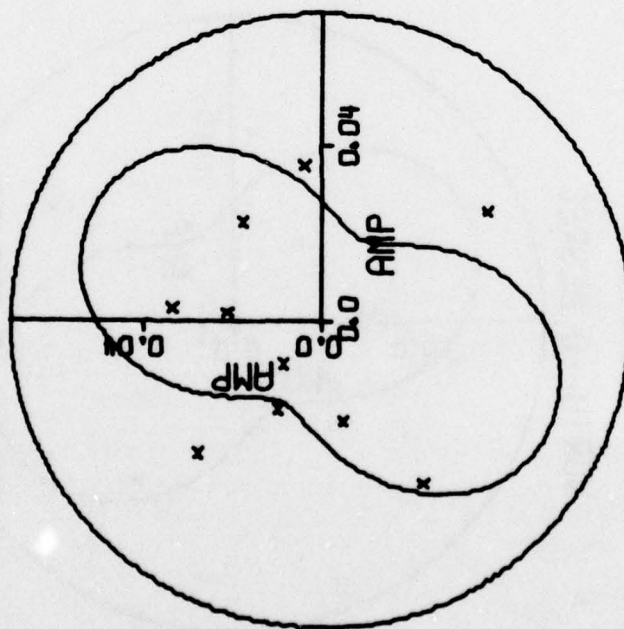


FIGURE V-31
 SURFACE WAVE RADIATION PATTERNS FOR EVENT EKZ/704/76
 (PAGE 3 OF 18)

EKZ/704/76
 DOUBLE COUPLE EXPLOSION
 LR--PERIOD=35.0
 NORTH--0 DEGREE



EKZ/704/76
 DOUBLE COUPLE EXPLOSION
 LQ--PERIOD=35.0
 NORTH--0 DEGREE

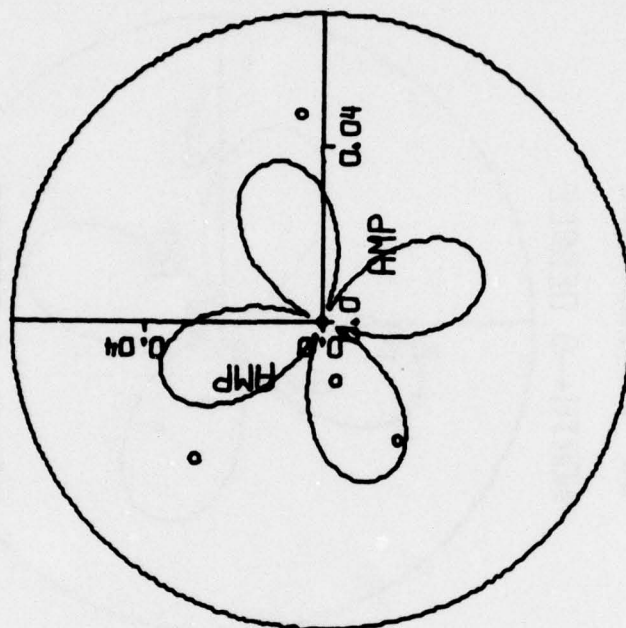
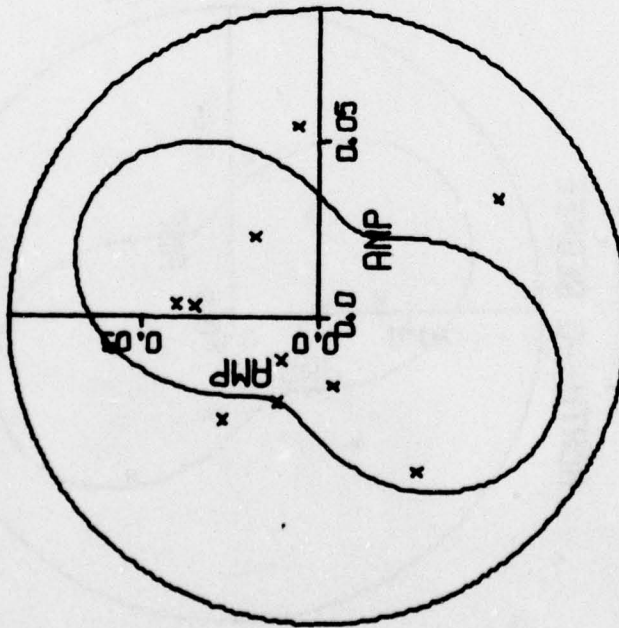


FIGURE V-31
 SURFACE WAVE RADIATION PATTERNS FOR EVENT EKZ/704/76
 (PAGE 4 OF 18)

EKZ/704/76
 DOUBLE COUPLE EXPLOSION
 LR--PERIOD=30.0
 NORTH--0 DEGREE



EKZ/704/76
 DOUBLE COUPLE EXPLOSION
 LQ--PERIOD=30.0
 NORTH--0 DEGREE

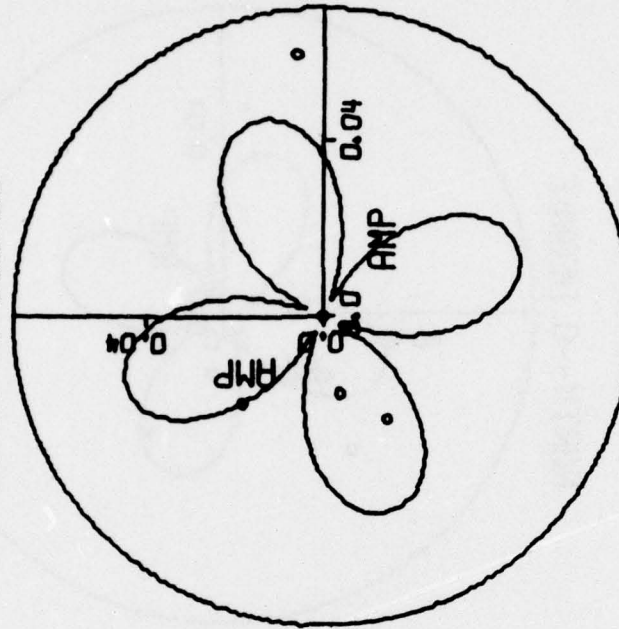
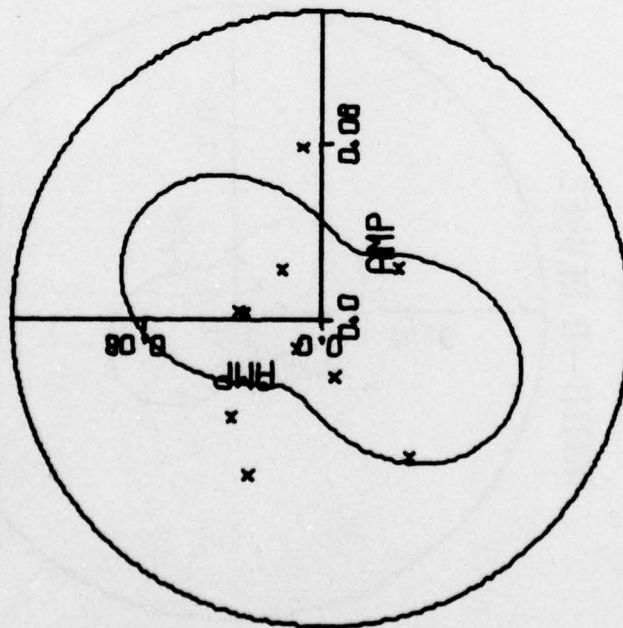


FIGURE V-31
 SURFACE WAVE RADIATION PATTERNS FOR EVENT EKZ/704/76
 (PAGE 5 OF 18)

EKZ/704/76
 DOUBLE COUPLE EXPLOSION
 LR--PERIOD=25.0
 NORTH--0 DEGREE



EKZ/704/76
 DOUBLE COUPLE EXPLOSION
 LQ--PERIOD=25.0
 NORTH--0 DEGREE

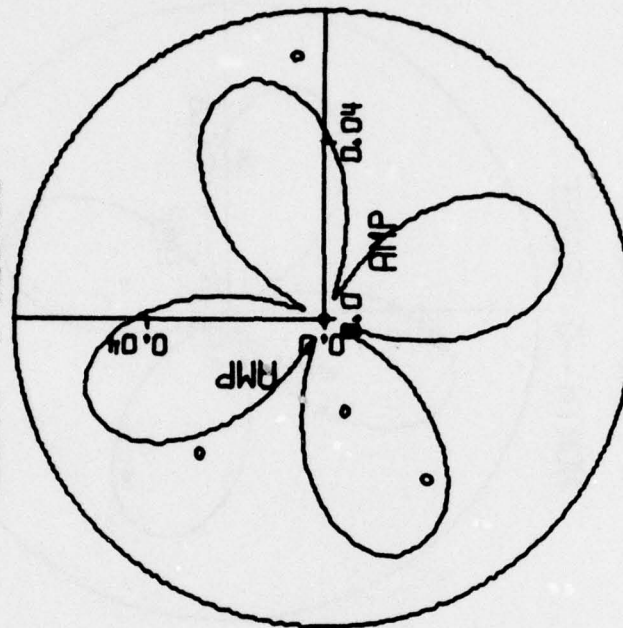
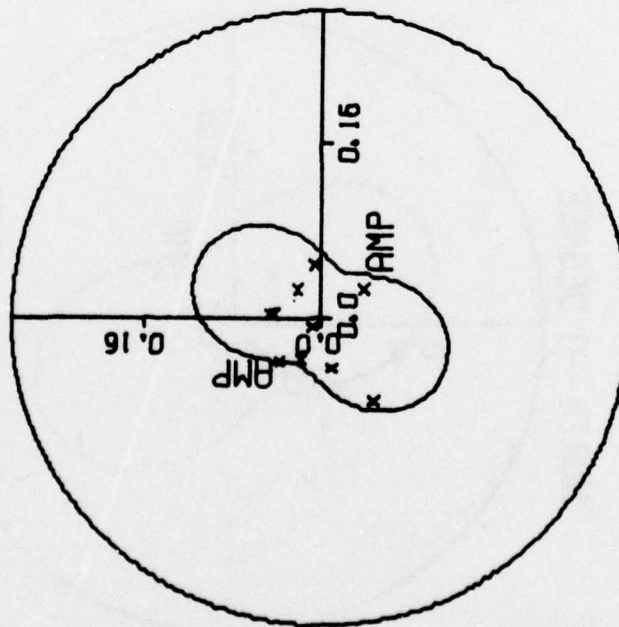


FIGURE V-31
 SURFACE WAVE RADIATION PATTERNS FOR EVENT EKZ/704/76
 (PAGE 6 OF 18)

EKZ/704/76
 DOUBLE COUPLE EXPLOSION
 LR--PERIOD=20.0
 NORTH--0 DEGREE



EKZ/704/76
 DOUBLE COUPLE EXPLOSION
 LQ--PERIOD=20.0
 NORTH--0 DEGREE

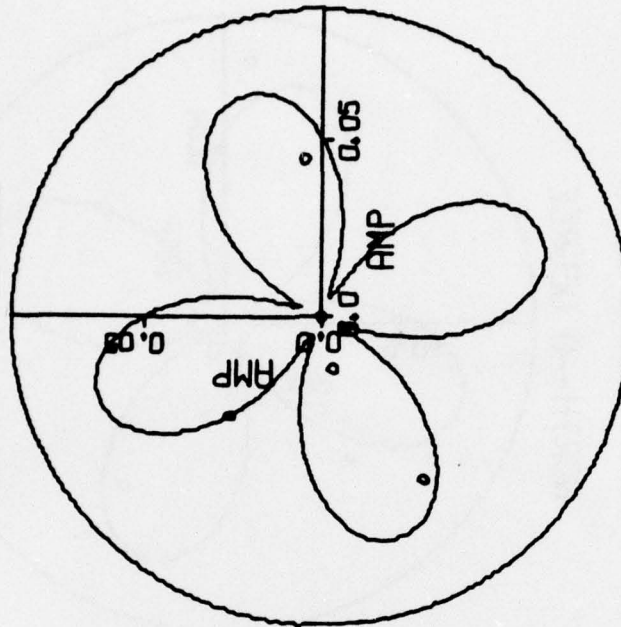
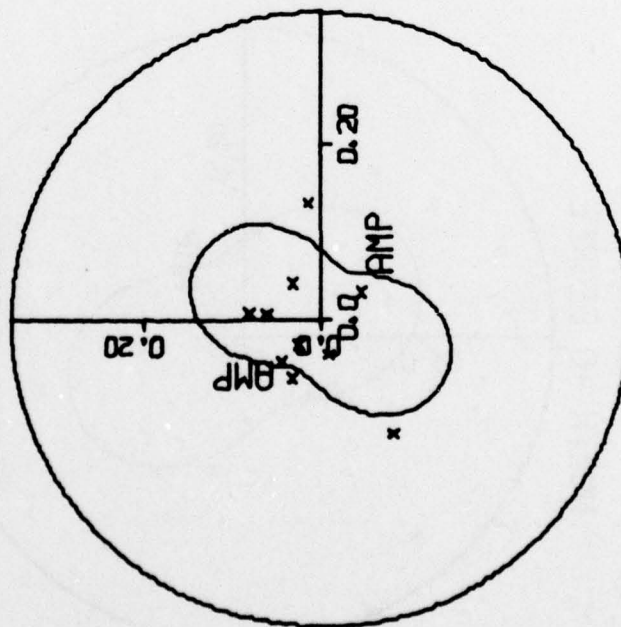


FIGURE V-31
 SURFACE WAVE RADIATION PATTERNS FOR EVENT EKZ/704/76
 (PAGE 7 OF 18)

EKZ/704/76
 DOUBLE COUPLE EXPLOSION
 LR--PERIOD=15.0
 NORTH--0 DEGREE



EKZ/704/76
 DOUBLE COUPLE EXPLOSION
 LQ--PERIOD=15.0
 NORTH--0 DEGREE

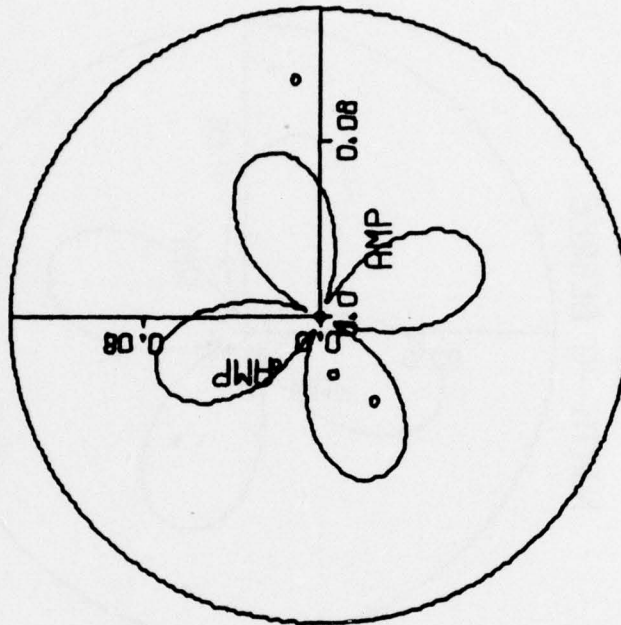
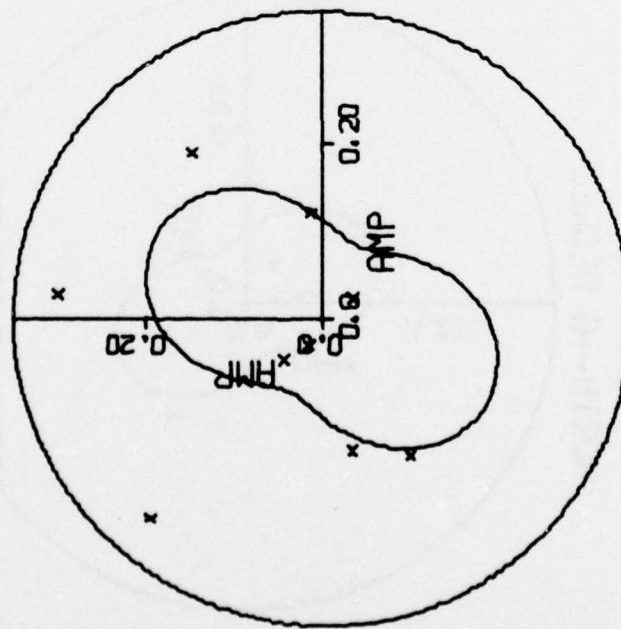


FIGURE V-31
 SURFACE WAVE RADIATION PATTERNS FOR EVENT EKZ/704/76
 (PAGE 8 OF 18)

EKZ/704/76
DOUBLE COUPLE EXPLOSION
LR--PERIOD=10.0

NORTH--0 DEGREE



EKZ/704/76
DOUBLE COUPLE EXPLOSION
LQ--PERIOD=10.0

NORTH--0 DEGREE

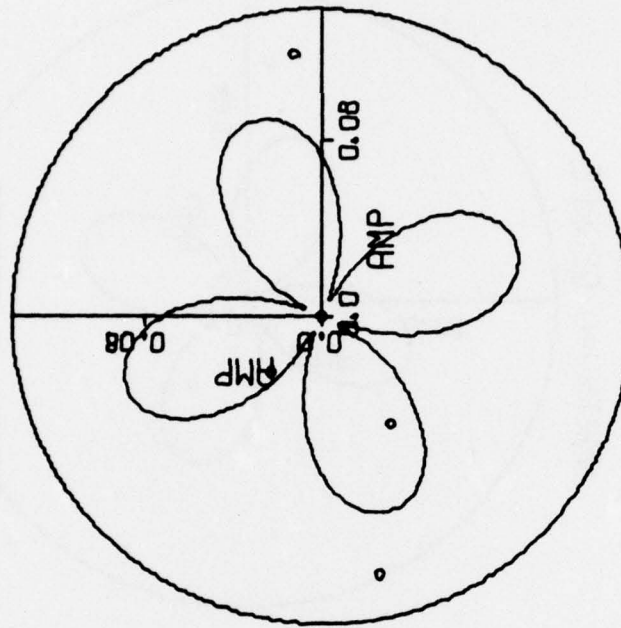


FIGURE V-31
SURFACE WAVE RADIATION PATTERNS FOR EVENT EKZ/704/76
(PAGE 9 OF 18)

EKZ/704/76
DOUBLE COUPLE EXPLOSION
LQ/LR--PERIOD=50.0
NORTH--0 DEGREE

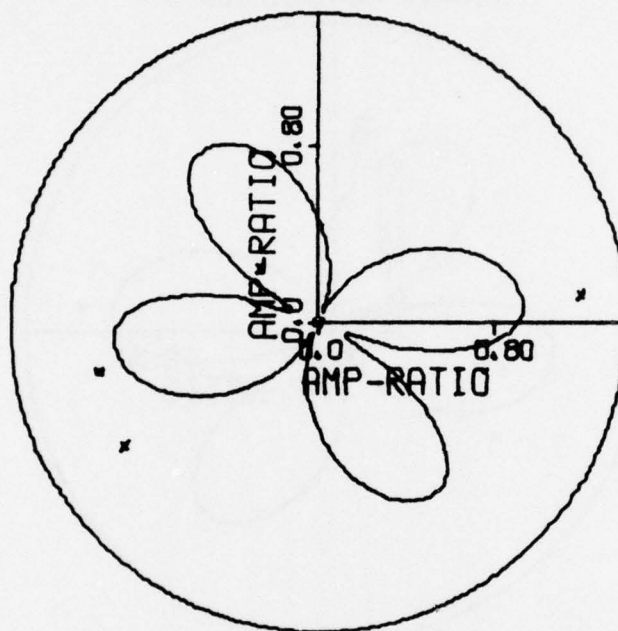


FIGURE V-31
SURFACE WAVE RADIATION PATTERNS FOR EVENT EKZ/704/76
(PAGE 10 OF 18)

EKZ/704/76
DOUBLE COUPLE EXPLOSION
LQ/LR--PERIOD=45.0
NORTH--0 DEGREE

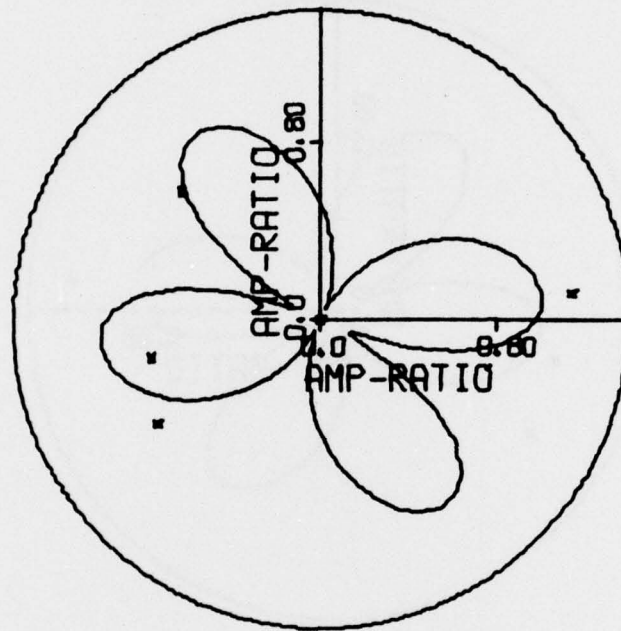


FIGURE V-31
SURFACE WAVE RADIATION PATTERNS FOR EVENT EKZ/704/76
(PAGE 11 OF 18)

EKZ/704/76
DOUBLE COUPLE EXPLOSION
LQ/LR--PERIOD=40.0

NORTH--0 DEGREE

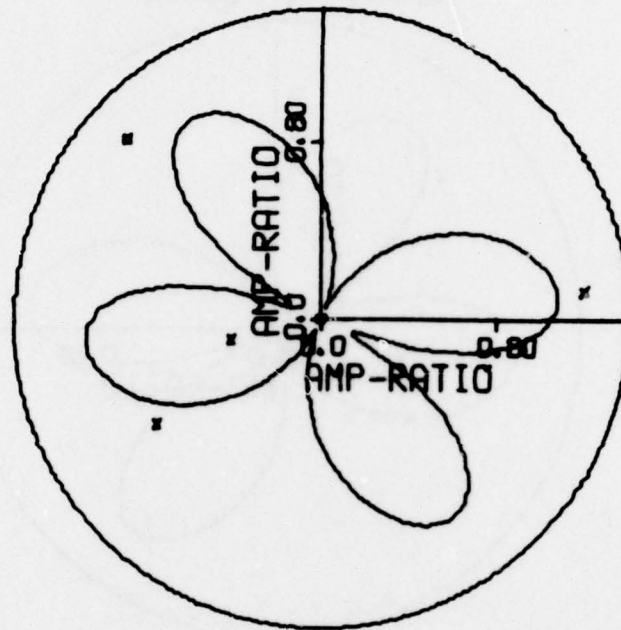


FIGURE V-31
SURFACE WAVE RADIATION PATTERNS FOR EVENT EKZ/704/76
(PAGE 12 OF 18)

EKZ/704/76
DOUBLE COUPLE EXPLOSION
LQ/LR--PERIOD=35.0
NORTH--0 DEGREE

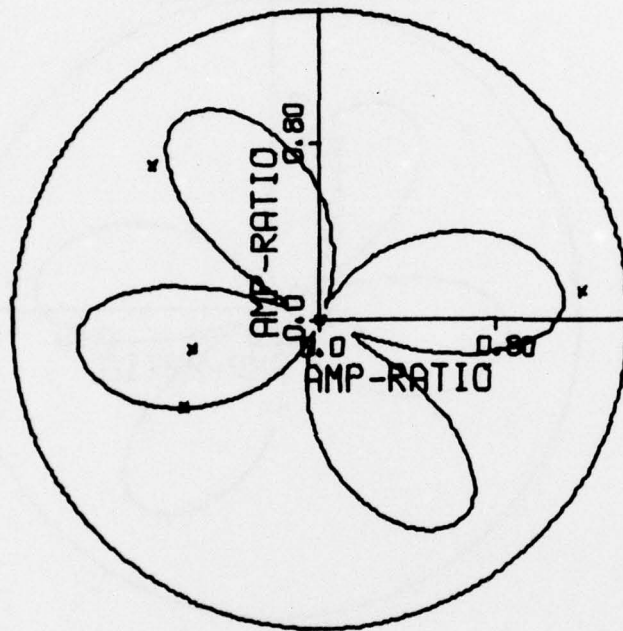


FIGURE V-31
SURFACE WAVE RADIATION PATTERNS FOR EVENT EKZ/704/76
(PAGE 13 OF 18)

EKZ/704/76
DOUBLE COUPLE EXPLOSION
LQ/LR--PERIOD=30.0
NORTH--0 DEGREE

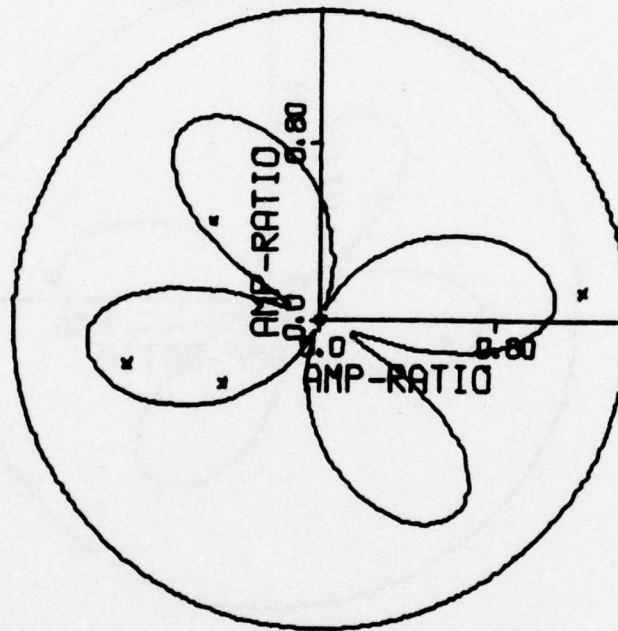


FIGURE V-31
SURFACE WAVE RADIATION PATTERNS FOR EVENT EKZ/704/76
(PAGE 14 OF 18)

EKZ/704/76
DOUBLE COUPLE EXPLOSION
LQ/LR--PERIOD=25.0
NORTH--0 DEGREE

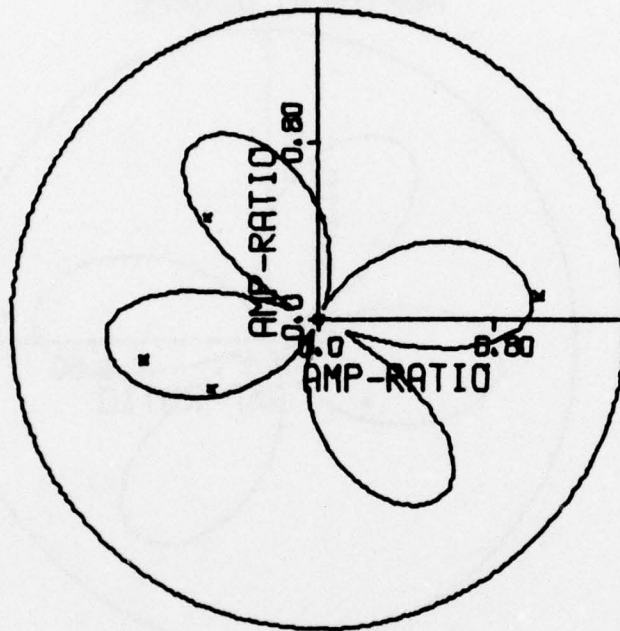


FIGURE V-31
SURFACE WAVE RADIATION PATTERNS FOR EVENT EKZ/704/76
(PAGE 15 OF 18)

EKZ/704/76
DOUBLE COUPLE EXPLOSION
LQ/LR--PERIOD=20.0

NORTH--0 DEGREE

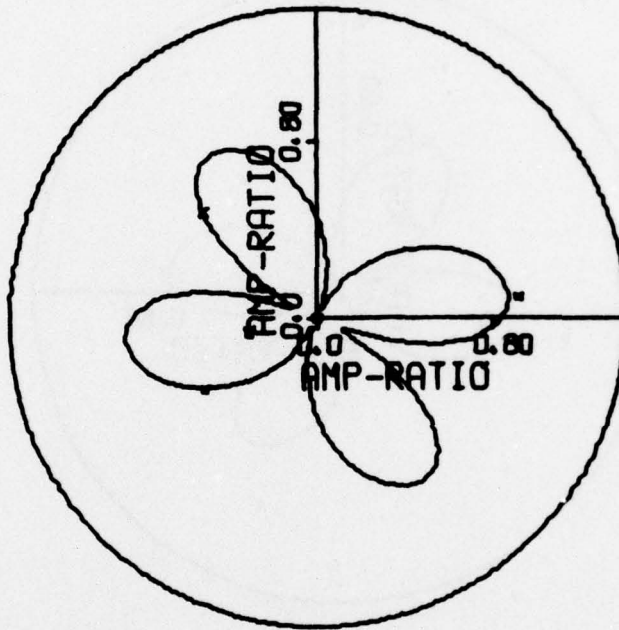


FIGURE V-31
SURFACE WAVE RADIATION PATTERNS FOR EVENT EKZ/704/76
(PAGE 16 OF 18)

EKZ/704/76
DOUBLE COUPLE EXPLOSION
LQ/LR--PERIOD=15.0
NORTH--0 DEGREE

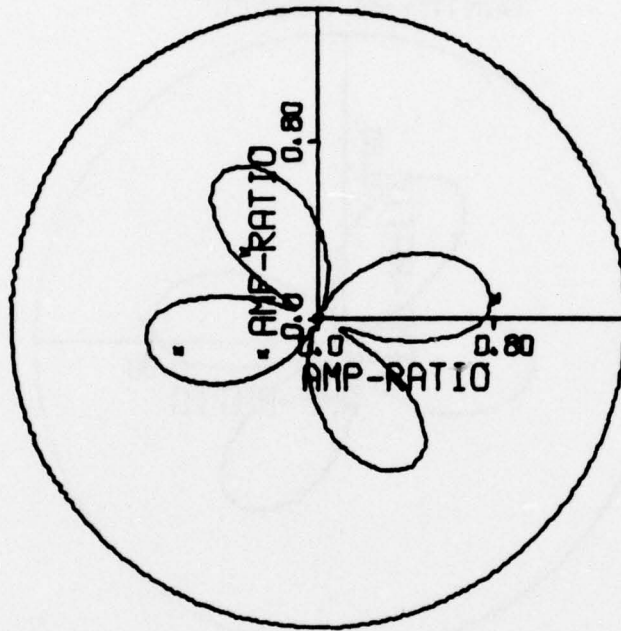


FIGURE V-31
SURFACE WAVE RADIATION PATTERNS FOR EVENT EKZ/704/76
(PAGE 17 OF 18)

EKZ/704/76
DOUBLE COUPLE EXPLOSION
LQ/LR--PERIOD=10.0

NORTH--0 DEGREE

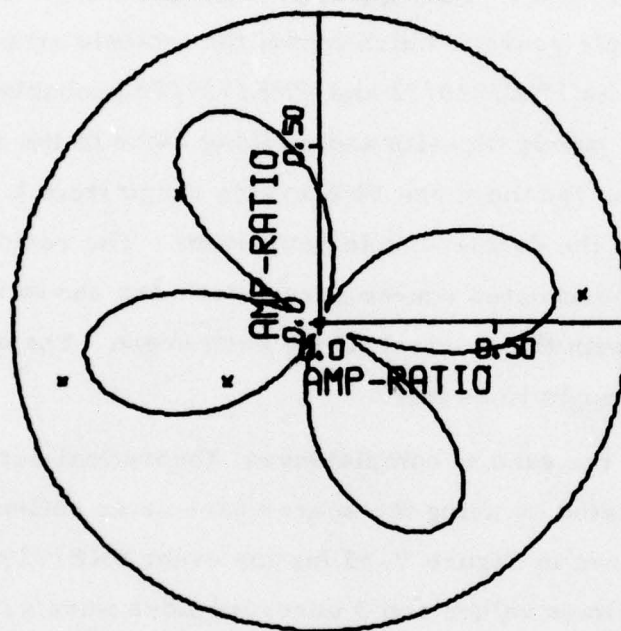


FIGURE V-31
SURFACE WAVE RADIATION PATTERNS FOR EVENT EKZ/704/76
(PAGE 18 OF 18)

3. The PNE Events

For the selected PNE events, estimates of source parameters based on the minimum-residual criterion are listed in Table V-11. Those based on the residual distributions are listed in Table V-12. Again, as observed for the NTS and EKZ events, the depth estimates of these events are all very shallow (0.5 km). The dip, slip, and strike angle estimates indicate that the double-couple sources which model the tectonic strain releases associated with the events PNE/820/72 and PNE/729/76 probably have very similar orientations, i. e., purely dip-slip and striking close to the E-W direction. The estimated F values for the three PNE events range from 1.0 to 1.25, indicating the existence of the double-couple component. The residual distributions with respect to the estimated source parameters are shown in Figures V-32 to V-34, together with the spectral fit for each event. The spectral fits for these events are thought to be fair.

For the sake of completeness, theoretical surface wave radiation patterns generated by using the source parameter estimates listed in Table V-11 are shown in Figure V-35 for the event PNE/729/76. Again 5 observed Rayleigh wave values and 3 observed Love wave values available at each period are also plotted in this figure. The general agreement between the theoretical Rayleigh and Love wave radiation patterns and the observed values is good. Especially, the three observed LQ/LR values fall quite close to the theoretical LQ/LR radiation patterns for most of the periods.

4. Comparison Among the Selected NTS, EKZ, and PNE Events

From source parameter estimates of the selected NTS, EKZ and PNE events discussed above, it seems that differences in the source parameter estimates are not obvious among these three groups of explosion events. The results of comparing these three groups of explosion events can be interpreted as follows:

TABLE V-11

ESTIMATIONS OF SOURCE PARAMETERS OBTAINED BY AMPLITUDE
SPECTRAL FITTING BASED ON THE MINIMUM-RESIDUAL
CRITERION: SELECTED PNE EVENTS

Event I. D.	Optimal Solution					
	Depth h km	Dip Angle δ°	Slip Angle λ°	Strike $N\phi^\circ E$	Moment M_E 10^{25} dyne-cm	M_X
PNE/1222/1	0.5	30	-30	135	0.186×10^{-1}	0.186×10^{-1}
PNE/820/72	0.5	40	-90	105	0.635×10^{-2}	0.793×10^{-2}
PNE/729/76	0.5	70	-90	110	0.117×10^{-1}	0.177×10^{-1}
						F
						1.00
						1.25
						1.00

TABLE V-12

ESTIMATIONS OF SOURCE PARAMETERS OBTAINED BY AMPLITUDE
SPECTRAL FITTING BASED ON THE RESIDUAL DISTRIBUTIONS:
SELECTED PNE EVENTS

Event I. D.	Source Parameters							
	Depth h km		Dip Angle δ°		Slip Angle λ°		Strike $N\phi^\circ E$	
	Probable Range	% Fre- quency	Probable Range	% Fre- quency	Probable Range	% Fre- quency	Probable Range	% Fre- quency
PNE/1222/1	0.5 ~ 1.5	92	30 ~ 50 70 ~ 80	59 33	-30 ~ +30	86	135 ~ 150	74
PNE/820/72	0.5 ~ 1.5	98	40 ~ 60	65	-30 ~ -90	84	100 ~ 150	91
PNE/729/76	0.5	81	30 60 ~ 90	19 65	-90 0 ~ -60	28 55	100 ~ 120 145 ~ 170	30 70

(a) Residual Distributions

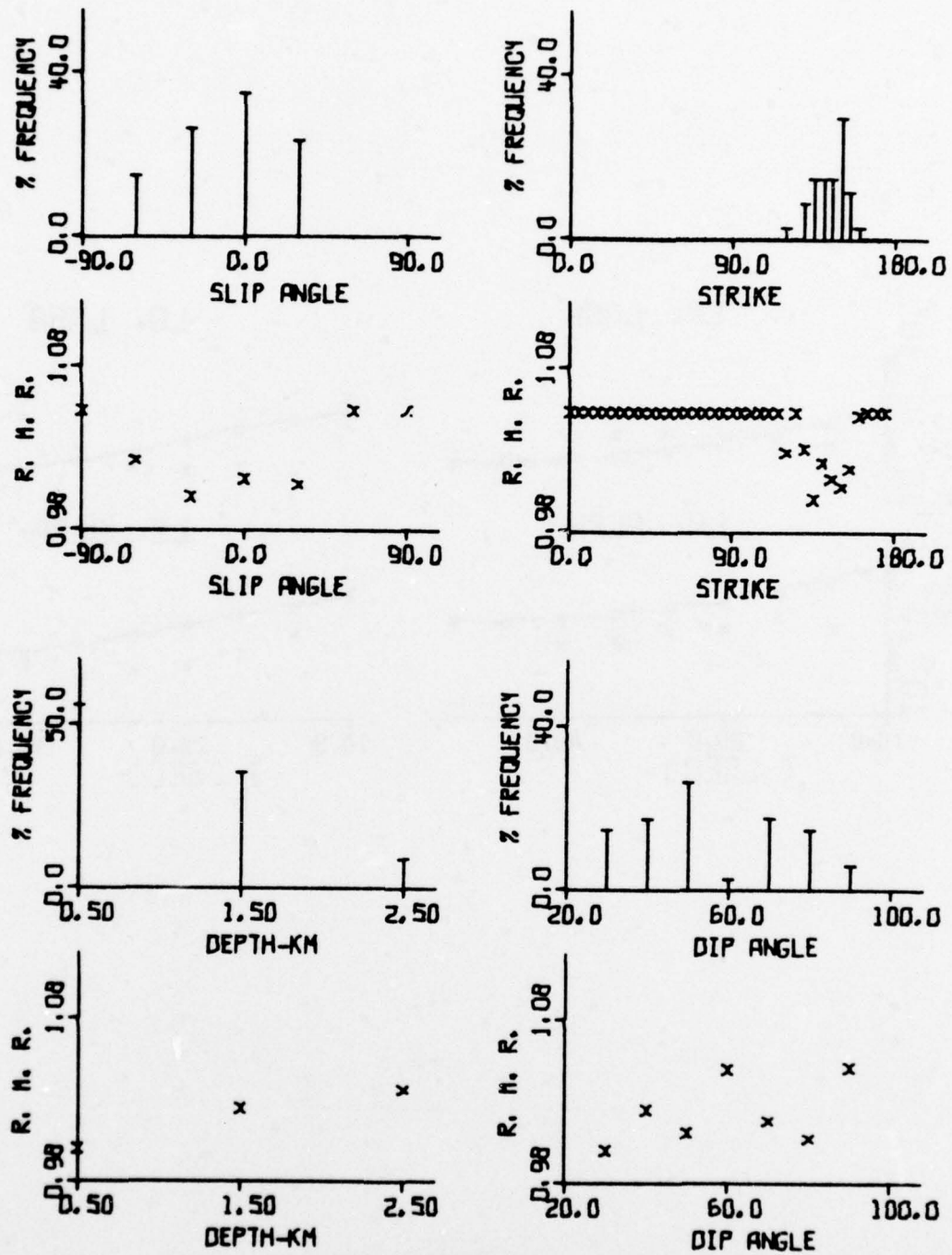


FIGURE V-32

RESULTS FROM AMPLITUDE SPECTRAL FITTING: PNE/1222/1
(PAGE 1 OF 2)

(b) Spectral Fits

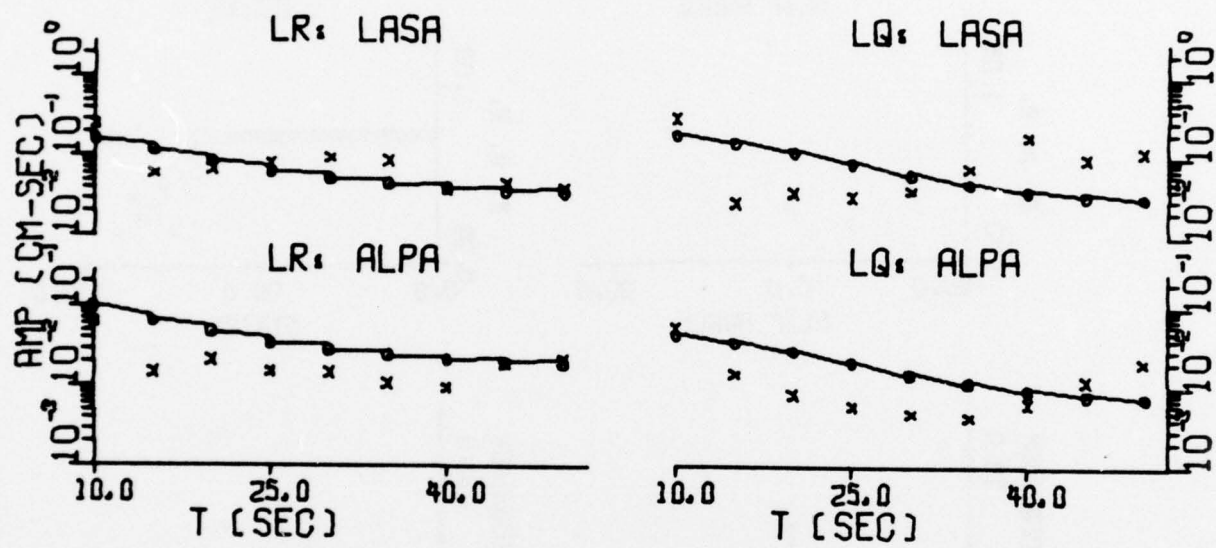


FIGURE V-32
RESULTS FROM AMPLITUDE SPECTRAL FITTING: PNE/1222/1
(PAGE 2 OF 2)

(a) Residual Distributions

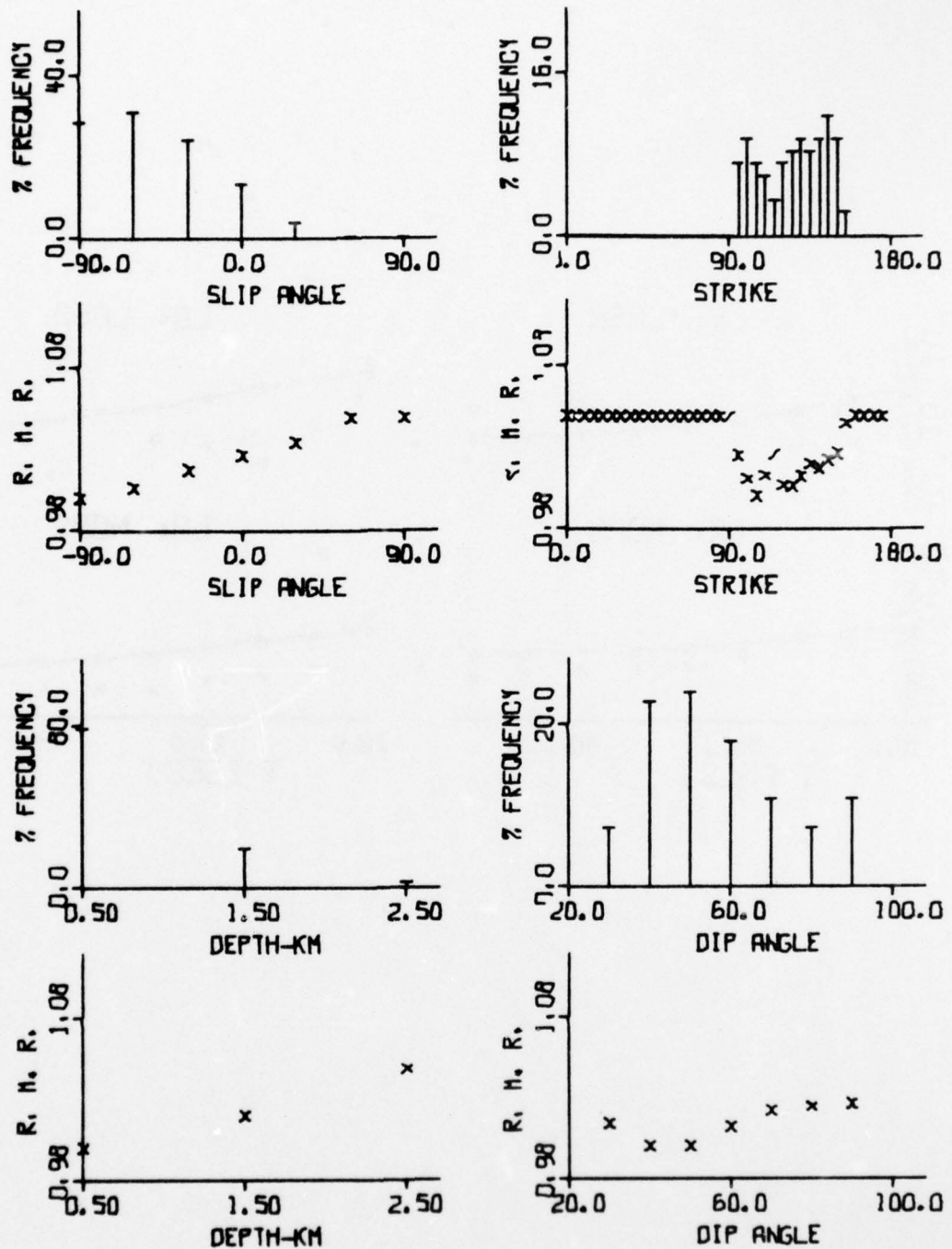


FIGURE V-33

RESULTS FROM AMPLITUDE SPECTRAL FITTING: PNE/820/72
(PAGE 1 OF 2)

(b) Spectral Fits

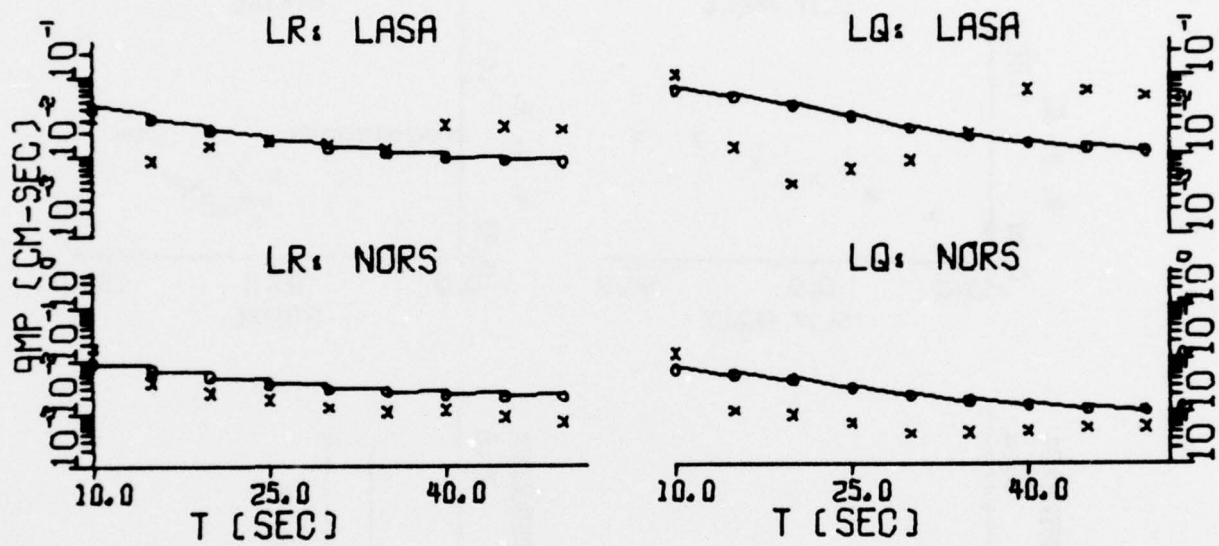


FIGURE V-33

RESULTS FROM AMPLITUDE SPECTRAL FITTING: PNE/820/72
(PAGE 2 OF 2)

(a) Residual Distributions

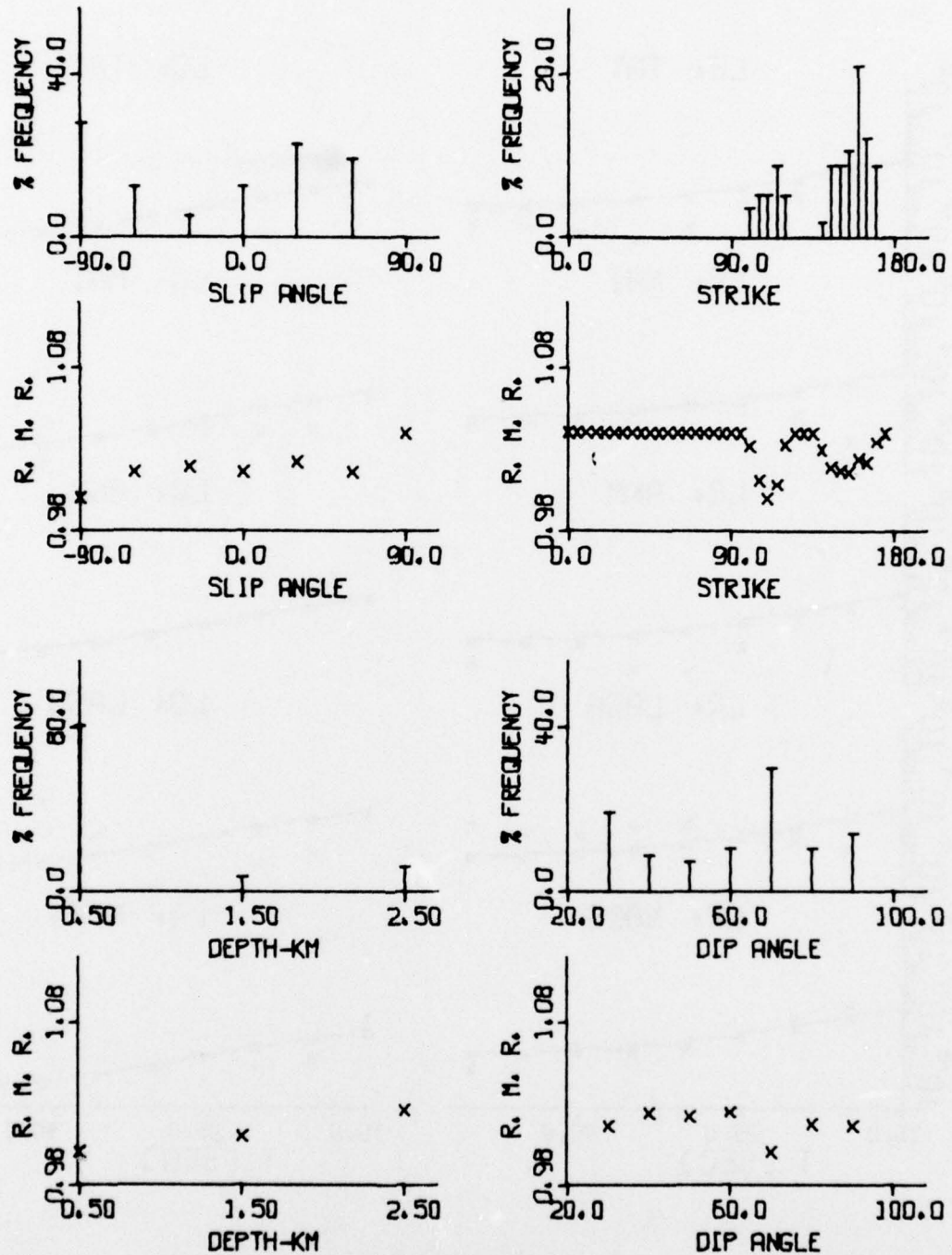


FIGURE V-34

RESULTS FROM AMPLITUDE SPECTRAL FITTING: PNE/729/76
(PAGE 1 OF 2)

(b) Spectral Fits

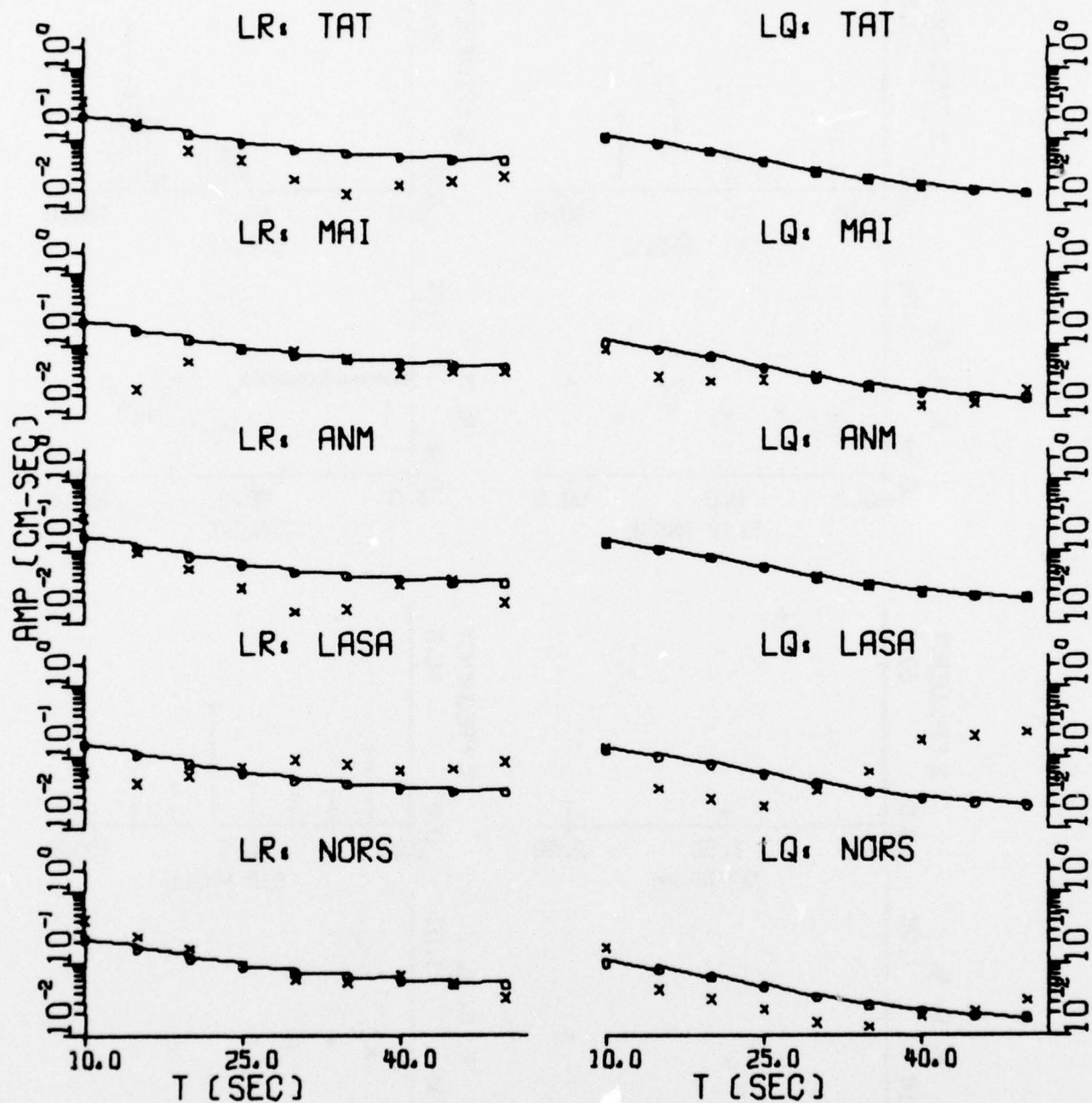
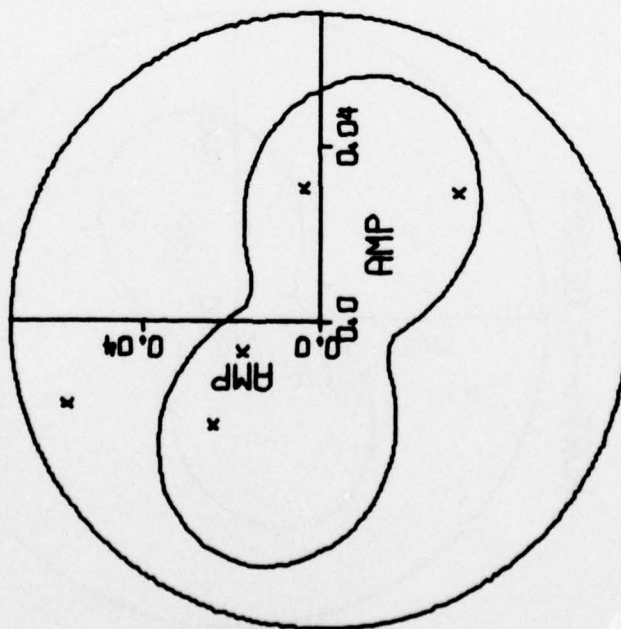


FIGURE V-34

RESULTS FROM AMPLITUDE SPECTRAL FITTING: PNE/729/76
(PAGE 2 OF 2)

PNE/729/76
 DOUBLE COUPLE EXPLOSION
 LR--PERIOD=50.0
 NORTH--0 DEGREE



PNE/729/76
 DOUBLE COUPLE EXPLOSION
 LQ--PERIOD=50.0
 NORTH--0 DEGREE

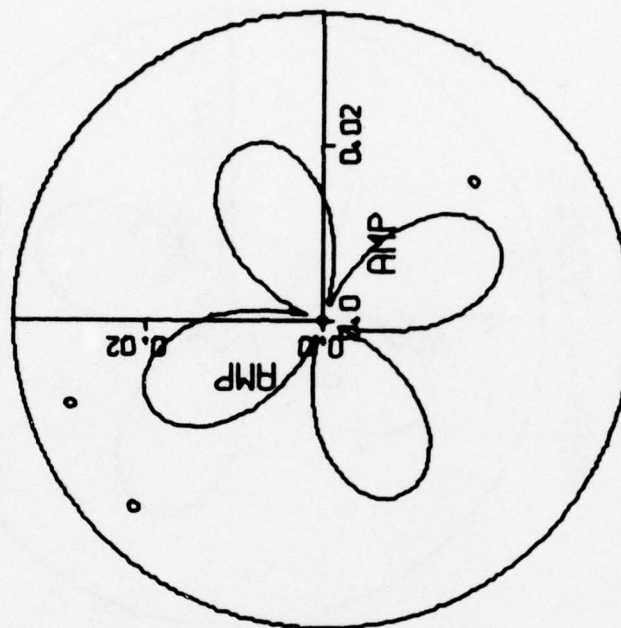
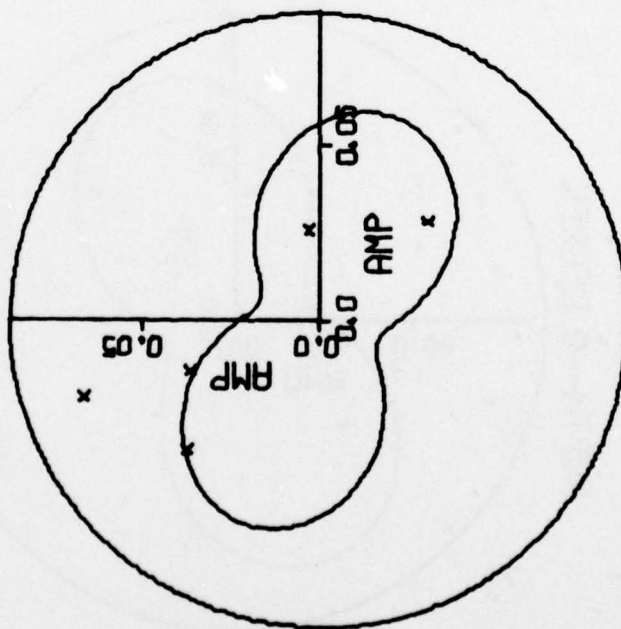


FIGURE V-35
 SURFACE WAVE RADIATION PATTERNS FOR EVENT PNE/729/76
 (PAGE 1 OF 18)

PNE/729/76
 DOUBLE COUPLE EXPLOSION
 LR--PERIOD=45.0
 NORTH--0 DEGREE



PNE/729/76
 DOUBLE COUPLE EXPLOSION
 LQ--PERIOD=45.0
 NORTH--0 DEGREE

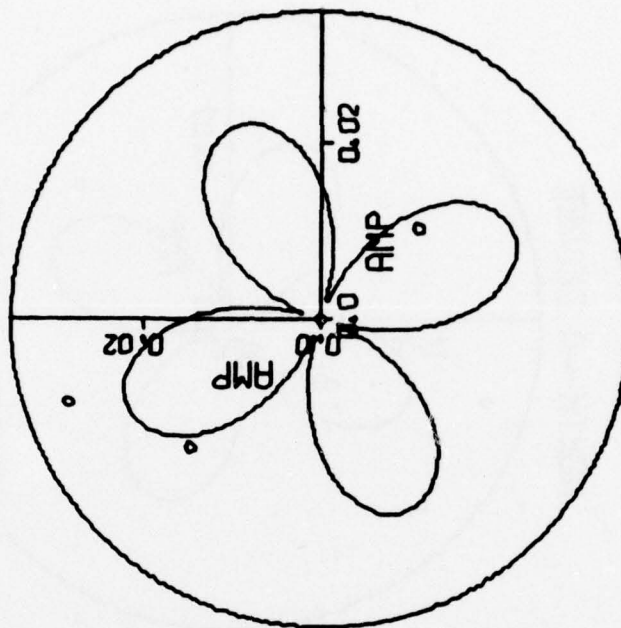
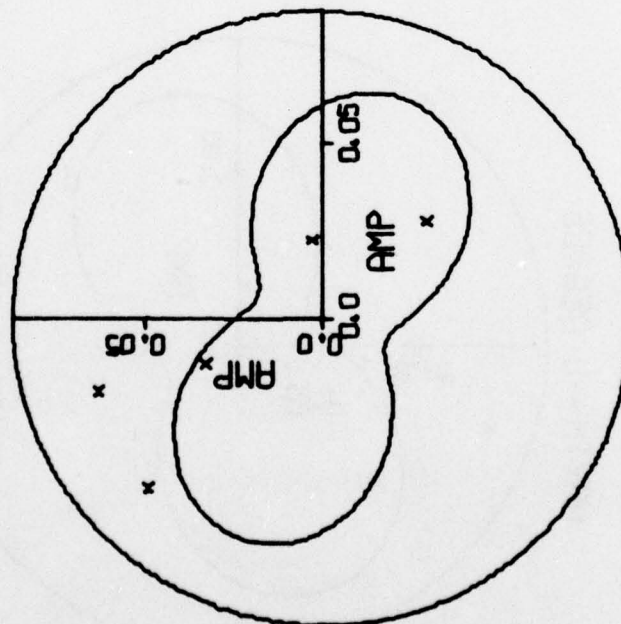


FIGURE V-35
 SURFACE WAVE RADIATION PATTERNS FOR EVENT PNE/729/76
 (PAGE 2 OF 18)

PNE/729/76
 DOUBLE COUPLE
 LR--PERIOD=40.0

NORTH--0 DEGREE



PNE/729/76
 DOUBLE COUPLE
 LQ--PERIOD=40.0

NORTH--0 DEGREE

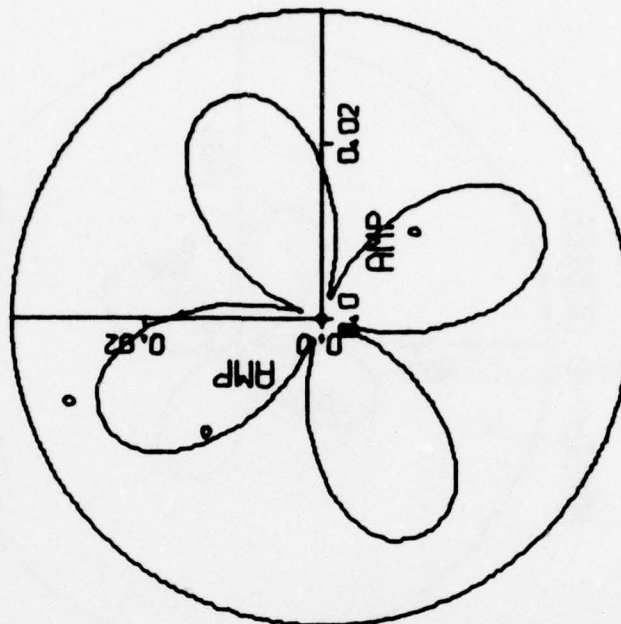
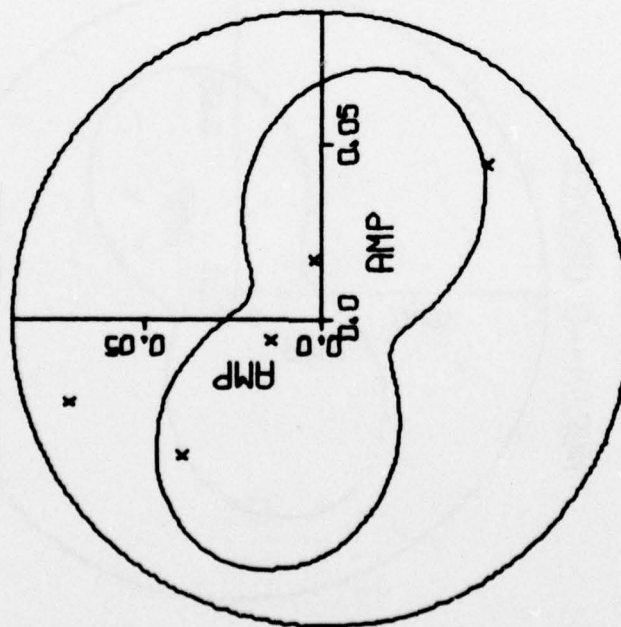


FIGURE V-35
 SURFACE WAVE RADIATION PATTERNS FOR EVENT PNE/729/76
 (PAGE 3 OF 18)

PNE/729/76
 DOUBLE COUPLE EXPLOSION
 LR--PERIOD=35.0

NORTH--0 DEGREE



PNE/729/76
 DOUBLE COUPLE EXPLOSION
 LQ--PERIOD=35.0

NORTH--0 DEGREE

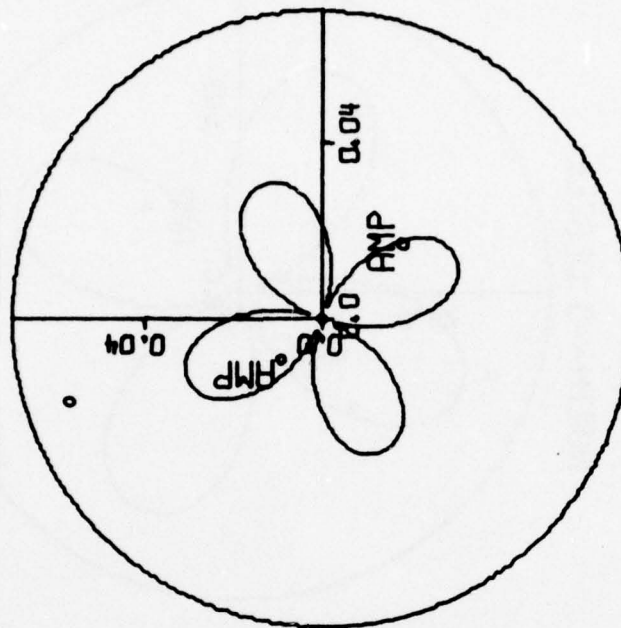
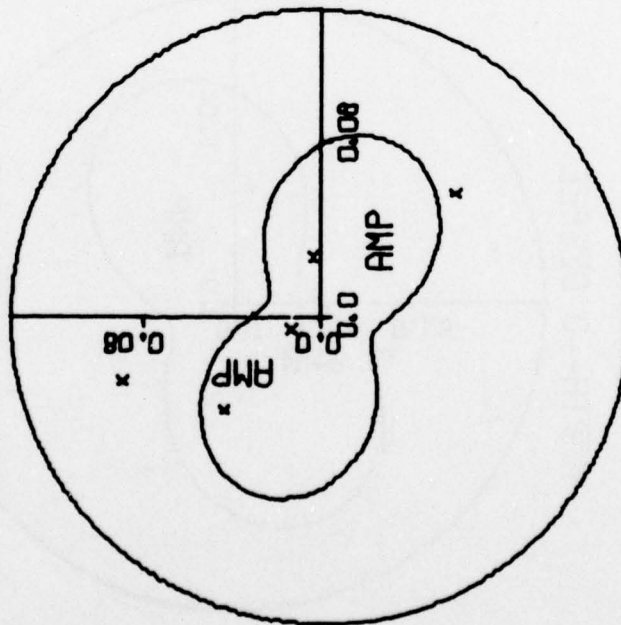


FIGURE V-35
 SURFACE WAVE RADIATION PATTERNS FOR EVENT PNE/729/76
 (PAGE 4 OF 18)

PNE/729/76
 DOUBLE COUPLE EXPLOSION
 LR--PERIOD=30.0
 NORTH--0 DEGREE



PNE/729/76
 DOUBLE COUPLE EXPLOSION
 LQ--PERIOD=30.0
 NORTH--0 DEGREE

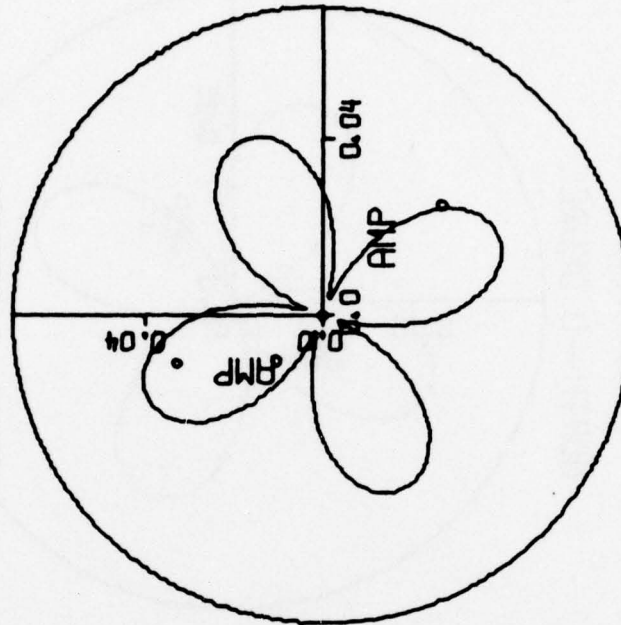
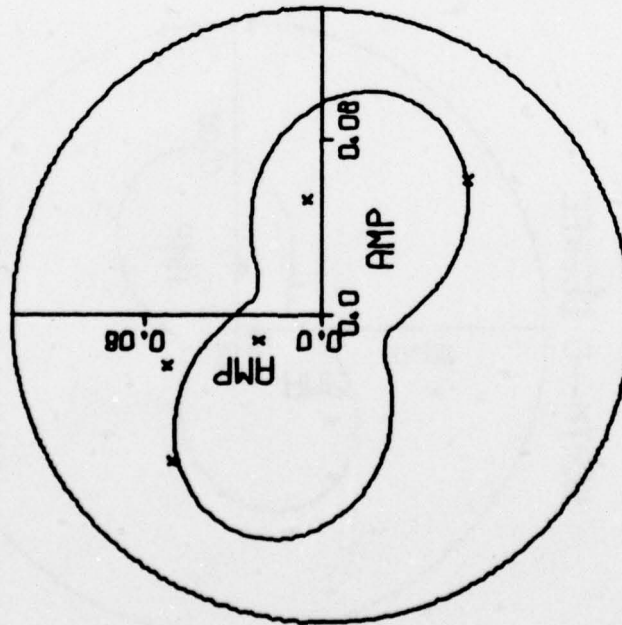


FIGURE V-35
 SURFACE WAVE RADIATION PATTERNS FOR EVENT PNE/729/76
 (PAGE 5 OF 18)

PNE/729/76
DOUBLE COUPLE EXPLOSION
LR--PERIOD=25.0

NORTH--0 DEGREE



PNE/729/76
DOUBLE COUPLE EXPLOSION
LQ--PERIOD=25.0

NORTH--0 DEGREE

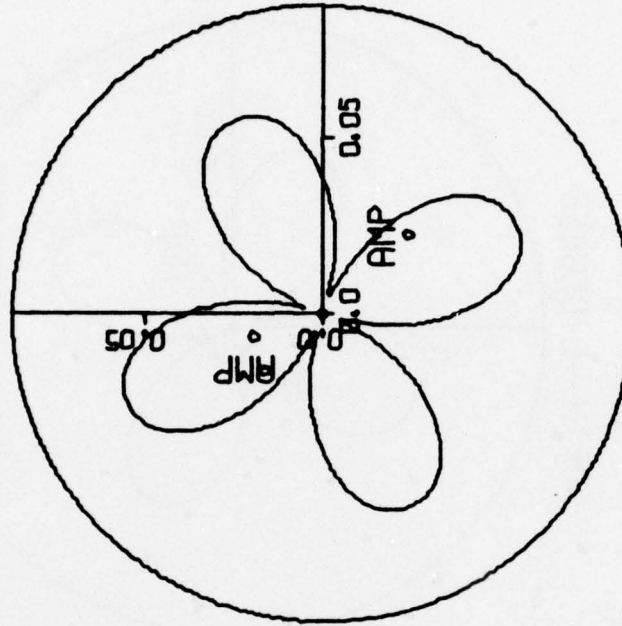
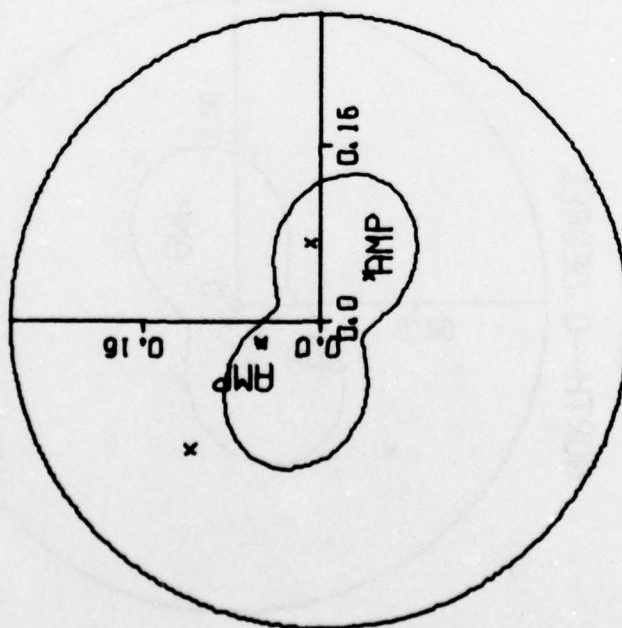


FIGURE V-35
SURFACE WAVE RADIATION PATTERNS FOR EVENT PNE/729/76
(PAGE 6 OF 18)

PNE/729/76
 DOUBLE COUPLE EXPLOSION
 LR--PERIOD=20.0

NORTH--0 DEGREE



PNE/729/76
 DOUBLE COUPLE EXPLOSION
 LQ--PERIOD=20.0

NORTH--0 DEGREE

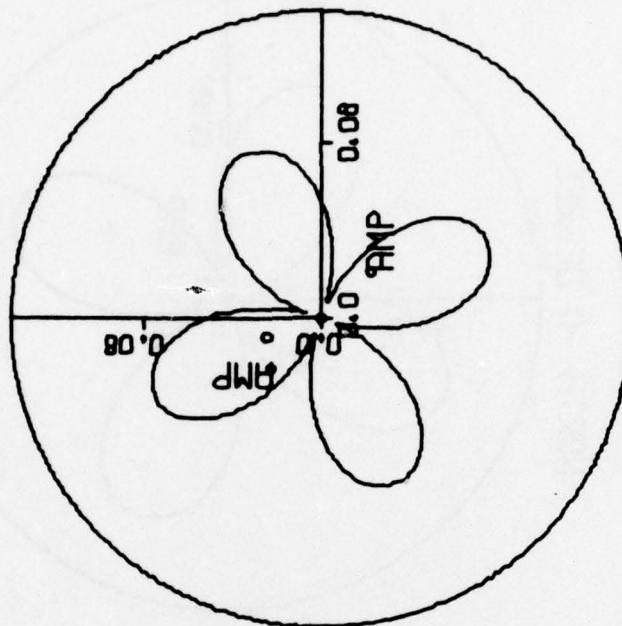
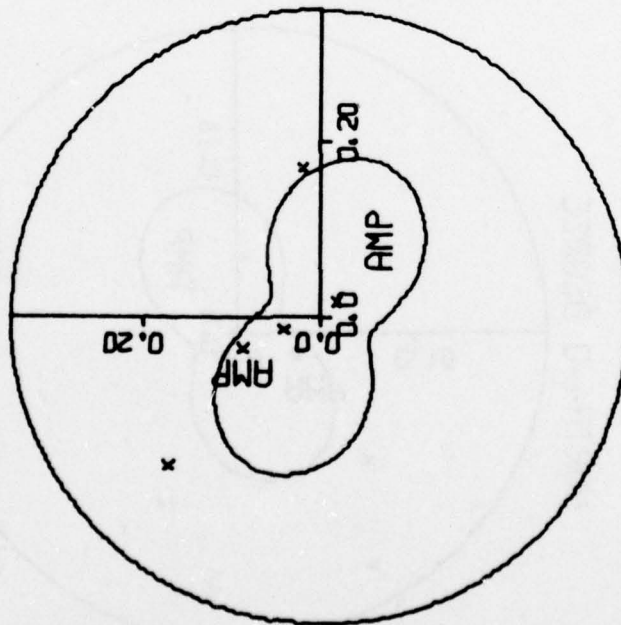


FIGURE V-35
 SURFACE WAVE RADIATION PATTERNS FOR EVENT PNE/729/76
 (PAGE 7 OF 18)

PNE/729/76
 DOUBLE COUPLE EXPLOSION
 LR--PERIOD=15.0

NORTH--0 DEGREE



PNE/729/76
 DOUBLE COUPLE EXPLOSION
 LQ--PERIOD=15.0

NORTH--0 DEGREE

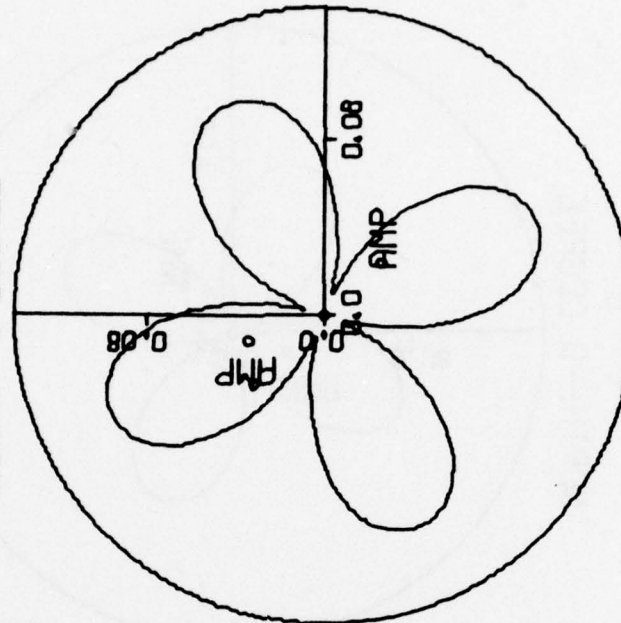
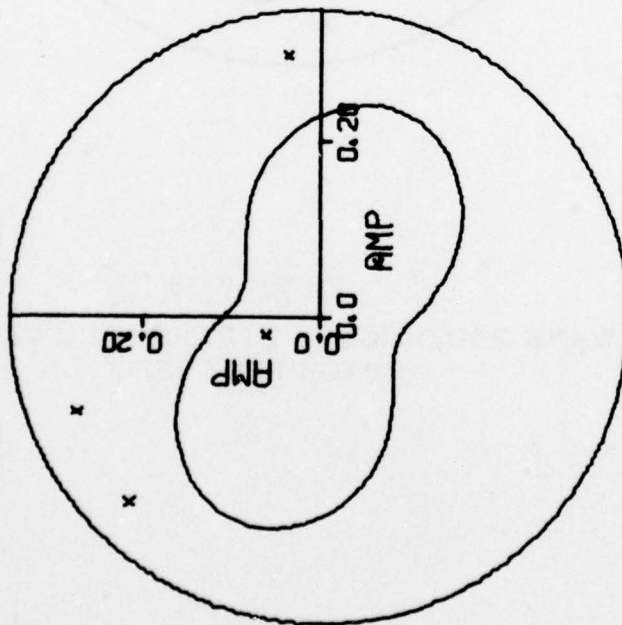


FIGURE V-35

SURFACE WAVE RADIATION PATTERNS FOR EVENT PNE/729/76
 (PAGE 8 OF 18)

PNE/729/76
 DOUBLE COUPLE
 LR--PERIOD=10.0
 NORTH--0 DEGREE



PNE/729/76
 DOUBLE COUPLE
 LQ--PERIOD=10.0
 NORTH--0 DEGREE

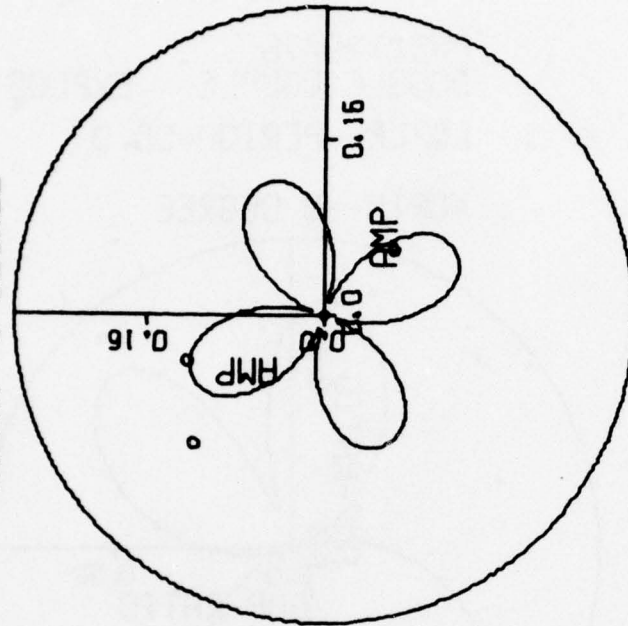


FIGURE V-35
 SURFACE WAVE RADIATION PATTERNS FOR EVENT PNE/729/76
 (PAGE 9 OF 18)

PNE/729/76
DOUBLE COUPLE EXPLOSION
LQ/LR--PERIOD=50.0
NORTH--0 DEGREE

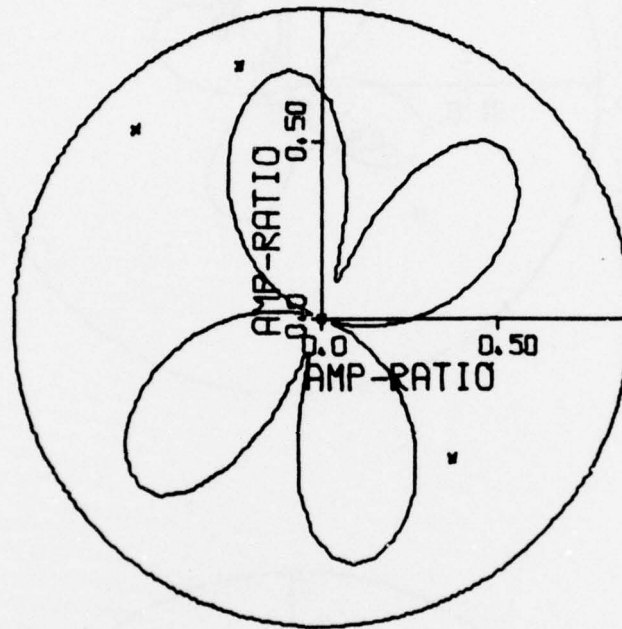


FIGURE V-35
SURFACE WAVE RADIATION PATTERNS FOR EVENT PNE/729/76
(PAGE 10 OF 18)

PNE/729/76
DOUBLE COUPLE EXPLOSION
LQ/LR--PERIOD=45.0
NORTH--0 DEGREE

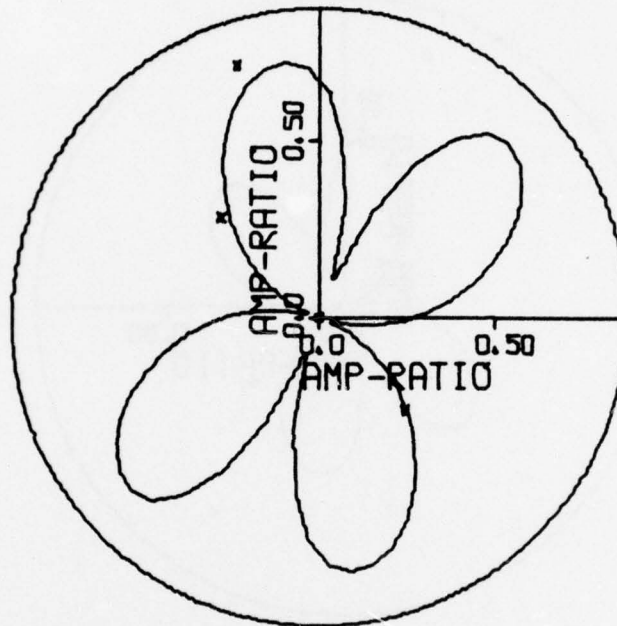


FIGURE V-35
SURFACE WAVE RADIATION PATTERNS FOR EVENT PNE/729/76
(PAGE 11 OF 18)

PNE/729/76
DOUBLE COUPLE EXPLOSION
LQ/LR--PERIOD=40.0
NORTH--0 DEGREE

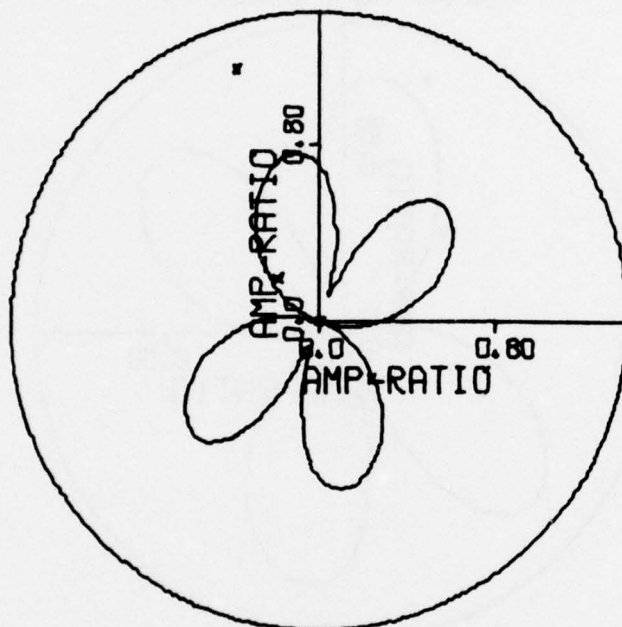


FIGURE V-35
SURFACE WAVE RADIATION PATTERNS FOR EVENT PNE/729/76
(PAGE 12 OF 18)

PNE/729/76
DOUBLE COUPLE EXPLOSION
LQ/LR--PERIOD=35.0
NORTH--0 DEGREE

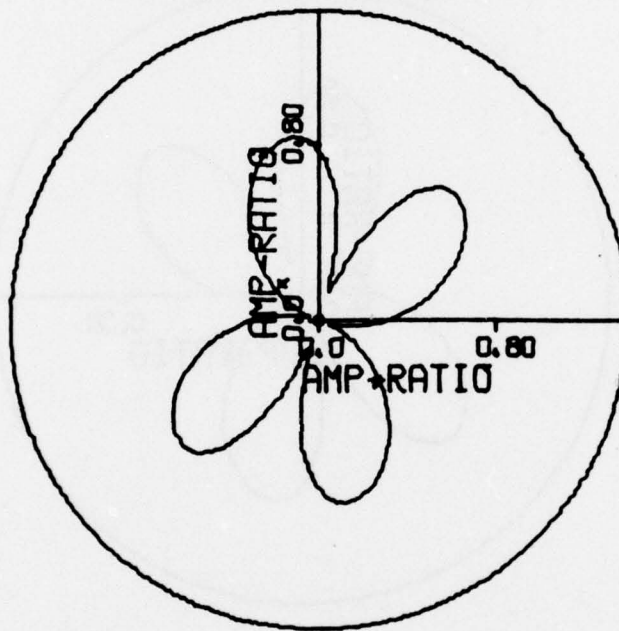


FIGURE V-35
SURFACE WAVE RADIATION PATTERNS FOR EVENT PNE/729/76
(PAGE 13 OF 18)

PNE/729/76
DOUBLE COUPLE EXPLOSION
LQ/LR--PERIOD=30.0
NORTH--0 DEGREE

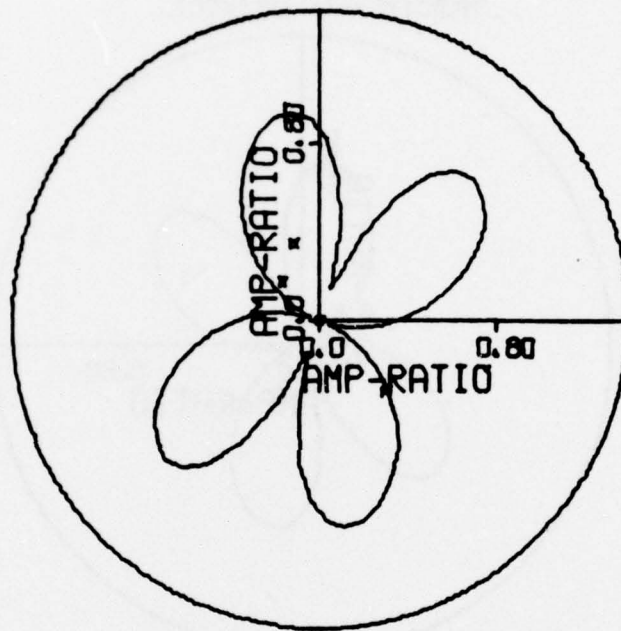


FIGURE V-35
SURFACE WAVE RADIATION PATTERNS FOR EVENT PNE/729/76
(PAGE 14 OF 18)

PNE/729/76
DOUBLE COUPLE EXPLOSION
LQ/LR--PERIOD=25.0
NORTH--0 DEGREE

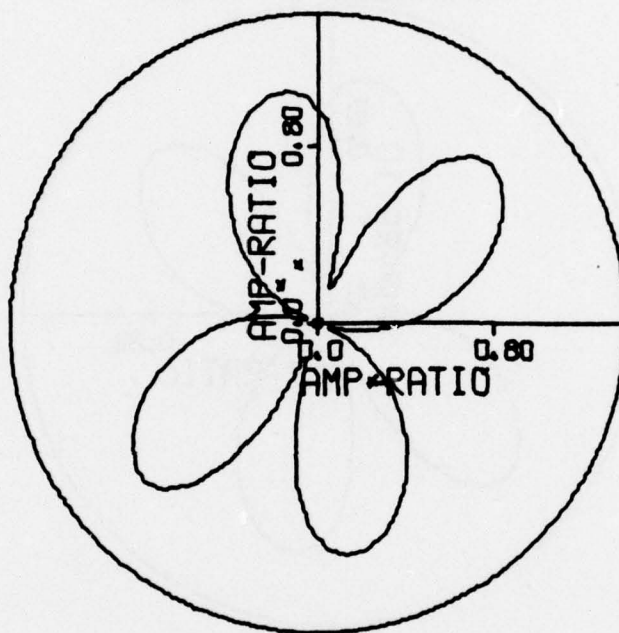


FIGURE V-35
SURFACE WAVE RADIATION PATTERNS FOR EVENT PNE/729/76
(PAGE 15 OF 18)

PNE/729/76
DOUBLE COUPLE EXPLOSION
LQ/LR--PERIOD=20.0
NORTH--0 DEGREE

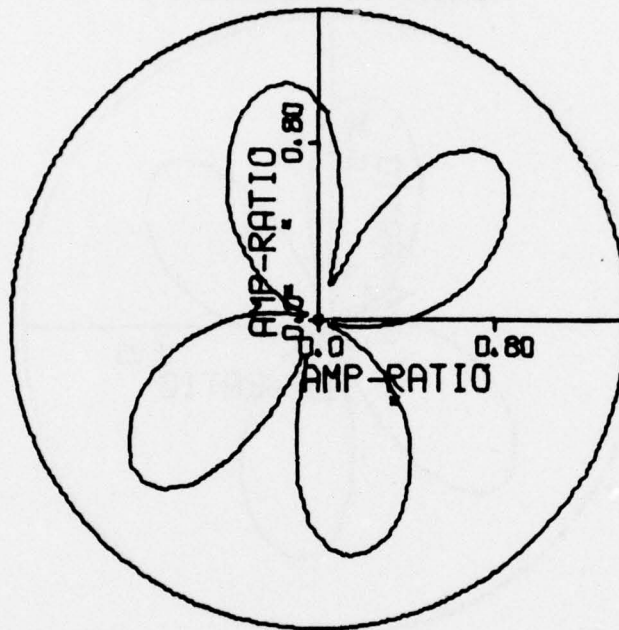


FIGURE V-35
SURFACE WAVE RADIATION PATTERNS FOR EVENT PNE/729/76
(PAGE 16 OF 18)

PNE/729/76
DOUBLE COUPLE EXPLOSION
LQ/LR--PERIOD=15.0
NORTH--0 DEGREE

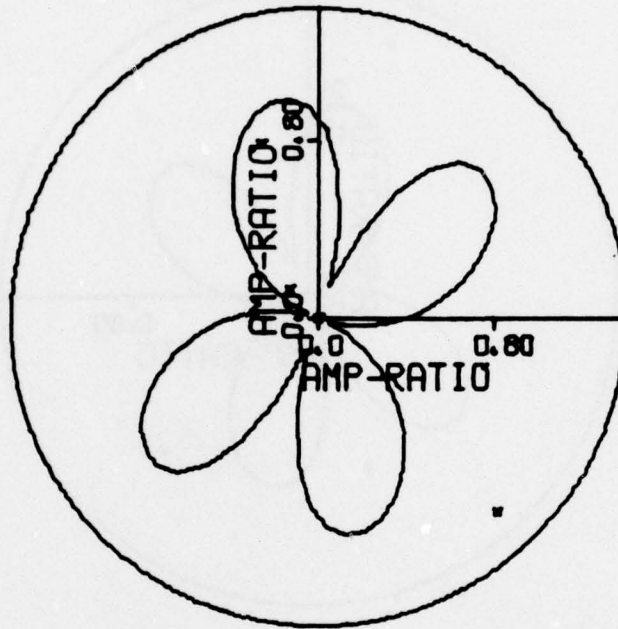


FIGURE V-35
SURFACE WAVE RADIATION PATTERNS FOR EVENT PNE/729/76
(PAGE 17 OF 18)

PNE/729/76
DOUBLE COUPLE EXPLOSION
LQ/LR--PERIOD=10.0
NORTH--0 DEGREE

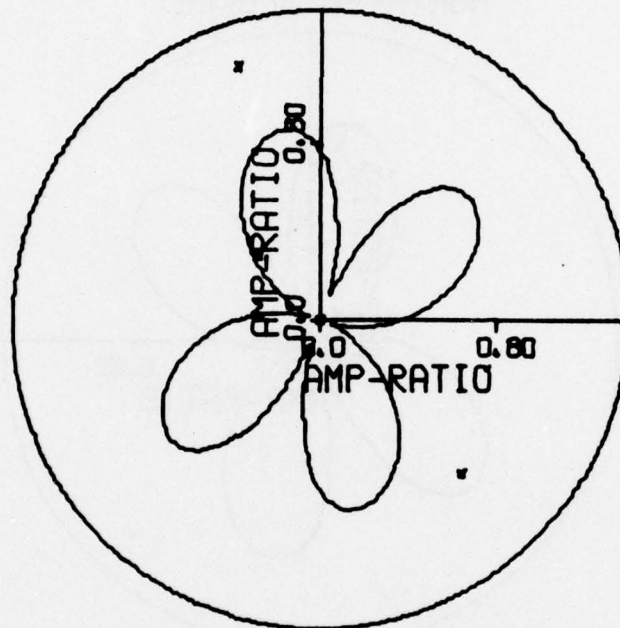


FIGURE V-35
SURFACE WAVE RADIATION PATTERNS FOR EVENT PNE/729/76
(PAGE 18 OF 18)

- More good quality surface wave data are available for the NTS events than for the EKZ or PNE events. There are more Love wave recordings available for the NTS events. However, lack of good Love wave recordings for the EKZ events does not necessarily imply that the EKZ events radiated less Love waves. In fact, for the EKZ events, if the observation stations have Love wave recordings, the observed Love wave signals are compatible with the observed Rayleigh wave signals, in terms of data quality and signal level.
- The depth estimates of the selected NTS, EKZ, and PNE events are all very shallow. This is to be expected, since these events are presumed underground explosions.
- The estimates of dip and slip angle of the double-couple sources of tectonic strain release vary among these events. Most NTS events seem to have more of a *strike-slip type of mechanism*. Most EKZ events seem to have more of a dip-slip type of mechanism.
- The strike angle estimates of the double-couple sources for the NTS events are generally in the N-S direction, while those for PNE events are close to the E-W direction. It seems that there is no trend in the strike angle estimates of the EKZ events.
- The estimated F values vary among the events in each group and among these three groups of explosion events. They all indicate that these presumed explosions have associated tectonic strain release. The range of variation of the estimated F values are not significantly different among these three groups. However, for the events with the same m_b , the estimated seismic moments (given in Tables V-7, V-9, and V-11

as M_E) of the tectonic strain releases associated with the selected NTS events are noticeably larger than those associated with selected EKZ or PNE events. Also, the variations of minimum residuals, with respect to the tested F values in the amplitude spectral fitting process, are quite different between the selected NTS events and the selected EKZ or PNE events. Figure V-36 shows the residual variations with respect to the tested F values for the events NTS/1028/5, EKZ/704/76, and PNE/729/76. For the NTS events, the minimum residual increases drastically when the tested F value increases from the estimated F value and the residual only increases very slightly when the tested F value decreases from the estimated F value. For the EKZ and PNE events, the residual increases slowly in both directions.

To see if the source parameter estimates of these selected NTS, EKZ, and PNE events can be used for discrimination among these three groups of events or between earthquakes and explosions, the estimates of the source parameters, which are thought to be relevant, are plotted as functions of the event m_b . Figure V-37 displays the estimated F values versus the event m_b for the selected NTS, EKZ, and PNE events. It is noticed that there is no apparent correlation between the F value and the event m_b . That is, the larger m_b does not necessarily imply smaller or larger F values. The estimates of the moments of the explosive sources (given in Tables V-7, V-9, and V-11 as M_X) for these events as a function of the event m_b are shown in Figure V-38. Also plotted in this figure are the previously obtained seismic moment estimates of various central Eurasian earthquakes (Tsai and Shen, 1972; Turnbull, et al., 1973, 1974; Sun, 1976) and the theoretically predicted relation (given by L_E in the figure) between the seismic moment and the event m_b for the earthquakes (Tsai, 1972b).

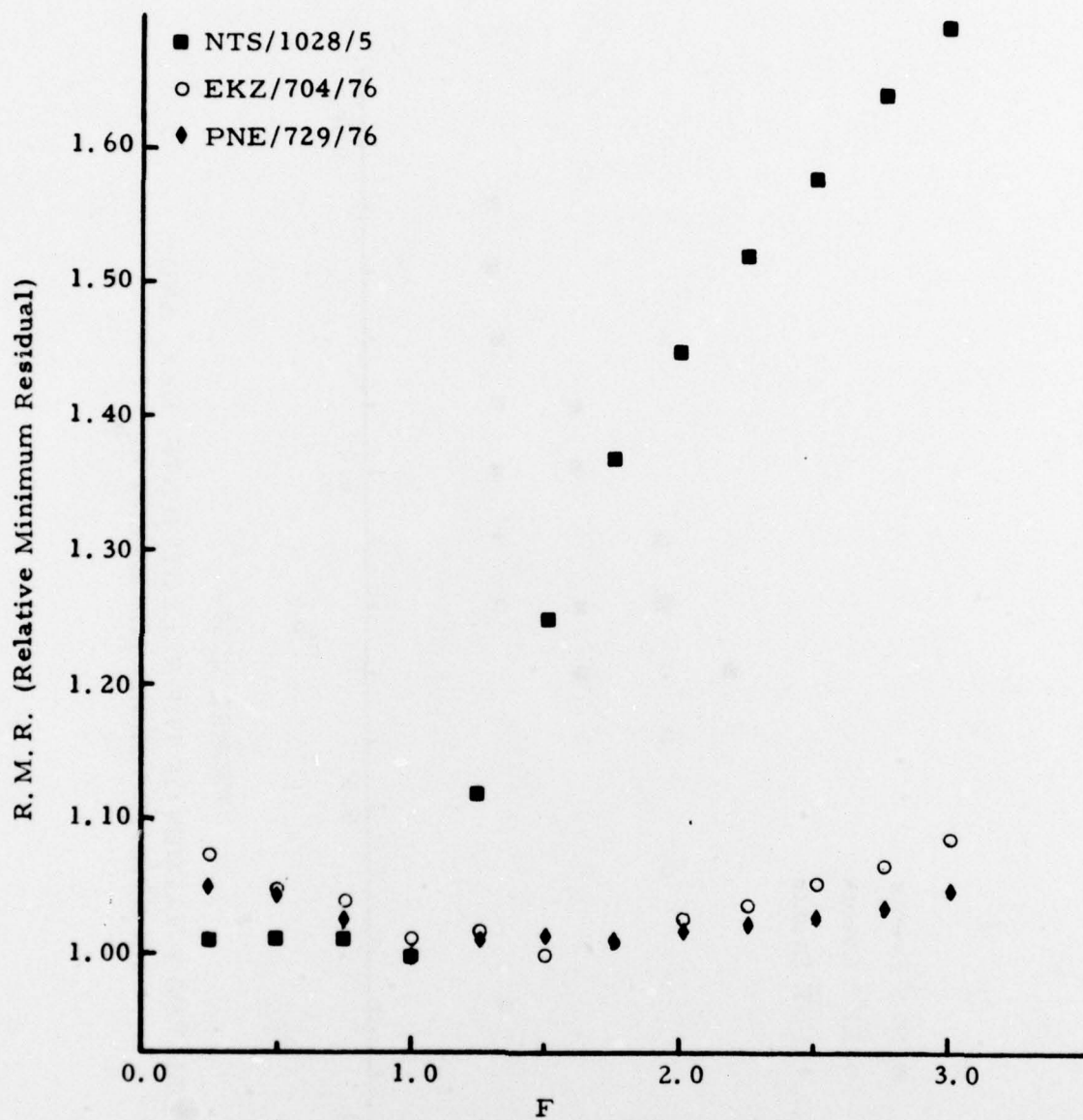


FIGURE V-36

TYPICAL RESIDUAL VARIATION WITH RESPECT TO THE TESTED
F VALUES FOR THE SELECTED NTS, EKZ, AND PNE EVENTS

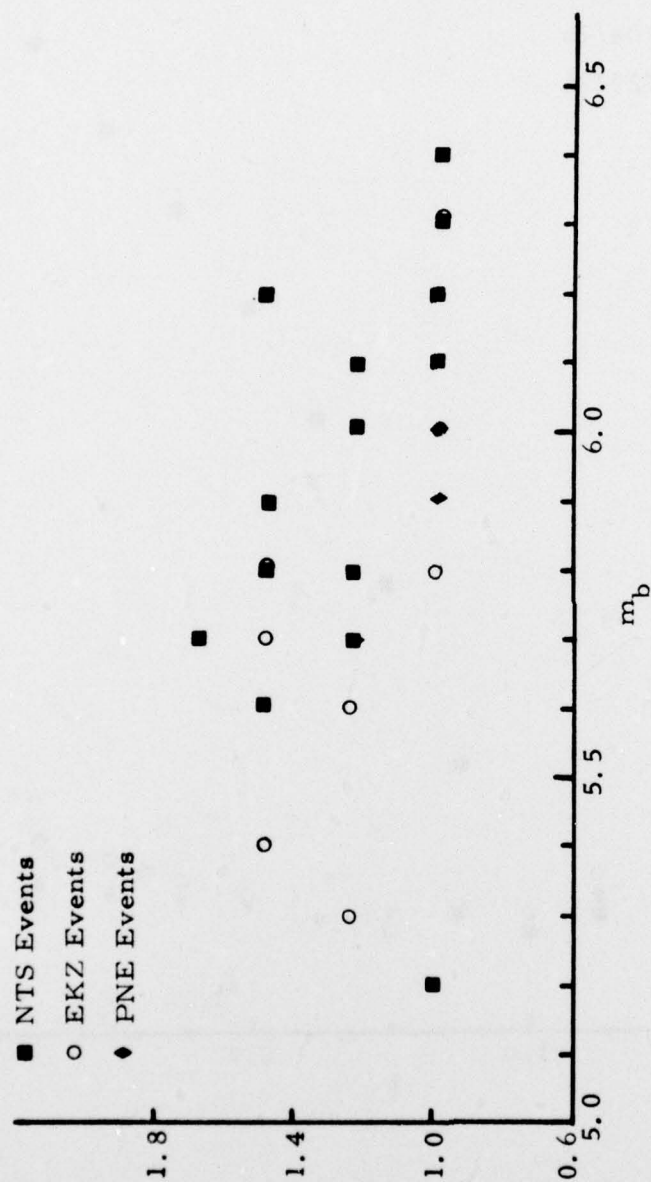


FIGURE V-37
ESTIMATED F VALUES OF THE SELECTED NTS, EKZ, AND
PNE EVENTS VERSUS THE EVENT m_b

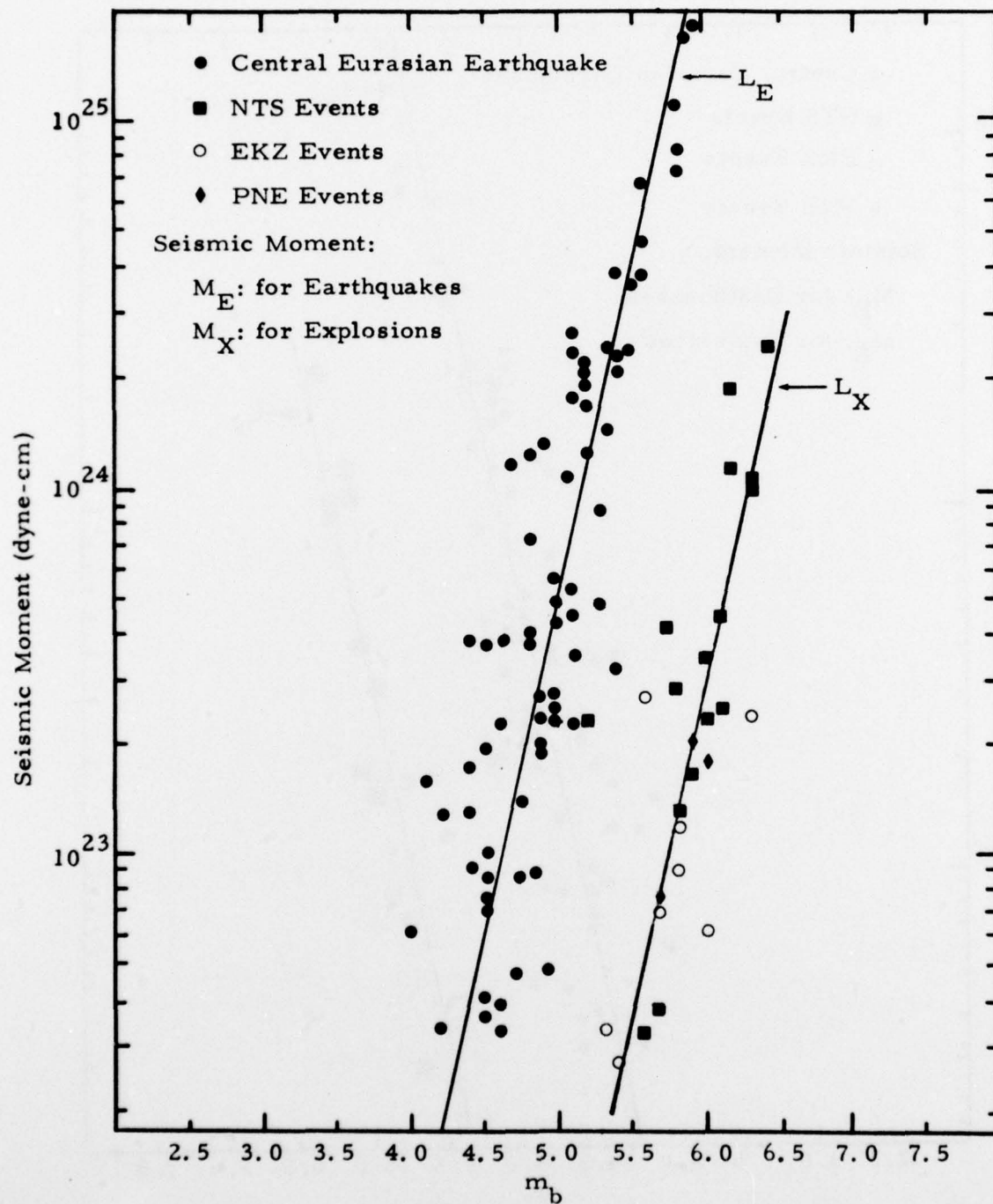


FIGURE V-38
 MOMENT VERSUS m_b PLOT
 (PAGE 1 OF 2)

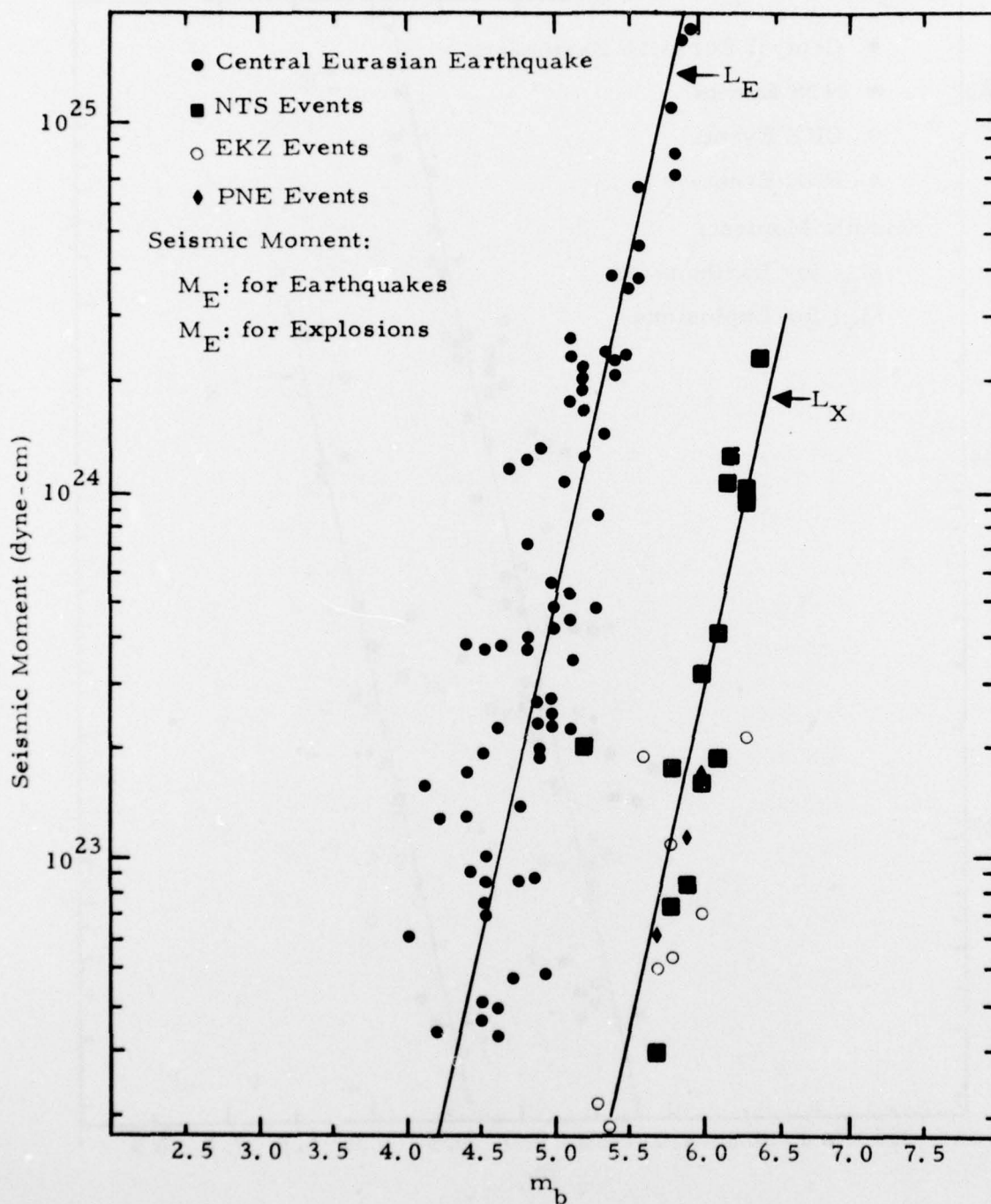


FIGURE V-38
 MOMENT VERSUS m_b PLOT
 (PAGE 2 OF 2)

The results from the examination of this figure can be summarized as follows:

- The theoretically predicted relation between the seismic moment and the event m_b for the earthquakes explains the previously estimated seismic moments of the central Eurasian earthquakes very well, for m_b from 4.5 to 6.0.
- In general, for the events with similar m_b , the moment estimates of the explosive sources for the NTS events are larger than those for the EKZ or the PNE events.
- The moment estimates, M_X , of the explosive sources for the selected NTS, EKZ, and PNE events can be well fitted with a straight line (indicated by L_X in the figure) parallel to the theoretically predicted line L_E for the earthquakes. The separation of these two lines is about one m_b unit. This separation in the moment versus m_b plot can be used to discriminate the earthquake population against the explosion population.
- Comparing with the conventional M_s versus m_b plot, the moment versus m_b plot seems to offer better discrimination in several respects. First, the separation between the earthquake populations is less in the moment versus m_b plot. Second, earthquake and explosion populations are less scattered in the moment versus m_b plot. Third, in the moment versus m_b plot, the explosions at NTS and EKZ can be considered as one explosion population; while in the M_s versus m_b plot, the NTS events and the EKZ events behave very differently, with the NTS events quite often extending into the earthquake population, making the M_s versus m_b plot ineffective for discrimination purposes.

SECTION VI

CONCLUSIONS

The far-field long-period surface waves, both Rayleigh and Love, observed at the long-period seismic network have been studied for the presumed underground nuclear explosions at the United States Nevada Test Site (NTS) and Russian eastern Kazakh (EKZ), and for the peaceful nuclear explosions (PNE) in the north Caspian Sea region. A total of twenty-seven recent NTS, EKZ, and PNE events have been analyzed in terms of their surface wave dispersion characteristics, the Rayleigh wave attenuation along the travel path involved, their Rayleigh and Love wave spectra, and their seismic source parameter estimates.

The collective behavior of the Rayleigh and Love wave fundamental mode group velocities for each travel path involved has been obtained. For some travel paths, the theoretical surface wave dispersions for the normal continental or oceanic path can explain the observed group velocities quite well. However, the deviations of the observed group velocities from the theoretical group velocity curves are very noticeable in many cases. Therefore, the collection of the representative surface wave group velocity curves, which have been obtained here, along the travel paths from NTS, EKZ, and the north Caspian Sea region to ALPA, NORSAR, LASA, VLPE stations, SRO, and the SDCS stations will be helpful and can be used as guidelines for the future analysis of the surface waves of the seismic events in these three areas.

The Rayleigh wave attenuation coefficients (for periods from 10 to 50 seconds at 5 second increments) have been obtained for the continental and mixed paths from NTS to the observation stations, for those from

EKZ to the observation stations, for oceanic paths from the NTS to stations in the Pacific Ocean, and for one path across the Atlantic Ocean (KON-ZLP). The agreement between the attenuation values obtained here and those calculated by other investigators is fairly good. In general, Tryggvason's attenuation curve has yielded quite reasonable attenuation corrections and is thought suitable for the average travel paths.

From the examination of the observed Rayleigh and Love wave amplitude spectra of these NTS, EKZ, and PNE events, it has been shown that the seismic sources of these explosions have various degrees of double-couple component in addition to the explosive source. The evidence of this double-couple component in these explosion events is indicated by the presence of Love wave motions observed at various recording stations and the azimuthal variations of the observed surface wave amplitude spectra. However, we have not observed any case where the Love wave amplitude is always less than the corresponding Rayleigh wave amplitude at a given station, as found by Lambert et al. (1972). The observed LQ/LR spectral ratios are found compatible with the average fundamental mode LQ/LR spectral ratios for the shallow earthquakes theoretically modeled by double-couple sources. This does not quite agree with the observations made by Lambert et al. (1972), that the LQ/LR spectral ratios for explosions are less than 1.0 and are much less than those for earthquakes. Although it has been found that there is a difference between earthquakes and explosions in the average frequency dependence of LQ/LR ratios, this difference is not thought to be sufficiently significant to be used as a discriminative feature between earthquakes and explosions, as implicitly suggested by Lambert et al. (1972).

The source parameter estimates of selected NTS, EKZ, and PNE events have been obtained by fitting the observed surface wave amplitude spectra with the theoretically calculated surface wave spectra of a combined source, which consists of the explosive source and the double-couple source.

The double-couple source is used to model the possible tectonic strain release associated with the explosion. The depth estimates of these events indicate that most of them took place at very shallow depths (0.5 km). The very shallow depth estimates are thought to be very reasonable, since those events are presumed underground nuclear explosions. The dip and slip angle estimates of the NTS events do not quite agree with the assumption made by some authors (Toksöz, et al., 1965; Lambert, et al., 1972; Mitchell, 1975) that tectonic strain release associated with the NTS events can be modeled by a double-couple source with a vertical strike-slip type of mechanism (i. e., $\delta = 90^\circ$, $\lambda = 0^\circ$). The strike angle estimates for the selected NTS events are generally in the N-S direction, while those for the selected PNE events are close to the E-W direction. However, there is no general trend observed in the strike angle estimates for the EKZ events. No apparent correlation between the estimated F values and the event m_b has been found for these events. The F values estimated for the NTS, EKZ, and PNE events are 1.0-1.75, 1.0-1.5, and 1.0-1.25, respectively. However, for the events with the same m_b , the estimated seismic moments of the tectonic strain releases associated with the selected NTS events are in general larger than those associated with the selected EKZ or PNE events.

From the source parameter estimations for those NTS, EKZ, and PNE events, the moment versus m_b plot has been found to be very promising for the purpose of discrimination between earthquakes and explosions. Several advantages of using the moment versus m_b plot over the conventional M_s versus m_b plot have been found, such as less scattering in both populations and wider separation, in terms of m_b , between the two populations. However, it must be mentioned here that the earthquakes, shown in Figure V-38 for the moment versus m_b plot, are modeled by the double-couple source only instead of the combined source which is used to model the explosion events studied here. It is believed that the moment versus m_b plot shown in Figure V-38 will not be significantly altered by modeling the earthquakes with the combined

source, since the double-couple source alone has been producing very satisfactory results for the earthquakes. Nevertheless, for a fair comparison, the earthquake events should be treated in the same way as the explosion events by using the combined source in the source parameter estimation for earthquakes.

SECTION VII
REFERENCES

- Aki, K., 1964; A Note on Surface Wave Generation from the Hardhat Nuclear Explosion, J. Geophys. Res., 69, 1131-1134.
- Alexander, S. S., 1963; Surface Wave Propagation in the Western United States, Ph.D. Thesis, California Institute of Technology, Pasadena, California.
- Anderson, D. L., 1964; The Anelasticity of the Earth, J. Geophys. Res., 69, 2071-2084.
- Arabasz, W. J., W. D. Richins, and C. J. Langer (1975); Detailed Characteristics of March 1975 Idaho-Utah Border Earthquake Sequence, EOS, 56, 1022.
- Bache, T. E., and D. G. Lambert, 1977; Earthquake Ground Motion From The 1975 Pocatello Valley Earthquake, Quarterly Status Report, AFGL Contract F19628-77-C-0004, Hanscom Air Force Base, Massachusetts.
- Battis, J. C., and K. J. Hill, 1977; Analysis of Seismicity and Tectonics of the Central and Western United States, Interim Scientific Report No. 1, Texas Instruments Report No. ALEX(02)-ISR-77-01, AFOSR Contract Number F44620-76-C-0063, Texas Instruments Incorporated, Dallas, Texas.
- Ben-Menahem, A., and D. G. Harkrider, 1964; Radiation Patterns of Seismic Surface Waves from Buried Dipolar Point Source in a Flat Stratified Earth, J. Geophys. Res., 69, 2605-2620.

- Brune, J. N., and P. W. Pomeroy, 1963; Surface Wave Radiation Patterns for Underground Nuclear Explosions and Small-Magnitude Earthquakes, *J. Geophys. Res.*, 68, 5005-5028.
- Eaton, J. P., 1963; Crustal Structure from San Francisco, California, to Eureka, Nevada, from Seismic-Refracton Measurements, *J. Geophys. Res.*, 68, 5759-5806.
- Harkrider, D. G., 1964; Surface Waves in Multilayered Elastic Media: I. Rayleigh and Love Waves from Buried Sources in a Multilayered Elastic Half-Space, *Bull. Seismol. Soc. Amer.*, 54, 627-680.
- Herrmann, R. B., 1974; Surface-Wave Generated by Central United States Earthquakes, Ph.D. Dissertation, Saint Louis University, Saint Louis, Missouri.
- Herrmann, R. B., and B. J. Mitchell, 1975; Statistical Analysis and Interpretation of Surface Wave Anelastic Attenuation Data for the Stable Interior of North America, *Bull. Seismol. Soc. Amer.*, 65, 1115-1128.
- Hoel, P. G., 1962; Introduction to Mathematical Statistics, John Wiley & Sons, New York.
- Lambert, D. G., E. A. Flinn, and C. B. Archambeau, 1972; A Comparative Study of the Elastic Wave Radiation from Earthquakes and Underground Explosions, *Geophys. J. R. Astr. Soc.*, 29, 403-432.
- Mitchell, B. J., 1975; Regional Rayleigh Wave Attenuation in North America, *J. Geophys. Res.*, 80, 4904-4916.
- Mitchell, B. J., L. W. B. Beite, Y. K. Yu, and R. B. Herrmann, 1976; Attenuation of Love and Rayleigh Waves Across the Pacific at Periods Between 15 and 110 Seconds, *Bull. Seismol. Soc. Amer.*, 66.
- Nordyke, M. P., 1973; A Review of Soviet Data on the Peaceful Uses of Nuclear Explosions, Report No. UCRL-51414, Lawrence Livermore Laboratory, University of California/Livermore.

- Press, F., and C. B. Archambeau, 1962; Release of Tectonic Strain by Underground Nuclear Explosions, *J. Geophys. Res.*, 67, 337-343.
- Rodriguez, R. G., 1969; Atlas of Asia and Eastern Europe to Support Detection of Underground Nuclear Testing, Vol. V - Crust and Mantle Conditions, U.S. Geological Survey.
- Smith, R. B., and M. L. Shar, 1974; Contemporary Tectonics and Seismicity of the Western United States with Emphasis on the Intermountain Seismic Belt, *Geol. Soc. Am. Bull.*, 85, 1205-1218.
- Sun, D., 1976; Source Studies in the Near- and Far-Field, Semi-Annual Technical Report No. 6-Part A, Texas Instruments Report No. ALEX(02)-TR-76-01-Part A, AFOSR Contract Number F44620-73-C-0055, Texas Instruments Incorporated, Dallas, Texas.
- Sun, D., and J. S. Shaub, 1977; Analysis of Seismic Surface Waves Using PDP-15 Interactive Graphics, *Proc. of the International Symposium on Computer Aided Seismic Analysis and Discrimination*, Falmouth, Massachusetts.
- Toksöz, M. N., A. Ben-Menahem, and D. G. Harkrider, 1964; Determination of Source Parameters of Explosions and Earthquakes by Amplitude Equalification of Seismic Surface Waves: 1. Underground Nuclear Explosions, *J. Geophys. Res.*, 69, 4355-4366.
- Toksöz, M. N., D. G. Harkrider, and A. Ben-Menahem, 1965; Determination of Source Parameters by Amplitude Equalification of Seismic Surface Waves: 2. Release of Tectonic Strain by Underground Nuclear Explosions and Mechanisms of Earthquakes, *J. Geophys. Res.*, 70, 907-922.
- Tryggvason, E., 1965; Dissipation of Rayleigh Wave Energy, *J. Geophys. Res.*, 70, 1449-1455.

- Tsai, Y. B., 1972a; Utility of Tsai's Method for Seismic Discrimination: Semi-Annual Technical Report No. 1, AFOSR Contract Number F44620-71-C-0112, Texas Instruments Incorporated, Dallas, Texas.
- Tsai, Y. B., 1972b; Utility of Tsai's Method for Seismic Discrimination: Semi-Annual Technical Report No. 2, AFOSR Contract Number F44620-71-C-0112, Texas Instruments Incorporated, Dallas, Texas.
- Tsai, Y. B., and K. Aki, 1969; Simultaneous Determination of the Seismic Moment and Attenuation of Seismic Surface Waves, Bull. Seismol. Soc. Amer., 59, 275-287.
- Tsai, Y. B., and W. W. Shen, 1972; Utility of Tsai's Method for Seismic Discrimination: Final Report, AFOSR Contract Number F44620-71-C-0112, Texas Instruments Incorporated, Dallas, Texas.
- Turnbull, L. S., 1976; Determination of Seismic Source Parameters Using Far-Field Surface Wave Spectra, Ph.D. Thesis, The Pennsylvania State University, State College, Pennsylvania.
- Turnbull, L. S., D. F. D. Sun, and J. S. Shaub, 1973; Determination of Seismic Source Parameters from Frequency Dependent Rayleigh and Love Wave Radiation Patterns, Semi-Annual Technical Report No. 1-Part C, Texas Instruments Report No. ALEX(02)-TR-73-01-Part C, AFOSR Contract Number F44620-73-C-0055, Texas Instruments Incorporated, Dallas, Texas.
- Turnbull, L. S., D. Sun, and D. G. Black, 1974; Determination of Seismic Source Parameters from Long-Period Teleseismic Waves, Semi-Annual Technical Report No. 2-Part A, Texas Instruments Report No. ALEX(02)-TR-74-01-Part A, AFOSR Contract Number F44620-73-C-0055, Texas Instruments Incorporated, Dallas, Texas.

Turnbull, L. S., and J. C. Battis, 1974; Interpretation of Strong-Motion Earthquake Accelerograms: The Bear Valley Event of 1973, Final Report, Texas Instruments Report No. ALEX(02)-FR-74-01, AFOSR Contract Number F44620-72-C-0073, Texas Instruments Incorporated, Dallas, Texas.

Turnbull, L. S., J. C. Battis, D. Sun, and A. C. Strauss, 1975; Source Studies in the Near- and Far-Field, Semi-Annual Technical Report No. 4-Part A, Texas Instruments Report No. ALEX(02)-TR-75-01-Part A, AFOSR Contract Number F44620-73-C-0055, Texas Instruments Incorporated, Dallas, Texas.